MATERIALS DEVELOPMENT FOR COMMERCIAL MULTILAYER CERAMIC CAPACITORS

Ronald Mikkenie

Materials Development for Commercial Multilayer Ceramic Capacitors

Ronald Mikkenie

R. Mikkenie
Materials Development for Commercial Multilayer Ceramic Capacitors
Ph.D. Thesis University of Twente, Enschede, The Netherlands

ISBN: 978-90-365-3275-4
DOI: 10.3990/1.9789036532754

Printed by Datawyse B.V., Maastricht, The Netherlands.

MATERIALS DEVELOPMENT FOR COMMERCIAL MULTILAYER CERAMIC CAPACITORS

PROEFSCHRIFT

ter verkrijging van
de graad van doctor aan de Universiteit Twente,
op gezag van de rector magnificus,
Prof. dr. H. Brinksma,
volgens besluit van het College voor Promoties
in het openbaar te verdedigen
op donderdag 17 november 2011 om 16:45 uur

door

Ronald Mikkenie
geboren op 8 augustus 1971
te Detmold (Duitsland)

Dit proefschrift is goedgekeurd door de promotoren:
Prof.dr.ing. A.J.H.M. Rijnders
Prof.dr.ir. J.E. ten Elshof

Contents

Summary

Electronic devices like notebooks, smart phones, GPS units, LED TVs and other daily life applications are produced with increased functionality and complexity from year to year. Today's electronic devices must be equipped with new smart electronic circuitry designs to add more functionality within a single device, while not making them larger in size. As the electronic circuits are made of various components, active semiconducting chips and passive components, like resistors, capacitors and inductors, more and more components are needed per single unit. While the number of components increases all components are subject to miniaturization to increase the volume efficiency. As capacitors are one of the more important passive components and every device consists of more than one hundred capacitors, a lot of effort is put on developing smaller sized capacitors.

Capacitors can be made from a wide variety of dielectrics and the components can have various shapes. The majority are surface mount capacitors and especially multilayer ceramic capacitors are one of the more popular types. These multilayer ceramic capacitors are mainly used in today's electronic devices and these types of capacitors are discussed in this thesis.

As the name multilayer ceramic capacitor already suggests the components are made up of a body, in which alternating layers of dielectrics and conducting metal electrodes are embedded. In Chapter 2 the manufacturing of multilayer ceramic capacitors is explained in more detail. In the 1980s and 1990s the majority of multilayer capacitors were made with expensive noble metals like palladium or platinum. Due to the price increase of these noble metals at the end of the 20th century, the passive component industry started to develop new dielectric materials suitable for co-firing with less expensive noble metals like pure silver or silver-palladium alloys. Another way to decrease metal costs is to implement base metals like nickel and copper as electrode material. Therefore new types of dielectric materials had to be developed in order to be co-fired with nickel or copper in a reducing atmosphere to prevent the metals from oxidizing.

Multilayer ceramic capacitors can be made of a wide variety of materials and depending on the electrical characteristics they are employed in different applications. This thesis describes dielectrics, personally developed for use in commercial multilayer capacitors, which show high stability towards temperature, frequency and voltage in Chapter 3. These dielectrics have low or moderate permittivity values and they are primarily used for filtering, smoothing and temperature control applications. Chapter 3 also describes multilayer capacitors

having relatively high permittivities. These are based on barium-neodymium-titanates and zinc-magnesium-titanates. These materials are suitable for co-firing with pure silver or silver-palladium alloys. It is described how to modify the dielectric composition in order to co-fire with high silver content electrodes and which strategy has to be followed in order to get reliable multilayer capacitors.

Furthermore, it is described how high-permittivity temperature stable capacitors having copper electrodes can be produced. These types of dielectrics have very low equivalent series resistance characteristics. Such capacitors can be used in high frequency applications especially. Various multilayer capacitors with electrodes of silver-palladium alloys, copper and nickel electrodes were made. The equivalent series resistance characteristics were determined to compare these capacitors with respect to their performance at high frequencies. Multilayer capacitors with the lowest equivalent series resistances are obtained when metals having the lowest possible bulk resistivity, like copper or silver, are selected.

The second part, Chapter 4, describes multilayer capacitors that are used for decoupling and bypassing purposes in electronic circuitry. These capacitors consist of dielectrics which are based on modified ferroelectric barium titanates. Typically they have very high permittivity values. They are less stable towards temperature changes, but they are important for their high capacitive volume efficiency. The multilayer ceramic capacitors are already produced with low cost metals, in particular nickel electrodes. Development is mainly focused on increasing the capacitive volume efficiency by decreasing the dielectric layer thickness and by maximizing the number of electrodes layers. Various strategies are described to make high capacitance multilayer capacitors.

The dielectrics layers of these high capacitance multilayer capacitors were already decreased down to 1 μm thickness in recent years. The grain size of the ceramics is typically 200–250 nm and efforts are made to decrease the grain size further, while maintaining reliable capacitor characteristics. The influence of the applied electrical field on the dielectric layers is explained in this chapter, and a strategy is presented how to develop new high permittivity dielectrics effectively. The influence of raw materials properties, particle size distribution of raw materials, and formulation on electrical properties and microstructures of the ceramics is described, while a conventional production method is used. With an alternative method it is possible to make ceramics having high permittivity values as well. In that process raw materials are used, which have high concentrations of yttrium oxide and copper oxide in the barium titanate lattice. These doped barium titanate powders are then mixed with pure barium titanate powders, together with extra dopant elements, to produce a new type of dielectrics.

Samenvatting

Tegenwoordig is een leven zonder elektrische apparaten niet meer weg te denken. Dagelijks wordt ons leven beheerst door verschillende elektronica zoals mobiele telefoons, televisies, laptops, GPS-ontvangers en andere apparatuur die ons leven kunnen veraangenamen. Zoals iedereen weet worden deze apparaten steeds compacter, maar tegelijkertijd bevatten ze ook meer functies per toestel. Kijk maar naar de mobiele telefoon. In de jaren negentig werden de mobiele telefoons gemaakt om, zoals de naam al zegt, ermee te kunnen bellen. Tegenwoordig is bellen maar een nevenfunctie van de mobiele telefoon. Het is ondertussen een compact en handzaam apparaat geworden dat meer weg heeft van een kleine computer, waarmee onder andere gesurft kan worden op het internet. Zelfs navigatie met GPS is al een standaard functie. Of kijk naar de televisies. Na de analoge zwart-wit TV's en later de kleuren televisies is het huidige digitale tijdperk tijd voor televisies waarin verschillende functies zijn geïntegreerd. Naast het grotere aanbod van kanalen, waarvan sommige te bekijken zijn in een hogere resolutie, zijn er ook andere functies mogelijk. Vaak is het al mogelijk om ze als een internet-tv te gebruiken. Huidige LED-TV's hebben al de mogelijkheid om in 3D- beeld uit te zenden. Daar komt bij dat deze apparaten steeds platter zijn geworden. In ieder geval zijn de meeste elektronische toestellen steeds complexer geworden en hiervoor moeten ook de gebruikte componenten aangepast worden. En dit proces zal in de toekomst ook door blijven gaan.

De meeste elektronische apparaten bevatten een grote variëteit aan componenten. Wie ooit wel eens een apparaat van binnen heeft gezien, kent wel het groene plastic plaatje waarop een groot aantal kleine componenten zitten. Er wordt een grote verscheidenheid aan componenten gebruikt, die onderling verschillende functies hebben. Naast de onvermijdelijke chips, batterijen, spoeltjes en dergelijke bestaat het grootste deel uit weerstanden en condensatoren. Deze componenten zijn onmisbaar in elk elektronisch circuit. Deze studie beschrijft het materiaal onderzoek voor condensatoren. Condensatoren zijn componenten die elektrische lading en energie kunnen opslaan en zijn derhalve onmisbaar in elektrische circuits.

Om in een condensator de elektrische lading te kunnen opslaan hebben we een niet-geleidend materiaal, het diëlektricum, nodig dat tussen twee geleiders wordt geplaatst. Bij gelijkstroom heeft een van de elektrodes een positieve lading en de andere elektrode een negatieve lading. Er wordt zo een elektrische veld gecreëerd waarbij de negatief geladen deeltjes, de elektronen, bewegen naar de positieve

elektrode, totdat de maximale capaciteit van de condensator is bereikt. De stroom zal dan geblokkeerd worden. Echter wanneer er een wisselstroom aangelegd wordt over een condensator dan wordt de stroom niet geblokt maar doorgelaten. De mate waarin dit gebeurt, is afhankelijk van de aangelegde spanning, de frequentie van de wisselstroom, de eigenschappen van het diëlektricum en de vormgeving van het component.

Er bestaan verschillende soorten condensatoren en ze worden vaak ingedeeld op basis van de materialen waarmee ze gemaakt worden. Er bestaan papieren, kunststof film, elektrolytische en tantaal elektrolytische condensatoren. In dit onderzoek worden de keramische condensatoren besproken. Deze kunnen gemaakt worden als een plaat- condensator, waarbij contact met het elektrisch circuit wordt gemaakt via twee draden. Of ze worden gemaakt als een opbouwcomponent (Surface Mount Device) en dan worden ze meerlaagscondensatoren genoemd. Meerlaags keramische condensatoren bestaan uit lagen van diëlektrisch keramiek, die tussen geleidende metaal elektroden liggen, en om en om contact maken met een van de twee buitenelektroden. Met deze opbouw kunnen hoge capaciteiten bereikt worden. Voor het diëlektrisch keramiek kan gekozen worden uit een grote verscheidenheid aan materialen, die verschillende eigenschappen hebben. Voor de binnenelektroden wordt vaak palladium, palladium-zilverlegeringen of nikkel metalen gebruikt. De buitenelektroden zijn vaak van zilver of koper houdende elektroden, de keuze is gebaseerd op het type metaal van de binnenelektrode. Bijvoorbeeld als de binnenelektrode van nikkel is, dan is de buitenelektrode gemaakt van een koper houdende elektrode.

De ontwikkeling van keramische meerlaagscondensatoren is voornamelijk gebaseerd op twee hoofdfactoren. Enerzijds is de kostprijs van het component van belang. Dat betekent dat er goedkopere metalen voor de elektroden gebruikt moeten worden. In het verleden werden de elektroden namelijk gemaakt van dure metalen zoals platina of palladium. Nu worden deze voornamelijk gemaakt van het goedkopere nikkel en soms van koper. In sommige toepassingen worden, vanwege de kwaliteitseisen, ook legeringen van zilver en palladium gebruikt, waarbij een zo hoog mogelijke concentratie aan zilver in de legering wordt gehanteerd. Anderzijds is de technologische ontwikkeling gebaseerd op het feit dat de componenten steeds kleiner moeten worden. Aangezien de elektrische apparaten steeds kleiner worden, betekent dit ook dat de componenten kleiner moeten zijn. De combinatie van de twee factoren betekent dat er nieuwe diëlektrische materialen ontwikkeld moeten worden om een zo hoog mogelijke capaciteitsopbrengst per volume te krijgen.

Er bestaan zeer veel keramische materialen die voor meerlaagscondensatoren gebruikt kunnen worden. Afhankelijk van de materiaaleigenschappen kunnen de condensatoren geclassificeerd en toegepast worden voor specifieke doeleinden. Verschillende typen van deze keramische materialen en hun eigenschappen worden

in mijn onderzoek besproken aan de hand van het specifieke gebruik van de condensator in het elektrische circuit.
In Hoofdstuk 1 wordt uitgelegd wat het doel van het onderzoek is. In Hoofdstuk 2 worden de fabricagemethoden en de verschillende manieren van karakteriseren van de eigenschappen van de condensatoren besproken. Materiaalonderzoek voor temperatuur stabiele condensatoren is in Hoofdstuk 3 het hoofdthema. Temperatuur stabiele condensatoren hebben een lage diëlektrische constante, meestal een stuk lager dan 200. Bovendien hebben ze een zeer lage capaciteitsafhankelijkheid ten opzichte van de temperatuur. Deze componenten kennen verschillende toepassings-mogelijkheden. Echter ze worden meestal gebruikt in applicaties die werken bij hoge frequenties. Voor dit type condensatoren is het voornaamste doel het vinden van temperatuur stabiele diëlektrische materialen die samen met zilver-rijke zilver-palladium legeringen, puur zilver of koper metaal elektroden kunnen sinteren. Van verschillende, door mij, ontwikkelde diëlektrische materialen worden de eigenschappen van de condensatoren beschreven.

De totale weerstand van condensatoren, of meer specifiek de impedantie, is een belangrijke eigenschap, die de frequentie-afhankelijke complexe weerstand van de elektrische stroom in een condensator beschrijft. Het onderzoek laat zien dat de impedantie voornamelijk bepaald wordt door de keuze van het metaal voor de binnenelektroden. De laagste impedantie wordt namelijk verkregen door puur zilver of koper te gebruiken voor de binnenelektroden, omdat deze metalen een lage specifieke weerstand hebben. Doordat de impedantie afhankelijk is van de frequentie en de impedantie zo laag mogelijk moet zijn, omdat anders teveel warmte wordt gegenereerd, wordt de weerstand in een condensator zo laag mogelijk gehouden, hierdoor kunnen deze typen condensatoren gebruikt worden in toepassingen die werken bij hoge frequenties, zoals mobiele telefoons.

In Hoofdstuk 4 worden condensatoren besproken, die een zo hoog mogelijke diëlektrische capaciteitsdichtheid hebben. In meerlaagscondensatoren kan dat bereikt worden door veel diëlektrische en elektroden lagen in een vast volume te bouwen, daarom moeten deze lagen wel zo dun mogelijk zijn. Op dit moment worden condensatoren gemaakt die diëlektrische en elektrode- laagdikten hebben van ongeveer 1 micrometer en de componenten kunnen tot 1000 lagen bevatten afhankelijk van de grootte van de component. Om condensatoren met steeds dunnere diëlektrische lagen te kunnen maken, moeten er nieuwe materialen ontwikkeld worden die betrouwbaar zijn en tegen een relatief hogere elektrische veld kunnen.

In dit werk worden verschillende diëlektrische materialen besproken die een hoge diëlektrische constante hebben, ongeveer rond de 5000, en een relatief lage temperatuurafhankelijkheid ten opzichte van de capaciteit. Dit type elektrokeramiek wordt gemaakt op basis van bariumtitanaat waaraan verschillende elementen, de zogenaamde doteringen, zijn toegevoegd. Doel is om een zo hoog mogelijke

diëlektrische constante te krijgen. De elektrische eigenschappen en de microstructuren van keramiek worden in detail besproken: op basis van de gebruikte grondstoffen, de compositie en de deeltjesgrootte van de vaste stof materialen. Tevens worden de eigenschappen van de condensatoren toegelicht.

Met een door mij bedachte alternatieve synthese methode kan een keramiek met een hoge diëlektrische constante worden gemaakt. Hierbij wordt eerst een precursor van yttrium en koper gedotteerd bariumtitanaat gesynthetiseerd. Deze precursor wordt vervolgens samen met puur bariumtitanaat en ander metaaloxiden, doteringen, gesinterd tot een materiaal meteen hoge diëlektrische constante en een vlakke temperatuurafhankelijkheid.

Chapter 1

Introduction to multilayer ceramic capacitors

In electronics one of the important passive components are capacitors. Without capacitors modern electronic devices like computers, cell phones, televisions, microwave ovens, car electronics and other daily life applications cannot exist. There are many types of capacitors in use and they can be classified according the shape, the used materials and electrical characteristics. Capacitors come in two major categories; capacitors with two leads and surface mount device (SMD) capacitors. The SMD type capacitors are currently the most popular ones and they are used in a wide variety of applications. The SMD type capacitors come with a variety of dielectric materials and are commonly classified accordingly. So electrolytic, film, paper, tantalum, niobium and ceramic capacitors exist, among others. Each material has its specific electrical properties and they are designed and used in electronics for specific needs. However, ceramic capacitors have distinctive properties like high frequency and temperature stability, high reliability, high breakdown resistance and high volumetric efficiency.[1] Especially these ceramic capacitors are used in high numbers, over hundred components, in applications like car electronics, computers and mobile phones.[2–3] Furthermore, these ceramic capacitors have a market share of about 90 % in part volume.[3] To achieve a high volumetric efficiency (capacitance per volume) the ceramic capacitors are produced in a multilayered embodiment, which is the most popular configuration.

Construction multilayer capacitor. Multilayer ceramic capacitors (MLCC) are made up of a ceramic body in which alternating layers of conductive metal electrodes are embedded, see Figure 1.1. The inner electrodes are connected in parallel on each side of the capacitor with a conductive termination electrode, which consists of glass-metal matrix. The MLCCs have nickel barrier terminations, which allow soldering at higher temperatures without dissolving electrode metal into the solder. Therefore an intermediate layer of nickel is electroplated on top of the glass-metal termination, usually copper or silver. Thereafter a tin layer is electroplated on top to improve solderability. The capacitance of a MLCC is determined by[2]

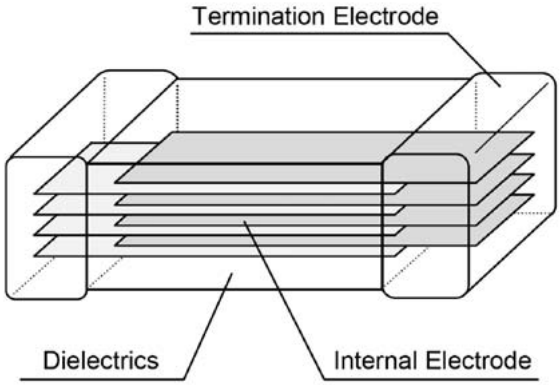

Figure 1.1: Construction of a MLCC.

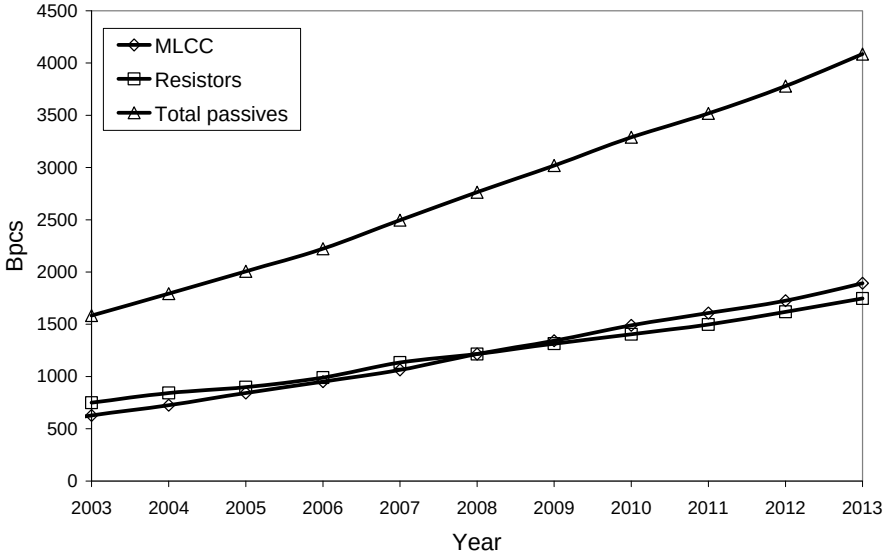

Figure 1.2: Market growth for passive components. (Data provided by Yageo Europe B.V, the Netherlands).

$$C = \frac{\varepsilon_r \varepsilon_0 (n\text{-}1) A}{d} \qquad (1.1)$$

were C is the capacitance in Farad, ε_r the dimensionless relative permittivity, ε_0 is vacuum permittivity of $8{,}854 \cdot 10^{-12}$ F/m, n is the number of inner electrodes, A is the overlap of the electrodes in m^2 and d is the dielectric thickness in m. Typically, the thickness of the electrodes is around 1.5 µm. The thickness of the dielectric layers decreased over the years to about 1 µm nowadays. The number of electrodes can range between 2 and 1000, depending on dielectric type and case size of the capacitors.

Market trend. The MLCCs are widely used in electronic devices and the market is still growing each year. The number of passive components sold and the outlook for coming years is that the market continues to grow and will reach the number of 3 to 4 trillion pieces sold each year, see Figure 1.2. The increase of the total number of passive components, including resistors, capacitors, inductors and thermistors, is due to the ever increasing complexity of the electronic devices and functionality added to the electronics is increased from year to year. Due to the increased complexity of the electronic circuitry more and more passive components are needed. However, this also puts a large constraint on the number of MLCCs on a circuit board, because less space is available on the circuit boards as the devices are subject to miniaturization. Therefore the volumetric efficiency of the ceramic capacitors has to be increased to fulfil these requirements.[4]

Case size multilayer ceramic capacitor. The dimensions of the capacitors, length, width and height, are defined with narrow tolerances by the Electronic Industries Alliance (EIA).[5] The case sizes of the capacitors are described with a four digit code. The first two digits defines the length and the last two the width of the MLCCs. Normally the units are described in 0.001 inch. However, also in some cases the metric system is used. Thus the very popular case size notation of 0402 MLCCs can be expressed in the metric system as 1005. In industry these standard case sizes are important in view of the production process to make electronic board circuits. Figure 1.3 shows an overview of multilayer capacitors in various case sizes. This overview shows clearly the large difference in size of the multilayer capacitors.

In the 1990s the case sizes were primarily the bigger sizes like 1210, 1206 and 0805, see Figure 1.4. However, due to the continuing miniaturization of electronic devices the market share for the smaller components grew steadily and currently the 0402 and 0201 MLCCs are the most popular sizes to be used in electronic devices.[1, 4] Even the smallest MLCC, 01005 with a length of 0.4 mm x 0.2 mm (a small deviation of the normal convention), is currently available on the market and already used in various applications.[3] Thus the aim for high capacitance per volume unit is currently a major development target.

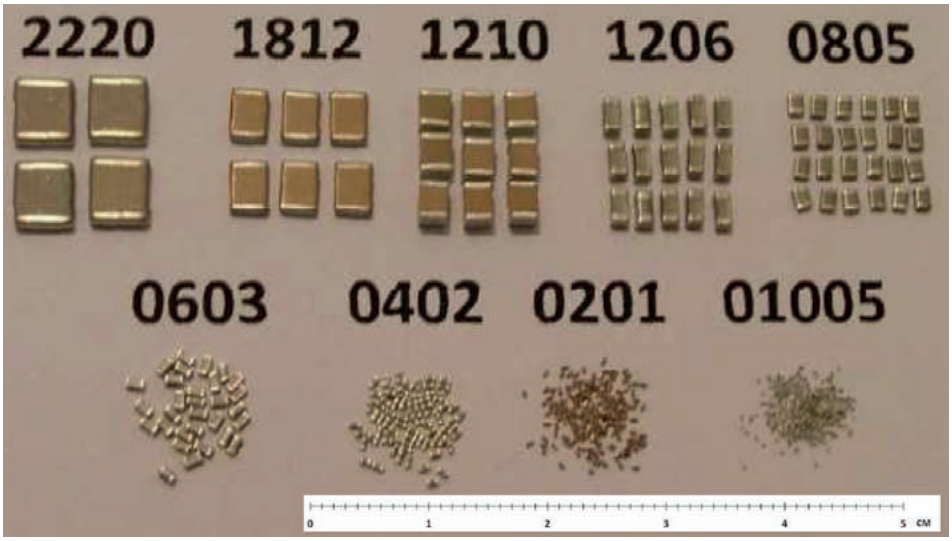

Figure 1.3: Overview of various case size capacitors.

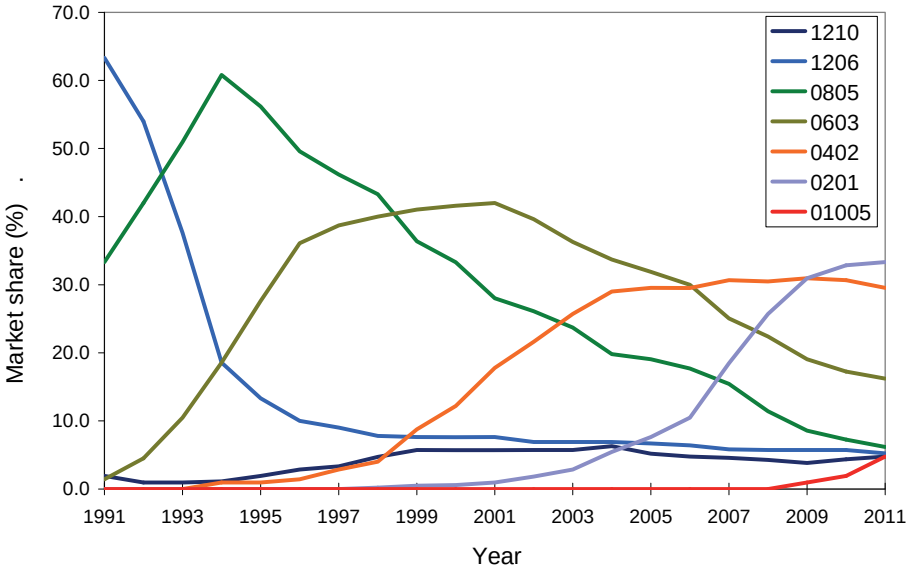

Figure 1.4: The trend in market share of multilayer capacitors for the various case sizes. (Data provided by Yageo Europe B.V, the Netherlands).

Table 1.1: Classification of dielectrics as specified by EIA.

Class 1	Class 2	Class 3
Low ε_r	Moderate ε_r	High ε_r
< 200	1000 – 4000	8000 – 20000
Temperature stable	Large temperature drift	Large temperature drift
Low dissipation factor	Moderate voltage dependence	Voltage dependence
Low voltage dependence	Moderate frequency dependence	Frequency dependence
Low Frequency dependence	High reliable in high temperature applications	High volumetric efficiency
Low volumetric efficiency	Aging	Aging
No aging		
C0G/NP0	X5R, X6S or X7R	Y5V or Z5U

Classification. The use of MLCCs is mainly divided in two types of applications. In the first category capacitors are used in filters and resonant circuits for high frequency applications. In high frequency applications the MLCCs should exhibit a high temperature stability regarding permittivity, frequency and voltage. Furthermore, this type of MLCC should exhibit low electric losses to avoid much energy dissipation during use of the electronic device. The other major category are MLCCs for power supply bypassing and decoupling.[3] In these applications the requirements towards stability are less. The focus is more directed towards achievement of a high capacitive density and the MLCC may exhibit a moderate loss and have a low dependency of capacitance on temperature, frequency or voltage.

Nowadays a wide variety of dielectrics are fabricated and the relative permittivity values range from 5 to over 20,000. Not only the relative permittivity of the capacitors show a large variation, but also other electrical properties, such as temperature stability, voltage stability, aging and so on, are material dependent. The EIA specified the commercially available capacitors into three important classes, see Table 1.1. In Class 1 the low ε_r dielectrics have low dissipation factors, typically much lower than 0.01. However, these capacitors show high temperature stability. In Class 1 dielectrics like mica, porcelain, steatite, forsterite, aluminum oxides and other low ε_r materials are present.[3, 6] Higher permittivity values are obtained in rutile TiO_2 or perovskite ceramics like $(Ca,Mg)TiO_3$, modified $(Ca,Sr)(Zr,Ti)O_3$ or $Ba(Zn_{1/3}Ta_{2/3})O_3$. Highest permittivity values, above 100, can be achieved by BaO-Nd_2O_3-TiO_2 and BaO-PbO-Nd_2O_3-TiO_3 ceramics.[7]

In Class 2 and Class 3 the dielectric characteristics are described of materials which exhibit high ε_r -values. A special group of dielectrics are based on modified ferro-electric $BaTiO_3$ and have ε_r values ranging from 1000 to 20000. Furthermore,

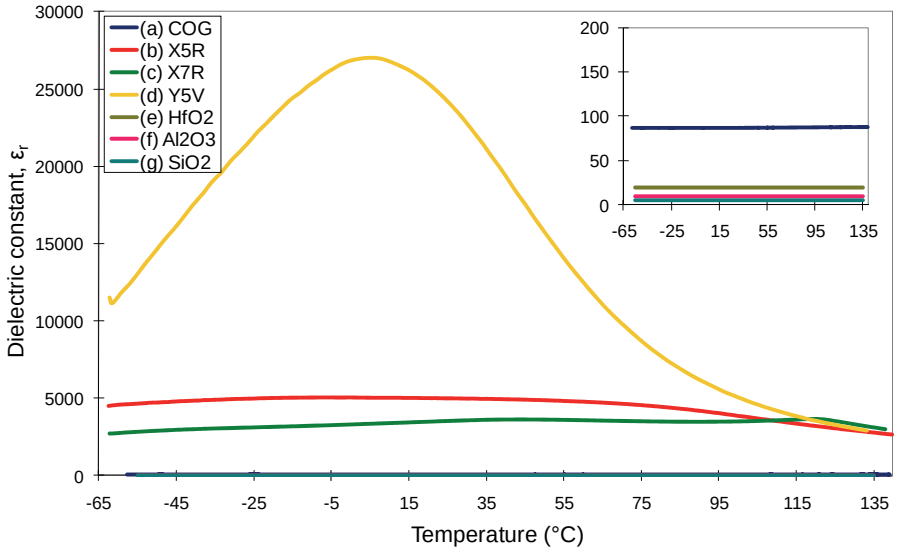

Figure 1.5: The change of dielectric constant as a function of temperature for (a) Class 1 C0G, (b) Class 2 X5R, (c) Class 2 X7R, (d) Class 3 Y5V, (e) HfO_2, (f) Al_2O_3 and (g) SiO_2 dielectrics.

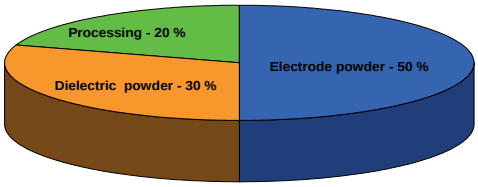

Figure 1.6: Average cost price distribution of Class 1 MLCC (C0G-type; Capacitance drift from -55 to 125°C less than ±30 ppm/°C) to raw materials and processing. (Data provided by Yageo Europe BV, the Netherlands).

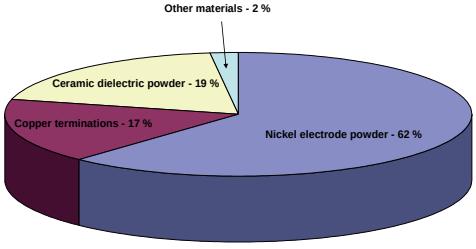

Figure 1.7: Material costs to produce high capacitance MLCC with a large number of inner electrodes of nickel.[9]

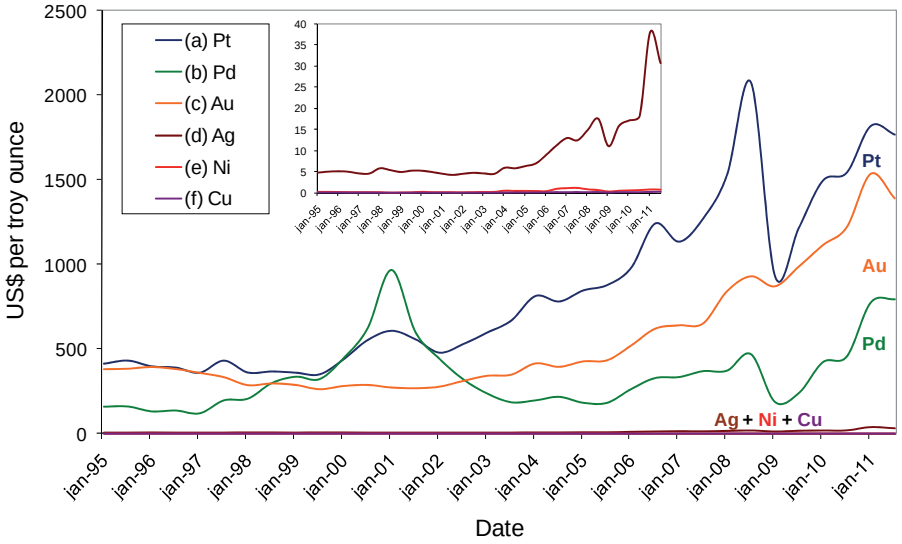

Figure 1.8: Price chart of precious metals (a) platinum, (b) palladium, (c) gold and (d) silver. For comparison the price chart of the base metals (e) nickel and (f) copper in US$ per troy ounce (1 troy ounce = 31.1034 gram).[10]

the dissipation factors are also higher, which range between 0.01 and 0.03, than Class 1 dielectrics. The ε_r of Class 2 dielectrics, typically modified $BaTiO_3$, vary more on temperature, voltage and frequency compared to Class 1 ceramics. Moreover the ε_r stability of Class 3, such as modified $(Ba,Ca)(Ti,Zr)O_3$, is less stable than the Class 2 dielectrics as they show even larger variations towards these parameters. In Figure 1.5 the relative permittivity dependency on temperature for various typical examples of each class is shown.

There is a Class 4 defined, which describes capacitors made of barrier layer ceramics, consisting of a conductive core and a thin isolating shell.[3, 6] These dielectrics have a very low breakdown voltage and high losses. In general the electrical properties are very instable and actually these types of capacitors are not manufactured for the commercial market any more.

Cost of materials. In the 1980s and early 1990s most of the Class 1, Class 2 and Class 3 multilayer capacitors had inner electrodes which were made with expensive noble metals palladium or palladium rich silver-palladium alloys.[2, 8] The cost price to produce Class 1 type multilayer capacitors is mainly dominated by the cost price of the metal powders, which are used in the inner electrodes and terminations, see Figure 1.6. Depending on the total amount of inner electrodes in a MLCC these costs can vary between 30 to 60 % of the total cost price of a MLCC. For Class 2 and Class 3 type MLCCs the volumetric density is important. Besides using high ε_r

dielectrics, the volumetric efficiency is increased by the combination of an increasing number of inner electrodes and a reduction of the dielectric thickness for a specific case size capacitor. Especially the large number of inner electrodes, for some MLCCs already up to 1000 layers, will contribute to the high costs of these materials, see Figure 1.7.[4] Therefore in the mid 1990s the huge increase of the Pd price, see Figure 1.8, accelerated the use of silver rich Ag-Pd alloys and base-metals like Ni and Cu.

However, the average price of copper and nickel increased during the last couple of years. The advantage is still to be able to use the base metal electrode (BME) materials instead of pure palladium or platinum, when only the metal costs are considered. The drawback of using BME materials is that these have to be sintered in an atmosphere of low partial oxygen pressure to prevent the metals to oxidize during sintering. So costs increased when a kiln suitable to handle reducing atmospheres, like a wet hydrogen-nitrogen atmosphere, was used. In any case the need to develop new dielectric materials, able to sinter with BME technology, had to be developed.

Scope of this thesis

Miniaturization and cost reduction have an impact on the requirements of dielectric materials used in multilayer ceramic capacitors. As there is a wide variety of ceramic materials that are used in the 2 main specific applications, the MLCCs described in this work are divided in 2 major categories as well. The scope of this thesis is to explore the possibilities to implement new dielectric and/or electrode materials for each of the 2 categories MLCCs. The first part consists of several chapters describing Class 1 multilayer capacitors, in particular the most temperature stable capacitors. The influence of replacement of expensive palladium metal by low cost electrode metals on development of dielectric ceramics and their electrical properties is described. The effect on the equivalent series resistance is demonstrated for various combinations of dielectric materials and electrode materials.

The second part of this thesis describes high capacitive capacitors having nickel inner electrodes and very thin dielectric layers. As the development of Class 3 capacitors, described in Chapter 4, was already discontinued in the last decade, effort was put into development of Class 2 capacitors. These Class 2 capacitors have dielectric thicknesses of at least 1 to 2 microns. Work was done to develop new dielectric materials which can be used to improve the capacitive density efficiency. Therefore, the effects of composition and processing on various electrical properties of the dielectrics were investigated. The aim of that work was to make MLCCs with

dielectric layers with the highest possible permittivity, and relative stability towards temperature variations.

References

1) Pithan, C.; Hennings, D. and Waser, R. *Progress in the synthesis of nanocrystalline $BaTiO_3$ powders for MLCC*; International Journal of Applied Ceramic Technology, 2005 **2**(1): p. 1–14.
2) Yoon, D. H. *Tetragonality of barium titanate powder for a ceramic capacitor application*; Journal of Ceramic Processing Research, 2006 **7**(4): p. 343–354.
3) Pan, M. J. and Randall, C. A. *A Brief Introduction to Ceramic Capacitors*; IEEE Electrical Insulation Magazine, 2010 **26**(3): p. 44–50.
4) Randall, M.; Skamser, D.; Kinard, T.; Qazi, J. and Tajuddin, A. *Thin film MLCC*; Conference paper CARTS USA, 2007: p. 1–12.
5) EIA-198–1F *Ceramic Dielectric Capacitors Clasess I, II, III and IV - part 1: Characterization and requirements*; 2002.
6) *Electroceramics*; 2nd ed.; Moulson, A. J. and Herbert, J. M.; John Wiley & Sons Ltd.: Chichester, 2003; p. 269-289.
7) Fiedziuszko, S. J.; Hunter, I. C.; Itoh, T.; Kobayashi, Y.; Nishikawa, T.; Stitzer, S. N. and Wakino, K. *Dielectric materials, devices, and circuits*; IEEE Transactions on Microwave Theory and Techniques, 2002 **50**(3): p. 706–720.
8) Choi, Y. J.; Park, J. H.; Nahm, S. and Park, J. G. *Middle- and high-permittivity dielectric compositions for low-temperature co-fired ceramics*; Journal of the European Ceramic Society, 2007 27(4): p. 2017–2024.
9) www.ttiinc.com/object/me_zogbi_20070305
10) www.kitco.com

Chapter 2

Sample preparation and characterization

2.1 Production method of Multilayer Ceramic Capacitors

A MLCC is a component made of dielectric layers with alternating layers of metal inner electrodes, which are connected with the termination electrodes, as shown in Figure 1.1. The fabrication of these multilayer components happens via several process steps. Figure 2.1 shows the process steps schematically in the process flow. The process starts with the mixing and milling of ceramic powders together with solvents and dispersants to prepare a slurry. The milling of slurries is normally carried out in a large ball mill. However, in recent years bead mills and pearl mills are used instead to reach more efficiently smaller particle sizes. When the target particle size distribution is reached, the slurries are separated from the milling beads and an appropriate amount of binder solution is added. After the suspension, often also called slip, is homogeneously mixed and degassed, thin foils are casted.

When the foils are dried a pattern of rectangular metal electrodes is printed on the sheets via screen printing. The printed sheets are stacked layer-by-layer with precise alignment to produce alternating layers of electrodes in a ceramic body. Figure 2.2 shows the schematic representation of the stacking process of the screen-printed foils. The stack are then uniaxially pressed to laminate the layers to form a compact plate, which is thereafter cut into separate green MLCC chips. To remove the organic materials the individual chips are subjected to binder burnout at moderate temperatures. Thereafter the chips are sintered at high temperatures to obtain dense bodies. After that the sintering process and the chips undergo a tumbling process to make them a bit rounded. In order to make the connection between the inner electrodes on both ends of the chips a termination paste, made of a glass-metal matrix embedded in an organic vehicle, is applied. The termination paste is dried and thereafter cured in a conveyor furnace to sinter the terminations to high density. To protect the termination during soldering against leaching, meaning to prevent diffusion of melted termination metals into the solder, a nickel barrier layer

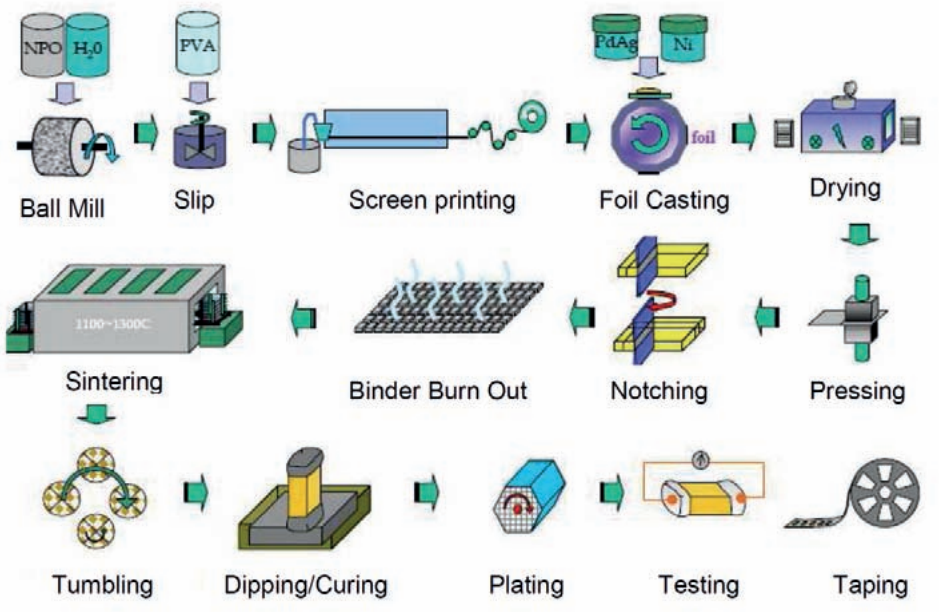

Figure 2.1: Flow chart of MLCC water based Philips Generation 3 fabrication process.

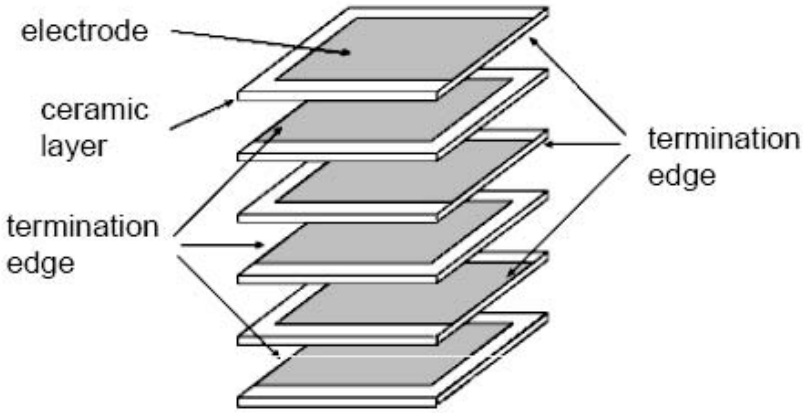

Figure 2.2: Schematic representation of the stacking process.

Table 2.1: Materials used in water en solvent-based foils.

	Materials	Water based	Solvent based
Slurry	Solids	Formulation of metal oxides	Formulation of metal oxides
	Dispersant	Dispex® A40[1]	Malialim® AKM-0531[2]
	Solvent	Water	Ethanol/Toluene
Binder solution	Binder	PVA (Poly Vinyl Alcohol)	PVB (Poly Vinyl Butyral)
	Plasticizer	TEG (Triethylene Glycol), PEG400, Glycerol	BBP (n-butyl benzyl phthalate)
	Anti-foam	Triton® CF32[3]	-
	Realease agent	TPnB (Tripropylene glycol n-butylether)	-
	Wetting agent	Sermul[4]	BYK®-333[5]

is made by electroplating and on top a tin layer is applied to improve solderability.

The multilayer capacitors described in this thesis were fabricated according to two methods, which can be categorized as water or solvent-based technology. This categorization refers to the solvents used in the slip to cast foils. The environmentally friendly system based on water, known as Philips Generation 3 technology, is a tape casting method in which the foils are self-supporting. This means that no carrier tape is used. This foil casting method was used to prepare the multilayer capacitors that are discussed in Chapter 3. Because the water based system does not allow the casting of foils thinner than 6 microns, the multilayer capacitors described in Chapter 4 were fabricated with an organic solvent-based technology. This technique makes use of a carrier tape made of polyethylene terephtalate having a silicone coating.

The difference in the type of solvents has an impact on the composition of the ceramic suspension (slip), see Table 2.1, but also on the production process. The dispersants, binders and other organics have to be soluble in the respective solvents. In the water-based system an ammonium polyacrylate dispersant, called Dispex® A40, was used to de-agglomerate the ceramic grains. To give the foil its strength a polyvinyl alcohol (PVA) in combination with a plasticizer was added to the slip composition. The other organic components were added in order to be able to cast

[1] Dispex® A40 (Ciba) = Ammonium polyacrylate based phosphate
[2] Malialim® AKM-0531 (NOF) = polyoxyalkalene comb-shaped surfactant
[3] Triton® CF32 (DOW) = alkylamino polyethoxy polypropoxy propanol
[4] Sermul® AE (BASF) = nonyl phenol phosphate
[5] BYK®-333 (Disperbyk) = polyether modified dimethylpolysiloxane

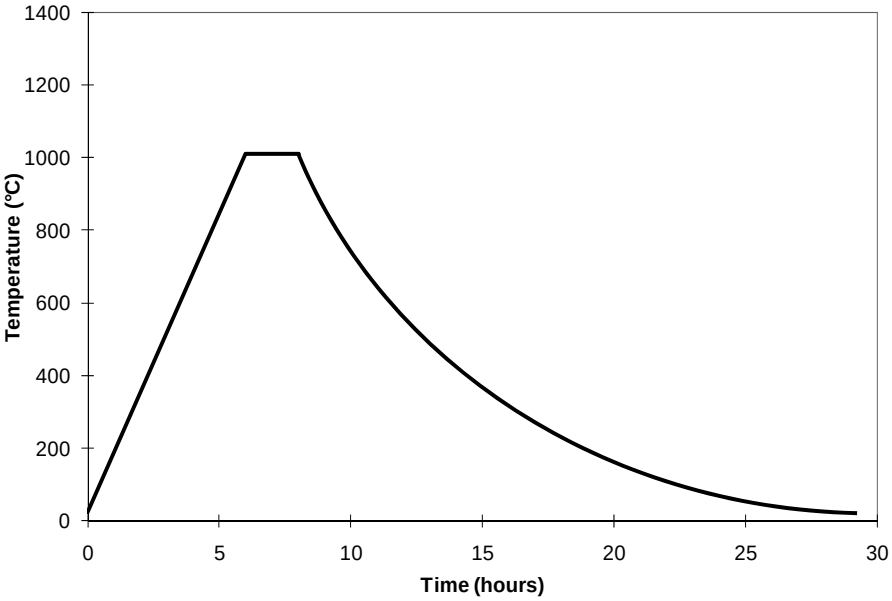

Figure 2.3: Sintering profile for NME and Cu MLCCs.

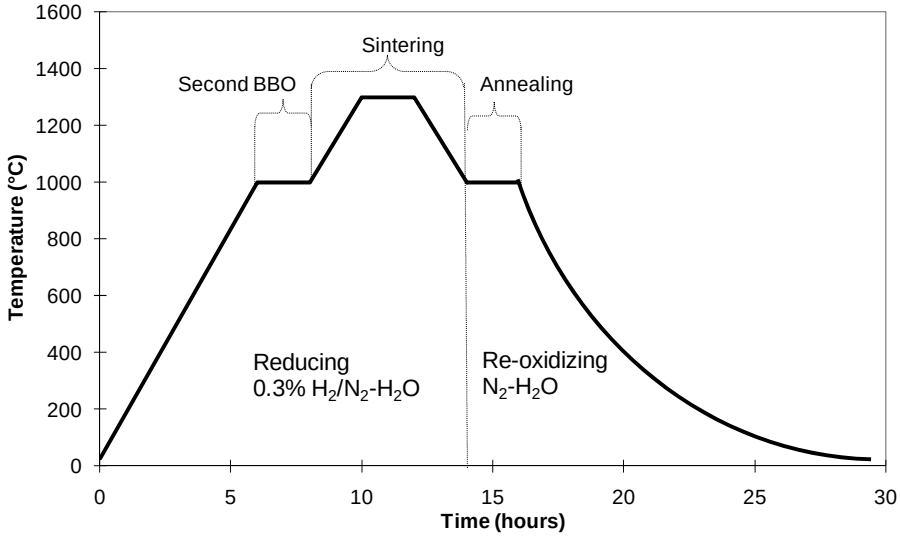

Figure 2.4: Sintering and re-oxidation profile for Ni-MLCCs.

foils without imperfections such as holes, thickness variations, sticking and others. The water based slips were cast directly on a steel belt and the foils were dried successively in a furnace. In contrast to the organic-based foils, which consisted of a dispersant based on styrene-maleic acid resin, AKM 0531, a polyvinylbutyral (PVB) binder and plasticizer butylbenzylphtalate (BBP). The slurries and slips were made with an ethanol-toluene solvent mix. These organic slips were cast via slot die coating on a carrier tape using a roll-to-roll technology. The foils were subsequently dried in a tunnel furnace. Typically these type of ceramic foils have green bulk densities of about 50 % of theoretical ceramic density.

The fabrication of laminated plates, with the alternating layers of dielectrics and metal electrodes, occurs more or less according to the same process steps. However, the binder composition has an influence on the material properties of the foils, but also on the strength and flexibility of the plates. The plates made via the water process are rigid and brittle. To produce single green multilayers these plates underwent a notching-breaking process. This is in contrast to the more flexible plates with PVB binders, which had to be cut with a knife at a moderate temperature of around 60 °C to make individual green multilayer capacitors. Big case size green capacitors, larger than 1206 or 1210, are often too difficult to separate using a notching-breaking or cutting process. Alternative separation processes are dicing the green plates with a diamond saw, using Disco dicing equipment, or laser cutting.

The green multilayer capacitors consisted of a lot of binders, which have to be removed, to avoid damage of the internal structure during sintering. Therefore the multilayer capacitors were given a binder burn-out treatment in air. That is done by increasing the temperature gradually to 300 °C over a long period of time. This has to be done in a controlled way to prevent too much gas formation during decomposition, because the internal structure may be damaged by a strong release of gases. Therefore the total binder cycle takes more than 24 hours to complete.

The multilayer capacitors with noble metal electrodes (NME), like Ag-Pd and pure Ag inner electrodes, and the MLCCs with Cu electrodes were sintered according a simple firing profile, see Figure 2.3. Sintering of the NME MLCCs were done in a Linn oven in air. The MLCCs with Cu electrodes were sintered in a tube kiln (Carbolite) in a low partial oxygen pressure atmosphere made of moist N_2.

Instead the MLCCs with nickel electrodes were sintered with a more complex firing profile, see Figure 2.4. The first step was to complete binder burn-out (BBO) as the BBO at moderate temperatures did not remove all carbon. The binder step and sintering were carried out in a moist H_2/N_2 atmosphere to control the oxygen partial pressure pO_2 during the firing process. After the sintering step the products were re-oxidized at a lower temperature of 1000 °C in a higher pO_2 atmosphere made of moist N_2.

After sintering the following process steps are more or less equal for all types of MLCCs. Only the type of materials used for the external terminations made a difference in the curing process. The MLCC having NME inner electrodes were applied with a glass containing Ag paste. After drying the terminations were cured at 750 °C for 45 minutes in a conveyer furnace (BTU) in air. While the MLCC having BME electrodes were terminated with a glass containing Cu paste, which was fired in a N_2 atmosphere at 800 to 900 °C in a Sierratherm conveyer furnace for 45 minutes.

2.2 Preparation of Ceramic Disc Capacitors

For easy evaluation of sintering behaviour and dielectric properties of the dielectric compositions ceramic disc capacitors (CDC) were fabricated. The CDCs consisted of a ceramic body with 2 electrodes on the sides. The process, shown in Figure 2.5, to make these CDCs starts with weighing the raw materials according to a given formulation. The powders were then de-agglomerated and milled to the required particle size distribution in a polyethyelene (PE) flask with 2 mm yttria-stabilized zirconia (YTZ®) milling beads. The media could be based either on water or 2-propanol. Slurries based on 2-propanol were milled to desired particle size distribution and the powders were dried afterwards. These powders had more or less homogeneously distributed fine powder particles. Another way to prepare homogeneously distributed powder particles was to prepare slurries based on water and to flocculate the solution. Therefore slurries with the metal oxides, water and surfactant, Dispex® A40, were made. The materials were put in a PE flask together with 2 mm YTZ milling beads and rolled on a roller bench at 65 rpm. The powders were de-agglomerated and milled towards the required particle size distribution. The slurries based on water-dispex formulation were flocculated with a flocculent (ZETAG®), added to Dispex® A40 in a ratio of 2 to 1, after separation of the milling beads. The flocculation step was done to avoid sedimentation during drying.

The homogeneous powders were mixed with a glycerine solution (10 weight% in water) and thereafter the grounded powder was sieved over 300 μm to get granules. The granules were then uniaxially pressed (Fontijne, SRA100) with a pressure of 8 bar into pellets of 8 or 10 mm in diameter and between 1 to 2 mm in height.

Two different ways of making CDCs were employed and the choice of the actual method that was used depended on the dielectrics and matching metallization. In Figure 2.5 process flow A shows the preparation method for CDC capacitors in which the ceramics body is sintered prior to the metallization process. This method was used to prepare the majority of samples discussed in Chapter 3. The alternative

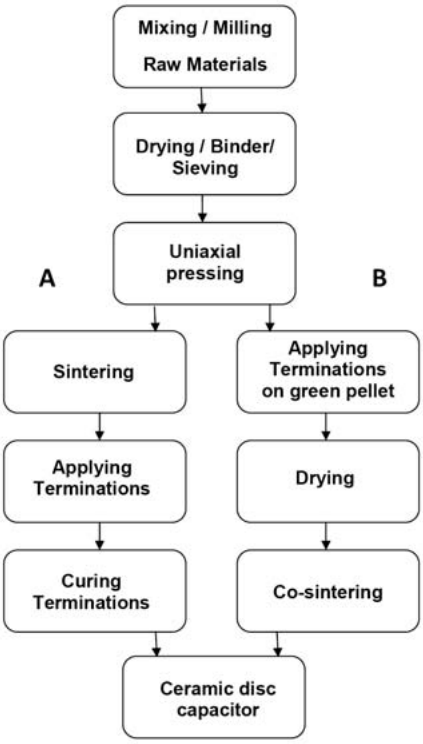

Figure 2.5: Flow chart of preparation of CDCs made via (a) sintering of ceramic body and afterwards applied terminations and (b) green pellets with dried terminations co-sintered.

method, process flow B, applies the metallization paste onto the green discs prior to the co-sintering process. After the metallization paste is dried the body and the metal electrodes are sintered simultaneously to get a good adhesion of dense dielectric body and terminations. This method was predominantly used for making the samples discussed in Chapter 4.

All samples discussed in Chapter 3 were sintered according to a simple firing profile as shown in Figure 2.3. However, sintering was performed in air or moist nitrogen atmosphere, depending on the materials used. The samples of Chapter 3.2 and 3.3 were all sintered in air in a Linn box furnace. These sintered discs got a Ag metallization paste applied, which thereafter was dried and cured in a conveyor furnace (BTU) in an air atmosphere at 750 °C.

The samples as discussed in Chapter 3.4 were prepared according to both methods. One part was sintered in a tube kiln (Carbolite) in air according to a simple heating cycle and then the discs were metalized using a Ag termination paste. Other samples were metalized with Cu terminations using either method. The green discs

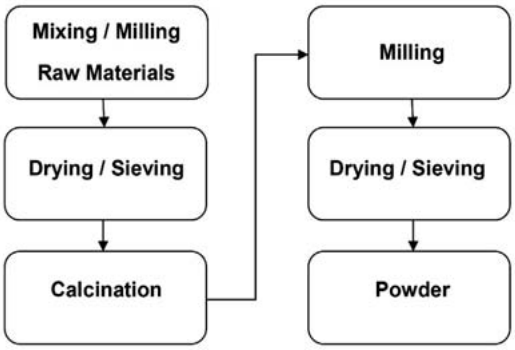

Figure 2.6: Flow chart of mixed oxide powder preparation.

and green CDCs were sintered in the Carbolite tube kiln in a moist N_2 atmosphere. The sintered discs received Cu terminations by applying a glass containing Cu paste on both sides and after drying the CDCs in a conveyor furnace (Sierratherm) at around 800–900 °C in a N_2 atmosphere.

The CDCs of Chapter 4 were mainly prepared using method B, where the green discs were applied with a Ni paste. After drying the CDCs were sintered according to the heating profile shown in Figure 2.4. Sintering of these CDCs occurred in a tube kiln (Carbolite), which had a similar heating profile as used in production. First the products got a second binder burn-out step in order to be certain that all organics were burnt off. Then sintering was performed in a defined forming gas atmosphere for some time, before the samples were re-oxidized during the annealing step.

2.3 Preparation of raw materials and sintering aids

In the next chapters several various types of dielectrics materials are discussed. In most cases the raw materials were commercially available powders. However, in some cases the sintering aids, as described in Chapter 3.2 and Chapter 3.4, had to be synthesized. In that case the mixed oxide (solid state) preparation method was used, see Figure 2.6. The process starts with weighing the raw materials in appropriate mass ratios. Then the powders were put in a PE flask together with 2 mm YTZ milling beads in either water or an organic solvent. Depending on the type of solvent a specific surfactant was added. However, when the powders were de-agglomerated and milled in 2-propanol, no surfactant was added to the slurry, because a homogeneous powder could be obtained after drying. When the powders were mixed and milled to the desired particle size distribution, the slurries were dried and sieved over a 300 µm metal sieve. Calcination was done by firing the powders in a Nabertherm batch kiln with a specific temperature profile. The temperature profile

was chosen in such way that homogenously distributed fine powders were obtained. Furthermore, the powder should not contain many hard agglomerates in order to be able to mill the powders easily after the calcination step. The powders were milled to the required particle size distribution using a PE flask filled with 2 mm YTZ beads, a solvent and, when necessary, surfactant. After the milling step the powders were dried, sieved over 300 μm and ready to use.

2.4 Characterization methods

Particle Size Distribution by laser diffraction method. This technique allows to measure the particle size distribution of a well dispersed sample of particles in a water or solvent solution. To stabilize the dispersion a sodium hypophosphite solution is added under fierce ultrasonic stirring for 3 minutes, to prevent the large particles from sedimenting. Because the dispersion is measured via one (red) or two (red and blue) laser beams the solution has to be more or less transparent in order to pass the dispersion to scatter the light beam. The diffracted light will be detected by the automated equipment and the angle of the diffracted light is a measure of the particle size. After proper input of the required parameters the particle size distribution is automatically calculated by using the proper mathematical equation. Light scattering is dependent on the refractive index of the solid powders and solvents and these factors must be taken into account. The range of particle sizes that can be measured by this method can range from 0.05 to 1000 μm.

Density measurements. The density of the ceramics were analyzed using Archimedes method. Hereby the weight of the ceramic pellets were measured in air and in water respectively. The measured density (ρ) can then be calculated by following formula:

$$\rho = \frac{M_a \cdot \rho_w}{M_a - M_w} \qquad (2.4.1)$$

were M_a and M_w is respectively the weight in gram of the pellet measured in air and in water. The ρ_w is the density of pure water in g/cm^3. The theoretical density (ρ_{th}) can be derived from X-Ray diffraction data, which gives the unit cell parameters, and the molar mass of the unit cell according following formula:

$$\rho_{th} = \frac{Z \cdot M \cdot u}{V} \qquad (2.4.2)$$

were Z is the number of formula unit per unit cell, M is the molar mass of the composition in g/mol, u the atomic mass unit of $1.66057.10^{-27}$ kg and V the volume of the unit cell in m^3.

Thermo-Mechanical Analysis (TMA). In order to determine the sintering behavior of the ceramics a TMA helps to define the optimum sintering temperature and gives insight into the sintering process. Equipment is used that can measure the sample dimensions with a measuring probe during a heating cycle. During the heating cycle the temperature is measured with a thermocouple near the location of the sample. The relationship between the dimensions of the sample, in particularly length, and temperature can then be examined. The NETSCH DIL 402 C dilatometer allows to program a heating cycle and the measurement can be automatically executed to obtain a sintering profile. The samples for this measurement were made according the process described above. However, the samples described in Chapter 3.2 were made differently. Instead of making discs of 10 mm in diameter and 2 mm in height, the powders were pressed uniaxially (Fontijne SRA100) with a pressure of 8 bar into discs of 8 mm diameter and around 7.5 mm in height. Thereafter these pellets were further compactized by cold isostatic pressing (EPSI) at 4000 bar for 3 minutes.

Sample preparation and analysis by optical microscope or scanning electron microscope. To examine the ceramic discs or MLCCs the specimens are embedded in a transparent resin. Therefore the samples are placed in a mould, which is then filled with a 2-component resin, solid and liquid, of methyl methacrylate (Technovit 4004, Hereaus), that polymerizes to a solid transparent body at room temperature. To avoid large pores during the polymerization the samples were placed in a pressure pot (Technomat) under a pressure of 2 bar for 30 minutes to harden the resin. Thereafter the specimens were grinded with SiC-paper, whereby the material is removed, using step by step a finer grade of SiC paper to obtain a relatively smooth surface. To achieve a very smooth surface the samples were polished using a diamond containing lubricant on a cloth. For the grinding and polishing process various types of machines of Struers, automatic and manual types, were used. The specimen can then be examined using an optical microscope or scanning electron microscopy.

Microstructure analysis by scanning electron microscope. Before the microstructure of the ceramics could be examined, the potted samples were chemically etched with a 1%HCl / 1%HF solution for several seconds. Then the etched surface was thoroughly cleaned and dried. The ceramics surface was examined using a scanning electron microscope (Philips XL20 or HR-SEM LEO1550).

Microstructure analysis by scanning transmission electron microscope. The samples were prepared using a traditional sample preparation technique. Samples were mechanical thinned to around 100 um. Then dimple ground using a Gatan model 656 dimple grinder. Samples were then thinned further using a Fischione Model 1010 ion mill. The microstructures of the samples were examined using two transmission electron microscopes; Technai 20 and JEOL 2010F. Both transmission electron microscope field emission guns operated at 200 kV. The energy dispersive spectroscopy (EDS) was performed using an Oxford Instrument ISIS system.

Average Grain Intercept method. The Average Grain Intercept method is a technique to quantify the average grain size of a ceramic material. The ceramic surface is polished and if necessary chemically etched, to highlight the grain boundaries and a photograph of the microstructure is taken using a scanning electron microscope. Then 5 randomly positioned lines are drawn on the micrograph and each grain boundary is pointed out on the line. Each grain is then marked by intersection lines. The number of these intercepts marks every grain crossed on each line. Because it is known how large the line actual is, because a length marker in microns is given in each micrograph, the average grain size can be calculated. The calculated average of the 5 lines will give finally the average grain size of the ceramics.

X-ray diffraction. The crystalline phases of powders and ceramics, were identified by X-ray diffraction analysis (PanAnalytical PW180) using Cu-Kα radiation. The patterns were taken with 2θ starting from 5° to 90°. The XRD patterns were analyzed using the X'pert Highscore software to identify the phase structures by comparing the results with reference patterns provided by the International Centre for Diffraction Data (ICDD). Phase fractions were calculated on basis of comparing the heights of peaks of various phase structures in a single ceramic sample.

Capacitance and Tan δ. The electrical properties, capacitances and tan δ, were measured using a HP4284A LCR meter. The CDCs and MLCCs with capacitance values below 100 pF were measured with an AC current of 1 MHz and 1 V_{rms}, following the guidelines provided by the Electronics Industries Alliance (EIA). The capacitance values in the range of 100 pF to 10 μF, with a rated voltage of 6.3 V or more, were measured with an AC current of 1 kHz and $1V_{rms}$. Otherwise the capacitance and tan δ were measured at 1 kHz and 0.5 V_{rms}. When the capacitance exceeded 10 μF an AC current of 120 Hz and 0.5 V_{rms} was used. The tan δ values were always measured simultaneously with the capacitance measurement. The relative permittivity values were calculated using Equation 1.1, taking into account

the discontinuity of the electrodes, which were analyzed using an optical microscope and software, to determine the active area between the electrodes.

Temperature Coefficient of Capacitance. The temperature coefficient of capacitance (TCC) of the samples were measured from -55 °C to +160 °C using a HP4284A LCR meter. The applied AC current depended on the capacitance of the sample as described above. The temperature was measured using a Keithley 740 system scanning thermometer. The measurement setup was controlled by a computerized system equipped with automated data acquisition. The acquired data show the dependency between capacitance and temperature.

Insulation Resistance. Before the insulation resistance measurements the capacitors were fully discharged. Then the insulation resistance of the CDCs and MLCCs were measured after the required voltage had been applied for 60 seconds. The measurements were carried out with a high resistance meter (Agilent 4339B).

Equivalent Series Resistance. The ESR of the MLCCs were measured with an Agilent LCR meter 4287a and fixture 16196A. The measuring frequency range was 30 MHz up to 3 GHz with 32 measuring points.

P-E hysteresis loops. The polarization versus applied electrical field (P-$U_{applied}$) hysteresis loops of the Ceramic Disc Capacitors were measured using a RT6000 HVS-2 analyzer (Radiant Technologies Inc.). From the slope of the P-$U_{applied}$ curves the relative permittivity values were calculated.

Chapter 3

Temperature stable multilayer ceramic capacitors

Chapter 3.1

An introduction to temperature stable multilayer capacitors

In electronic equipment, capacitors are used in various applications, which can be categorized in two major types.[1] In one category, capacitors are used for power supply bypassing and decoupling, in which capacitors with high capacitances with moderate voltage and temperature dependence characteristics are needed. In the other category, temperature stable capacitors are used in resonant circuits and filtering applications. In these applications the temperature stable capacitors generally operate at Radio Frequencies (RF) between 100 MHz and 30 GHz.[2–3] Typical applications for wireless operated devices are notebooks, mobile phones, wireless LAN and other wireless communication systems.[4] To meet the requirements in a RF circuit the capacitors should have a relatively high dielectric constant (ε_r) to accomplish high volumetric efficiency in applications which are subject to miniaturization. The capacitors should have a high quality factor (Q) to store electromagnetic energy, to filter and to transport current with the lowest possible losses ($Q = 1/\tan \delta$). Furthermore, to minimize frequency drift as response to temperature fluctuations a low temperature coefficient of frequency (τ_f) is needed.[2, 5]

Classification. Dielectrics used for passive components are classified by the Electronics Industries Alliance (EIA) in several classes depending on the electrical properties of the materials.[6] The EIA provides guidelines describing how the electrical properties should be measured and it specifies the dielectric materials accordingly. The temperature stable dielectrics are classified as Class 1 dielectrics. These dielectrics exhibit the most stable capacitance values towards voltage, temperature and frequency variation. The loss factors, tan δ, of these dielectrics have the lowest possible values, even at frequencies above 1 GHz. The EIA codes of Class 1 dielectrics are according the electrical properties and the code consists of three characters in which the first digit provides the significant digits of temperature coefficient. The second digit provides the multiplier and the third digit the tolerance.

Table 3.1.1: Coding of Class 1 capacitors according EIA specification.[1]

Significant digits of temperature coefficient α		Multiplier		Tolerance in ppm/°C	
C	0.0	0	-1	G	± 30
B	0.3	1	-10	H	± 60
L	0.8	2	-100	J	± 120
A	0.9	3	-1000	K	± 250
M	1.0	5	+1	L	± 500
P	1.5	6	+10	M	± 1000
R	2.2	7	+100	N	± 2500
S	3.3	8	+1000		
T	4.7				
V	5.6				
U	7.5				

For example R2H has a capacitance drift of -220±60ppm/°C.

In Table 3.1.1 the EIA codes for Class 1 dielectrics are shown. This table shows that many possible dielectric properties regarding capacitance drift can be specified. However, in practice only a few types are used. One of the most important types of capacitors is the one coded as C0G. The C0G dielectrics have a zero temperature coefficient and a tolerance of ± 30 ppm/°C. C0G dielectrics are the most accurate materials for capacitors towards temperature drift.

Temperature stable properties. In the passive component industry C0G dielectrics are often also called NP0, which is an abbreviation for Negative Positive Zero. Besides a near zero temperature coefficient of capacitance (TCC), the materials possess a near-zero temperature coefficient of permittivity (τ_ε) and near zero temperature coefficient of resonance frequency (τ_f). These three coefficients are closely related to each other.[7–9] The TCC is related to τ_e by:

$$TCC = \tau_\varepsilon + \alpha_L \qquad (3.1.1)$$

where α_L is the linear expansion coefficient. Equation 3.1.1 is valid under the assumption that that the expansion coefficients in all directions are identical. Thus the dielectric should be an isotropic material. The variables τ_ε and τ_f are related via the equation:

$$\tau_f = - (½ \tau_\varepsilon + \alpha_L) \qquad (3.1.2)$$

Table 3.1.2: Various materials with temperature stable C0G characteristics.

	ε_r	τ_f (ppm/K)	$Q \cdot f_o$ (GHz)	Reference
$MgTiO_3$-$CaTiO_3$	22	- 3	45000	10-12
$Ba[Sn_x(Mg_{1/3}Ta_{2/3})_{1-x}]O_3$	25	-5 to +5	80000	10, 12–13
$CaZrO_3$	29	- 20	14000	11, 14
$Ba(Zr,Zn,Ta)O_3$	30	-5 to +5	100000	10, 13
$Nd_2Ti_2O_7$*	36	- 118	1800	7, 11, 15
$(Zr,Sn)TiO_4$	38	0 ~ 5	30000	10-11, 13
$BaTi_4O_9$	39	~ 4	44500	11–12, 15
$Ba_2Ti_9O_{20}$	40	~ 4	5000	7, 10, 15
$BiNbO_4$	40	+ 30	8000	7
BaO-Nd_2O_3-$4TiO_2$	80	+ 88	6000	15
BaO-Bi_2O_3-Nd_2O_3-TiO_2	91	+ 6	6100	7, 11
$(Ba_{0.5}Pb_{0.5})O$-Nd_2O_3-$5TiO_2$	95	+ 8	5600	10-11, 13
TiO_2*	100	+ 400	17000	14, 16–17
$MgTiO_3$*	17	- 45	22000	10, 14, 16
$CaTiO_3$*	170	+ 800	1800	10, 14, 16
Al_2O_3*	10	+ 50	33000	14, 17
HfO_2*	25	n.a.	n.a.	18
SiO_2*	3.9	n.a.	n.a.	18

* Included for comparison.

For resonator circuits and filtering applications the resonant frequency requires a low frequency drift to avoid large variations of the transmitted frequency signal during operation.[10] Since the resonance frequency is dependent on permittivity and size of the components, a balanced control between τ_ε and linear expansion coefficient is needed to obtain a near-zero τ_f.

An important feature of C0G dielectrics is the large quality factor (Q), which is approximately equal to 1/tan δ. A high Q-factor is needed in RF applications to increase the possible number of channels in a given frequency range and to avoid the risk of overlap of the transmitted frequency bands. Therefore the losses must be kept low and the intensity of the signals kept optimal.[8, 10] For high frequency dielectrics Q-factors should be more than 1000 in the range of 500 Mhz to 20 GHz.[10, 15] The Q-factor decreases with increasing frequency (f) and the product $Q \cdot f$ will be constant for any given material in the operating frequency range. In practice materials give higher $Q \cdot f$ values when measured at higher frequencies. The materials are normally

measured at the resonance frequency (f_0) and to compare various dielectrics the $Q \cdot f_0$ values are usually quoted.[8]

Dielectrics and electrical characteristics. C0G dielectrics are commonly made of para-electric materials with a ε_r between 10 and 120. The dielectrics are composed of $MgTiO_3$, $CaTiO_3$ or $CaZrO_3$, and have a relatively low permittivity of 20 to 30.[19] C0G materials with higher permittivity values are based on TiO_2 rich rare earth titanates like $BaTi_4O_9$ or $BaNd_2Ti_5O_{14}$. The highest permittivity values have been found in materials like $BaO\text{-}Bi_2O_3\text{-}Nd_2O_3\text{-}TiO_2$ and $(Ba_{0.5}Pb_{0.5})O\text{-}Nd_2O_3\text{–}5TiO_2$, which have ε_r values up to 100. In Table 3.1.2 a summary of C0G materials that have been developed for high frequency applications is listed.

Single phase materials like $MgTiO_3$, and $CaTiO_3$ have large τ_f values, i.e. -45 and 800 ppm/°C, respectively. The $MgTiO_3\text{-}CaTiO_3$ phases form a solid solution after sintering and the dielectrics have as a near zero τ_f. However C0G materials can also be composed of 2 or more single phase compounds, such as $BaO\text{-}Nd_2O_3\text{-}TiO_2$ dielectrics, in order to accomplish near-zero TCC values. Each phase has its own characteristic electrical properties for ε_r, Q and τ_f. The dielectric properties of a new mixture can be tailored by mixing the various phases, following the logarithmic mixing rules. The average ε_r, Q and τ_f can be calculated for a dielectric composition, in the example below with three phase fractions v_1, v_2 and v_3, via[20–26]

$$\ln \varepsilon_r = v_1 \ln \varepsilon_{r,1} + v_2 \ln \varepsilon_{r,2} + v_3 \ln \varepsilon_{r,3} \qquad (3.1.3)$$

$$Q^{-1} = v_1 Q_1^{-1} + v_2 Q_2^{-1} + v_3 Q_3^{-1} \qquad (3.1.4)$$

$$\tau_f = v_1 \tau_{f,1} + v_2 \tau_{f,2} + v_3 \tau_{f,3} \qquad (3.1.5)$$

The dielectrics listed in Table 3.1.2 can only be densified at temperatures above 1300°C.[27] Therefore the ceramics have to be co-fired with a metal with a high enough melting point that is stable in an oxidizing sintering atmosphere. Commonly platinum or palladium inner electrodes were used to produce multilayer ceramic capacitors. The drive to lower costs promoted use of cheaper metals like silver, copper or nickel to replace the expensive noble metals palladium and platinum. However, a change of inner electrode materials has an influence on the chemistry of the dielectric materials. The choice of another metal to be used for the electrodes will create new conditions and requirements that the dielectrics must fulfil. But a change of materials for dielectrics and inner electrodes may not influence the electrical properties of the multilayer capacitors. The C0G characteristics for capacitance, TCC, Q-factor and equivalent series resistance (ESR) must follow the specifications. To develop MLCCs with low cost electrode materials three major conditions must be fulfilled. The first condition is that the dielectrics of the MLCCs

can be co-fired with the inner electrodes below the melting point of the metal or alloy. The second condition is that the dielectrics should withstand an atmosphere of low partial oxygen pressure during sintering to prevent the metal electrode, that is made from copper or nickel, to oxidize. The third condition is related to the electrode series resistance (ESR) of the capacitors. Multilayer capacitors used in high frequency applications must have low ESR values. The ESR is derived from material dependent parameters such as the dissipation in dielectrics, electrode resistivity and termination resistivity. Furthermore, the ESR is also dependant on the construction of the MLCC such as size, number of electrodes, electrode thickness and so forth.

All factors that contribute to the ESR of the MLCCs should be kept a small as possible at high frequencies, avoiding high losses during capacitor operation. As mentioned earlier the multilayer capacitors should have a high *Q*-factor value. There is a relationship between *Q*-factor and ESR and it is described by:

$$Q = \frac{1}{\tan \delta} = \frac{X_c}{\mathrm{ESR}} = \frac{1}{2\pi f C} \qquad (3.1.6)$$

where X_c is the capacitive reactance in Ω, f is the frequency in Hz and C is the capacitance in F.[3] The ESR of the capacitors is equal to the electrode resistance and related to the dielectric loss of the dielectric materials and the equation is described by[28–29]

$$\mathrm{ESR} = R_{el} + \frac{\tan \delta}{2\pi \cdot f \cdot C} \qquad (3.1.7)$$

where R_{el} is the resistance of the inner electrodes. The ESR will be equal to R_{el} at frequencies higher than 100 MHz.[30] Therefore the specific resistivity of the metals should be as small as possible to get the lowest possible ESR values.

Electrode materials and properties. In Table 3.1.3 the physical properties of common electrodes materials are listed. Before the mid 1990s palladium and platinum metals were commonly used for the electrodes in MLCCs. However alternative metals, like Ag, Cu and Ni, have lower melting points than Pd and Pt. When MLCC are sintered near the melting point of the metals, the electrodes will coagulate and physical transport of metal from the chip due to evaporation can occur, which would result in inhomogeneous electrodes. As a rule of thumb MLCCs are sintered about 50 °C below the melting point of the used metals or alloys. In this research sintering temperatures for systems having high silver content electrodes needs to be sintered even at lower temperatures to prevent excessive silver diffusion or silver evaporation during firing, as is described in Chapter 3.2.

Table 3.1.3: Physical properties of conductors.[31–33]

Metal	Melting Temperature (°C)	Specific resistivity at 20 °C (μΩ·cm)	Density (g/cm^3)	Thermal expansion coefficient (10^{-6}/K)
Ag	961	1.6	10.5	19
Cu	1083	1.7	9.0	17
Au	1063	2.3	19.3	14
Mo	2610	5.2	10.2	5
W	3410	5.7	19.3	5
Ni	1453	6.8	8.9	13
Pt	1772	10.6	21.4	9
Pd	1552	10.8	12.0	11
Pb	327	20.6	11.4	29

The specific resistivity is another important feature, especially concerning the ESR of the MLCCs. The specific resistivity values of Pd and Pt are comparable, 11 μΩ·cm at 20 °C. Except for lead all other metals have lower bulk resistivity values compared to palladium and platinum. Thus most of these metals can be used as an alternative when the ESR is concerned. However, other factors have to be considered as well. For instance gold can be used, but that metal is expensive and therefore not a candidate to replace palladium or platinum electrodes. Best alternatives to produce high *Q* MLCCs are silver or copper, because these two metals have the lowest bulk resistivity. If silver and copper are used the best performance to ESR is expected when one of these two metals is applied. The drawback of silver is its low melting point. Dielectrics must be developed which must to be sintered well below 961 °C to avoid coagulation or diffusion into the dielectrics during sintering. However, copper has a higher melting point, i.e. 1083°C. The drawback of copper is the fact that it easily oxidizes when sintered at high temperatures in an oxygen-containing atmosphere like air. Therefore copper has to be sintered in a reducing atmosphere such as H_2/N_2 or CO/CO_2, in which the partial oxygen pressure (pO_2) is low, to protect the copper from oxidation.[34]

The oxidation stability of various metals were calculated. The oxidation reactions of metals for the different oxidation states can be described by[35]

$$xM + \tfrac{1}{2}n(O_2)_g \leftrightarrow M_xO_n \qquad (3.1.8)$$

where M represents the metal and $(O_2)_g$ is gaseous O_2. The digits *x* and *n* represent reaction coefficients to balance the equation and integer numbers, respectively. The

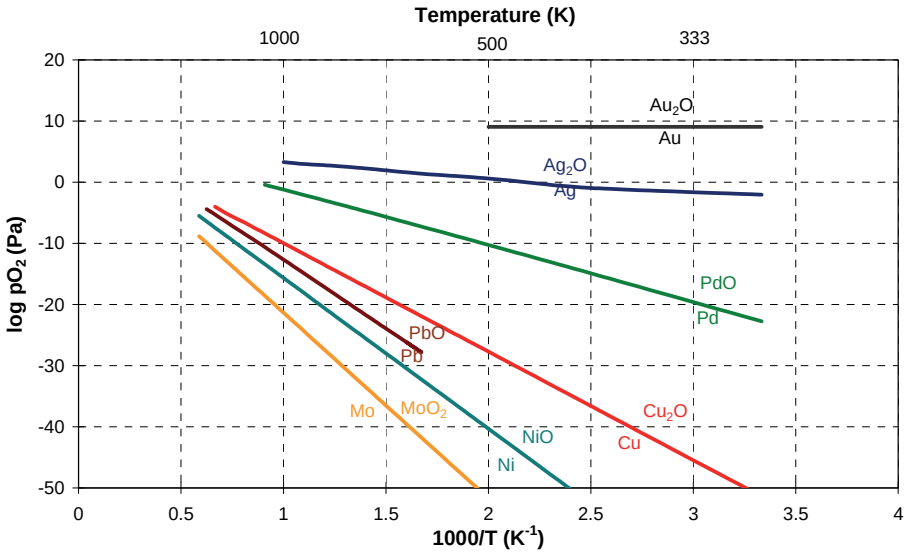

Figure 3.1.1: Calculated pO_2 with temperature of conducting metals.[31, 36]

Gibbs free energy ($\Delta G°$) of oxidation reactions is negative and the oxygen partial pressure of O_2 (pO_2) is quite low. The relation between $\Delta G°$ and pO_2 can be described for these reactions by;

$$\Delta G° = - RT \ln (pO_2)^{-n/2} \qquad (3.1.9)$$

For Equation 3.1.9 it is assumed that the activity coefficients (a_M and a_{MxOn}) is 1 for all solid metals and their oxides. To calculate the oxidation stability the data of $\Delta G°$, the two-term equation, in J/mol from the CRC Handbook of Chemistry and Physics was used.[36] The results of the calculations of various metals are shown in Figure 3.1.1.

From the results shown in Figure 3.1.1 it becomes evident that copper, lead nickel and molybdenum have to be sintered at low O_2 partial pressures. Lead, molybdenum and tungsten are not candidates to replace palladium or platinum, because dielectrics have to sustain very low pO_2 levels during sintering. It is noted that tungsten has the same pO_2-temperature relationship as molybdenum has. Therefore the aim is to use silver, copper or nickel as electrodes in multilayer capacitors.

Silver is an interesting alternative to use as electrode material. However, the melting point of pure silver is 960 °C and it will be difficult to develop a dielectric material that can be sintered at such a low temperature. Instead an alloy of silver-

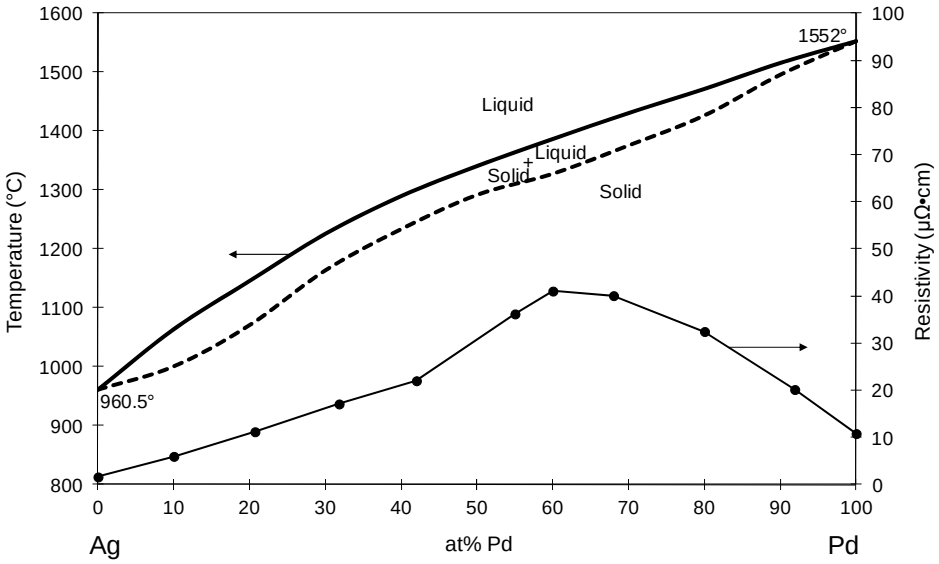

Figure 3.1.2: Phase diagram and specific resistivity of Ag-Pd system.[31]

palladium can be used as inner electrode. Both metals Ag and Pd have the same crystal structure (FCC) and are complete miscible to form a continuous solid solution (alloy).[31, 35, 37] The solidus and liquidus temperature curves, see Figure 3.1.2, of the Ag/Pd alloys increase gradually from the low melting point of Ag at 960 °C to the melting point of Pd at 1552 °C. Thus, a wide range of sintering temperatures can be chosen to co-fire the multilayered structures, depending on the requirements. However, the bulk resistivity is not linearly dependent to the silver-palladium ratio. When silver is added to palladium the bulk resistivity first increases to a maximum value of 41 μΩ·cm at a Pd-content of 60 atomic percent (at%), before the resistivity is reduced to 1.6 μΩ·cm for pure silver. The resistivity of 20 at% Pd alloy is approximately equal to the resistivity of pure palladium. Therefore to meet the ESR requirements the silver-palladium alloy should have a Pd-content between 0 and 20 at%. This assumption is only valid when both metals are compared in MLCCs with the same construction and when the same electrode thickness is used.

Scope of this chapter. In the 1990s the C0G MLCC were primarily made with 80Ag/20Pd and 70Ag/30Pd alloys. Therefore sintering temperatures of these MLCCs were carried out at around 1080 to 1100 °C. In this chapter the effort to replace these MLCCs with other electrode metals and ceramics will be described. Therefore dielectrics which sinter at 1050 °C or preferably lower temperatures had to be developed.

In the first chapters material systems will be described that are suitable to sinter with silver rich Ag-Pd and pure Ag electrodes. Chapter 3.2 describes a material

system for 95Ag/5Pd and 90Ag/10Pd electrodes based on $BaO\text{-}Nd_2O_3\text{-}Gd_2O_3\text{-}TiO_2$ dielectrics. In Chapter 3.3 dielectrics based on $(Zn,Mg)TiO_3$ to which a sintering aid of $Bi_2O_3\text{-}ZnO\text{-}B_2O_3$ is added, is reported. The sintering temperature of these dielectrics was reduced to below 900 °C and MLCCs with pure Ag electrodes were examined.

Multilayer capacitors with Cu electrodes require a sintering temperature of 1000–1040 °C. These capacitors have to be sintered in a reducing atmosphere. A $BaO\text{-}Nd_2O_3\text{-}Gd_2O_3\text{-}TiO_2$ material was chosen at which sintering aids were added to produce reliable dielectrics. In Chapter 3.4 the material properties of the dielectrics and the electrical performance of the MLCCs with Cu electrodes are described.

For MLCCs with nickel electrodes the ceramic material can be sintered at higher temperatures and in practice the ceramics are sintered at around 1300 °C in mass production kilns. The dielectrics are commonly based on $CaZrO_3$ and $(Ba,Sr)(Zr,Ti)O_3$, compositions in which the ratio between the elements are balanced to achieve high permittivity, high *Q*-factors and near zero TCC. Often some acceptor dopants are added to these dielectrics to get reduction stable dielectrics.[14, 38–41] In Appendix A-1 a summary of the electrical properties of dielectrics used for MLCC with Ni electrodes are described. In Chapter 3.5 the ESR performance of C0G MLCCs made with various dielectrics – metal electrode combinations are compared. The MLCCs were all similarly constructed. The scope of this chapter is to evaluate MLCCs with various metal electrodes and to compare them for their frequency response on ESR.

References

1) Pan, M. J. and Randall, C. A. *A Brief Introduction to Ceramic Capacitors*; IEEE Electrical Insulation Magazine, 2010 **26**(3): p. 44–50.
2) Rawn, C. J.; Birnie, D. P.; Bruck, M. A.; Enemark, J. H. and Roth, R. S. *Structural investigation of $Ba_{6-3x}Ln_{8+2x}Ti_{18}O_{54}$ (x = 0.27, Ln = Sm) by single crystal x-ray diffraction in space group Pnma (No. 62)*; Journal of Materials Research, 1998 **13**(1): p. 187–196.
3) Randall, M. S. et al *Capacitor considerations for Power Management*; conference paper CARTS 2006, p. 97–111.
4) Ohsato, H. *Research and development of microwave dielectric ceramics for wireless communications*; Journal of the Ceramic Society of Japan, 2005 **113**(1323): p. 703–711.
5) Haga, K.; Ishii, T.; Mashiyama, J. and Ikeda, T. *Dielectric-properties of 2-phase mixture ceramics composed of rutile and its compounds*; Japanese Journal of Applied Physics; 1992, **31**: p. 3156–3159.
6) EIA-198–1F Ceramic Dielectric Capacitors Clasess I, II, III and IV - part 1: Characterization and requirements; 2002.
7) Wersing, W. *Microwave ceramics for resonators and filters*; Current Opinion in Solid State & Materials Science, 1996 **1**(5): p. 715–731.

8) Reaney, I. M. and Iddles, D. *Microwave dielectric ceramics for resonators and filters in mobile phone networks*; Journal of the American Ceramic Society, 2006 **89**(7): p. 2063–2072.
9) *Electroceramics*; 2nd ed.; Moulson, A. J. and Herbert, J. M.; John Wiley & Sons Ltd.: Chichester, 2003; p 298–302.
10) Cava, R. J. *Dielectric materials for applications in microwave communications*; Journal of Materials Chemistry, 2001 **11**(1): p. 54–62.
11) Choi, J. H.; Kim, J. H.; Lee, B. T.; Kim, Y. M. and Moon, J. H. *Microwave dielectric properties of Ba-Nd-Ti-O system doped with metal oxides*; Materials Letters, 2000 **44**(1): p. 29–34.
12) Fiedziuszko, S. J.; Hunter, I. C.; Itoh, T.; Kobayashi, Y.; Nishikawa, T.; Stitzer, S. N. and Wakino, K. *Dielectric materials, devices, and circuits*; IEEE Transactions on Microwave Theory and Techniques, 2002 **50**(3): p. 706–720.
13) Wakino, K.; Nishikawa, T.; Ishikawa, Y. and Tamura, H. *Dielectric resonator materials and their applications for mobile communication-systems*; British Ceramic Transactions and Journal, 1990 **89**(2): p. 39–43.
14) Kell, R. C.; Greenham, A. C. and Olds, G. C. E. *High permititivity temperature-stable ceramic dielectrics with low microwave loss*; Journal of the American Ceramic Society, 1973 **56**(7): p. 352–354.
15) Suvorov, D.; Valant, M. and Kolar, D. *The role of dopants in tailoring the microwave properties of* $Ba_{6-x}R_{8+2/3x}Ti_{18}O_{54}$ *R = (La-Gd) ceramics*; Journal of Materials Science, 1997 **32**(24): p. 6483–6488.
16) Sohn, J. H.; Inaguma, Y.; Yoon, S. O.; Itoh, M.; Nakamura, T.; Yoon, S. J. and Kim, H. J. *Microwave dielectric characteristics of ilmenite-type titanates with high Q-values*; Japanese Journal of Applied Physics, 1992 **33**: p. 5466–5470.
17) *Electroceramics*; 2nd ed.; Moulson, A. J. and Herbert, J. M.; John Wiley & Sons: Chichester, 2003; p 304–306.
18) Wilk, G. D.; Wallace, R. M. and Anthony, J. M. *High-kappa gate dielectrics: Current status and materials properties considerations*; Journal of Applied Physics, 2001 **89**(10): p. 5243–5275.
19) Kim, D. W.; Kim, B. K.; Je, H. J.; Park, J. G.; Kim, J. R. and Hong, K. S. *Degradation mechanism of dielectric loss in barium niobate under a reducing atmosphere*; Journal of the American Ceramic Society, 2006 **89**(10): p. 3302–3304.
20) Chaouchi, A.; Aliouat, M.; Marinel, S.; d'Astorg, S. and Bourahla, H. *Effects of additives on the sintering temperature and dielectric properties of* $ZnTiO_3$ *based ceramic*; Ceramics International, 2007 **33**(2): p. 245–248.
21) Chen, H. C.; Weng, M. H.; Horng, J. H.; Houng, M. P. and Wang, Y. H. *Effect of bismuth addition on sintering behavior and microwave dielectric properties of zinc titanate ceramics*; Journal of Electronic Materials, 2005 **34**(1): p. 119–124.
22) Hsieh, M. L.; Chen, L. S.; Wang, S. M.; Sun, C. H.; Weng, M. H.; Houng, M. P. and Fu, S. L. *Low-temperature sintering of microwave dielectrics* $(Zn,Mg)TiO_3$; Japanese Journal of Applied Physics Part 1-Regular Papers Brief Communications & Review Papers, 2005 **44**(7A): p. 5045–5048.
23) Kim, H. T.; Kim, Y.; Valant, M. and Suvorov, D. *Titanium incorporation in* Zn_2TiO_4 *spinel ceramics*; Journal of the American Ceramic Society, 2001 **84**(5): p. 1081–1086.

24) Kobayashi, H. and Hosokawa, Y. *Dielectric-constant characteristics of a new composite dielectric material*; Journal of the American Ceramic Society, 1990 **73**(6): p. 1774–1776.
25) Wu, J. M.; Chang, M. C. and Yao, P. C. *Reaction sequence and effects of calcination and sintering on microwave properties of (Ba,Sr)O-Sm_2O_3-TiO_2 ceramics*; Journal of the American Ceramic Society, 1990 **73**(6): p. 1599–1605.
26) Zheng, H.; Reaney, I. M.; Muir, D.; Price, T. and Iddles, D. M. *Composite dielectric ceramics based on BaO-Ln_2O_3-TiO_2 (Ln = Nd, La)*; Japanese Journal of Applied Physics Part 1-Regular Papers Brief Communications & Review Papers, 2005 **44**(5A): p. 3087–3090.
27) Choi, Y. J.; Park, J. H.; Nahm, S. and Park, J. G. *Middle- and high-permittivity dielectric compositions for low-temperature co-fired ceramics*; Journal of the European Ceramic Society, 2007 **27**(4): p. 2017–2024.
28) *Electroceramics*; 2nd ed.; Moulson A.J., H. J. M.; John Wiley & Sons Ltd.: Chichister, 2003; p 255.
29) Lee, W. H.; Su, C. Y.; Huang, C. L.; Lee, Y. C.; Hu, C. L.; Yang, J.; Yang, T. and Lin, S. P. *Effect of inner electrode on electrical properties of (Zn,Mg)TiO_3-based multilayer ceramic capacitor*; Japanese Journal of Applied Physics Part 1-Regular Papers Brief Communications & Review Papers, 2005 **44**(12): p. 8519–8524.
30) Mandai H., S. Y., Canner J.P. *Multilayer ceramic NPO capacitors with copper electrode*; Ceramic Transactions; 1989 **15**: p. 313–327.
31) Wang, S. F.; Dougherty, J. P.; Huebner, W. and Pepin, J. G. *Silver-palladium thick-film conductors*; Journal of the American Ceramic Society, 1994 **77**(12): p. 3051–3072.
32) Burn, I. *Processing multilayers ceramics with internal copper conductors*; Ceramic Transactions, 1990 **15**: p. 375–384.
33) *Metals reference book*; 3rd ed.; Smithells, C. J.; Butterworths: London, 1962; Vol. 2, p 695.
34) Bernard, J.; Houivet, D.; El Fallah, J. and Haussonne, J. M. *$MgTiO_3$ for Cu base metal multilayer ceramic capacitors*; Journal of the European Ceramic Society, 2004 **24**(6): p. 1877–1881.
35) Wang, S. F. and Huebner, W. *Interaction of Ag Pd metallization with lead and bismuth oxide-based fluxes in multilayer ceramic capacitors*; Journal of the American Ceramic Society, 1992 **75**(9): p. 2339–2352.
36) *CRC Handbook of Chemistry and Physics*; 75th ed.; Lide, R. L.; CRC Press, Inc.: Boca Raton, FL, 1994; Vol., p 5–72 to 5–75.
37) Pepin, J. G. *Subsolidus phase-realtions in the system Pd-Ag-O and application to multilayer ceramic capacitors electrodes*; Advanced Ceramic Materials, 1988 **3**(5): p. 517–519.
38) Kishi, H.; Mizuno, Y. and Chazono, H. *Base-metal electrode-multilayer ceramic capacitors: Past, present and future perspectives*; Japanese Journal of Applied Physics Part 1-Regular Papers Short Notes & Review Papers, 2003 **42**(1): p. 1–15.
39) Lee, W. J.; Wakahara, A. and Kim, B. H. *Decreasing of $CaZrO_3$ sintering temperature with glass fritaddition*; Ceramics International, 2005 **31**(4): p. 521–524.
40) Pollet, M.; Marinel, S. and Desgardin, G. *$CaZrO_3$, a Ni-co-sinterable dielectric material for base metal-multilayer ceramic capacitor applications*; Journal of the European Ceramic Society, 2004 **24**(1): p. 119–127.
41) Cheon, C. I.; Kim, J. S. and Lee, H. G. *The correlation between tau(epsilon) and the tolerance factor in (Sr, Ca)(Ti, Zr)O_3 microwave dielectric ceramics*; Journal of Materials Research, 1998 **13**(5): p. 1107–1109.

Chapter 3.2

Diffusion of silver during sintering in high permittivity C0G dielectrics[1]

3.2.1. Introduction

In the last two decades the development on multilayer ceramic capacitors (MLCC) is focused on miniaturization and cost reduction. MLCCs are commonly used in electronics like personal computers, mobile phones and other devices. The market of these components is still growing due to global increase of the general usage of electronics. Besides miniaturization of electronic devices and components new technologies use more complex electronic circuits in which an increasing number of passive components, like MLCCs, are needed. In mobile phones, wireless LAN, notebooks, multilayer capacitors with excellent properties in Radio Frequency (RF) applications are needed. These type of MLCCs are fabricated with materials having low relative permittivity ε_r, temperature stable electrical properties and high quality factor Q.[1]

Temperature stable dielectrics, Class 1 dielectrics according to the Electronic Industries Alliance (EIA) specification, are used in RF applications. Here, stable capacitance towards temperature and aging is needed. The most stable type of dielectrics is encoded C0G by EIA and is often called NP0 ('negative positive zero') in industry. The temperature coefficient of relative permittivity of C0G dielectrics must be approximately zero and may not exceed ±30 ppm/°C in the temperature range between -55 °C and 125 °C. Dielectrics that consist of high ε_r and high Q can be made with a wide variety of dielectrics like $(Zr,Sn)TiO_4$, $Ba(Zn,Ta)O_3$, Ti-rich $BaO\text{-}TiO_2$, Ba-Ln-Ti-O, and $BaO\text{-}PbO\text{-}Nd_2O_3\text{-}TiO_2$.[2–3] For C0G MLCCs with palladium or palladium rich Ag/Pd electrodes, Ba-Nd-Ti-O (BNT) dielectrics are often used.[4]

[1] Published in Integrated Ferroelectrics

In this study a commercial dielectric based on non-ferroelectric $BaO\text{-}Nd_2O_3\text{-}Gd_2O_3\text{-}TiO_2$ (AD850DZ, Ferro) was used, which will be called hereafter K85. The sintering temperature of this dielectric is about 1200 °C depending on the sintering conditions. To lower the sinter temperature sintering aids were added to this dielectric compound, keeping C0G properties and the highest possible ε_r.

In the past, MLCCs were usually made with palladium or palladium rich electrodes. In order to reduce costs, the implementation of silver or silver rich electrodes was the main technological drive towards new dielectric material development. However, silver can diffuse as ions or transport as vapour into the ceramics during co-firing of multilayer ceramic components.[5] The influence of silver diffusion on the performance of ceramics was studied and published.[5–13] However, no literature is available on electrode continuity and electrode composition after sintering for silver and silver-rich electrodes in multilayer components.

During the development of MLCCs containing silver rich 95Ag/5Pd (wt%/wt%) electrodes it has been observed that a large variation of capacitance and ESR values was measured. Furthermore, it was observed that the electrode layers showed a discontinuity near the outside of the MLCC. For MLCCs the electrode continuity is important for the electrical properties in general, more specifically for the equivalent series of resistance (ESR) of the components. The problem was due to the fact that silver diffuses into the ceramics or evaporated in air during co-sintering. This causes the electrodes to become discontinuous.

In this chapter, the development of MLCCs, based on new dielectrics and silver rich Ag/Pd electrodes, with respect to electrode quality is described. A new dielectric composition was developed, based on commercial powder AD850DZ of Ferro. This commercial powder AD850DZ is called K85 in this paper. A sintering aid was used to decrease the sintering temperature of K85. MLCCs with this new dielectric formulation were made using 95Ag/5Pd and 90Ag/10Pd powders and are called K72 and K75, respectively. These K72 and K75 0805–100pF MLCCs consist of 10 electrodes. After co-firing the MLCCs at 950°C for 2 hours the electrodes were analyzed with SEM-EDS to detect Ag loss. The analysis revealed that silver diffusion can be avoided if the melting point of the Ag/Pd alloy exceeds the sintering temperature of the dielectric by at least 100°C. This knowledge can be used to select the best suitable Ag/Pd alloy for co-sintering with a certain new dielectric composition.

In order to measure the ESR, 0603–10pF MLCCs containing 5 electrode layers were prepared. Material combinations of K85 with pure palladium, K80 with 80Ag/20Pd alloy and K75 with 90Ag/10Pd alloy were tested. It was observed that the ESR properties improved when electrodes with high silver content were used.

3.2.2. Experimental

Sample preparation. The powders for K80 were made starting from K85 (AD850DZ, Ferro) and sintering aid 1. Sintering aid 1 consists of a compound called ZST and CuO (Pan-Continental Chemical Co, 99%). The compound ZST is based on 1 mol ZnO (Sigma Aldrich 99.0%), 1 mol SiO_2 (Degussa, aerosil R975) and 1 mol TiO_2 (Riedel de Haën, 99.0%), which is calcined at 1000 °C. The exact composition cannot be given as it is a dielectric material used currently in MLCCs production by Yageo. However, the addition of ZST to K85 is between 2 and 5 wt% and the CuO concentration is between 0.2 and 1.0 wt % to K85. The dielectric powders for K72 and K75 were made starting from K85 (AD850DZ, Ferro) and sintering aid 2, which is prepared from $Zn_4B_6O_{13}$ (Borax, 98%), ZnO (Sigma Aldrich 99.0%), SiO_2 (Degussa, aerosil R975), CuO (Pan-Continental Chemical Co, 99%) and Bi_2O_3 (Merck, 99%). The addition of the various elements cannot be exactly given, but the range of each added compound or metaloxide varies between 1 and 3 wt% to K85. The powders were weighed into a PE flask PE flask with 2 mm YTZ® beads. The powders were mixed for 16 hrs using isopropyl alcohol as medium. The powders were dried, grounded and uniaxially pressed (Fontijne SRA100) into discs of 8 mm diameter x 7.55 mm height. The discs were pressed cold isostatically (EPSI *Engineered Pressure Systems International* B.V.) at 4000 bar for 3 minutes. The discs were measured using a NETZCH Dil 402 C dilatometer. The samples were sintered at a 5 °C/min heating rate in static air. Then they were kept for 30 minutes at 1200 °C (K80 and K72) or at 1250 °C (K85) before the samples were cooled down at a rate of 10 °C/min.

Ag content characterization of electrodes. Green MLCC chips were produced on regular production equipment at Yageo in Roermond, the Netherlands. The 0805 MLCCs consisted of 10 electrode layers in a brick with an overall size of 2.0 mm x 1.25 mm x 0.6 mm. The dielectric thickness after sintering was 10 μm; the electrode thickness was 2.5 μm. The MLCCs of K80, dielectrics made from K85 and sintering aid 1, were made with 80Ag/20Pd paste. The MLCCs of K80 were sintered in air at 1080 °C for 2 hours. The MLCCs of K72 and K75, dielectrics made from K85 and sintering aid 2, were made of 95Ag/5Pd and 90Ag/10Pd paste, respectively. Both samples were sintered at 950 °C for 2 hours in an air atmosphere. The silver and palladium content of the electrodes were determined using a SEM (Philips XL20) equipped with an EDS system (EDAX).

ESR measurements. MLCCs of K85/100 Palladium, K80–80Ag/Pd20 and K72–90Ag/10Pd were prepared by making 0603 green chips in 1.6 mm x 0.8 mm x 0.8 mm with 5 electrodes. The MLCCs had a capacitance of 10 pF measured at 1MHz/1V after sintering. End contacts were applied onto the brick with glass containing silver paste. The ESR was measured with an Agilent LCR meter 4287a

Tabel 3.2.1: Sample overview of dielectrics, electrode composition and sintering temperature.

Material code	Dielectrics	Electrode Ag/Pd (wt%/wt%)	Sintering temperature (°C)
K85	AD850DZ	Pd	1180
K80	AD850DZ + sinter aid 1	80Ag/20Pd	1080
K75	AD850DZ + sinter aid 2	90Ag/10Pd	950
K72	AD850DZ + sinter aid 2	95Ag/5Pd	950

and fixture 16196A. The measuring frequency range was 30MHz up to 3GHz with 32 measuring points.

3.2.3. Results and Discussion

The MLCC samples were based on commercial BaO-Nd_2O_3-Gd_2O_3-TiO_2 dielectrics, AD850DZ, of Ferro. In this paper the commercial dielectric is called K85 and it sinters dense at temperature of around 1180 °C depending on sintering conditions. This material can be co-sintered with pure palladium or high content palladium like 20Ag/80Pd. For MLCCs with 80Ag/20Pd electrodes a dielectric composition was already developed using a sintering aid, see Table 3.2.1.

With the addition of sinter aid 1, which is based on a ZnO-SiO_2-CuO-TiO_2 compound, to K85 the sinter temperature was decreased. The samples made from this new formulation and 80Ag/20Pd electrodes are called K80. The sinter temperature for these K80 MLCCs is 1080°C when sintered in air for 2 hours. To use high silver content Ag/Pd alloys like 95Ag/5Pd another sinter aid was developed to obtain a dielectric formulation that could sinter below the melting temperature of pure silver. This material is called K72 and is based on K85 and sinter aid 2, which was made of a mixture of the following oxides: B_2O_3, ZnO, SiO_2, Bi_2O_3 and CuO. The dilatometer results, see Figure 3.2.1, show that K72 sintered dense at lower temperature than K80. In this study these dielectrics were first used in combination with 95Ag/5Pd electrodes and the samples are called K72. The samples made of the same new dielectrics in combination with 90Ag/10Pd are called K75. Both samples were sintered dense at 950 °C for 2 hours in air.

After sintering of the MLCC samples it was observed that the electrodes were discontinuous near the surface of the brick, see Figure 3.2.2. However, the electrodes in the middle of the brick are continuous. This discontinuity of the silver

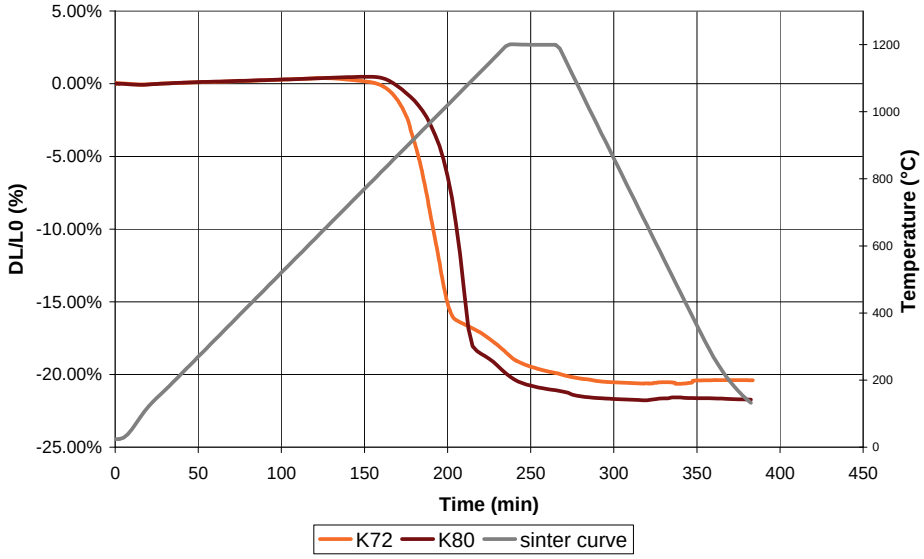

Figure 3.2.1: The thermomechanical analysis (TMA) curve of K80 and K72 dielectrics.

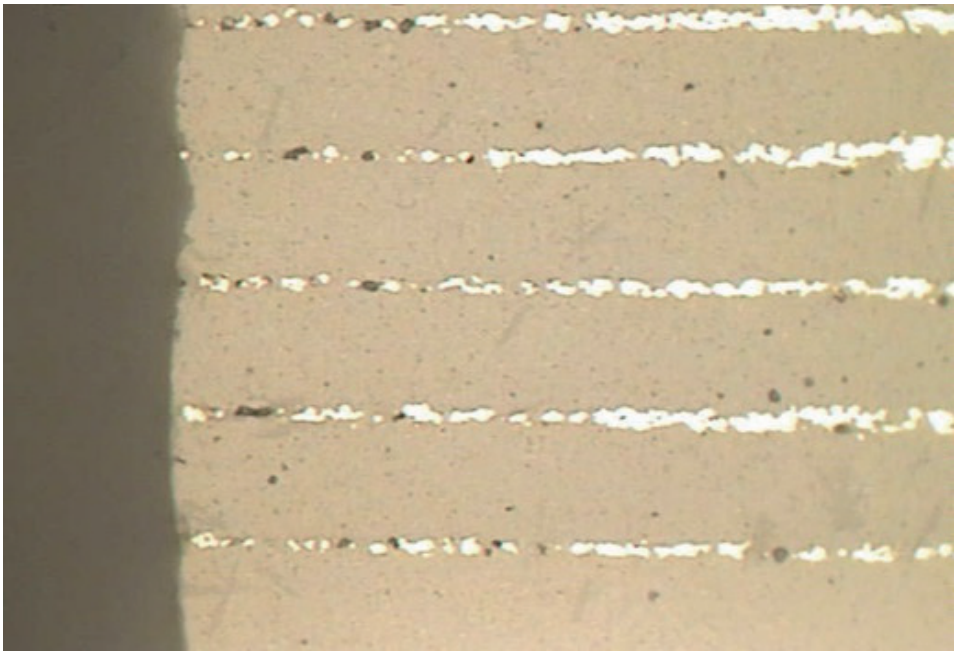

Figure 3.2.2: Discontinuous electrodes near surface of MLCC brick.

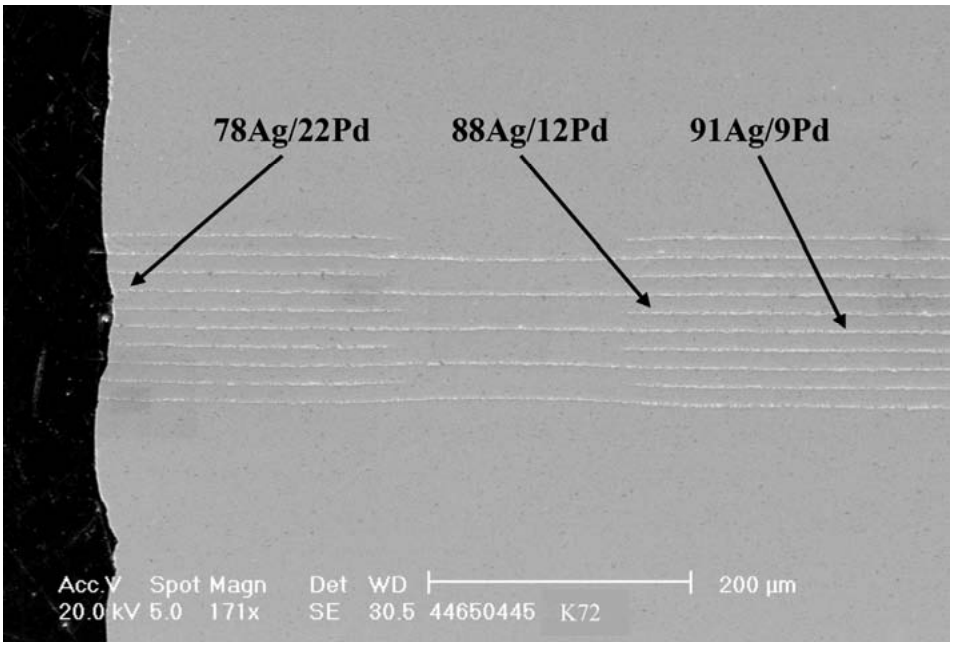

Figure 3.2.3: Quantitative analysis by SEM/EDS of K72–95Ag/5Pd electrodes.

palladium electrodes is due to evaporation or diffusion of silver during sintering. The elemental compositions of the electrodes were analyzed in detail by SEM/EDS using a spot size of 5 at 20kV. Because the silver and the palladium energy absorption bandwidth overlap partly a series of standards were made; 95Ag/5Pd, 90Ag/10Pd, 80Ag/20Pd and 70Ag/30Pd. Powder alloys were used to sinter 10 mm x 5 mm discs at 450–500 °C in air. These discs were used to calibrate for the EDS analysis. At several points the electrodes were analyzed, beginning near the outside of the brick at 10 µm depth, to about 560 µm inside the brick, see Figure 3.2.3.

The Ag/Pd ratios of the electrodes of the 3 MLCC samples were determined and the results are summarized in Table 3.2.2. From the results we can observe that for K80–80Ag/20Pd and K72–95Ag/5Pd the values of the measured Ag/Pd ratio at 10 µm depth were much different compared to the initial electrode composition. In K80 MLCCs an electrode ratio of 50Ag/50Pd was determined at 10 µm depth, which means that most of silver diffused into the interior, or evaporated during co-firing. Also for K72–95Ag/5Pd a large difference of Ag/Pd ratio compared to its initial value was found. However, in the K75–90Ag/10Pd system the difference between the initial and final Ag/Pd ratio is smaller. The results of the measuring point at a depth of 500 – 520 µm indicates that the sintered alloy is almost similar to the initial alloys used to prepare the samples.

To investigate the effect in more detail and to normalize these results a new calculation was performed. At each data point the remaining silver content was

quantified in terms of the ratio between the initial and final silver concentration in the electrode material. So the silver content before and after sintering is given as a percentage yield. The results are shown in Figure 3.2.4. The results show that for K80 and K72 at 10 μm from the edge of the chip only 20% of the initial silver content remained. For K75 around 60% of the initial silver remains in the electrode. Further down inside the brick at 500 to 560 μm depth the electrodes of K80 and K72 had 60 to 70% of the initial silver remaining. The measurement on the K75 sample showed that at 520 μm depth all silver remained.

Tabel 3.2.2: Quantitative analysis of elements in Ag/Pd electrodes by SEM-EDS.

K72 95Ag/5Pd		K80 80Ag/20Pd		K72 90Ag/10Pd	
Distance in brick from end-termination (μm)	Ag-Pd content (wt%/wt%)	Distance in brick from end-termination (μm)	Ag-Pd content (wt%/wt%)	Distance in brick from end-termination (μm)	Ag-Pd content (wt%/wt%)
100	78–22	10	50–50	10	85–15
400	88–12	520	73–27	520	89–11
500	91–9	560	70–30	560	87–13

These results show that selection of a high silver content electrode for a certain dielectric is important to achieve good electrode continuity. K80 was sintered at 1080°C and K72 was sintered at 950°C. If we plot these temperatures in the binary phase diagram of Ag/Pd,[14] as shown in Figure 3.2.5, we can determine that K80 is sintered 60°C below the melting point of 80Ag/20Pd. K72 dielectric was sintered 60°C below the melting point of 95Ag/5Pd. However, K72 and K75 dielectrics are sintered well below the melting point of 90Ag/10Pd. Here the difference is 110 °C and it is much larger than the other two systems. Due to this larger difference between the sintering temperature of the K75 MLCCs and the melting point of 90Ag/10Pd less silver will diffuse into the ceramics or evaporate during co-firing. Because less silver is lost, a qualitatively good and continuous electrode layer remained in the sintered MLCCs. Beside the improvement of the electrical properties, which are not discussed here, also the ESR of the MLCCs were improved when better quality electrodes were used.

The ESR is derived from various parameters such as the dissipation in dielectrics, electrode resistivity and termination resistivity. Its value also depends on the construction of the MLCC in terms of size, number of electrodes, electrode thickness, etc. The ESR was measured directly with the LCR analyzer and the

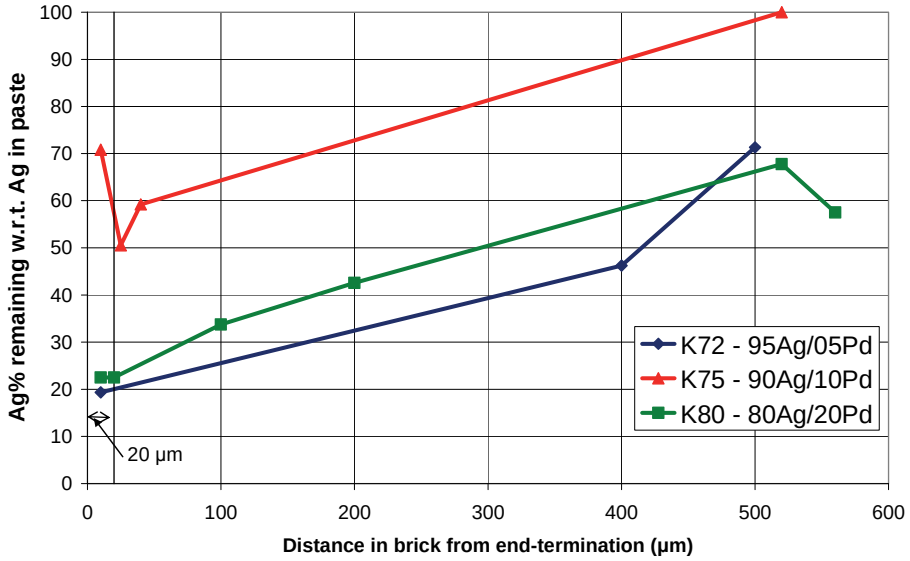

Figure 3.2.4: Ag (mol%) remaining in electrodes after sintering.

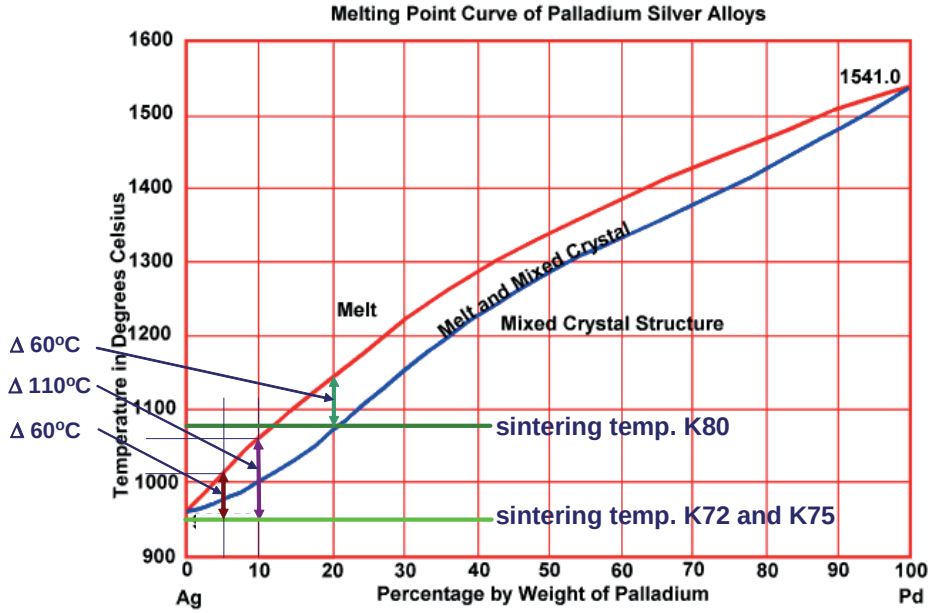

Figure 3.2.5: Binary phase diagram of Ag-Pd and sintering temperature of K72, K75 and K80.[14]

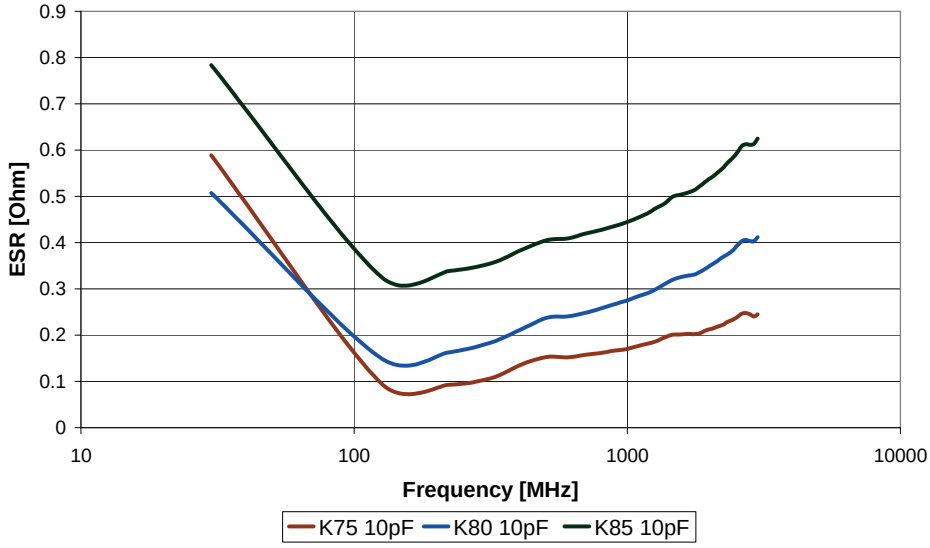

Figure 3.2.6: ESR as function of frequency for K85, K80 and K75 0603–10pF MLCCs.

results are plotted in Figure 3.2.6. The 0603 MLCCs used for these measurements had 5 metal electrodes. The capacitances of these MLCCs were 10 pF measured at 1 MHz/1 V. The dielectric thickness of the samples was 10 μm and the electrode thickness was 2.5 μm after sintering. The resonance frequencies of the 3 samples are around 125.8 MHz.

For K85 with pure Pd electrodes the ESR is larger than in the other two samples. This contrasts with the expectation that the ESR of K85-Pd is the same as K80–80Ag/20Pd, due to the fact that the bulk specific resistivity of palladium and 80Ag/20Pd alloy are the same, i.e. 11 μΩ.cm.[15] However, the ESR of the K80–80Ag/20Pd MLCC samples was considerably lower than K85-Pd. Thus, not only the resistivity contributes to the lower ESR of K80, but other parameters like the insulation resistance of the ceramics are important as well. At the resonance frequency the ESR of K75–90Ag/10Pd MLCC samples was lower than K80, as is expected from the specific resistivity values of Ag-Pd alloys. MLCCs made with K72 dielectrics and 90Ag-10Pd electrodes show an improvement of ESR compared to K80 MLCCs.

3.2.4. Conclusions

This study shows that in addition to the development of dielectrics towards C0G properties, the Ag/Pd alloy must also be chosen in such way that silver diffusion and evaporation are avoided. Therefore an Ag/Pd alloy must be chosen that melts at least

100 °C above the sintering temperature of the dielectrics. MLCCs made with low temperature sintering dielectrics and 90Ag/10Pd electrodes show lower ESR values than MLCCs made with 80Ag/20Pd electrodes. The use of silver-rich electrodes helps to decrease the ESR of MLCCs.

References

1) Ohsato, H. *Research and development of microwave dielectric ceramics for wireless communications*; Journal of the Ceramic Society of Japan, 2005 **113**(1323): p. 703–711.
2) Cava, R. J. *Dielectric materials for applications in microwave communications; Journal of Materials Chemistry*, 2001 **11**(1): p. 54–62.
3) Fiedziuszko, S. J.; Hunter, I. C.; Itoh, T.; Kobayashi, Y.; Nishikawa, T.; Stitzer, S. N. and Wakino, K. *Dielectric materials, devices, and circuits*; IEEE Transactions on Microwave Theory and Techniques, 2002 **50**(3): p. 706–720.
4) Xu, X. BME COG MLCCs; *The High Capacitance Class-I solution*; conference paper CARTS Europe 2007, 2007: p. 11–17.
5) Shih, S. J. and Tuan, W. H. *Solubility of silver and palladium in $BaTiO_3$*; Journal of the American Ceramic Society, 2004 **87**(3): p. 401–407.
6) Zuo, R. Z.; Li, L. T.; Gui, Z. L.; Ji, C. X. and Hu, X. B. *Vapor diffusion of silver in cofired silver/palladium - ferroelectric ceramic multilayer*; Materials Science and Engineering B-Solid State Materials for Advanced Technology, 2001 **83**(1–3): p. 152–157.
7) Tuan, W. H.; Cheng, Y. W. and Huang, Y. C. *Solubility of silver in non-stoichiometric barium titanate*; Journal of Electroceramics, 2008 **21**: p. 29–33.
8) Jean, J. H. and Chang, C. R. *Interfacial reaction kinetics between silver and ceramic-filled glass substrate*; Journal of the American Ceramic Society, 2004 **87**(7): p. 1287–1293.
9) Zuo, R. Z.; Li, L. T.; Gui, Z. L.; Hung, T. F. and Xu, Z. K. T*EM and EDS investigation of heterogeneous interfaces in cofired multilayer ceramic capacitors*; Materials Science and Engineering B-Solid State Materials for Advanced Technology, 2002 **95**(1): p. 1–5.
10) Lewis, D. J.; Gupta, D.; Notis, M. R. and Imanaka, Y. *Diffusion of Ag-110m tracer in polycrystalline and single-crystal lead-containing piezoelectric ceramics*; Journal of the American Ceramic Society, 2001 **84**(8): p. 1777–1784.
11) Zuo, R. Z.; Li, L. T. and Gui, Z. L. *Interfacial development and microstructural imperfection of multilayer ceramic chips with Ag/Pd electrodes*; Ceramics International, 2001 **27**(8): p. 889–893.
12) Chen, C. Y. and Tuan, W. H. *Evaporation of silver during cofiring with barium titanate*; Journal of the American Ceramic Society, 2000 **83**(7): p. 1693–1698.
13) Lee, W. H.; Su, C. Y.; Lee, Y. C.; Yang, J.; Yang, T. and Shih, P. L. *Effect of inner electrode on reliability of (Zn,Mg)TiO_3-based multilayer ceramic capacitor*; Japanese Journal of Applied Physics Part 1-Regular Papers Brief Communications & Review Papers, 2006 **45**(7): p. 5859–5864.
14) *Metals reference book*; 3rd ed.; Smithells, C. J.; Butterworths: London, 1962; Vol. 2, p 695.
15) Wang, S. F.; Dougherty, J. P.; Huebner, W. and Pepin, J. G. *Silver-palladium thick-film conductors*; Journal of the American Ceramic Society, 1994 **77**(12): p. 3051–3072.

Chapter 3.3

Multilayer capacitors with $(Zn,Mg)TiO_3$ dielectrics and pure Ag electrodes

3.3.1 Introduction to $(Zn,Mg)TiO_3$ dielectrics

In Chapter 3.2 multilayer capacitors (MLCC) based on high permittivity dielectrics were discussed in relation to high silver content silver-palladium alloys. But these dielectrics can't be used to produce MLCCs with pure silver inner electrodes, although it would be more favorable to produce multilayer capacitors with pure silver electrodes in order to decrease costs.[1] Another benefit of using pure silver electrodes is that, due to the low specific resistivity of silver, multilayer capacitors with low equivalent series resistance can be made. The aim is to develop a dielectric material that sinters well below the melting point of silver, 961 °C, in order to prevent diffusion and evaporation of silver during sintering, thereby realizing more reliable C0G MLCCs based on pure silver electrodes.

One type of dielectrics with promising C0G properties is based on $ZnO\text{-}TiO_2$ ceramics. These ceramics are a possible candidate to produce C0G MLCCs, which contain pure silver electrodes. The first studies on the $ZnO\text{-}TiO_2$ material system were done in the early 1960s and these were mainly focussed on identifying the phase diagram.[2–3] It has been reported that $ZnTiO_3$, Zn_2TiO_4 and $Zn_2Ti_3O_8$ are present in the $ZnO\text{-}TiO_2$ system. Later ceramics in the $ZnO\text{-}TiO_2$ system, formulated without additives, were also investigated in more detail regarding their electrical properties.[4–6] From these studies it was concluded that a mixture of $ZnTiO_3$ and TiO_2, sintered at 1300 °C for 2 hours, could have a near zero temperature coefficient of capacitance (TCC). However, the addition of sinter additives was needed to decrease the sintering temperatures down to 850 - 900 °C. The ceramics and the electrical properties of a solid solution of $ZnTiO_3$ and TiO_2, to which B_2O_3,[7–8] $ZnO\text{-}B_2O_3$ [9–10] and $ZnO\text{-}B_2O_3\text{-}SiO_2$ [8] were added, were investigated. Also the effect of Bi_2O_3 addition to a $ZnO\text{-}TiO_2$ material system was investigated with respect to

sintering temperature and electrical properties.[11] Unfortunately, the sintering temperatures of these ceramics were not below 1000 °C. Fortunately, the majority of the examined ZnO-TiO_2 based ceramics could be sintered well below the melting point of silver and some of these ceramics also had promising dielectric properties.

Although dielectrics with good electrical properties were produced the main problem was the reproducibility of the TCC values. It became evident that the TCC values were very sensitive to details in the sintering process in a specific temperature range. This was associated with the formation of various crystal structures during sintering. When the ceramics were sintered at a temperature between 850 and 950 °C, the $ZnTiO_3$ phase decomposed into various volume fractions, which consisted of Zn_2TiO_4 and TiO_2. The phase fractions varied from batch to batch, resulting in varying TCC values. A reproducible TCC near zero is therefore difficult to accomplish with these materials, which are only based on ZnO and TiO_2 as main components.

The addition of MgO to ZnO-TiO_2 dielectrics, formulated without sintering aids, was examined. The aim of the study was to determine if a more reliable dielectric towards the changes in the sintering process, and with better TCC reproducibility, could be developed. The strategy was to shift the decomposition of $ZnTiO_3$ to higher temperatures.[12–13] The studies showed that this was indeed possible and later this material system was examined in more detail. Besides the incorporation of MgO into the ZnO-TiO_2 material system also the effect of addition of $3ZnO$-B_2O_3,[14] Bi_2O_3,[15] $3ZnO$-B_2O_3 + Bi_2O_3 [16] and CaO-B_2O_3-SiO_2 [17] on the properties of the material were studied. These studies revealed that the addition of MgO into ZnO-TiO_2 and a sintering aid could result in dielectrics with a relative permittivity, ε_r, of around 25. In general these dielectrics had quality factors *Q* exceeding 4000 GHz and TCC values near zero. Thus, it should be possible to make C0G dielectrics with these types of compositions.

Multilayer capacitors with silver-palladium inner electrodes, which were produced to examine the electrical properties and reliability and which are described in literature, were based on the following materials: $Zn_{0.95}Mg_{0.05}TiO_3$,[18] $Zn_{0.95}Mg_{0.05}TiO_3$ + *0.25* mol% TiO_2 + *1* wt% $3ZnO$-B_2O_3,[19] and $Zn_{0.95}Mg_{0.05}TiO_3$ + *2* mol% Bi_2O_3 + *1* mol% Sb_2O_3.[20] In these studies the MLCCs were made with electrodes that consisted of 90Ag/10Pd, 95Ag/5Pd and 99Ag/1Pd alloys. In particular the effects of silver concentration on properties such as lifetime and insulation resistance were examined. However, these dielectrics were not evaluated in MLCCs with pure silver electrodes.

In this chapter $Zn_{0.95}Mg_{0.05}TiO_3$ + *0.25* mol% TiO_2, which will be called ZMT hereafter, will be discussed as the main dielectric component. The influence of $Zn_4B_6O_{13}$ and Bi_2O_3 addition on the sintering and electrical properties was investigated. The most optimal formulation described in this chapter, namely ZMT +

2 wt% $Zn_4B_6O_{13}$ + *2* wt% Bi_2O_3, can be sintered at a temperature of 900 °C. This composition was used to evaluate MLCCs with pure silver and 95Ag/5Pd electrodes.

3.3.2. Experimental – preparation of CDCs and MLCCs

Preparation and characterization of ceramic disc capacitors. The powders were made starting from $Zn_{0.95}Mg_{0.05}TiO_3$ + *0.25* mol% TiO_2 (ZMT, Kyoritsu Chemical Manufacturing). Slurries were prepared by weighing ZMT, $Zn_4B_6O_{13}$ (Borax, 98%) and Bi_2O_3 (Merck, 99%) in a PE flask with 2 mm YTZ beads and water. The powders were milled to a D_{50} of 0.7 μm. Then the powders were granulated with a glycerine solution (10 wt% in water) and uniaxially pressed (Fontijne SRA100) into pellets of 10 mm diameter x 1.2 mm height. The pellets were sintered at various temperatures in a tube kiln (Carbolite) in air. Silver terminations were applied onto the pellets using a silver termination paste (Yageo). Curing of the samples was done in a one hour cycle in a curing oven (Sierratherm) at 750 °C in air.
Preparation and evaluation of MLCC samples. Green MLCC chips were produced on regular production equipment at Yageo in Roermond, The Netherlands, as described in Chapter 2. The 0805 MLCCs consisted of 5 or 8 electrode layers in bricks with an overall size of 2.0 mm x 1.25 mm x 0.6 mm. The dielectric thickness after sintering was 14 μm; the electrode thickness was 2.5 μm. The MLCCs were made with a pure Ag or a 95Ag/5Pd (wt%/wt%) paste. The MLCCs were sintered at a temperature between 900 °C and 930 °C for 1 hour in air. Silver terminations (Yageo) were applied onto MLCCs using laboratory flat bed dipping equipment. The dried silver paste was cured in a Sierratherm kiln at 750 °C in air.

3.3.3. Results and Discussion

3.3.3.1 Material development using CDCs

A series of pellets with a composition of ZMT ($Zn_{0.95}Mg_{0.05}TiO_3$ + *0.25* mol% TiO_2) + *x* wt% $Zn_4B_6O_{13}$ + *y* wt% Bi_2O_3 were made and the pellets were sintered at various temperatures in a gradient kiln for one hour in air. In Figure 3.3.1 the results of the sintering behavior is shown by showing the percentage of shrinkage of the pellets as a function of sintering temperature. As already published in literature ZMT without sintering additives cannot be sintered dense below a temperature of 1100 °C.[9–10] With the addition of a $ZnO\text{-}B_2O_3$ compound, $Zn_4B_6O_{13}$, to ZMT the sintering temperature can be decreased down to 900 °C. This is in agreement with what is described in literature on the effect of $3ZnO\text{-}B_2O_3$ addition on the densification of

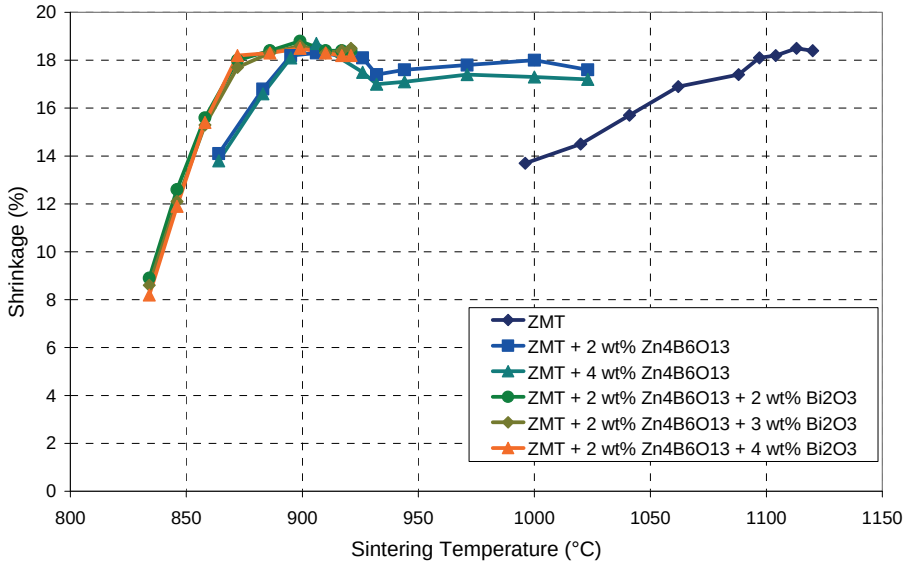

Figure 3.3.1: Shrinkage of the pellets measured after sintering.

$ZnO\text{-}TiO_2$ ceramics.[14] With a relatively small amount of *2* wt% of $Zn_4B_6O_{13}$ the sintering temperature can be reduced to 900 °C. Maybe a smaller amount of $Zn_4B_6O_{13}$ can be used, but we should be certain that the amount is sufficient to achieve dense ceramics after sintering. Therefore the composition of ZMT with *2* wt % $Zn_4B_6O_{13}$ was used as carrier composition to investigate if a further decrease of the sintering temperature was possible by adding Bi_2O_3.

Since a sintering temperature of 900 °C is most probably not sufficient to avoid silver diffusion and evaporation during sintering, see Chapter 3.2, the addition of Bi_2O_3 to ZMT + *2* wt% $Zn_4B_6O_{13}$ was examined. It is desired to decrease the sintering temperature to approximately 850 °C, which is approximately 100 °C below the melting point of silver, to minimize the effect of silver diffusion on the electrical properties and reliability of multilayer capacitors having pure silver electrodes. In Figure 3.3.1 the results show that with a small addition of *2* wt% Bi_2O_3 the sintering temperature can be decreased to 875 °C. This is the lowest possible sintering temperature, because larger amounts of Bi_2O_3 addition did not decrease the sintering temperature further. The small additions of Bi_2O_3 in combination with $Zn_4B_6O_{13}$ act as a strong sintering combination for liquid phase sintering and thus only a small amount of flux is needed to wet the ceramic surface of ZMT ceramics and to sinter the ceramics dense.

The densities of the various samples were measured and the results are listed in Table 3.3.1. The theoretical densities of the various compounds were calculated

from the densities of the raw materials. The theoretical density of $Zn_{0.95}Mg_{0.05}TiO_3$ was calculated using the known densities of $ZnTiO_3$ and $MgTiO_3$, which are 5.16 and 3.89 g/cm^3, respectively. Both $ZnTiO_3$, ecandrewsite, and $MgTiO_3$, geikielite, have the same ilmenite crystal structure ($FeTiO_3$). Since the ionic radius of Mg^{2+} (0.66 Å) is not much smaller than the ionic radius of Zn^{2+} (0.74 Å), the Mg^{2+} ion can easily substitute Zn^{2+} to form a $Zn_{1-x}Mg_xTiO_3$ solid solution.[14, 21] The density of $Zn_{0.95}Mg_{0.05}TiO_3$ was calculated using Vegards law to be 5.09 g/cm^3.[22]

The calculation of the theoretical density assumed that only the ilmenite type $ZnTiO_3$ was synthesized during sintering. But studies on ZnO-TiO_2 phase diagram revealed that various compounds, like $ZnTiO_3$, $Zn_2Ti_3O_8$, Zn_2TiO_3 and rutile TiO_2, could be formed during synthesis of 1 mol ZnO and 1 mol TiO_2.[2–3, 23] It was found that during synthesis of an equimolar ratio of ZnO and TiO_2 a series of reactions occurred, depending on sintering temperature. A phase diagram, see Figure 3.3.2, is proposed by Yang and Swisher based upon the former work by the other authors and their own findings.[23] From their work the reactions which occur during solid state sintering can be expressed by the following equations:

$$10\ ZnO + 10\ TiO_2 \xrightarrow{\approx 700\ ^\circ C} 10\ ZnTiO_3$$

$$\xrightarrow{700\text{-}900\ ^\circ C} 2\ ZnTiO_3 + 2\ Zn_2Ti_3O_8 + 2\ Zn_2TiO_4$$

$$\xrightarrow{900\text{-}950\ ^\circ C} 2\ ZnTiO_3 + 2\ Zn_2Ti_3O_8 + 2\ Zn_2TiO_4 + 2\ TiO_2$$

$$\xrightarrow{\geq 950\ ^\circ C} 5\ Zn_2TiO_4 + 5\ TiO_2$$

These results show that during sintering at lower temperatures first $ZnTiO_3$ is formed, but this compound decomposes at higher temperatures. Above 900 °C the hexagonal $ZnTiO_3$ is decomposed into cubic $Zn_2Ti_3O_8$, cubic Zn_2TiO_4 and rutile TiO_2. Above 950 °C only cubic Zn_2TiO_3 and cubic TiO_2 are present in the ceramics. The relative small addition of Mg^{2+} into the $ZnTiO_3$ ceramics influence the sintering temperature at which the ceramics decomposes. The decomposition of $(Zn,Mg)TiO_3$ ceramics occurs at higher temperatures. Therefore, it is presumed that this will form ceramics with more suitable properties for dielectric materials.

The calculated value of the theoretical density of ZMT was based on the idea that the sintered ceramics were only formed by the hexagonal phase $(Zn,Mg)TiO_3$, see Table 3.3.1. If the calculation was based on the formation of $(Zn,Mg)_2TiO_4$ and TiO_2 then the theoretical density of ZMT would be 4.85 g/cm^3. Thus the ZMT ceramics sintered at 1100 °C had a relative density of 97.5%. It was expected that the addition of $Zn_4B_6O_{13}$ to ZMT would decrease the density of the sintered ceramics, due to the lower specific density of the compound. But the data showed

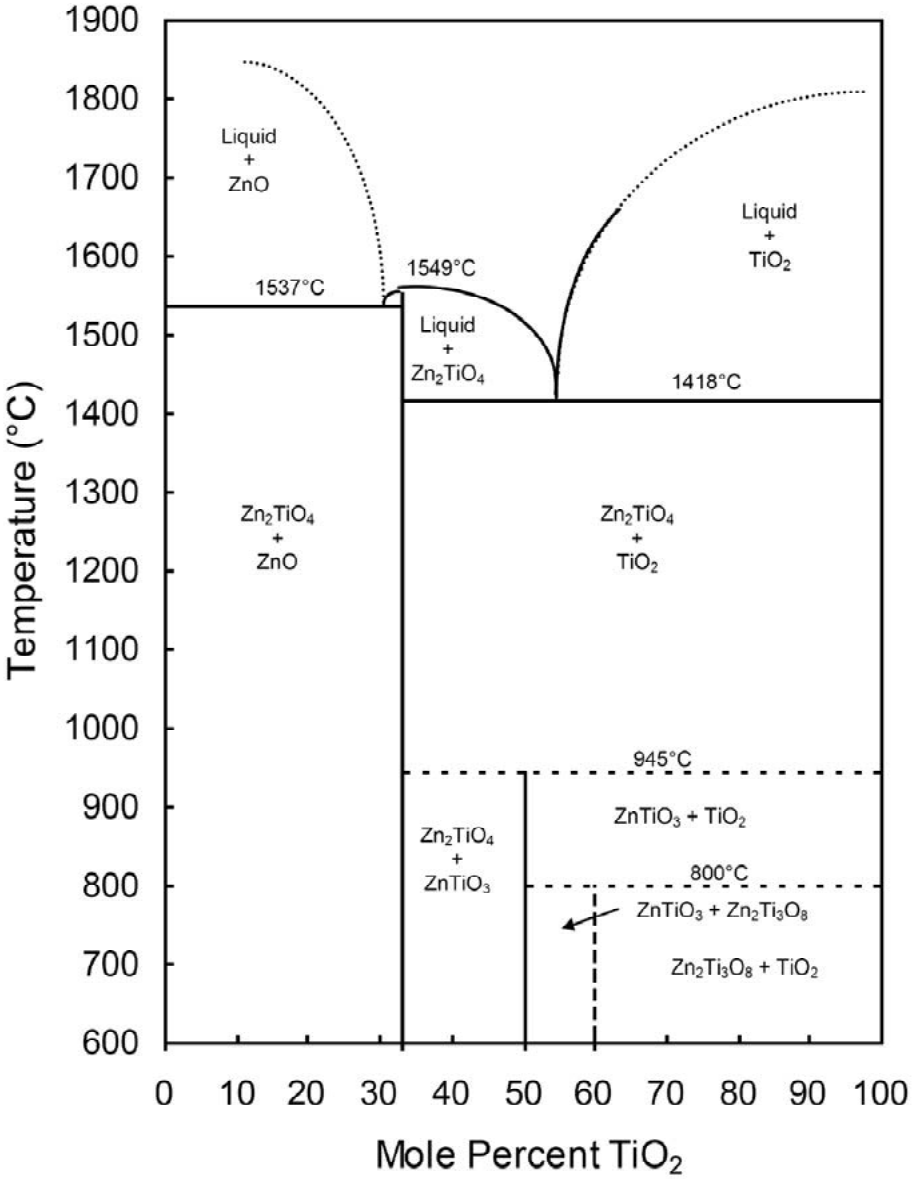

Figure 3.3.2: Phase diagram of ZnO-TiO_2 proposed by Yang and Swisher.[23]

Table 3.3.1: Densities of pellets sintered at various temperatures for a series $Zn_{0.95}Mg_{0.05}TiO_3$ + *0.25* mol% TiO_2 (ZMT) + *x* wt% $Zn_4B_6O_{13}$ + *y* wt% Bi_2O_3.

Ceramic Composition	Density (g/cm^3)					
	$\rho_{theor.}$	1100 °C	940 °C	920 °C	895 °C	875 °C
ZMT	5.09	4.73	Porous	Porous	Porous	Porous
ZMT + 2% $Zn_4B_6O_{13}$	5.05	-	4.74	4.78	4.92	Porous
ZMT + 4% $Zn_4B_6O_{13}$	5.00	-	4.72	4.91	4.82	Porous
ZMT+2%$Zn_4B_6O_{13}$+2% Bi_2O_3	5.12	-	-	4.93	4.89	4.84
ZMT+2%$Zn_4B_6O_{13}$+3% Bi_2O_3	5.16	-	-	4.94	4.93	4.91
ZMT+2%$Zn_4B_6O_{13}$+4% Bi_2O_3	5.19	-	-	4.94	4.96	4.94

that addition of $Zn_4B_6O_{13}$ to ZMT resulted in a higher density of the sintered ceramics. The samples sintered at 895 °C have the highest values and a decrease of measured density was observed when the samples were sintered at higher temperatures. Furthermore, the samples with $Zn_4B_6O_{13}$ addition sintered at 940 °C have similar values as ZMT sintered at 1100 °C. These results suggest that the ceramics did not decompose completely into Zn_2TiO_4 and TiO_2 and that $ZnTiO_3$ phase was present in the ceramics sintered at temperatures between 895 and 940 °C.

The addition of Bi_2O_3 to a mixture of ZMT + *2* wt% $Zn_4B_6O_{13}$ will increase the density of the ceramics due to the heavy Bi^{3+} ions. It was expected that Bi_2O_3 addition will also influence the decomposition reaction of ZMT. The trend of increasing density as function of increasing amount of Bi_2O_3 into ZMT + *2* wt% $Zn_4B_6O_{13}$ was clearly observed for the ceramics sintered at 895 °C. The density of the ceramics containing *2* and *3* wt% Bi_2O_3 was dependent on the sintering temperature. Thus the relative density is dependent on sintering temperature for these compositions. However, the ceramics with *4* wt% Bi_2O_3 was less dependent on sintering temperature and the ceramics had a relative density of 95%.

The electrical properties, relative permittivity (ε_r) and tan δ, of the samples are shown in Table 3.3.2. The ZMT ceramics had an ε_r of 35.4, which is slightly larger than a comparable dielectric found in literature.[14] The loss factor, tan δ, of the dielectric is low and the values exceed the specifications for C0G dielectrics (tan $\delta < 10^{-3}$). The samples ZMT + 2 wt% $Zn_4B_6O_{13}$ and ZMT + 4 wt% $Zn_4B_6O_{13}$ have lower relative permittivity compared to ZMT. The variation of the relative permittivity can be explained by the mixing rule for dielectrics, see Equation 3.1.3, Because the ceramics consists of several volume fractions of various phases, as explained above. Each phase in the ceramics has its own specific ε_r, *Q* and TCC values. Thus after sintering the average ε_r will be changed depending on the type and amount of added

compounds. When ZMT dielectrics are mixed with $Zn_4B_6O_{13}$ the average ε_r of the dielectrics will be lowered depending of the amount of $Zn_4B_6O_{13}$ added to ZMT. The extra addition of Bi_2O_3 will form a $Bi_2Ti_2O_7$ phase during sintering and the presence of this pyrochlore phase in the ceramics seems to increase the average relative permittivity.

Low losses, tan δ, were obtained when these dielectrics were sintered between 895 and 920 °C. These dielectrics had excellent *Q.f* factors, which were above 10000 MHz. However, when these dielectrics were sintered at 940 °C high tan δ values were measured. The higher values of tan δ are caused by the decomposition of ZMT into rutile TiO_2 and Zn_2TiO_4. Since rutile TiO_2 has a low tan δ the increase of tan δ should be caused by the large tan δ of the Zn_2TiO_4 ceramic.[21]

Table 3.3.2: Relative permittivities and loss factors measured at 1 MHz/1V_{rms} after sintering at various temperatures.

Ceramic Composition	1100 °C		940 °C		920 °C		895 °C		885 °C	
	ε_r	Tan δ (10^{-4})	ε_r	Tan δ (10^{-4})	ε_r	Tan δ (10^{-4})	ε_r	Tan δ (10^{-4})	ε_r	Tan δ (10^{-4})
ZMT	35	16.5	-	-	-	-	-	-	-	-
ZMT+2% $Zn_4B_6O_{13}$	-	-	35	17.0	30	1.0	28	1.0	-	-
ZMT+4% $Zn_4B_6O_{13}$	-	-	30	7.0	26	1.0	27	1.0	-	-
ZMT+2% $Zn_4B_6O_{13}$+2% Bi_2O_3	-	-	-	-	29	1.4	30	1.3	29	1.2
ZMT+2% $Zn_4B_6O_{13}$+3% Bi_2O_3	-	-	-	-	30	1.7	30	2.5	30	3.7
ZMT+2% $Zn_4B_6O_{13}$+4% Bi_2O_3	-	-	-	-	32	2.5	31	2.4	32	3.5

The ε_r and tan δ of ZMT + 2 wt% $Zn_4B_6O_{13}$ + x wt% Bi_2O_3 dielectrics were increased when the amount of Bi_2O_3 in the dielectrics was increased. These characteristics were caused by the presence of $Bi_2Ti_2O_7$ in the ceramics, which was formed during sintering. This is in agreement what is published by Lee and Lee, who found that *Q.f* values dropped when Bi_2O_3 was added to ZMT + $Zn_4B_6O_{13}$ ceramics.[16] However, the tan δ values of the measured samples are still low and meet the C0G specification well.

The ZMT samples, sintered at 1100 °C, had very large negative TCC values, which were -186 ppm/°C, see Table 3.3.3. This is due to the presence of Zn_2TiO_4 and TiO_2 in the ceramics. Because TiO_2 has a large negative TCC value, around -500 ppm/°C, the average TCC value is dominated by the TiO_2 phase.[6, 10] The TCC values of ZMT + *2* wt% $Zn_4B_6O_{13}$ and ZMT + *4* wt% $Zn_4B_6O_{13}$ dielectrics were

very dependent on the sintering temperature. In Figure 3.3.3 the complete TCC curves of ZMT + *2* wt% $Zn_4B_6O_{13}$, sintered at 900, 920 and 940 °C, respectively, are shown as an example to visualize the dependency of TCC to sintering temperature. The TCC curves are rotated clockwise when the sintering temperature is increased. When the dielectrics are sintered at 920 °C the TCC, measured at 125 °C, was -2 ppm/°C. However, when the dielectrics were sintered at 940 °C, the TCC curve rotated clockwise, which would indicate that more TiO_2 is present in the ceramics. When the dielectrics were sintered at 900 °C the TCC at 125 °C was 40 ppm/°C. These positive TCC value indicate that less TiO_2 was present in the dielectric composition compared to dielectrics sintered at higher temperatures. Thus the TCC of the ZMT + *2* wt% $Zn_4B_6O_{13}$ dielectrics are very dependent on the sintering temperature. Since a temperature window of 7 to 15 °C in mass production pusher kilns can occur it will be difficult to get reproducible TCC values when these ceramics are mass produced.

Table 3.3.3: The TCC of samples measured at 125 °C after sintering at various temperatures.

Ceramic Composition	1100 °C TCC (ppm/°C)	940 °C TCC (ppm/°C)	920 °C TCC (ppm/°C)	900 °C TCC (ppm/°C)	885° C TCC (ppm/°C)
ZMT	-186	-	-	-	-
ZMT+ 2% $Zn_4B_6O_{13}$	-	-47	-2	40	-
ZMT + 4% $Zn_4B_6O_{13}$	-	-86	-2	41	-
ZMT + 2%$Zn_4B_6O_{13}$ + 2% Bi_2O_3	-	-	38	27	25
ZMT + 2% $Zn_4B_6O_{13}$ + 3% Bi_2O_3	-	-	55	29	24
ZMT + 2% $Zn_4B_6O_{13}$ + 4% Bi_2O_3	-	-	55	28	22

The TCC values of ZMT + *2* wt% $Zn_4B_6O_{13}$ + *y* wt% Bi_2O_3 dielectrics were much less dependent on sintering temperature variations. All samples did have positive TCC values at 125 °C between 22 and 55 ppm/°C, depending on the amount of Bi_2O_3 and the sintering temperature. However, samples that were sintered at 920 °C had large TCC values, exceeding the C0G specification. In comparison, the samples sintered at 895 and 900 °C, the TCC values were respectively 22 and 29 ppm/°C. As an example the TCC curves of ZMT + *2* wt% $Zn_4B_6O_{13}$ + *2* wt% Bi_2O_3 dielectrics, which were sintered at three different sintering temperatures, are shown in Figure 3.3.4. In Figure 3.3.4 it can be observed that the TCC values of this dielectric composition is less dependent on sintering temperature.

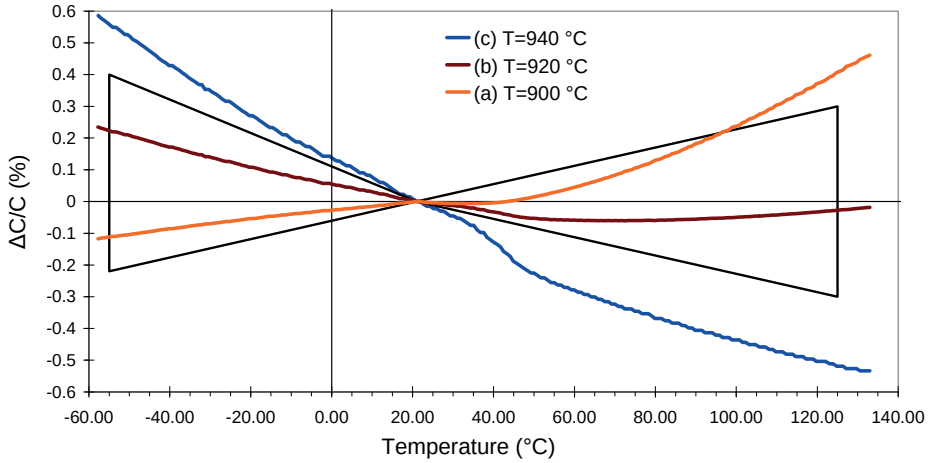

Figure 3.3.3: TCC curve of ZMT + 2 % $Zn_4B_6O_{13}$ sintered at (a) 900, (b) 920 and (c) 940 °C. The C0G specification box is drawn in the figure.

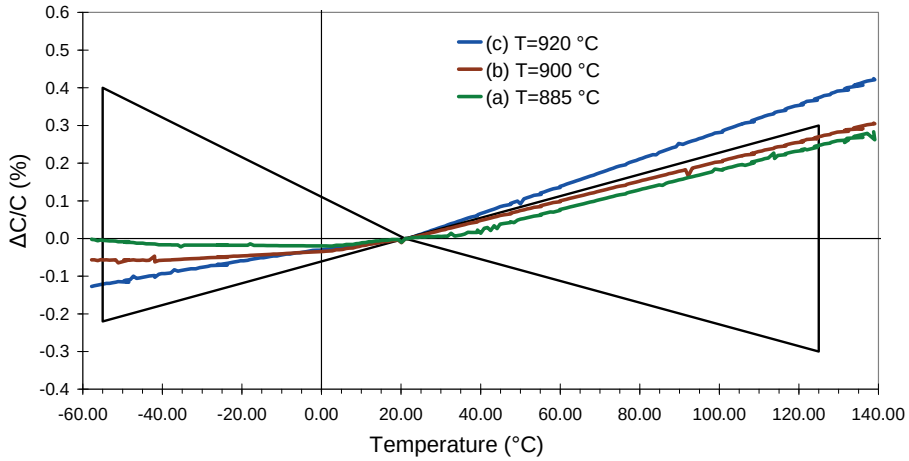

Figure 3.3.4: TCC curve of ZMT + 2 % $Zn_4B_6O_{13}$ + 2 % Bi_2O_3 sintered at (a) 885, (b) 900 and (c) 920°C. The C0G specification box is drawn in the figure.

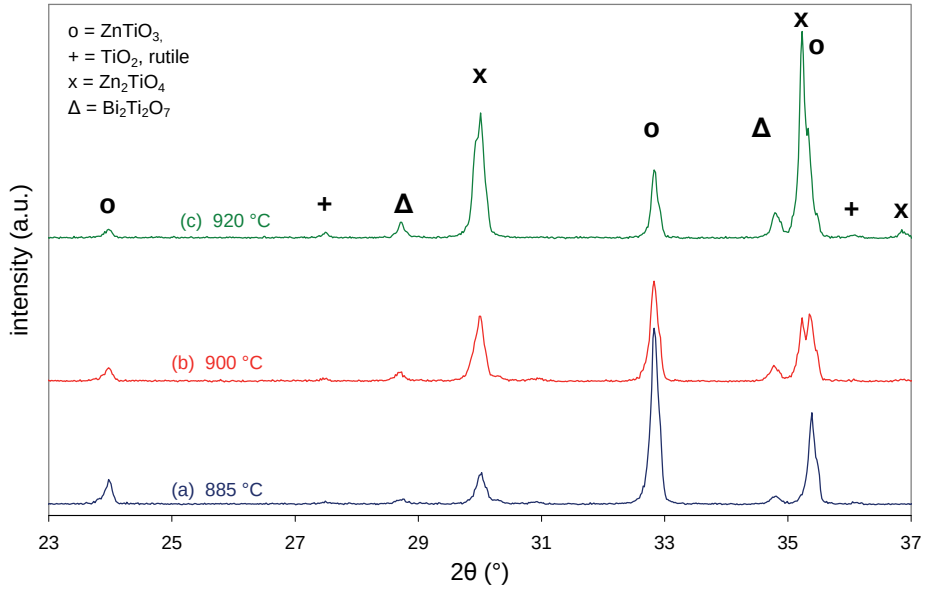

Figure 3.3.5: X-Ray diffraction patterns of ZMT + *2* wt% $Zn_4B_6O_{13}$ +*2* wt% Bi_2O_3 sintering at (a) 885 °C, (b) 900 °C and (c) 920 °C.

The crystal structures of the ZMT + *2* wt % $Zn_4B_6O_{13}$ + *2* wt % Bi_2O_3 ceramics, sintered at 885, 900 and 920 °C, were identified and four different crystal structures were detected, see Figure 3.3.5. The crystal structures identified were hexagonal $ZnTiO_3$,[24] cubic Zn_2TiO_4,[25] tetragonal TiO_2 [26] and cubic $Bi_2Ti_2O_7$.[27] The crystal structure $Zn_2Ti_3O_8$ was not found and it was most probably not present in the ceramics or it would be as a minor trace.

Table 3.3.4: XRD analysis of the phase fractions of ZMT + *2* wt% $Zn_4B_6O_{13}$+ *2* wt% Bi_2O_3 dielectrics sintered at 885, 900 and 920°C.

$T_{sintering}$	$(Zn,Mg)TiO_3$ (%)	$(Zn,Mg)_2TiO_4$ (%)	$Bi_2Ti_2O_7$ (%)	TiO_2 (%)
885 °C	80.7	6.8	11.0	1.6
900 °C	45.9	29.1	23.7	1.3
920 °C	19.0	57.2	22.3	1.4

The XRD analysis of the ceramics revealed that the phase fractions of the four identified phases are dependent on sintering temperature, see Table 3.3.4. In the ceramic sintered at 885 °C, hexagonal $ZnTiO_3$ was dominantly present and had a

phase fraction of 80.9 %. However, the content of $ZnTiO_3$ decreased to a phase fraction of 19 % when the ceramics were sintered at 920 °C. The phase fraction of cubic Zn_2TiO_4 increased when the ceramics were fired at increasing temperatures.

The amount of $Bi_2Ti_2O_7$ and TiO_2 seems to be less dependent on sintering temperature. The XRD results can be used to explain why the TCC curves for the dielectric composition are quite stable. The TCC values of $ZnTiO_3$, Zn_2TiO_4 and TiO_2 are +130, +160 and -880 ppm/°C, respectively,[5, 7–8, 15, 17] and $Bi_2Ti_2O_7$ has a positive TCC.[11] In our case we have to consider the TCC values of $(Zn,Mg)TiO_3$ and $(Zn,Mg)_2TiO_4$, but we do not know the amount of Mg^{2+} present in each phase. Furthermore, we do not know the exact ε_r, *Q* and TCC values of these different phases either. Normally the average ε_r. *Q* and TCC of the ceramics could be calculated by using the mixing rules for dielectrics, i.e. Eq. 3.1.3, Eq. 3.1.4 and Eq. 3.1.5, respectively. However, an explanation for the temperature dependence of these parameters will be given instead. Because the amount of TiO_2 in the ceramics is not dependent on sintering temperature, the ε_r, *Q* and TCC parameters were not influenced largely by TiO_2. The amount of $Bi_2Ti_2O_7$ was higher. The amount of this phase increased from 11.0 to 23.7 % when the ceramics were fired at 885 to 900 °C. No further increase was observed when the ceramics were fired at 920 °C. The phases $(Zn,Mg)TiO_3$ and Zn_2TiO_4 are the main cause of changing the ε_r, *Q* and TCC values, because these phase fractions changed the most. The $(Zn,Mg)TiO_3$ phase is largely present in the ceramics sintered at 885 °C, Table 3.3.4, while $(Zn,Mg)_2TiO_4$, is present even less than $Bi_2Ti_2O_7$. The ratio between $(Zn,Mg)TiO_3$ and $(Zn,Mg)_2TiO_4$ changed when the ceramics were sintered at 900 and 920 °C, respectively. In the ceramics sintered at 920 °C the $(Zn,Mg)_2TiO_4$ phase is mainly present in the ceramics, in contrast to $(Zn,Mg)TiO_3$ which amount decreased to 19%. These XRD results suggest that large differences of ε_r and tan δ would be found.

Furthermore, the results in Table 3.3.2 show that the ε_r of ZMT + *2* wt % $Zn_4B_6O_{13}$ + *2* wt % Bi_2O_3 is stable at the sintering temperature. The tan δ is increased slightly and is almost negligible. These results assume that ε_r and tan δ of $(Zn,Mg)TiO_3$ and $(Zn,Mg)_2TiO_4$ are roughly similar. The results of the TCC values, see Table 3.3.3 and Figure 3.3.4, would assume that the influence of the various phases in ZMT + *2* wt % $Zn_4B_6O_{13}$ + *2* wt % Bi_2O_3 is large. The difference between the TCC of $(Zn,Mg)TiO_3$ and $(Zn,Mg)_2TiO_4$ is approximately similar to $ZnTiO_3$ and Zn_2TiO_4. Therefore the shift in TCC due to sintering temperature can be explained by the larger TCC value of Zn_2TiO_4 than of $ZnTiO_3$. Thus, when more Zn_2TiO_4 is present in the ceramics than $ZnTiO_3$ the average TCC will be larger compared to ceramics in which more $ZnTiO_3$ than Zn_2TiO_4 is present. The results in Table 3.3.4 and in Table 3.3.3 indicate that this also happened in the ZMT + *2* wt % $Zn_4B_6O_{13}$ + *2* wt % Bi_2O_3 dielectrics.

3.3.3.2 Evaluation of MLCCs with pure Ag electrodes

The dielectric composition ZMT + *2* wt% $Zn_4B_6O_{13}$ + *2* wt% Bi_2O_3 was evaluated in 0805 MLCCs. Four types of MLCC samples were prepared, see Table 3.3.5. Two types of metals, silver and a 95 Ag/5Pd alloy were used as inner electrodes. The MLCCs were made into 2 constructions with 5 and 8 electrodes, respectively. The minimum sintering temperature of the ZMT + *2* wt% $Zn_4B_6O_{13}$ + *2* wt% Bi_2O_3 ceramics is approximately 900 °C, which is almost 60 °C below the melting point of silver. In Chapter 3.2 it was concluded that the difference between sintering temperature of the ceramics and the melting point of the electrode metal should be at least 100 °C. For the 95Ag/5Pd alloy the difference between sintering temperature of ZMT + *2* wt% $Zn_4B_6O_{13}$ + *2* wt% Bi_2O_3 and the melting point of the 95Ag/5Pd alloy is approximately 110 °C. The use of different metals for the inner electrodes was used to examine the quality of the multilayer capacitors after sintering. Especially excessive silver diffusion or evaporation, which can occur during sintering, can alter the electrical properties of the capacitors. In Table 3.3.6 the results of the electrical measurements on the MLCCs are shown.

Table 3.3.5: Overview of the MLCC samples with Ag and 95Ag-5Pd electrodes.

Exp. No.	Dielectric composition	Electrode composition (wt%/wt%)	No. electrodes
1	ZMT + 2% $Zn_4B_6O_{13}$ + 2% Bi_2O_3	100 Ag	5
2	ZMT + 2% $Zn_4B_6O_{13}$ + 2% Bi_2O_3	95 Ag / 5 Pd	5
3	ZMT + 2% $Zn_4B_6O_{13}$ + 2% Bi_2O_3	100 Ag	8
4	ZMT + 2% $Zn_4B_6O_{13}$ + 2% Bi_2O_3	95 Ag / 5 Pd	8

All MLCCs were first sintered at 930 °C to be certain that the ceramics were well dense. The results showed that the MLCCs of experiment 1 and 3, with pure silver electrodes, had lower capacitance values compared to MLCCs with 95Ag/5Pd electrodes. The lower values for the capacitance in experiment 1 and 3 can be explained by the fact that silver from the electrode was evaporated or diffused into the ceramics. The loss of silver in the electrodes was the cause of the discontinuity of the electrodes. When the electrodes are discontinuous lower capacitance values will be found.[19–20] The MLCCs of experiment 2 were also sintered at lower temperatures. The electrical properties, capacitance and tan δ, were not altered much by changing the sintering temperature. Next to the capacitance and tan δ measurements also the insulation resistance (IR) of the multilayer capacitors were measured at two different temperatures, 25 and 140 °C.

Table 3.3.6: The average values of capacitance, tan δ and insulation resistance, $IR_{20}$and IR_{140} for MLCCs samples (n=10).

Exp. No.	$T_{sintering}$	Capacitance 1 MHz/1 V	Tan δ 1 MHz/1 V	IR_{20} 20°C/50 V	IR_{140} 140°C/50 V
	(°C)	(pF)	(10^{-4})	(Ω)	(Ω)
1	930	11.6	2.8	$1.5 \cdot 10^{12}$	$< 10^5$
2	930	14.9	2.1	$6.2 \cdot 10^{12}$	$< 10^5$
2	915	14.5	2.7	$2.3 \cdot 10^{13}$	$< 10^5$
2	900	14.7	2.8	$3.2 \cdot 10^{13}$	$< 10^5$
3	930	79.6	1.9	$3.2 \cdot 10^{11}$	$< 10^5$
4	930	88.2	1.8	$7.2 \cdot 10^{11}$	$< 10^5$

The insulation resistance is an important property of a capacitor. In a direct current (DC) field an ideal capacitor has an infinite resistance, but in reality capacitors do not function ideally and some leakage currents occur during load. Therefore, capacitors have an insulation resistance which can be described for a plate capacitor by the following equation:

$$IR = \frac{\rho \cdot d}{A} \qquad (3.3.1)$$

in which ρ is the specific resistivity of the dielectrics in Ω·m, d the distance between the electrodes in meters, and A is the active area between the electrodes in m^2. A charged capacitor will be discharged according to the following equation:[28]

$$Q_t = Q_0 \exp^{-t/\tau} \qquad (3.3.2)$$

where Q_t is the charge of the capacitor at time t in coulombs and Q_0 the initial charge in Coulombs. The time constant τ of the capacitor and can be calculated by

$$\tau = IR \cdot C \qquad (3.3.3)$$

where IR is the insulation resistance in Ω and C is the capacitance in F. The time constant is only dependent on the material properties. For MLCC capacitors it is recommended that the time constant at 20 °C should be at least 1000 seconds. When the time constant is measured at 140 °C the values may not be lower than 100 seconds. Therefore, the insulation resistance of capacitors should be temperature stable in order to function properly in electronic equipment. The time constant τ_{20},

measured at 20 °C, for the MLCC samples varied between 17.4 and 470 seconds. The time constant, τ_{140}, dropped to values below 10^{-6} seconds. What the exact τ_{140} values were for these samples could not be determined due to the measuring limits of the used equipment.

The decrease of IR_{140} was caused by the presence of the semi-conductive $(Zn,Mg)_2TiO_4$ phase in the dielectric ceramics. The Zn_2TiO_4 phase is a spinel type of material, which conductivity shows Arrhenius-type behavior.[29–30] Therefore ceramics composed of a mix of dielectric ceramics such as TiO_2, $(Zn,Mg)TiO_3$ and Bi_2TiO_7 and a semi-conductive ceramics such as spinel-type Zn_2TiO_4, will result in a semi-conductive material when the phase fraction of Zn_2TiO_4 in the ceramics is large enough, or when the conductivity is not inhibited by other means such as grain boundary resistivity.

3.3.4. Conclusions

Dielectric ceramics with the composition $Zn_{0.95}Mg_{0.05}TiO_3$ + *0.25* mol% TiO_2 + *2* wt% $Zn_4B_6O_{13}$ + *2* wt% Bi_2O_3 were developed for use as dielectric material for multilayer capacitors with pure silver electrodes. This dielectric composition had a ε_r of 30, tan δ of $1.3 \cdot 10^{-3}$ and TCC of 27 ppm/°C. MLCCs with this dielectric composition were produced with silver and 95Ag/5Pd electrodes. Despite good values for capacitance and tan δ, the insulation resistance and the calculated time constant τ_{20}, measured at 20 °C, of the MLCCs were relatively low. Furthermore, the insulation resistance and time constant τ_{140} values measured at 140 °C were decreased substantially. This is due to the presence of semi-conductive spinel Zn_2TiO_4 ceramics in the dielectric composition. These dielectrics show a very large drift towards temperature change in the time constant and therefore these dielectrics cannot be used in applications where temperature stability is crucial.

References

1) Kishi, H.; Mizuno, Y. and Chazono, H. *Base-metal electrode-multilayer ceramic capacitors: Past, present and future perspectives*; Japanese Journal of Applied Physics Part 1-Regular Papers Short Notes & Review Papers, 2003 **42**(1): p. 1–15.
2) Bartram, S. F. and Slepetys, R. A. *Compound formation and crystal structure in the system ZnO-TiO$_2$*; Journal of the American Ceramic Society, 1961 **44**(10): p. 493–499.
3) Dulin, F. H. and Rase, D. E. *Phase equilibria in the system ZnO-TiO$_2$*; Journal of the American Ceramic Society, 1960 **43**(3): p. 125–131.
4) Kim, H. T.; Byun, J. D. and Kim, Y. *Microstructure and microwave dielectric properties of modified zinc titanates (I)*; Materials Research Bulletin, 1998 **33**(6): p. 963–973.

5) Kim, H. T.; Kim, Y.; Valant, M. and Suvorov, D. *Titanium incorporation in Zn_2TiO_4 spinel ceramics*; Journal of the American Ceramic Society, 2001 **84**(5): p. 1081–1086.
6) Haga, K.; Ishii, T.; Mashiyama, J. and Ikeda, T. *Dielectric-properties of 2-phase mixture ceramics composed of rutile and its compounds*; Japanese Journal of Applied Physics, 1992 **31**: p. 3156–3159.
7) Kim, H. T.; Kim, S. H.; Nahm, S.; Byun, J. D. and Kim, Y. *Low-temperature sintering and microwave dielectric properties of zinc metatitanate-rutile mixtures using boron*; Journal of the American Ceramic Society, 1999 **82**(11): p. 3043–3048.
8) Chaouchi, A.; Aliouat, M.; Marinel, S.; d'Astorg, S. and Bourahla, H. *Effects of additives on the sintering temperature and dielectric properties of $ZnTiO_3$ based ceramic*; Ceramics International, 2007 **33**(2): p. 245–248.
9) Mergen, A. and Goren, R. *Sintering of zinc metatitanate with zinc borate addition*; Key Engineering Materials, 2004 **264–268**: p. 1349–1352.
10) Chaouchi, A.; Marinel, S.; Aliouat, M. and d'Astorg, S. *Low temperature sintering of $ZnTiO_3/TiO_2$ based dielectric with controlled temperature coefficient*; Journal of the European Ceramic Society, 2007 **27**(7): p. 2561–2566.
11) Chen, H. C.; Weng, M. H.; Horng, J. H.; Houng, M. P. and Wang, Y. H. *Effect of bismuth addition on sintering behavior and microwave dielectric properties of zinc titanate ceramics*; Journal of Electronic Materials, 2005 **34**(1): p. 119–124.
12) Kim, H. T.; Nahm, S.; Byun, J. D. and Kim, Y. *Low-fired $(Zn,Mg)TiO_3$ microwave dielectrics*; Journal of the American Ceramic Society, 1999 **82**(12): p. 3476–3480.
13) Chang, U. S.; Chang, Y. H.; Chen, I. G. and Chen, G. J. *Synthesis and characterization of zinc titanate doped with magnesium*; Solid State Communications, 2003 **128**(5): p. 203–208.
14) Lee, Y. C.; Lee, W. H. and Shiao, F. T. *Microwave dielectric properties of $Zn_{0.95}Mg_{0.05}TiO_3+0.25TiO_2$ ceramics with $3ZnO-B_2O_3$ addition*; Japanese Journal of Applied Physics Part 1-Regular Papers Short Notes & Review Papers, 2004 **43**(11A): p. 7596–7599.
15) Hsieh, M. L.; Chen, L. S.; Wang, S. M.; Sun, C. H.; Weng, M. H.; Houng, M. P. and Fu, S. L. *Low-temperature sintering of microwave dielectrics $(Zn,Mg)TiO_3$*; Japanese Journal of Applied Physics Part 1-Regular Papers Brief Communications & Review Papers, 2005 **44**(7A): p. 5045–5048.
16) Lee, Y. C. and Lee, W. H. *Effects of glass addition on microwave dielectric properties of $Zn_{0.95}Mg_{0.05}TiO_3+0.25TiO_2$ ceramics*; Japanese Journal of Applied Physics Part 1-Regular Papers Brief Communications & Review Papers, 2005 **44**(4A): p. 1838–1843.
17) Li, B.; Zhang, S. R.; Yuan, Y.; Zhou, X. H. and Xiang, L. C. *Dielectric properties and microstructure of TiO_2 modified $(ZnMg)TiO_3$ microwave ceramics with $CaO-B_2O_3-SiO_2$*; Journal of Materials Science, 2009 **44**(18): p. 4993–4998.
18) Lee, W. H.; Su, C. Y.; Lee, Y. C.; Yang, J.; Yang, T. and Shih, P. L. *Effect of inner electrode on reliability of $(Zn,Mg)TiO_3$-based multilayer ceramic capacitor*; Japanese Journal of Applied Physics Part 1-Regular Papers Brief Communications & Review Papers, 2006 **45**(7): p. 5859–5864.
19) Lee, W. H.; Su, C. Y.; Huang, C. L.; Lee, Y. C.; Hu, C. L.; Yang, J.; Yang, T. and Lin, S. P. *Effect of inner electrode on electrical properties of $(Zn,Mg)TiO_3$-based multilayer ceramic capacitor*; Japanese Journal of Applied Physics Part 1-Regular Papers Brief Communications & Review Papers, 2005 **44**(12): p. 8519–8524.

20) Lee, W. H. and Su, C. Y. *Characterization of silver interdiffusion into (Zn,Mg)TiO_3 + x : Bi : Sb multilayer ceramic capacitor*; Journal of the American Ceramic Society, 2007 **90**(8): p. 2454–2460.
21) Sohn, J. H.; Inaguma, Y.; Yoon, S. O.; Itoh, M.; Nakamura, T.; Yoon, S. J. and Kim, H. J. *Microwave dielectric characteristics of ilmenite-type titanates with high Q-values*; Japanese Journal of Applied Physics, 1994 **33**: p. 5466–5470.
22) Vegard, L. *Die Konstitution der Mischkristalle und die Raumfüllung der Atome*; Zeitschrift für Physik, 1921 **5**(1): p. 17–26.
23) Yang, J. and Swisher, J. H. *The phase stability of $Zn_2Ti_3O_8$*; Materials Characterization, 1996 **37**(2–3): p. 153–159.
24) *ICSD powder diffraction card 00–026–1500: $ZnTiO_3$.*
25) *ICSD powder diffraction card 00–025–1164: Zn_2TiO_4.*
26) *ICSD powder diffraction card 00–021–1274: TiO_2.*
27) *ICSD powder diffraction card 00–032–0118: $Bi_2Ti_2O_7$.*
28) *Electroceramics*; 2nd ed.; Moulson, A. J. and Herbert, J. M.; John Wiley & Sons: Chichester, 2003; p 304–306.
29) Grigoryan, R. A. and Grigoryan, L. A. *Synthesis and properties of Zn_2TiO_4-Zn_2SnO_4-$ZnFe_2O_4$ solid solutions*; Inorganic Materials, 2004 **40**(3): p. 295–299.
30) Grigoryan, R. A. and Grigoryan, L. A. *Electrical properties of $Zn_2(Ti_aSn_b)_{1-x}Zr_xO_4$ solid solutions*; Inorganic Materials, 2010 **46**(1): p. 55–59.

Chapter 3.4

Multilayer capacitors with high-ε_r C0G dielectrics and Cu electrodes

3.4.1. Introduction to (Ba,Sr,Ca)O-$(Nd,Gd)_2O_3$-TiO_2 ceramics

As discussed in the introduction chapter, the cost of multilayer capacitors (MLCC) can be reduced by using base metals like copper or nickel instead of silver or silver palladium alloys. The disadvantage of copper or nickel is that the MLCCs have to be sintered in sintering atmospheres with low oxygen partial pressure to prevent the metals to oxidize during the sintering process.[1] However, it is still very interesting to use copper in MLCCs because of its low specific resistivity. MLCCs with very low equivalent series resistance (ESR) values can be produced and they can be used in applications which operate at very high frequencies. The aim is to develop a dielectric material which has a high relative permittivity (ε_r) to enable production of small case size multilayer capacitors. The dielectrics should have stable temperature characteristics towards electrical properties in order to make reliable temperature stable C0G MLCCs.

Dielectrics which consists of high ε_r, high *Q*-factor and near zero temperature coefficient of capacitance (TCC) can be made with a wide variety of dielectrics, see Chapter 3.1 for the details. For C0G MLCCs with an ε_r larger than 60, BaO-Nd_2O_3-TiO_2 and other rare earth based BaO-Re_2O_3-TiO_2 dielectrics are often used.[2–5]. However, these dielectrics ceramics can only be sintered at temperatures of 1300 °C or more. Therefore the inner electrodes of MLCCs have to be platinum, palladium or palladium rich silver-palladium alloys.[4, 6–7] In order to use Cu the sintering temperature has to be below the melting point of copper. Furthermore, sintering has to take place in an atmosphere of low oxygen partial (pO_2). Since copper must be protected from oxidation, sintering is performed in a reducing atmosphere. This requirement posed some limitations on the selection of dielectrics and sintering aids, because the ceramics should be able to withstand a reducing atmosphere during

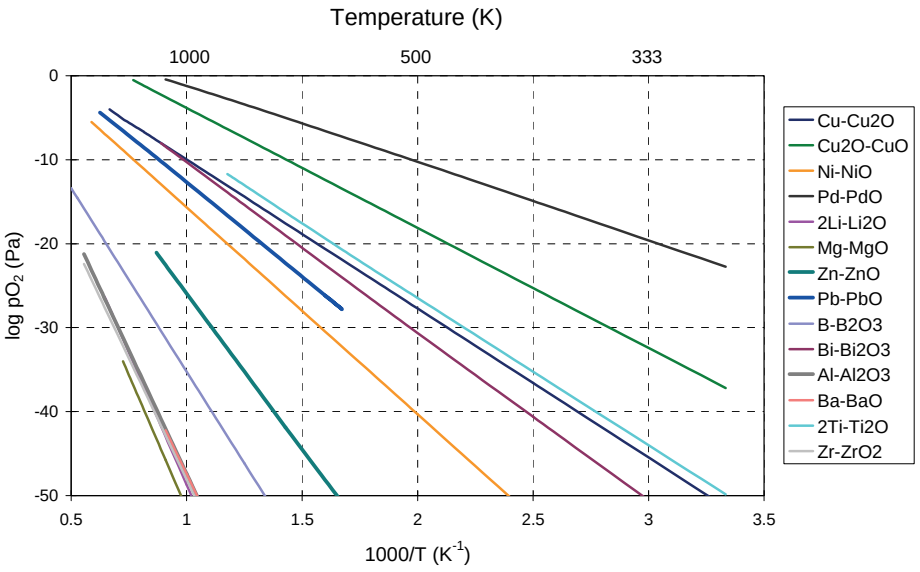

Figure 3.4.1: The oxidation stability of various metal oxides.[8–9]

sintering. This condition limits the choice of metal oxides that can be used in the dielectric composition. Consequently, the metal oxide must be thermodynamically stable at high temperatures and low oxygen partial pressure (pO_2), see Figure 3.4.1.

The first generation MLCCs with copper electrodes were based on $(Pb_{1.0}Ca_{0.01})[(Mg_{1/3}Nb_{2/3})_{0.8}Ti_{0.125}(Ni_{1/2}W_{1/2})_{0.075}]O_{3.01}$, $Pb(Mg_{1/3}Nb_{2/3})O_3$-$PbTiO_3$ and $0.95Pb(Mg_{1/3}Nb_{2/3})O_3$-$0.05PbTiO_3$-MgO-CaO-$PbSiO_3$ ceramics.[10–11] These multilayer capacitors had large capacitance deviations, ±15% or more when measured between -55 and 125 °C, compared to capacitance values measured at 25°C. Other examples of MLCCs with copper electrodes, having a high capacitance drift, were based on $BaTiO_3$ ceramics.[12] The sintering temperature of $BaTiO_3$ was lowered below the melting point of copper by adding a ZnO-B_2O_3 flux together with Li_2O. The ceramics were sintered at 1000 °C for 2 hrs in an atmosphere in which the pO_2 was $4.7.10^{-11}$ atm. The dielectric ceramics had a ε_r of 2270, a tan δ of about 0.01. These ceramics had a large capacitance drift, which was nonetheless within ±15% between -55 and 125 °C.

Multilayer capacitors with copper electrodes having C0G properties have been reported in literature. An example is a material based on BaO-SrO-SiO_2-ZrO_2 with small additions of Al_2O_3 and TiO_2. This dielectric was sintered near 1000 °C and had a relative permittivity of 15. The TCC values of these dielectrics were within ±30 ppm/°C.[13] Temperature stable C0G dielectrics can be made with $CaZrO_3$ ceramics. When $CaZrO_3$ is sintered together with a $LiNO_3$-SiO_2-$CaCO_3$-TiO_2

sintering aid, MLCCs with a ε_r of 28 and a τ_ε of -45 ppm/°C can be produced.[14–15] Dielectrics based on $CaZrO_3$ at which a Li_2O-B_2O_3 compound, SiO_2 and small additions of MnO_2 and $SrTiO_3$ were added, produced multilayer capacitors with a ε_r of 25, *Q*-factor values of 2500 and TCC between -10 and +20 ppm/°C between -55 and 125 °C.[16] Multilayer capacitors with copper electrodes were also made based on $MgTi_{0.975}O_{3+\delta}$ dielectric ceramics at which 8.24 mol% LiF flux was added. This dielectric material had a low relative permittivity of 18.[17] A study on MLCCs made with a $0.84Ba_5Nb_4O_{15}$ - $0.16BaNb_2O_6$ + 0.3 wt% B_2O_3 composition revealed that the ceramics, when sintered at 950 °C for 2 hrs, had C0G properties with a ε_r of 42, a *Q.f*-factor of 28000 GHz and τ_ε of 0 ppm/°C.[18] All mentioned dielectric ceramics are based on materials having a relatively low permittivity, the ε_r did not exceed 50, while dielectrics based on BaO-Re_2O_3-TiO_2 or BaO-PbO-Nd_2O_3-TiO_2 can achieve higher permittivity values up to 100, see Table 3.1.2. So far no reports are known about high permittivity C0G type dielectrics that are suitable for co-sintering with copper inner electrodes to produce MLCCs.

Table 3.4.1: Composition of (Ba,Sr,Ca)O-$(Nd,Gd)_2O_3$-TiO_2.

Component	Mol Fraction
BaO	0.231
CaO	0.050
SrO	0.020
Nd_2O_3	0.131
Gd_2O_3	0.103
TiO_2	1.000

In this chapter a commercial dielectric powder (Ba,Sr,Ca)O-$(Nd,Gd)_2O_3$-TiO_2 was used. The exact composition of the dielectric powder is shown in Table 3.4.1. The ceramics of the (Ba,Sr,Ca)O-$(Nd,Gd)_2O_3$-TiO_2 powder have a ε_r of approximately 80 and a TCC of 16 ppm/°C. However, these ceramics have to be sintered at a temperature between 1150 and 1200 °C and sintering is normally carried out in air. Because sintering temperature had to be lowered below the melting point of copper, sintering aids based on Li_2O-MgO-SiO_2 were prepared to add to (Ba,Sr,Ca)O-$(Nd,Gd)_2O_3$-TiO_2. In order to withstand the low pO_2 during sintering CuO, which act as an acceptor, was added to ceramic composition. The new composition was tested in MLCCs with copper electrodes.

3.4.2. Experimental - Powders, CDCs and MLCCs

Powder, Pellet and Ceramic Disc Capacitor preparation. Sintering aids based on Li_2O-MgO-SiO_2 were prepared by mixing Li_2CO_3 (Sigma Aldrich, 99%), MgO (Merck, 99%) and SiO_2 (Aerosil R972, Degussa) in 2-propanol using a PE flask with 2 mm YTZ beads. After 16 hours of mixing and milling were the powders calcined at 900 °C for 2 hours in an air atmosphere. After calcination were the powders milled to a D_{50} of 0.4 μm.

The powders were made starting from a commercial dielectric powder based on a (Ba,Sr,Ca)O-$(Nd,Gd)_2O_3$-TiO_2 composition (AD850DZ, Ferro), the sintering additives Li_2O-MgO-SiO_2 and CuO (Pan-Continental Chemical Co, 99%). Slurries were prepared by weighing the powders in a PE flask with 2 mm YTZ milling beads. The milling medium was a mixture of water and ethanol in the ratio 1:1. After mixing and the slurry was milled to a D_{50} of 1 μm. Before pressing the powders were mixed with a glycerine solution (10 wt% in water). Powder, 400 mg, was weighed and thereafter pressed uniaxially (Fontijne) into a pellets of 10 mm in diameter and 1 mm thickness. The samples used to evaluate the sintering temperature were sintered in a gradient tube kiln (Carbolite) in air. Thereafter silver terminations were applied on the discs using Ag paste (Yageo) and fired at 750 °C in a conveyor furnace (BTU). To study the dielectric material properties the samples were sintered in a reducing atmosphere, N_2/H_2O. Terminations of copper were applied using a copper paste (Yageo). The pellets with the copper electrodes were co-fired in a tube kiln (Carbolite) at 1040 °C in an N_2/H_2O atmosphere for 1 hour. Pellets with silver electrodes applied at room temperature were made of a silver paste (Leitsilber 200, Degussa).

MLCC preparation. Green MLCC chips were produced on regular production equipment at Yageo in Roermond, the Netherlands, as described in Chapter 2. The 0603 MLCCs consisted of 5 or 15 electrode layers in a brick with an overall size of 1.6 mm x 0.8 mm x 0.8 mm. The 1206 MLCCs consisted of 4 or 29 electrode layers in a brick with an overall size of 3.2 mm x 1.6 mm x 0.8 mm. The dielectric thickness varied between 20 and 66 μm depending on the MLCC construction. The electrodes were made with a copper paste (Yageo) and the electrode thickness was 4 or 10 μm. The MLCCs were sintered in a reducing atmosphere of wet N_2 at 1040°C for 1 hour. Copper terminations (Yageo) were applied on the MLCCs.

3.4.3. Results and Discussion

3.4.3.1. Material development

A commercial NP0 powder of Ferro based on (Ba,Sr,Ca)O-$(Nd,Gd)_2O_3$-TiO_2, which will be called K85 hereafter, was used as main dielectric material. The exact formula of K85 is given in Table 3.4.1. Pellets of K85 powder were sintered at 1200 °C in air and thereafter the crystal structure of the ceramics was determined by X-ray diffraction analysis. X-ray analysis of Figure 3.4.2 revealed that these ceramics have an orthorhombic $Ba_{4.5}Nd_9Ti_{18}O_{54}$ crystal phase.[19] No other crystal phases were observed in the XRD pattern and if other crystal phases were present than the amount would be so small that is was undetectable.

The K85 dielectrics can be sintered at sintering temperatures between 1150 and 1200 °C. To use K85 in MLCCs with copper electrodes some adjustments to enhance the material properties must be carried out. First the sintering temperature had to be decreased below the melting point of copper metal, 1084 °C, by adding sintering aids to K85. Secondly, BaO-Re_2O_3-TiO_2 ceramics are easily reduced when sintered in an atmosphere with a low oxygen partial pressure. The addition of the sintering aids should produce new dielectric ceramics which are reduction stable and acquire the desired C0G properties.

Table 3.4.2: Composition of GL1, GL2 and GL3 in mol%.

	GL1	GL2	GL3
Li_2O	6	30	25
MgO	39	18	11
SiO_2	55	52	64

In order to decrease the sintering temperature of the ceramics compositions based on of Li_2O-MgO-SiO_2 were chosen. These elements are reduction stable. The Li_2O-MgO-SiO_2 glasses react with K85 through liquid phase sintering without influencing the C0G characteristics too much.

Three sintering aids (SA), see Table 3.4.2 for the compositions, in the material system Li_2O-MgO-SiO_2 were investigated. The sintering compounds are called respectively GL1, GL2 and GL3. In Figure 3.4.3 the three Li_2O-MgO-SiO_2 compositions are shown in the phase diagram. The GL1 glass was a composition with a low Li^+ content. The other 2 glass compounds had higher Li^+ contents. Furthermore, GL3 is a composition, which is situated in the eutectic point at 930 °C.

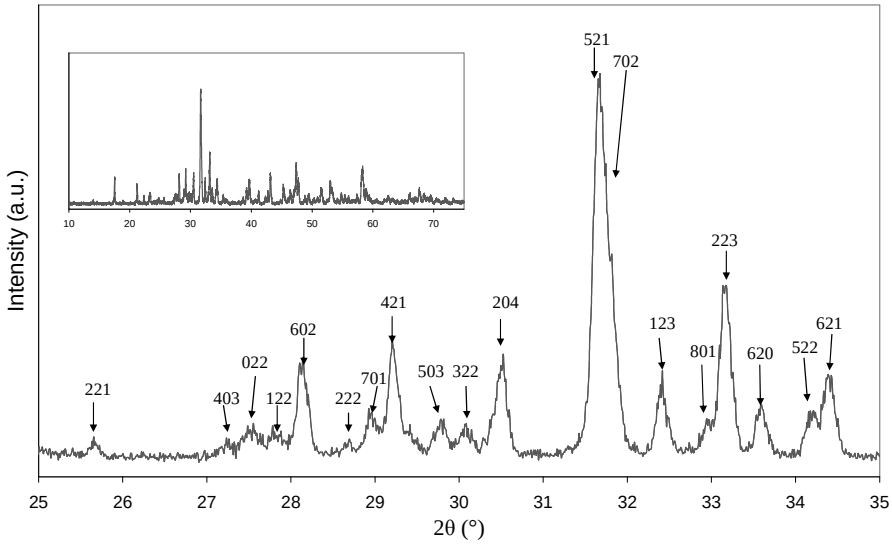

Figure 3.4.2: X-ray diffraction pattern of commercial AD850DZ (K85) powder sintered at 1200°C. The XRD pattern can be fully indexed using the orthorhombic $Ba_{4.5}Nd_9Ti_{18}O_{54}$ phase to indicate single phase ceramics.

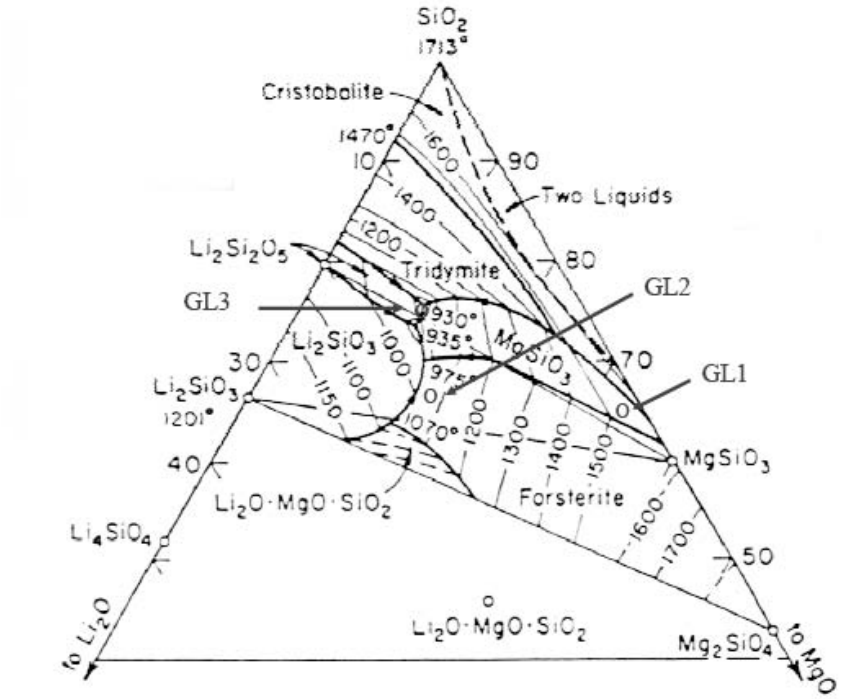

Figure 3.4.3: Phase diagram of Li_2O-MgO-SiO_2 in wt%.[20]

Table 3.4.3: Density (g/cm^3) of K85 + *5* wt % SA pellets sintered in air at various temperatures.

Material	ρ_{th}	1200 °C	1130 °C	1100 °C	1060 °C	1030 °C
K85	5.62	5.63	p	p	p	p
K85+5 % GL1	5.48	*	5.09	5.01	p	p
K85+5 % GL2	5.45	*	4.82	4.82	4.82	4.79
K85+5 % GL3	5.45	*	5.07	5.06	4.98	4.81

*= No sample, p = open porosity

In Tables 3.4.3 and 3.4.4 the results of a series of dense samples K85 + 5 wt% SA, where SA is GL1, GL2 or GL3, respectively, are shown. The samples were all fired for one hour in an air atmosphere at various temperatures. The K85 dielectrics sintered at 1200 °C were dense after firing and the density of these samples were equal to the values supplied by Ferro. In Table 3.4.3 it is shown that K85 was porous when sintered at temperatures equal to or below 1130 °C. Addition of Li_2O-MgO-SiO_2 to K85 decreased the sintering temperature for all three glass compounds. However, the addition of GL1 did not accomplish sintering temperatures below 1100 °C. Therefore this glass compound was not used for further evaluation. The addition of GL2 and GL3 to K85 was more successful, because the ceramics could be sintered dense at 1030 °C, which is 50 °C below the melting point of copper.

Table 3.4.4: Electrical properties of K85 + *5* wt% SA sintered in air at various temperatures and electrical properties measured at 1 MHz/1 V_{rms}.

	1200 °C		1130 °C		1100 °C		1060 °C	
Material	ε_r	Tan δ (10^{-4})	ε_r	Tan δ (10^{-4})	ε_r	Tan δ (10^{-4})	ε_r	Tan δ (10^{-4})
K85	80	2	-	-	-	-	-	-
K85+ 5 % GL2	-	-	55	10	55	11	-	-
K85+ 5 % GL2	-	-	53	8	53	8	58	9
K85+ 5 % GL2	-	-	63	7	53	8	58	10

- = pellet not fabricated or pellet not fully dense

The electrical properties of K85, sintered at 1200°C, were evaluated. These dielectrics had a high relative permittivity of 80 and a low loss factor tan δ of 2.10^{-4}. When Li_2O-MgO-SiO_2 additives were added to K85, the ε_r values dropped and tan δ values increased. This was probably due to the low relative permittivity values of Li_2O-MgO-SiO_2 compounds, which are approximately between 5 and 10. Moreover,

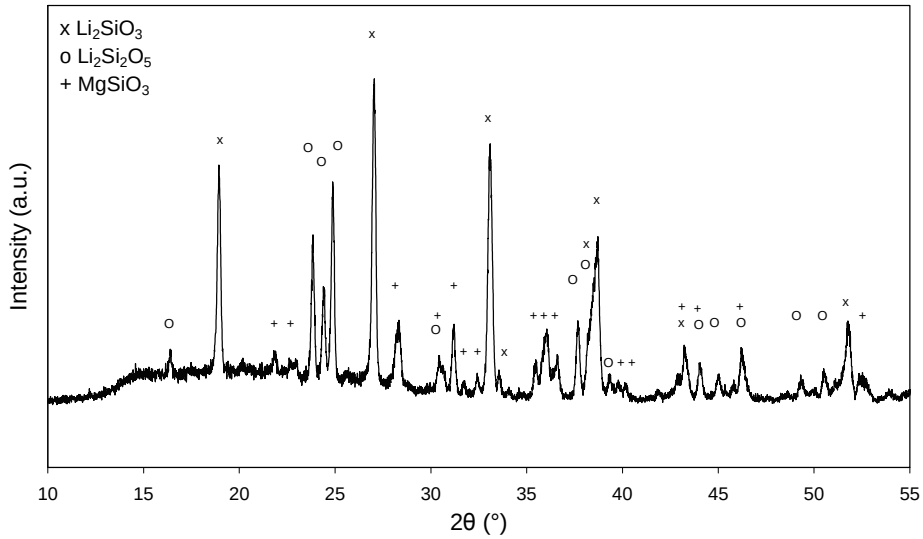

Figure 3.4.4: X-Ray diffraction pattern of Li_2O-MgO-SiO_2 compound GL2, after calcination at 900°C.

these materials also have higher loss factors. When ε_r and the *Q*-factor ($Q = 1/\tan \delta$) of K85 and Li_2O-MgO-SiO_2 are known, the average permittivity and tan δ can be calculated by the logarithmic mixing rules Equations 3.1.3 and 3.1.4, respectively. The two ceramic compositions that contained GL2 or GL3 had approximately equal values for ε_r and tan δ, when sintered at 1060 °C in air. The relative permittivity of these compounds was 58. Furthermore the tan δ values of both compounds was similar, with values between $9 \cdot 10^{-4}$ and $10 \cdot 10^{-4}$. However, the electrical properties of the dielectrics were equal for both sintering aids. The lithium-rich composition GL2 was chosen for further development in order to be sure that dense ceramics will be obtained.

The powders of GL2 sintering aid were made by calcination of a mixture of components at 900 °C for 2 hours in air. The crystal phases of the calcined powder were identified by X-ray powder diffraction analysis, see Figure 3.4.4. The analysis revealed that 3 crystal phases were present in the GL2 powder. The three crystal structures were Li_2SiO_3,[21] $Li_2Si_2O_5$ [22] and $MgSiO_3$.[23] The fact that these crystal phases were found in the powder is in agreement with the phase diagram of Li_2O-MgO-SiO_2 compounds, see Figure 3.4.3.

In Table 3.4.5 and Table 3.4.6 the results of ceramic compositions K85 + *x* wt% GL2, with *x* = 0, 3, 4, 5 and 6, are shown. The pellets were all sintered for one hour in air at temperatures varying between 1030 and 1130 °C. For K85 + *3* wt% GL2 the minimum sintering temperature was 1100 °C. In K85 + *4* wt% GL2 the sintering

temperature could be decreased to 1030 °C. Thus a minimum amount of *4* wt % GL2 to K85 was needed to reach the minimum sintering temperature. Higher amounts of GL2 did not help to decrease the sintering temperature any further.

Table 3.4.5: Densities (g/cm^3) of K85 + *x* wt% GL2 ceramics sintered in air.

Material	$\rho_{th.}$	1210 °C	1130 °C	1100 °C	1060 °C	1030 °C
K85	5.62	5.63	p	p	p	p
K85+3 % GL2	5.53	*	5.12	5.08	p	p
K85+4 % GL2	5.50	*	5.04	5.03	5.01	4.92
K85+5 % GL2	5.47	*	4.82	4.82	4.82	4.79
K85+6 % GL2	5.45	*	4.72	4.72	4.71	4.75

*no sample, p = open porosity

The density of the pellets decreased to lower values when the addition of GL2 was increased from *3* to *6* weight percent. The theoretical density of GL2 composite is approximately 2.55 g/cm^3, while K85 has a density of 5.6 g/cm^3. Mixing these two materials will result in lower density for the mixture compound, when it is assumed that no substantial reaction between the materials occurs during sintering. The GL2 phases would then be located at the grain boundaries and at triple points in the ceramic matrix.

The relative permittivity decreased when the amount of GL2 is increased due to lower relative permittivity of $LiSiO_3$, $Li_2Si_2O_5$ and $MgSiO_3$. The logarithmic mixing rules Equation 3.4.1 and 3.4.2 predict that a mixture of a high and low permittivity dielectric will result in an average ε_r with a value somewhere between the highest and lowest ε_r. In this case the average ε_r decreases from 80 for K85 to 54 for K85 + *6* wt% GL2. The decrease of ε_r is significant, indicating that the relative permittivity of the GL2 mixture is very low and near 1. However, when the theoretical ε_r is calculated for K85 + *6* wt% GL2 with ε_r of GL2 of about 5, the relative permittivity would be approximately 70. The fact that lower values were found for these samples can be attributed to unknown reactions between K85 and GL2 components. Probably elements of K85 diffused into one or more components of GL2 during sintering. This led to larger phase fractions in the ceramic compositions, thus lowering the average permittivity. Another argument could be that the glass from the Ag paste, which was located between the ceramics and the Ag termination, may have contributed to a lower permittivity than expected.

Table 3.4.6: Electrical properties of K85 + *x* wt% GL2 sintered in air at various temperatures, and measured at 1 Mhz/1 V_{rms}.

	1210 °C		1130 °C		1100 °C		1060 °C		1030 °C	
Material	ε_r	Tan δ (10^{-4})	ε_r	Tan δ (10^{-4})	ε_r	Tan δ (10^{-4})	ε_r	Tan δ (10^{-4})	ε_r	Tan δ (10^{-4})
K85	80	2	-	-	-	-	-	-	-	-
K85+ 3 % GL2	-	-	65	10	65	8	-	-	-	-
K85+ 4 % GL2	-	-	61	8	60	13	57	24	56	35
K85+ 5 % GL2	-	-	63	8	53	8	58	9	x	x
K85+ 6 % GL2	-	-	53	7	54	6	54	5	54	8

- = pellet not fabricated or pellet not fully dense, x pellet not measured.

The sintering properties of K85 + *x* wt% GL2 ceramics are quite sensitive to the partial oxygen pressure. This can be illustrated by applying various terminations onto the pellets of K85 + *4* wt% GL2 ceramics. First, these pellets were sintered at 1040 °C for one hour in a wet N_2 atmosphere. Then three types of terminations were applied onto the pellets. The Leitsilber paste was applied at room temperature in air. Thus, the dielectric properties of the ceramics were not changed by any heat treatment. The Ag paste was applied on the sintered pellets by curing the paste at 750 °C for one hour in air. The ceramic disc capacitors (CDC) with the Cu terminations were processed in two ways. In the first method the Cu paste was applied onto the pellets after they had been sintered in air. Thereafter the CDCs with the dried Cu terminations were cured at 880 °C for one hour in a dry N_2 atmosphere. In the second approach the Cu paste was printed on both sides of the pellets before sintering. Then the CDCs were co-fired at 1040 °C in a wet N_2 atmosphere. The influence of various processes to apply different terminations showed that curing conditions have a large effect on the electrical properties, as can be noticed in Table 3.4.7.

Table 3.4.7: Results of CDCs, made of K85 + *4* wt% GL15 dielectric ceramics, with various terminations applied at different temperatures and atmospheres.

Termination Material	Curing Temperature (°C)	Curing Atmosphere	ε_r	Tan δ	IR (Ω)
Leitsilber	20	Air	132	0.230	$3 \cdot 10^6$
Ag-paste	750	Air	63	0.003	$1.5 \cdot 10^8$
Cu-paste	880	N_2	679	0.380	$< 10^5$
Cu-paste	1040*	N_2/H_2O	59	0.00025	$2.8 \cdot 10^9$

*cofiring

The CDCs made with Leitsilber electrodes had an ε_r of 132, tan δ of $2300 \cdot 10^{-4}$, and an insulation resistance (IR) of $3 \cdot 10^6$ Ω. The CDCs, onto which copper terminations were applied at 880 °C in a N_2 atmosphere, gave the following results: ε_r of 697, tan δ of $3800 \cdot 10^{-4}$, IR << 10^5 Ω. The process in which Cu paste was cured in a reducing atmosphere yielded higher ε_r and tan δ values. The large values of ε_r and tan δ indicate that the ceramics had changed, compared to the same ceramics sintered in air. This can be explained as follows. In a reducing atmosphere oxygen vacancies can be formed in Ba-Re_2O_3-TiO_2 and (Ba,Sr,Ca)O-$(Nd,Gd)_2O_3$-TiO_2 ceramics. The formation of these oxygen vacancies and conduction electrons during a reduction reaction can be expressed, using the Kröger-Vink notation, by:[24]

$$O_o \quad \leftrightarrow \quad \tfrac{1}{2}\, O_2 + V_o^{\cdot\cdot} + 2e' \qquad (3.4.3)$$

and

$$K_{red} = [V_o^{\cdot\cdot}][e']^2\sqrt{pO_2}/[O_o] \sim [V_o^{\cdot\cdot}]\,[e']^2\sqrt{pO_2} \qquad (3.4.4)$$

where K_{red} is the equilibrium constant. Depending on pO_2 more or less oxygen vacancies and conduction electrons are formed. When a higher concentration of charge carriers is present in the ceramics, its conductivity is increased. In this way the drop of IR in both experiments can also be explained, because the conduction electrons contribute to the decrease of insulation resistance. However, during re-oxidation the following equilibrium reactions occurred, which are described by:

$$V_o^{\cdot\cdot} + \tfrac{1}{2}\, O_2 \quad \leftrightarrow \quad O_o + 2h^{\bullet} \qquad (3.4.5)$$

and

$$K_{ox} = [O_o]\,[h^{\bullet}]^2/[V_o^{\cdot\cdot}]\,\sqrt{pO_2} \;\sim\; [h^{\bullet}]^2/[V_o^{\cdot\cdot}]\sqrt{pO_2} \qquad (3.4.6)$$

where K_{ox} is the equilibrium constant. The holes, $h^{\bullet}$, created during oxidation (Eq.3.4.5), recombine with conduction electrons, e', (Eq.3.4.3) to yield ceramics with less or nil charge carriers. The re-oxidation of the ceramics occurred when the CDCs, onto which silver terminations were applied, were cured at 750 °C in air. The re-oxidized ceramics yielded a ε_r of 63, a tan δ of $30 \cdot 10^{-4}$ and IR of $1.5 \cdot 10^8$ Ω. These results clearly indicate that good dielectrics can be established by re-oxidation. In any case, the best dielectric properties were achieved when the pellets were co-sintered with copper electrodes.

Figure 3.4.5: Schematic construction of a MLCC made of K85 + 5wt% GL15 and Cu electrodes after sintering at 1040 °C in wet N_2.

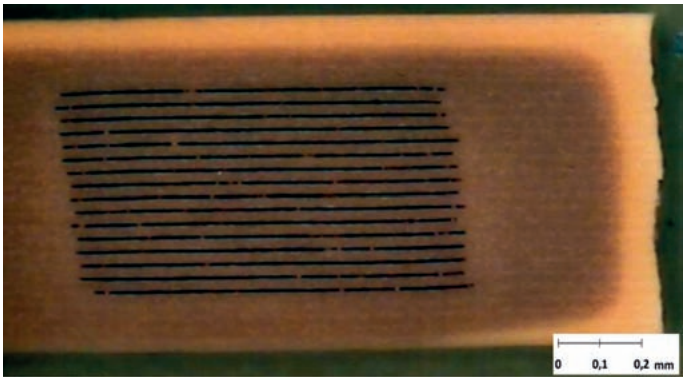

Figure 3.4.6: Cross section of MLCC of K85 + 5 wt% GL15 and Cu electrodes fired at 1040 °C in wet N_2.

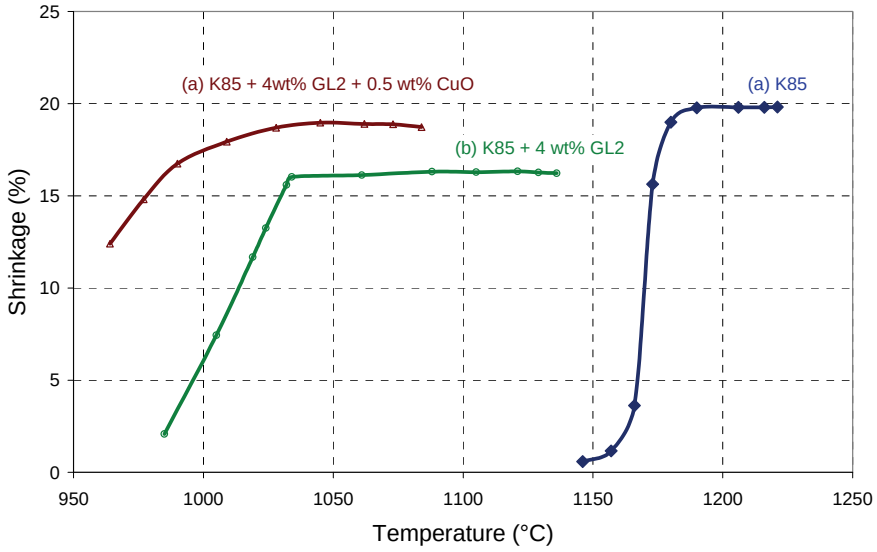

Figure 3.4.7: Sintering characteristics and densification of (a) K85, (b) K85+ *4* wt% GL2 and (c) K85 + *4* wt%G L2 + *0.5* wt% CuO.

Table 3.4.8: Density and electrical properties of K85 + *4* wt% GL2 + *y* wt% CuO, in which *y = 0, 0.5, 1* and *2*, were co-fired with Cu terminations at 1040 °C in N_2/H_2O.

Material	ρ_{th} (g/cm^3)	Density (g/cm^3)	ε_r	Tan δ (10^{-4})	IR 20°C/50V (Ω)	TCC (ppm/°C)
K85+4 % GL2	5.50	4.97	66	2.8	$1 \cdot 10^{10}$	*
K85+4 % GL2+0.5% CuO	5.51	5.20	65	2.8	$4 \cdot 10^{9}$	-18
K85+4 % GL2+1.0 % CuO	5.51	5.15	69	3.5	$1 \cdot 10^{10}$	-16
K85+4 % GL2+2.0 % CuO	5.52	5.30	59	2.2	$3 \cdot 10^{10}$	-15

* = TCC out of specification with a non linear curve

MLCCs with K85 + 5wt% GL2 dielectrics and copper electrodes were fabricated and these multilayer capacitors were sintered at 1040 °C in a wet N_2 atmosphere. It was observed that Cu was migrated from the electrodes into the ceramics during sintering. In Figure 3.4.6 this phenomenon can be clearly observed in the cross-section of a sintered MLCC brick. The copper, which diffused from the electrodes into the ceramics colored the ceramics darker between and near the electrodes. Where no copper diffused, the near-surface area of the brick was colored light brown. Less clearly visible, but schematically drawn in Figure 3.4.4, the diffusion of copper from the inner electrodes into the dielectric caused an extra shrinkage of the ceramics in the active area of the MLCC. Therefore the MLCCs had a peculiar shape. The middle of the MLCC was thinner than the outside of the brick. To avoid this peculiar shape the diffusion of Cu during sintering between copper electrode and dielectrics should be avoided. The addition of Cu^{+} or Cu^{2+} into the ceramics was needed to avoid inhomogeneous $Cu^{1+/2+}$ diffusion into the ceramics. However, the presence of copper ions in the ceramics improved the dielectric properties, as can be observed in Table 3.4.7 in the results on MLCC co-sintered with copper outer terminations. In these samples a large $Cu^{1+/2+}$ source was available, which diffused partly into the ceramics. The dielectric properties were improved when $Cu^{1+/2+}$ ions were incorporated at the Ti^{4+} site in the crystal lattice as $Cu^{1+/2+}$ ions will act as an acceptor. For these reasons CuO was also added to K85 + *x* wt% GL2 ceramics.

In Figure 3.4.7 the shrinkage behavior of K85, K85 + *4* wt% GL2 and K85 + *4* wt% GL2 + *0.5* wt% CuO ceramics with respect to sintering temperature is shown. The K85 + *4* wt% GL2 ceramics had a minimum sintering temperature of 1030 °C and reached a maximum shrinkage of 16%. When 0.5 wt % CuO was added to K85 + *4* wt% GL2 the sintering temperature could be reduced further to approximately 1000 °C. The pellets of K85 + *4* wt% GL2 + *0.5* wt% CuO had a maximum shrinkage of 19 %. The difference in final shrinkage of the pellets was explained by the difference in final density of the ceramics as described in

Table 3.4.5. The K85 + *4* wt % GL2 ceramics were probably not completely dense. Furthermore, the pellets of K85 + *4* wt% GL2 + *0.5* wt% CuO shrunk 19% and these ceramics had a relative density of 94 %, based on the calculated values of Table 3.4.8. The difference in density of the ceramics was an extra argument to explain the concave shape of the MLCCs as shown in Figure 3.4.5.

The effect of CuO on densities and electrical properties of the CDCs based on K85 + *4* wt% GL2 ceramics are listed in Table 3.4.8. The CDCs were co-sintered with Cu terminations at 1040 °C in a wet N_2 atmosphere. The densities of the pellets reached a relative density between 90.4 and 96.0 %. The relative permittivity of the samples ranged from 59 to 69, depending on the amount of CuO present in the ceramic composition. The tan δ values were low with an average of $3 \cdot 10^{-4}$ for all samples. The insulation resistance of the CDCs were measured at 50 V for 1 sec and these values varied a little and the average IR was $1 \cdot 10^{10}$ Ω. The TCC curve of K85 + *4* wt% GL2 CDCs was out of the C0G specification and they had a non-linear shape.

The peculiar shape of the TCC curve was caused by the higher porosity of the ceramics. The CDCs made with dielectrics containing CuO exhibited a linear dependency of capacity as the temperature varied from -55 to 125 °C. With an increasing concentration the TCC shifted from -18 to -15 ppm/°C when the CuO concentration in the ceramics increased from 0.5 to 2 wt%.

3.4.2.1. Evaluation of MLCCs with Cu electrodes

The dielectric composition K85 + *4* wt% GL2 + *0.5* wt% CuO was evaluated in 0603 and 1206 MLCCs. Four types of MLCCs were prepared and the used constructions are given in Table 3.4.9. The ceramic foil, which was used to make these MLCC samples, had a thickness of approximately 22 μm after sintering. By stacking the foils the ceramic thickness was increased from 22 μm to 66 μm. The electrode thickness of the first 2 samples was 10 μm, which is larger than in samples 3 and 4. This is due to different screen-printing screens used for printing the Cu paste. One type of Cu paste, without ceramic additives, was used in all four different MLCC samples. Terminations were applied onto the MLCC bricks, by curing the Cu termination paste at 700 °C in dry N_2, after sintering the MLCC bricks at 1040 °C in wet N_2.

The electrical values were measured at 1 MHz and 1 V_{rms} for the first 3 samples. However, the fourth sample was measured at 1 kHz and 1 V_{rms} according to the guidelines of EIA,[25] because capacitances above 1 nF have to be measured with an AC current of 1 kHz and 1 V_{rms}. The results of these measurements are shown in Table 3.4.6. They illustrate that a relative permittivity of 70 was achieved. Furthermore, the dielectrics had a low tan δ with values between $2 \cdot 10^{-4}$ and $4 \cdot 10^{-4}$.

Table 3.4.9: Overview of the MLCC samples regarding construction and materials.

No	Dielectric ceramics	Electrode material	Caze Size	No. electrodes	Dielectric thickness (μm)	Electrode thickness (μm)
1	K85+4% GL2+0.5% CuO	Cu	0603	5	66	10
2	K85+4 % GL2+0.5% CuO	Cu	0603	15	42	10
3	K85+4 % GL2+0.5% CuO	Cu	1206	4	22	4
4	K85+4 % GL2+0.5% CuO	Cu	1206	29	20	4

The *Q.f* factors of these dielectrics were between 2000 and 8000 MHz. The TCC of all samples are within C0G specification and were between 12 and 30 ppm/°C in the range between -55 and 125 °C.

As discussed in section 3.3 the insulation resistance (IR) and the time constant (τ) are important features of a capacitor. For MLCC capacitors it is recommended by MLCC manufacturers like Yageo, that the time constant would be at least 1000 seconds at 20 °C and exceed 100 seconds at 140 °C. The insulation resistance of the capacitor should be temperature stable in order to function well in electronic equipment. The time constant, τ_{20}, for sample numbers 1 and 2 were 150 and 155 seconds, respectively, when measured at 20 °C. This is less than required. The time constant, τ_{140}, dropped to 45 and 13 seconds for sample 1 and 2, respectively. Although the time constant is small, it is quite stable within the required temperature range.

Table 3.4.10: The electrical properties of the MLCC samples sintered at 1040 °C in wet N_2.

Sample	Sintering Temperature (°C)	Capacitance 1MHz/1V (pF)	ε_r	Tan δ (10^{-4})	TCC (ppm/°C)	IR 20°C/50V (Ω)	IR 140°C/50V (Ω)
1	1040	7.5	71	5.0	13	$2 \cdot 10^{13}$	$6.0 \cdot 10^{12}$
2	1040	31.0	71	3.7	30	$5 \cdot 10^{12}$	$4.2 \cdot 10^{11}$
3	1040	185.2	70	1.2	14	$4.7 \cdot 10^{10}$	-
4	1040	1908*	71*	8.0*	12*	$4.5 \cdot 10^{10}$	-

*Measured at 1 kHz/1 V_{rms}.

3.4.4. Conclusions

A material based upon a commercial powder of (Ba,Sr,Ca)O-$(Nd,Gd)_2O_3$-TiO_2 could be sintered below the melting point of copper due to the addition of a Li_2O-MgO-SiO_2 sintering aid. The Li_2O-MgO-SiO_2 compound was a mixture of $LiSiO_3$, $Li_2Mg_2SiO_5$ and $MgSiO_3$. By adding CuO, which was used as an acceptor dopant, reduction stable ceramics were developed that could be used for co-sintering in MLCCs with copper electrodes in a wet nitrogen atmosphere. MLCCs of K85 + *4* wt% Li_2O-MgO-SiO_2 compound + *0.5* wt% CuO had a relative permittivity of 70, *Q.f* of 8000 MHz and a TCC of +15 ppm/°C, which meet the C0G specifications for high frequency applications. The time constant of the capacitors is 150 seconds.

References

1) Kishi, H.; Mizuno, Y. and Chazono, H. *Base-metal electrode-multilayer ceramic capacitors: Past, present and future perspectives*; Japanese Journal of Applied Physics Part 1-Regular Papers Short Notes & Review Papers, 2003 **42**(1): p. 1–15.
2) Suvorov, D.; Valant, M. and Kolar, D. *The role of dopants in tailoring the microwave properties of $Ba_{6-x}R_{8+2/3x}Ti_{18}O_{54}$ R = (La-Gd) ceramics*; Journal of Materials Science, 1997 **32**(24): p. 6483–6488.
3) Fiedziuszko, S. J.; Hunter, I. C.; Itoh, T.; Kobayashi, Y.; Nishikawa, T.; Stitzer, S. N. and Wakino, K. *Dielectric materials, devices, and circuits*; IEEE Transactions on Microwave Theory and Techniques, 2002 **50**(3): p. 706–720.
4) Choi, Y. J.; Park, J. H.; Nahm, S. and Park, J. G. *Middle- and high-permittivity dielectric compositions for low-temperature co-fired ceramics*; Journal of the European Ceramic Society, 2007 **27**(4): p. 2017–2024.
5) Cava, R. J. *Dielectric materials for applications in microwave communications*; Journal of Materials Chemistry, 2001 **11**(1): p. 54–62.
6) Xu, X. *BME COG MLCCs; The High Capacitance Class-I solution*; conference paper CARTS Europe 2007: p. 1–7.
7) Zheng, H.; Reaney, I. M.; Muir, D.; Price, T. and Iddles, D. M. *Composite dielectric ceramics based on BaO-Ln_2O_3-TiO_2 (Ln = Nd, La)*; Japanese Journal of Applied Physics Part 1-Regular Papers Brief Communications & Review Papers, 2005 **44**(5A): p. 3087–3090.
8) *CRC Handbook of Chemistry and Physics*; 75th ed.; Lide, R. L.; CRC Press, Inc.: Boca Raton, FL, 1994; Vol., p 5–72 to 5–75.
9) Wang, S. F.; Dougherty, J. P.; Huebner, W. and Pepin, J. G. *Silver-palladium thick-film conductors*; Journal of the American Ceramic Society, 1994 **77**(12): p. 3051–3072.
10) Kato, J.; Yokotani, Y.; Kagata, H. and Niwa, H. *Multilayer ceramic capacitor with copper electrode*; Japanese Journal of Applied Physics Part 1-Regular Papers Short Notes & Review Papers, 1987 **26**: p. 90–92.
11) Hirakata, K.; Sato, S. I.; Uchikoba, F.; Kosaka, Y. and Sawamura, K. *Multilayer capacitors with copper inner electrodes*; Ferroelectrics, 1992 **133**(1–4): p. 139–144.

12) Song, T. H. and Randall, C. A. *Copper cofire X7R dielectrics and multilayer capacitors based on zinc borate fluxed barium titanate ceramic*; Journal of Electroceramics, 2003 **10**(1): p. 39–46.
13) Mandai H., S. Y., Canner J.P. *Multilayer ceramic NPO capacitors with copper electrode*; Ceramic Transactions, 1989 **15**: p. 313–327.
14) Pollet, M.; Hochart, X. and Marinel, S. *Copper electrodes multilayer ceramic capacitors - Part II - Chips fabrication, optimisation and characterisation*; Journal of Materials Science, 2004 **39**(6): p. 1959–1966.
15) Pollet, M. and Marinel, S. *Copper electrodes multilayer ceramic capacitors - Part I - The dielectric composition*; Journal of Materials Science, 2004 **39**(6): p. 1943–1958.
16) Yoneda, Y.; Kimura, T.; Haratani, T. and Asakura, K. *Reliability and application of low fired multilayer capacitor having copper inner electrode*; conference paper CARTS Europe 1997: p. 106–113.
17) Bernard, J.; Houivet, D.; El Fallah, J. and Haussonne, J. M. *$MgTiO_3$ for Cu base metal multilayer ceramic capacitors*; Journal of the European Ceramic Society, 2004 **24**(6): p. 1877–1881.
18) Kim, D. W.; Kim, B. K.; Je, H. J.; Park, J. G.; Kim, J. R. and Hong, K. S. *Degradation mechanism of dielectric loss in barium niobate under a reducing atmosphere*; Journal of the American Ceramic Society, 2006 **89**(10): p. 3302–3304.
19) *ICSD powder diffraction card 01–070–9069: $Ba_{4.5}Nd_9Ti_{18}O_{54}$.*
20) Murthy, M. K. and Hummel, F. A. *Phase equilibria in the system lithium metasilicate - forsterite -silica*; Journal of the American Ceramic Society, 1955 **38**(2): p. 55–63.
21) *ICSD powder diffraction card 00–029–0829: Li_2SiO_3.*
22) *ICSD powder diffraction card 00–040–0376: $Li_2Si_2O_5$.*
23) *ICSD powder diffraction card 00–022–0714: $MgSiO_3$.*
24) Smyth, D. M. *Comments on the defect chemistry of undoped and acceptor-doped $BaTiO_3$*; Journal of Electroceramics, 2003 **11**(1–2): p. 89–100.
25) EIA-198–1F *Ceramic Dielectric Capacitors Clasess I, II, III and IV - part 1: Characterization and requirements*; 2002

Chapter 3.5

Low equivalent series resistance of temperature stable multilayer capacitors with nickel, copper and silver-palladium electrodes

3.5.1. Introduction and overview of used materials

In battery operated electronic devices like mobile phones, notebooks, personal digital players and personal digital assistant devices, multilayer ceramic capacitors (MLCC) are used which operate at high frequencies. Typically for these applications, which require high reliability and frequency stability, temperature compensating capacitors, encoded C0G, are used to operate at high frequencies. To avoid high losses during operation at high frequencies, typically above 100 MHZ, there is a strong development to decrease the equivalent series resistance (ESR) and equivalent series inductance (ESL) of the multilayer capacitors. The ESR should be as low as possible in these capacitors to avoid much energy dissipation during load. A range of capacitance and frequency stable MLCCs made of various dielectric and electrode materials were already developed and are currently in mass production. But to reduce material costs capacitors are being produced with cheap base metals like copper or nickel, which replace the expensive noble metals palladium or silver-palladium alloys.[1–2]

In literature electrical properties like relative permittivity, quality factor (Q = 1/tan δ), TCC, and reliability of dielectric ceramics for capacitors are published. However, almost nothing is published about the ESR performance of MLCCs in relation to high permittivity dielectrics and base metal electrodes (BME) like copper and nickel. It is interesting to know if MLCCs with nickel electrodes perform equal to or better than MLCC with other metals like silver, silver-palladium or copper with

regard to ESR characteristics. Because the ESR performance at high frequencies is related to the resistivity of the electrode metal, a difference between ESR outputs was expected. Therefore MLCCs were produced with silver-palladium alloys, copper and nickel electrodes to make the evaluation in ESR performance. Because MLCCs were made with various metals, various dielectrics powders were used, which could be co-sintered with the respective metals.

Table 3.5.1: Sample overview of dielectrics, electrode materials and sintering conditions.

Code	Dielectrics	Electrode	Sintering temperature (°C)	Sintering atmosphere
K85	$BaO\text{-}(Nd,Gd)_2O_3\text{-}TiO_2$	Pd	1300	Air
K80	$BaO\text{-}(Nd,Gd)_2O_3\text{-}TiO_2$ + SA 1	80Ag/20Pd	1080	Air
K75	$BaO\text{-}(Nd,Gd)_2O_3\text{-}TiO_2$ + SA 2	90Ag/10Pd	950	Air
K72	$BaO\text{-}(Nd,Gd)_2O_3\text{-}TiO_2$ + SA 2	95Ag/5Pd	950	Air
K70	$BaO\text{-}(Nd,Sm)_2O_3\text{-}TiO_2$+ SA 3	95Ag/5Pd	950	Air
K55	$BaO\text{-}Re_2O_3\text{-}TiO_2$	Pd	1300	Air
K60	$BaO\text{-}(Nd,Gd)_2O_3\text{-}TiO_2$ + SA 4	Cu	1040	N_2/H_2O
K30	$Ca_xSr_{1-x}ZrO_3$'	Ni	1300	$H_2/N_2/H_2O$

Table 3.5.2: Overview of dielectric composition and relative permittivity.

Code	Dielectric Ceramics	Sintering Aid	ε_r
K85	$(Ba_{0.231}Ca_{0.05}Sr_{0.02})O\text{-}(Nd_{0.131}Gd_{0.103})_2O_3\text{-}TiO_2$	-	85
K80	$(Ba_{0.231}Ca_{0.05}Sr_{0.02})O\text{-}(Nd_{0.131}Gd_{0.103})_2O_3\text{-}TiO_2$	$ZnO\text{-}SiO_2\text{-}TiO_2\text{-}CuO$	80
K75	$(Ba_{0.231}Ca_{0.05}Sr_{0.02})O\text{-}(Nd_{0.131}Gd_{0.103})_2O_3\text{-}TiO_2$	$Zn_4B_6O_{13}\text{-}ZnO\text{-}SiO_2\text{-}CuO\text{-}Bi_2O_3$	77
K72	$(Ba_{0.231}Ca_{0.05}Sr_{0.02})O\text{-}(Nd_{0.131}Gd_{0.103})_2O_3\text{-}TiO_2$	$Zn_4B_6O_{13}\text{-}ZnO\text{-}SiO_2\text{-}CuO\text{-}Bi_2O_3$	77
K70	$BaO\text{-}Sm_2O_3\text{-}Nd_2O_3\text{-}TiO_2$	$Zn_4B_6O_{13}$-[(Mg,Cu,Ba,Zn)O-$(Al,Bi)_2O_3\text{-}SiO_2$]	67
K55	$Ba\text{-}Re_2O_3\text{-}TiO_2$	-	54
K60	$(Ba_{0.231}Ca_{0.05}Sr_{0.02})O\text{-}(Nd_{0.131}Gd_{0.103})_2O_3\text{-}TiO_2$	$Li_2O\text{-}MgO\text{-}SiO_2\text{-}CuO$	71
K30	$Ca_{(0.72}Sr_{0.28)}O\text{-}(Zr_{0.96}Ti_{0.04})O_2$ + 1 mol% SiO_2 + 0.5 mol% MnO + 0.1 mol% Nb_2O_5	-	32

In Table 3.5.1 an overview of the various MLCCs samples is shown. The dielectrics were made from commercially available powders. However, some adjustments to some dielectric powders, depending on the metal choice for the electrodes, were carried out to fulfil the requirements to produce the various types of C0G-MLCCs. The modifications were achieved by adding sintering aids (SA), which are based on metal oxides (see Table 3.5.2 for an overview), to the commercial powders.

The multilayer capacitors with noble metal electrodes (NME) were based on high permittivity BaO-$(Nd,Gd)_2O_3$-TiO_2 powders. The exact composition of this commercial powder is given in Table 3.4.1 and was used to fabricate K85, K80, K75 and K72 multilayer capacitors. However, to co-fire these MLCCs with Pd, 80Ag/20Pd, 90Ag/10Pd and 95Ag/5Pd (ratio in wt%/wt%), respectively, certain sintering aids, see Table 3.5.2, were added to the BaO-$(Nd,Gd)_2O_3$-TiO_2 powder to meet the requirements for co-sintering with the respective metals. In Chapter 3.2 the performance and properties of these MLCCs have been discussed. Another dielectric powder based on BaO-$(Nd,Sm)_2O_3$-TiO_2 was used to produce K70-MLCCs with 95Ag/5Pd electrodes to compare the ESR characteristics with K72-MLCCs. The K85-MLCCs were compared with MLCCs made with K55 and pure palladium electrodes. The commercial K55 dielectrics are based on a BaO-Re_2O_3-TiO_2 formulation. For K60-MLCCs with copper electrodes the same dielectric powder as K85 was used. In Chapter 3.4 the composition of the dielectrics used for K60-MLCCs were discussed in detail. So far the MLCC described were made with high permittivity dielectrics, which are difficult to sinter in a reducing atmosphere.

However, in dielectrics for MLCCs with nickel electrodes the ceramics were based on $SrZrO_3$ and $CaZrO_3$, which are known to be reduction stable during sintering. The $SrZrO_3$ and $CaZrO_3$ dielectrics exhibit good electronic properties in high frequency applications. The dielectrics have a relative permittivity (ε_r) of 38 and 30, respectively, and the TCC values are +120 and +40 ppm/°C, respectively. Tan δ is approximately $3 \cdot 10^{-4}$ for both dielectrics. They can be used for C0G capacitors when the TCC properties of the zirconates, having positive TCC, are mixed with titanates, having a negative TCC. For instance, $SrZO_3$ can be mixed with $SrTiO_3$ to obtain C0G dielectrics.[3–4] Solid state $CaZrO_3$ and $SrZrO_3$ powders are sintered dense at temperatures above 1450 °C, therefore the dielectrics have to be adjusted to sinter below the melting temperature of nickel of 1435 °C. To protect the nickel electrodes from oxidation the multilayer capacitors have to be sintered in a reducing atmosphere. To meet these conditions the addition of sintering aids, doping of acceptor dopants, and process conditions were investigated and have been reported in literature. Ceramics with C0G properties and good breakdown strength are available on the market. A dielectric powder, based on (Sr,Ca)O-$(Zr,Ti)O_2$, developed by Yageo was used to produce the K30-MLCCs.[4–10] In Appendix A.1, the

MLCC with medium relative permittivity based on (Sr,Ca)O-(Zr,Ti)O_2 are discussed in more detail.

The NP0-MLCCs having BME or NME electrodes were evaluated with respect to the ESR response to frequency. Furthermore, the effect of the dielectric composition was evaluated on ESR response to frequency. The goal is to find out which types of MLCCs can operated at high frequencies with low losses.

3.5.2. Preparation of multilayer ceramic capacitor samples

MLCC preparation and measurements. Multilayer ceramic capacitors of various dielectric and electrode metal combinations were prepared by making green bricks in 0603 dimensions with 5 electrodes to obtain a capacitance of 10 pF measured at 1MHz and 1V_{rms}. An overview of all used materials can be found in Table 3.5.1 and Table 3.5.2. Green MLCC bricks were produced on regular production equipment at Yageo in Roermond, the Netherlands, as described in Chapter 2. The MLCCs with palladium and silver-palladium alloys were sintered in air at sintering temperatures as listed in Table 3.5.1. The MLCCs with copper and nickel were sintered in a reducing atmosphere of N_2/H_2O at 1040°C and 1 % $H_2/N_2/H_2O$ at 1300 °C, respectively, for 1 hour. Terminations (Yageo) were applied on the MLCCs. For MLCCs with palladium and silver-palladium electrodes a silver paste was used. The silver terminations were cured at 750 °C in air for 1 hour. On MLCCs with copper and nickel inner electrodes a Cu termination paste was used and the dried Cu paste was cured at 900 °C in a nitrogen atmosphere in one hour cycle.

3.5.3. Theory of equivalent series resistance in capacitors

In battery operated applications like portable notebooks, mobile phones and portable music players an extended battery life is achieved upon using capacitors with low losses. Energy dissipation of capacitors, when a radio frequency (RF) AC voltage is applied, must be kept as low as possible to maximize output power and increase battery life. This can be achieved by using low loss C0G capacitors. These C0G capacitors exhibit high *Q*-factors. The *Q* factor is a dimensionless number. It expresses the energy dissipation of the capacitor and is a measure of the capacitor's ability to store energy without loss. The *Q*-factor is related to the capacitive reactance of the capacitor (X_c) and ESR via the following relationships:

$$Q = \frac{1}{\tan \delta} = \frac{X_c}{\mathrm{ESR}} = \frac{1}{2\pi \cdot f \cdot C} \qquad (3.5.1)$$

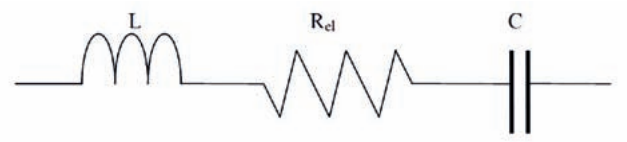

Figure 3.5.1: Capacitor circuit model for high frequencies.

Here tan δ is the dissipation factor, δ is the loss angle, X_c the capacitive reactance in Ω, ESR the equivalent series resistance of the capacitor in Ω, *f* the frequency in Hz and *C* the capacitance in F. From Equation 3.5.1 it is evident that the *Q*-factor can be changed by frequency, capacitance and ESR. The fact that capacitors dissipate power means that they are not ideal. An ideal capacitors would not dissipate energy when an AC voltage would be applied. The ESR of ideal capacitors would be zero. Since the capacitors are not ideal and the capacitor dissipates energy due to electrode resistance, insulation resistance of the dielectrics and dielectric loss. These factors contribute to the ESR and thus also to the quality factor of the capacitors. A non-ideal capacitor can be represented by an equivalent circuit model as shown in Figure 3.5.1.

This circuit model represents a non-ideal capacitor operating at high frequencies, typically above 100 MHz. The *L* in Figure 3.5.1 represents the inductance of the capacitor. R_{el} represents the electrode resistance of the multilayer capacitor. When capacitors are operated at lower frequencies an insulation resistance (IR) would be present in parallel to the capacitor *C*. But the IR is very large for ceramic capacitors with values exceeding 10^{12} Ω. Thus, the IR does not contribute to the capacitor's performance at RF frequencies. The absolute impedance of capacitors ($|Z|$), represented by the equivalent circuit model, responds to frequency via:

$$|Z| = \sqrt{ESR^2 + 2\pi \cdot f \cdot L - \frac{1}{2\pi \cdot f \cdot C}} \qquad (3.5.2)$$

where $|Z|$ is the absolute impedance of the capacitor in Ω, *f* the frequency in Hz, *L* is the inductance of the capacitor in nH and *C* is the capacitance in F. The impedance response to frequency, as described in Equation 2, is shown in Figure 3.5.2 for a typical 0603 - 10 pF capacitor. Minimum impedance is achieved at the resonance frequency of the capacitor. When a capacitor is used in a coupling application the AC current will pass in this specific frequency range near the resonance frequency, while AC currents above and below the resonance frequencies are blocked. In an electronic circuit a capacitor can be selected for use in a specific

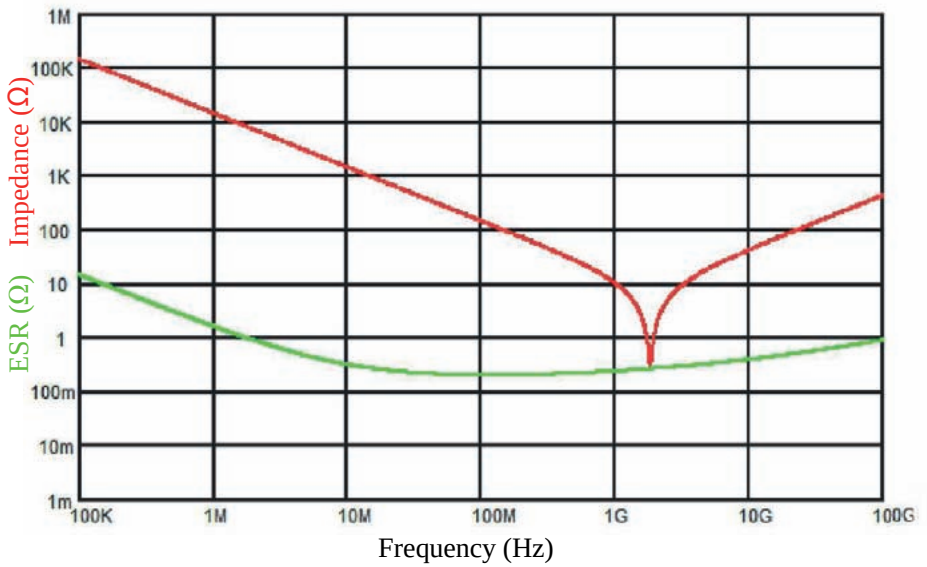

Figure 3.5.2: Frequency response on impedance and ESR of a 0603–10pF MLCC.

frequency range by calculation of the resonance frequency. The resonance frequency is given by

$$f_0 = \frac{1}{2\pi\sqrt{L \cdot C}} \qquad (3.5.3)$$

were f_0 is the resonant frequency in Hz, C the capacitor in F and L the inductance in nH. The reactance of a capacitor above the resonance frequency is inductive and can be large for some type of capacitors. The inductance of a capacitor is associated with its design. For small capacitors, like 0402 and 0603 case sizes, the inductance is low and can neglected in most cases.

In Figure 3.5.2 the response of ESR to frequency is also shown. The ESR, as described in Equation 3.5.2, of a capacitor that operates at RF frequencies, can be represented by

$$\mathrm{ESR} = R_{el} + \frac{\tan\delta}{2\pi \cdot f \cdot C} \qquad (3.5.4)$$

where R_{el} is the resistance of the electrodes. The equation shows that ESR is the sum of conductive and dielectric losses. Both parameters are frequency dependent. The

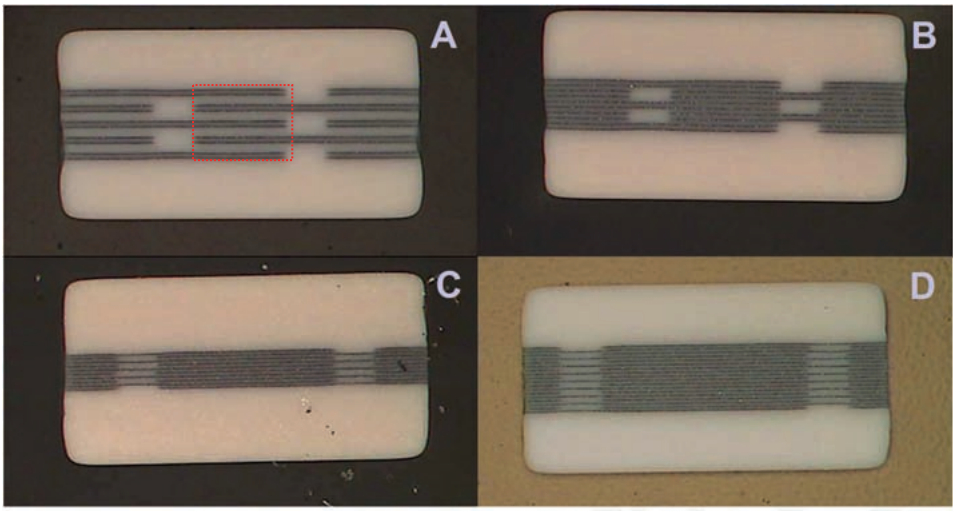

Figure 3.5.3: Various constructions of 0603 C0G MLCCs with capacitances of (a) 10 pF, (b) 22 pF, (c) 100 pF and (d) 220 pF.

dielectric losses are associated with the ceramic properties, as described by the second term of Equation 3.5.4. Parameters such as ceramic composition, impurity level and microstructure of the ceramics, like grains size, morphology and porosity, contribute to the dielectric loss factor. The dielectric losses are dominant in measurements at low frequencies between 1 kHz and 1 MHz. At these frequencies typically dielectric loss, tan δ, is measured. But at higher frequencies, between 10 and 30 MHz, the contribution of dielectric loss drops to a very low value or in some cases to zero. At higher frequencies the ESR is dominated by resistivity losses of the metals. In a multilayer capacitor the resistivity losses R_{el} is the sum of the resistivity of the inner electrodes, the terminations, the resistivity between interface of inner electrode and termination, and other barrier layers. MLCC construction parameters such as number of electrodes, double electrode layers, electrodes thickness etc., contribute to the ESR during measurements at high frequencies, especially when ESR is measured above 30 MHz. See Figure 3.5.3 for some examples of commercially available MLCCs. Note that for the 0603–10pF MLCC, Figure 3.5.3a, the active capacitive volume is highlighted with a red box in the middle of the capacitor.

The values of R_{el} at these frequencies are quite constant. However, when higher frequencies are applied to the capacitor the skin effect will play an important role. R_{el} will increase too due to the skin effect. When the skin effect occurs an AC current flows near the outside of the electrodes, because the resistivity in the middle of the electrodes is increased by the interaction with electromagnetic waves that oscillate the charge carriers back and forth.[11] Therefore the average AC current is

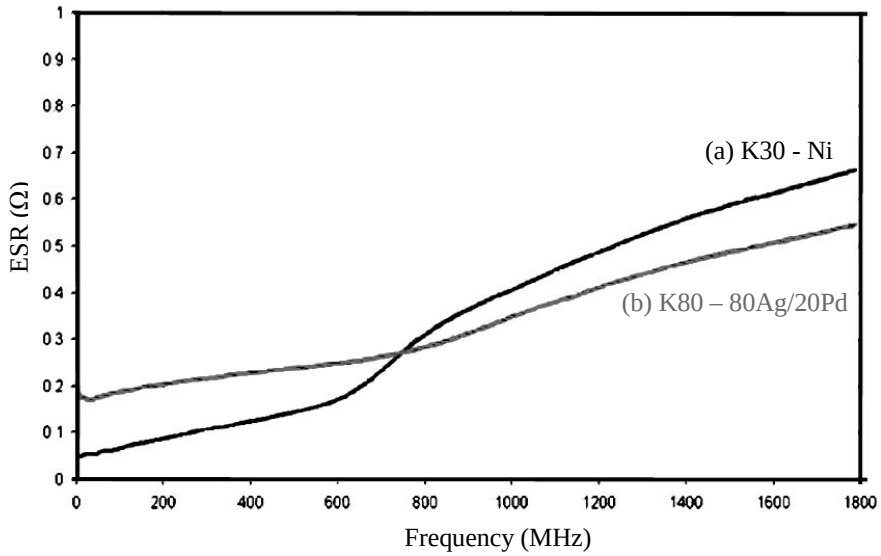

Figure 3.5.4: ESR response to frequency of 0603–10 pF MLCCs with (a) K30 dielectrics and nickel electrodes, (b) K80 dielectrics with 80Ag/20Pd electrodes.

cancelled out. The skin effect is frequency dependent and the associated skin depth, the depth near the surface of the electrode where current flows, decreases with increasing frequency. The resistivity of the electrodes and the ESR increase with decreasing skin depth.[2, 12–15]

3.5.3. Discussion of ESR results of various MLCCs

Nowadays MLCCs with Ni electrodes are mass produced and were mainly developed to replace the organic film capacitors.[1] However, Ni-MLCCs can partially replace the expensive MLCCs made with silver palladium electrodes. For RF applications it is important that impedance and ESR of Ni-MLCCs are low to avoid large energy dissipation. To study the electrical performance, 0603–10pF MLCCs were fabricated with nickel and 80Ag/20Pd inner electrodes to compare the ESR properties of the MLCCs. The 80Pd/20Ag-MLCCs were made with K80 dielectric ceramics, while Ni-MLCCs were made with K30 dielectrics. These dielectrics have C0G properties and the relative permittivity values are 80 and 30, respectively. To compensate for the difference in relative permittivity, different constructions were used to make multilayer capacitors to obtain a final capacitance of 10pF. In the design of the capacitors the dielectric thicknesses and electrode thickness were kept

Table 3.5.3: Physical properties of metals.[16–17]

Metal	Melting Temperature (°C)	Specific resistivity at 20 °C (μΩ·cm)
Pd	1552	10.8
80Ag/20Pd	1070	11.0
90Ag/10Pd	1000	6.0
95Ag/5Pd	980	3.8
Ag	961	1.6
Cu	1083	1.7
Ni	1453	6.8

equal. However, the number of electrodes and the overlap of the electrodes were varied to adjust the capacitance. Therefore a comparison of the impedance and ESR measurements is possible. Figure 3.5.4 shows the relationship between ESR and frequency of 10 pF 0603 MLCCs.

The ESR values of the Ni-MLCC between 30 and 700 MHz were lower compared to the 80Pd/20Ag-MLCCs. Above 800 MHz the ESR of Ni-MLCC was increased and values were higher compared to 80Pd/20Ag-MLCCs. The 80Pd/20Ag-MLCCs show a more or less linear increase of ESR in relation to frequency. However, the Ni-MLCCs responded differently to frequency as the ESR increased sharply between 600 and 800 MHz to values above the ESR values of Ag/Pd-MLCCs. The ESR of the Ni-MLCC was lower at relatively low frequencies because the specific resistivity of nickel is lower than the specific resistivity of 80Ag/20Pd alloy, see Table 3.5.3. Therefore, R_{el} and ESR of the Ni-MLCC between 30 and 700 MHz are smaller than in the 80Pd/20Ag-MLCCs.

The increase of ESR of Ni-MLCC at frequencies >600 MHz can be attributed to two phenomena. The first is related to the skin effect, because the skin depth is dependent on material properties, i.e., the specific resistivity and the magnetic permeability of the metals. The skin depth can be calculated by[14]

$$\delta = \sqrt{\frac{1}{\pi \cdot f \cdot \mu \cdot \sigma}} = \sqrt{\frac{\rho}{\pi \cdot f \cdot \mu}} \qquad (3.5.5)$$

were δ is the skin depth in meter, f the frequency in Hz, μ the magnetic permeability in Henry per meter, σ the conductivity in Ω/m and ρ the specific resistivity of the electrodes in Ω·m. In Equation 3.5.5 the skin depth is also dependent on the magnetic permeability of the metals. The silver-palladium alloys of 80/20 ratio are

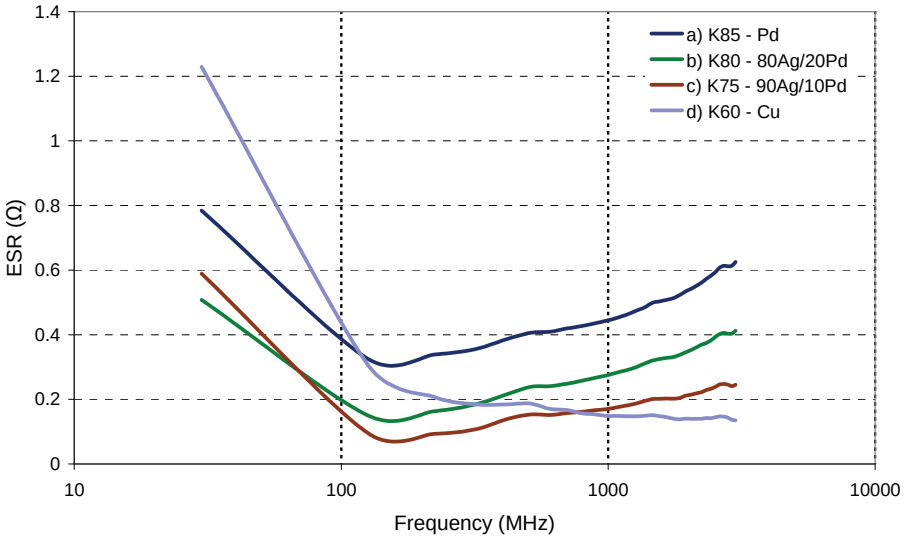

Figure 3.5.5: The ESR response to frequency of 0603–10 pF MLCCs with (a) K85 dielectrics and Pd electrodes, (b) K80 dielectrics and 80Ag/20Pd electrodes, (c) K75 dielectrics and 90Ag/10Pd electrodes and (d) K60 dielectrics and Cu electrodes.

known to be diamagnetic, while nickel is known to be ferromagnetic.[18] Due to the larger magnetic permeability of nickel compared to 80Ag/20Pd, the skin depth is smaller in nickel electrodes. Furthermore, the ferromagnetic behaviour the magnetic dissipation loss of nickel is probably dependent on frequency. A lot of magnetic energy and most probably an increase of the electrode resistivity can be expected at high frequencies in ferromagnetic materials.

The other phenomenon that probably caused the ESR of the Ni-MLCCs to increase can be related to the electrode quality. When thin nickel electrodes are sintered in a MLCC the nickel phase will form a microstructure of droplets of nickel, which are formed at high temperatures. This phenomenon is known also coagulation of nickel during sintering and contributes to the spatial discontinuity of the electrodes. The level of discontinuity of the nickel electrodes depends largely on the applied electrode thickness. When the electrode thickness is large enough the electrodes will be continuous. To minimize costs and avoid sintering mismatch during sintering the electrode thicknesses are kept as low as possible. Therefore the nickel electrodes show some degree of discontinuity after sintering. This also causes the resistivity of the electrodes to increase. At high frequencies, when the skin effect also plays a role, the ESR may be increased due to the sharp decrease of available conductance area compared to a situation with a ideal electrode geometry.

It is believed that the ESR of multilayer capacitors at high frequencies is mainly dependent on the electrode materials. This can be demonstrated by comparing the ESR characteristics of MLCCs with different electrodes like palladium, 80Ag/20Pd alloy, 90Ag/10Pd alloy and Cu. MLCCs with 0603 case size and a capacitance of 10 pF were therefore fabricated. That ESR does not depend significantly on electrode resistivity, as can be concluded when the ESR values of Pd-K85-MLCCs and 80Ag/20Pd-K80-MLCCs are compared. The specific resistivities of these two metals are almost equal, but at resonance frequency, which is around 130 MHz, the ESR of Pd-MLCC was 0.32 Ω and ESR of 80Ag/20Pd-MLCC was 0.15 Ω. The difference must be caused by other parameters like the microstructure of the metals, grain size and porosity, or on parameters that are related to the magnetic properties of the metals. Palladium is known as a paramagnetic material and has a larger susceptibility, $\mu = 7 \cdot 10^{-4}$ cm^3/mol, compared to 80Ag/20Pd, which is a diamagnetic materials with a molar susceptibility $\mu = -0.24 \cdot 10^{-4}$ cm^3/mol.[18] Therefore the skin depth in a Pd electrode is smaller than in 80Ag/20Pd electrodes. A larger ESR of Pd electrodes can thus be expected.

The ESR of the 90Ag/10Pd-MLCCs is 0.09 Ω, measured at the resonance frequency, which is lower than the ESR of the 80Ag/20Pd-MLCCs. Because the magnetic permeability of the two silver/palladium alloys is equal, the difference between ESR values is only attributed to the difference between the specific resistivities of the metals. The higher ESR values of the 90Ag/10Pd-MLCCs at 30 MHz can be attributed by the higher dielectric loss of the ceramics. Also the Cu-MLCCs have a high ESR at 30 MHz, which is also due to the high dielectric loss of the ceramics. But the ESR decreases with increasing frequency. The low ESR values at high frequencies are predominantly caused by the low specific resistivity of copper. Even at very high frequencies the ESR is not increased due to the skin effect. Therefore multilayer capacitors that have to be operated at frequencies above 1 GHz can best be made with copper electrodes.

Although the ESRs of MLCCs are predominantly dependent on the electrode metals, the influence of the dielectric ceramics on ESR was investigated nonetheless. MLCCs with pure palladium electrodes were fabricated based on two different types of C0G dielectrics with different relative permittivity values. The K85 and K55 dielectrics have a relative permittivity of around 80 and 55, respectively. Because the relative permittivities are different the constructions of the two MLCC types were slightly different. However, only the overlap of the electrodes was changed in order to achieve the same capacitance of 10 pF for both capacitors. The dielectric thickness and electrode thickness were kept equal. The other two MLCC types, with the 95Ag/5Pd inner electrodes, were also based on $BaO\text{-}Re_2O_3\text{-}TiO_2$ ceramics. K72 was based on $BaO\text{-}(Nd,Gd)_2O_3\text{-}TiO_2$ and K70 was based on $BaO\text{-}(Nd,Sm)_2O_3\text{-}TiO_2$.

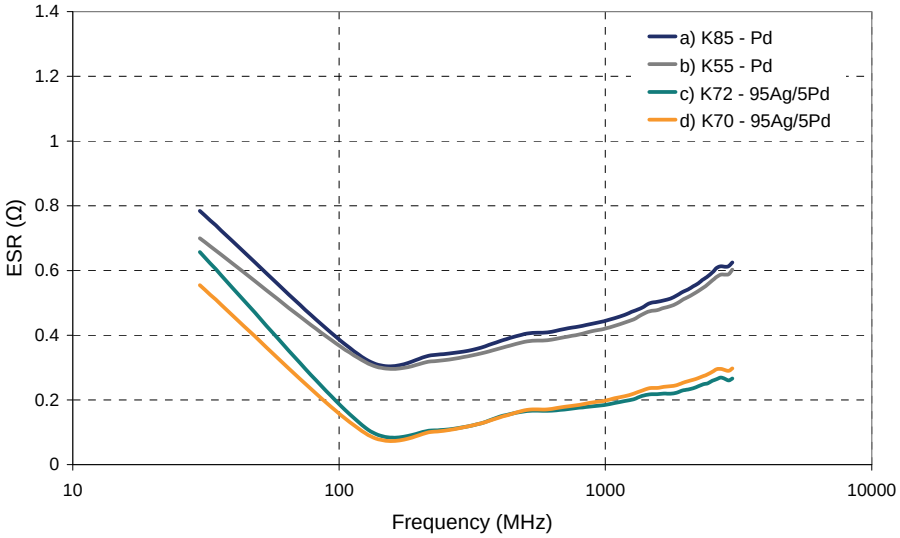

Figure 3.5.6: The ESR response to frequency of 0603–10 pF MLCCs with (a) K85 dielectrics and Pd electrodes, (b) K55 dielectrics and Pd electrodes, (c) K72 dielectrics and 95Ag/5Pd electrodes and (d) K70 dielectrics and 95Ag/5Pd electrodes.

In order to prevent the silver from evaporating and to avoid silver diffusion during sintering, sintering aids were added to the dielectric powders. Each sintering aid was uniquely designed to produce C0G dielectrics which could be sintered below the melting point of 95Ag/5Pd alloy, see Table 3.5.1. The ESR values of the four MLCC types were measured and the results are shown in Figure 3.5.6.

The difference in ESR between Pd and 95Ag/5Pd-MLCCs can be observed clearly. The K85 and K55 capacitors have approximately the same ESR values with respect to frequency. At resonance frequency the ESR of K85 and K55 was 0.3 Ω. The ESR of K72 and K70 at resonance frequency is approximately 0.09 Ω. The overlap of the ESR curves of the Pd and 95Ag/5Pd based MLCCs show clearly that ESR is predominantly dependent on the electrode properties. If one compares the ESR results of K72 and K70 to the K75–90Ag/10Pd capacitors, the ESR values are approximately similar. One would expect that the ESR of K72 and K70 would be lower than the K75 MLCCs. But the K72 and K70 capacitors were not sintered well below the melting point of the 95Ag/5Pd alloy. Silver was evaporated and some silver was diffused into the ceramics during sintering, which caused the formation of discontinuous electrodes near the surface of the brick, as has been explained in chapter 3.2. Due to this discontinuity of the electrodes the resistivity was increased, which led to higher ESR values.

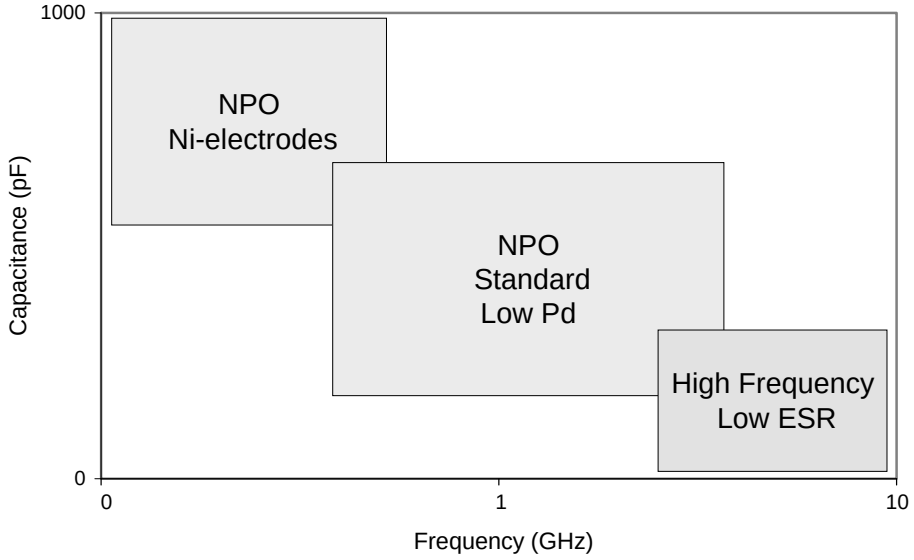

Figure 3.5.7: Overview application areas for the various C0G multilayer capacitor types.

3.5.4. Conclusions

Multilayer capacitors with various dielectric ceramic and inner electrode combinations were manufactured to investigate their ESR characteristics. It was found that low cost capacitors with nickel electrodes show low ESR values when measured at the lower part within the frequency range 30 to 3000 MHz. Above 800 MHz the capacitors with nickel electrodes exhibit a sharp increase of ESR. This is related to the skin effect, induced by the ferro-magnetic properties of nickel, and the discontinuity of the nickel electrodes.

Silver evaporation and silver diffusion should be avoided. These processes may occur during sintering, and discontinuous electrodes will increase the resistivity of the electrodes and produce higher losses during load in an electronic circuit.

The best performance concerning low energy and ESR losses are gained with capacitors with copper electrodes. These Cu-MLCCs exhibit very low ESR values at frequencies above 1000 MHz. The low losses for Cu-MLCC can be attributed to the low resistivity of copper and a good electrode continuity. The dielectric composition has no large effect on energy losses of the capacitors when applied at high frequencies. The losses are completely dependent on the material properties of the metals used for the electrodes.

In practice, Ni-MLCCs are usually used in applications that operate at relatively low frequencies, see Figure 3.5.7, while MLCCs based on Ag/Pd alloys operate at intermediate frequencies. For very high frequencies, typically above 2 GHz, MLCCs with copper electrodes are used. These Cu-MLCC have very low ESR and are therefore suitable for use in this frequency range. Cu-MLCCs are normally made from $CaZrO_3$ or $SrZrO_3$ based ceramics. Typically these MLCCs exhibit low capacitance values.

References

1) Kishi, H.; Mizuno, Y. and Chazono, H. *Base-metal electrode-multilayer ceramic capacitors: Past, present and future perspectives*; Japanese Journal of Applied Physics Part 1-Regular Papers Short Notes & Review Papers, 2003 **42**(1): p. 1–15.
2) Randall, M. S.; Blais, P.; Prymak, J.; Prevallet, M.; Skamser, D.; Grav, A.; Pinceloup, P.; Xu, X. and Tajuddin, A. *Capacitor considerations for power management*; Conference paper CARTS 2006, p. 97–111.
3) Kell, R. C.; Greenham, A. C. and Olds, G. C. E. *High permititivity temperature-stable ceramic dielectrics with low microwave loss*; Journal of the American Ceramic Society, 1973 **56**(7): p. 352–354.
4) Lee, W. J.; Wakahara, A. and Kim, B. H. *Decreasing of $CaZrO_3$ sintering temperature with glass fritaddition*; Ceramics International, 2005 **31**(4): p. 521–524.
5) Tsurumi, T.; Teranishi, T.; Wada, S.; Kakemoto, H.; Fukunaga, O.; Nakada, M. and Akedo, J. *Ultra wide range dielectric spectroscopy of strontium titanate-strontium zirconate solid solution*; Journal of the Ceramic Society of Japan, 2006 **114**(1333): p. 774–781.
6) Hu, X.; Ling, Z. Y.; Guo, D. and He, X. H. *Effective Sintering Aids of Boric Frit and Lithium Salts for Low-Temperature Sintering of Dielectric Ceramics*; Ferroelectrics, 2009 **388**: p. 120–127.
7) Kim, B. H.; Lee, G. Y.; Lee, W. J. and Kim, J. H. *Dielectric properties in $(1-x)CaZrO_3$–$0.1CaTiO_3$-$xTiO_2$ system*; Materials Science and Engineering B-Solid State Materials for Advanced Technology, 2004 **113**(3): p. 198–202.
8) Pollet, M. and Marinel, S. *Lowering of $CaZrO_3$ sintering temperature using lithium-calcium fluoride flux addition*; Materials Science and Engineering a-Structural Materials Properties Microstructure and Processing, 2003 **362**(1–2): p. 167–173.
9) Pollet, M.; Marinel, S. and Desgardin, G. *$CaZrO_3$, a Ni-co-sinterable dielectric material for base metal-multilayer ceramic capacitor applications*; Journal of the European Ceramic Society, 2004 **24**(1): p. 119–127.
10) Lee, W. S.; Su, C. Y.; Lee, Y. C.; Lin, S. P. and Yang, T. *Effects of dopant on the dielectric properties of $CaZrO_3$ ceramic sintered in a reducing atmosphere*; Japanese Journal of Applied Physics Part 1-Regular Papers Brief Communications & Review Papers, 2006 **45**(7): p. 5853–5858.
11) *Electroceramics*; 2nd ed.; Moulson, A. J. and Herbert, J. M.; John Wiley & Sons Ltd.: Chichester, 2003; p 296.

12) Stevenson, P. E. *One-kilohertz dissipation factor testing is inadequate for medical implant EMI filters and other high frequency MLC capacitor applications*; Conference paper CARTS Europe 2003 p.54
13) www.atceramics.com.
14) Lee, W. H.; Su, C. Y.; Huang, C. L.; Lee, Y. C.; Hu, C. L.; Yang, J.; Yang, T. and Lin, S. P. *Effect of inner electrode on electrical properties of (Zn,Mg)TiO_3-based multilayer ceramic capacitor*; Japanese Journal of Applied Physics Part 1-Regular Papers Brief Communications & Review Papers, 2005 **44**(12): p. 8519–8524.
15) *Electroceramics*; 2nd ed.; Moulson A.J., H. J. M.; John Wiley & Sons Ltd.: Chichister, 2003; p 253–255.
16) Wang, S. F.; Dougherty, J. P.; Huebner, W. and Pepin, J. G. *Silver-palladium thick-film conductors*; Journal of the American Ceramic Society, 1994 **77**(12): p. 3051–3072.
17) *Metals reference book*; 3rd ed.; Smithells, C. J.; Butterworths: London, 1962; Vol. 2, p 6 95.
18) Sanger, W. and Voitlander, J. *Dependence of the magnetic-susceptibility of the palladiumsilver alloy system on temperature and composition*; Zeitschrift Fur Physik B-Condensed Matter, 1981 **44**(4): p. 283–291.

Chapter 4

High capacitance multilayer ceramic capacitors

Chapter 4.1

Introduction to high capacitance multilayer capacitors

In the electronics industry the developments in the market for electronic devices and components are focused on miniaturization and cost reduction. In battery operated applications like mobile phones, notebooks, personal digital players and personal digital assistant devices, multilayer ceramic components like multilayer capacitors are used for a variety of functions. In the previous chapter the development of temperature stable capacitors was discussed. These types of capacitors usually have low capacitances, normally not exceeding 1 nF, and are mainly used at frequencies between 10 MHz and 30 GHz in resonance circuits and filtering applications. These temperature compensating capacitors exhibit low volumetric efficiency. However, for other applications like decoupling and noise reduction between frequencies of 1 and 40 MHz capacitors with high volumetric efficiency are required. These high capacitance multilayer capacitors (MLCC) have capacitance values in the range of 1nF to 100 μF. Because the trend in electronics is miniaturization, the focus is to increase the volumetric efficiency of multilayer capacitors. A lot of effort is taken in material and process development to produce capacitors in smaller case sizes with reliable electrical properties.[1–2]

4.1.1 High-ε_r ceramics

Hence, the trend is to develop and manufacture small case size capacitors with high volumetric efficiency. The capacitance of multilayer capacitors is dependent on permittivity and construction and is described by:

$$C = \varepsilon_r \cdot \varepsilon_0 \frac{(n\text{-}1) \cdot A}{d} \qquad (4.1.1)$$

where C is the capacitance in Farad, ε_0 the permittivity of vacuum, $\varepsilon_0 = 8.85 \cdot 10^{-12}$ F/m, ε_r the relative permittivity, n is number of electrodes, A the overlap area of the electrodes in m^2, and d the thickness of the dielectric layer in meter. Currently capacitors are produced with electrode layer numbers ranging from 500 to 1000 depending on the case size of the MLCCs. Dielectric thicknesses were already decreased below 1 μm and are almost equal to the electrode thickness, which are of the order of 0.8 to 1 μm for nickel electrodes. Because the volume of the capacitor can be described by $n(d+t)O$, the volumetric efficiency for the high layer count capacitors is:

$$\frac{C}{V} = \varepsilon_r \cdot \varepsilon_0 \frac{(n-1) \cdot A}{d \cdot n \cdot (d+t) \cdot O} \qquad (4.1.2)$$

were V is volume of the capacitor in m^3, t is the thickness of the electrodes in meter and O is the size of capacitor in m^2. The volumetric efficiency of the capacitors can be increased by following parameters: (i) use of materials having a higher dielectric constant, (ii) increasing the number of dielectric layers, (iii) increase of electrode overlap area by stacking precision of the electrodes, and (iv) decreasing the thickness of the dielectric and/or electrode layers. In practice, the improvement of a combination of above-mentioned parameters is targeted to produce multilayer capacitors with larger capacitance values for a given case size.

Classification. The MLCC which have a high volumetric efficiency should exhibit large relative permittivity values. However, the loss factor (Q) and temperature drift of capacitance are also relatively large for these types of MLCCs. Dielectrics are classified by Electronics Industries Alliance (EIA) in terms of temperature, voltage and frequency drift. The specification provides guidelines to classify capacitors as class 2 and 3 dielectrics. Class 2 materials are more stable and more reliable at higher operating temperatures than Class 3 materials. In Table 4.4.1 an overview of the EIA designations for high capacitance MLCCs is shown.[3]

The limits of minimum and maximum temperature are specified together with maximum capacitance change from the reference capacitance value measured at 25°C. In Table 4.1.1 all possible combinations of dielectric ceramics are shown. However, in practice only a few combinations like X5R, X7R, Y5V and Z5U are commonly manufactured in multilayer capacitors. The dielectrics of X7R, Z5U and Y5V exhibit large relative permittivity values which are around 3000, 8000 and 18000, respectively. With these types of dielectric ceramics high volumetric capacitive densities in multilayer capacitors can be achieved. They are therefore used in applications in which cost reduction is an important issue and factors like accuracy, stability, loss factor and aging are considered less important.[4–5]

Table 4.1.1: EIA coding of Class 2 and 3 capacitors.

EIA Code Lower Limit Temperature	Lower Limit Temperature (°C)	EIA Code Upper Limit Temperature	Upper Limit Temperature (°C)	EIA Code Capacitance change	Capacitance change (%)
X	-55	4	+65	A	±1.0
Y	-30	5	+85	B	±1.5
Z	+30	6	+105	C	±2.2
		7	+125	D	±3.3
		8	+150	E	±4.7
				F	±7.5
				P	±10.0
				R	±15.0
				S	±22.0
				T	+22 to -33
				U	+22 to -56
				V	+22 to -82

For example: X7R has a capacitance drift of ± 15% over temperature range of -55 to 125 °C and belongs to EIA specified class 2.

Perovskite crystal structure. The dielectrics used in high K capacitors ($K = \varepsilon_r$) are based on modified $BaTiO_3$ ceramics. The crystal structure of $BaTiO_3$ ceramics is named after the mineral Perovskite, $CaTiO_3$, and the structure is often represented as ABO_3. The generalized ABO_3 unit cell has the face centered cubic (FCC) structure. In the ideal Perovskite structure the metal ions located at the A^{2+} site are surrounded by 12 O^{2-} ions. The metal ions at the B^{4+} sites are located in the octahedral interstices of the unit cell, see Figure 4.1.1.[6]

In the ideal ABO_3 crystal structure the axis, *a*, of the cubic cell depends on the ionic radii. When the ions are regarded as rigid balls the lattice parameter *a* can be calculated according to the following relationships;[7–8]

$$a = \sqrt{2}\,(R_A + R_O) = 2\,(R_B + R_O) \qquad (4.1.3)$$

were R_A, R_B and Ro are respectively the ionic radii of A^{2-}, B^{4-} and O^{2-} ions, using the values as described by for instance Shannon.[9] This equation only holds for the ideal situation of the cubic Perovskite structure. However, in practise combinations of various elements, having each different ionic radii, are used to produce Perovskite type materials. In the 1920s the tolerance factor *t* for the Perovskite structure was

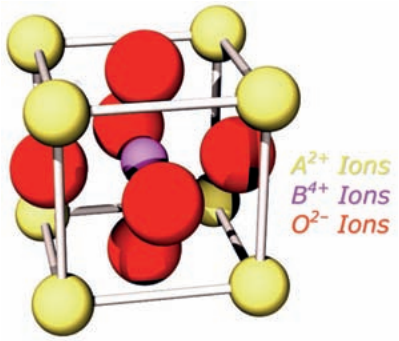

Figure 4.1.1: Cubic Perovskite structure, ABO_3.

proposed by Goldschmidt in order to predict or to evaluate the stability of the cubic Perovskite structure.[10] The tolerance factor is described by the following equation;[10]

$$t = \frac{R_A + R_O}{\sqrt{2}\,(R_B + R_O)} \qquad (4.1.4)$$

The most ideal cubic closed packed layer structure is found in $SrTiO_3$ and $BaZrO_3$, having tolerance factors t of approximately 1.[11–13] When the cation on the A-site is smaller than its cavity or the cation located on the B-site is too lare, than $t < 1$. This indicates that the cation on the A-site will have much room to vibrate. To minimize the lattice energy the octahedral lattices must be tilted to fill the space.[6] Due to this distortion the symmetry of the structure will be lowered. Hence the mineral Perovskite, $CaTiO_3$, the tolerance factor t is approximately 0.97, has the orthorhombic crystal structure.[8, 11, 14] On the other hand, when $t > 1$, the cavity of the ions located on the B-site will be enlarged and thus these ions have more space to vibrate. When $t > 1$, the most stable Perovskite crystal structures are variants of the hexagonal unit cells.[8] In the case of $BaTiO_3$, which has a tolerance factor of about 1.06 at roomtemperature, has the tetragonal crystal structure.[13, 15]

Above 120 °C the unit cell of $BaTiO_3$ has the cubic crystal structure. When the temperature is lower than 120 °C the central Ti^{4+} ions and the surrounding O^{2-} ions move in opposite directions away from the centre of the unit cell, whereas the Ba^{2+} remain at the same location. Due to this shift of the Ti^{4+} and O^{2-} ions the unit cell is distorted in the *c*-axis direction and an electric dipole moment is created, which leads to a spontaneous polarization along the *c*-axis of the unit cell. The unit cell therefore changes from cubic to tetragonal. The critical temperature at which the equilibrium positions of ions, and the unit cell structure is changed, is called the Curie temperature.[3, 6, 16] Besides the phase transformation of $BaTiO_3$ at 120 °C from cubic to tetragonal, two other crystal structure transformations occur at lower Curie

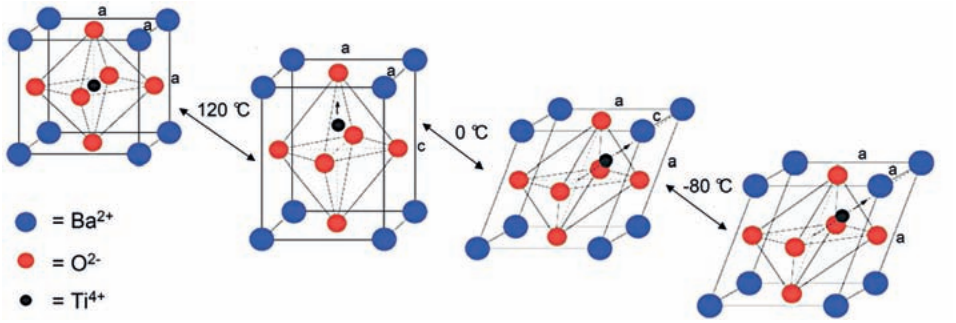

Figure 4.1.2: Unit cell distortions of $BaTiO_3$ at transition temperatures.

temperatures, see Figure 4.1.2. At approximately 0 °C the crystal structure of tetragonal $BaTiO_3$ changes to orthorhombic. Below the Curie temperature of -80 °C the unit cell is rhombohedral. In both orthorhombic and rhombohedral structures the Ti^{4+} and surrounding O^{2-} ions are displaced from the centre of the unit cell. The spontaneous polarization in both structures is oriented along the diagonal of the unit cell. The materials in which spontaneous polarization occurs, are ferroelectric. However, cubic $BaTiO_3$ has a high internal unit cell symmetry and spontaneous polarization does not occur. In this case cubic $BaTiO_3$ is called paraelectric.

In tetragonal, orthorhombic and rhombohedral $BaTiO_3$ ceramics the ion displacements form a dipole moment in the unit cell and the cell unit is distorted in a particular direction. Thus, spontaneous polarization is direction dependent and therefore for $BaTiO_3$ ceramics material properties like the relative permittivity are strongly anisotropic in a single crystal. The relative permittivity ε_r along the *a*-axis has values that exceed 2000–4000, while ε_r along the *c*-axis is low with values of about 200, see Figure 4.1.3.

Curie point shifters. The Curie temperatures and the transition of the $BaTiO_3$ crystal structures can be shifted by incorporation of isovalent substituents. The isovalent substituents, also called 'shifters' of Ba^{2+}, like Ca^{2+} and Sr^{2+}, will shift the Curie point to lower temperatures, see Figure 4.1.4.[17–18] Only the incorporation of Pb^{2+} in $BaTiO_3$ will shift the Curie temperature to higher temperatures. These elements can be mixed in any concentration as it forms a solid solution with $BaTiO_3$. The isovalent substituents Zr^{4+} and Sn^{4+}, used to replace Ti^{4+}, strongly lower the Curie temperature of the cubic-tetragonal transition. The Curie points of the other two phase transitions will be shifted to higher temperatures. For B-site substituted solid solutions of $Ba(Ti_{1-x}B_x)O_3$ the three phase transitions overlap at a higher concentration x=0.10–0.15 to one phase transition. The phase transition will change from cubic to rhombohedral around a temperature of 50 °C. High permittivity values are found for these types of dielectric materials.

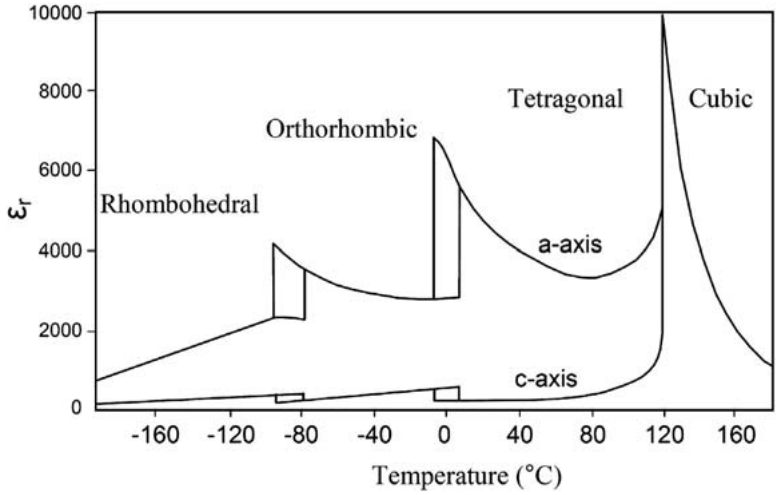

Figure 4.1.3: ε_r vs temperature of $BaTiO_3$ measured in a and c directions.[19]

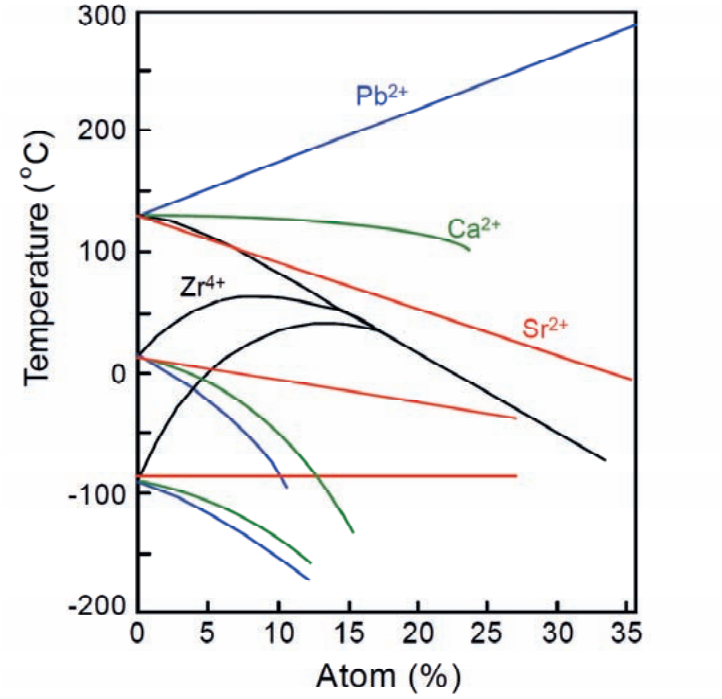

Figure 4.1.4: Curie Temperature changes after incorporation of isovalent shifters in $BaTiO_3$.[17]

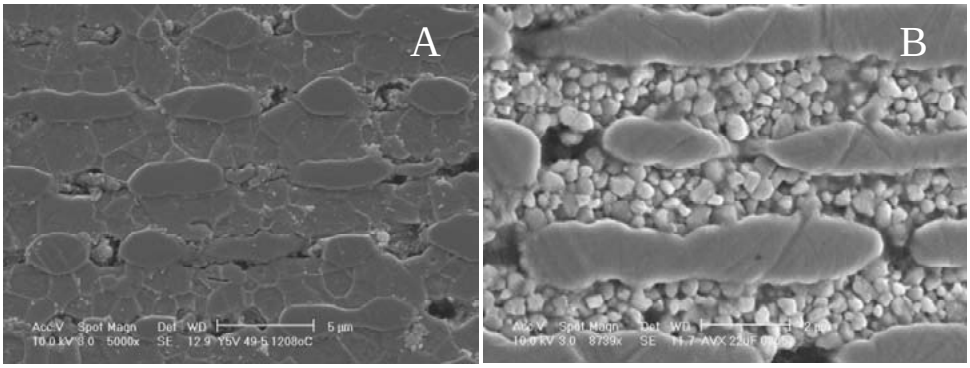

Figure 4.1.5: SEM micrographs of (a) an etched Y5V MLCC with a dielectric thickness of 3 μm and (b) an etched X5R MLCC with a dielectric thickness of 1.5 μm..

The Ba^{2+} and Ti^{4+} elements can also be substituted by other ions. However, the solubility of the ions can be limited, depending on ion properties like ionic radius and A/B ratio. Furthermore, the charge balance can also be distorted and affect the electrical properties of the dielectrics.

Y5V dielectric capacitors. For high capacitance multilayer capacitors a wide variety of materials has been developed. The dielectrics with very high relative permittivities are based on acceptor/donor doped $(Ba,Ca)(Ti,Zr)O_3$ solid solutions, which exhibit Y5V electrical characteristics with ε_r values of 14,000 or more. The ε_r of these type of ceramics is very dependent on the average grain size. The larger the average grain size, the larger the ε_r will be. Typically Y5V ceramic have large grains, however the minimum average grain size to obtain high relative permittivity values, larger than 5000, is limited to a minimum size of 2 to 3 μm, see Figure 4.1.5a. In Figure 4.1.6 the trend lines of the maximum dielectric constant, measured at the Curie point, as function of the average grain size for quite a number of Y5V compositions are shown.[20–21] The compositions are based on acceptor or acceptor/donor doped $(Ba_{1-x}Ca_x)(Ti_{1-y}Zr_y)O_3$ ceramics, with $x \leq 0.04$ and, $y \leq 0.18$. The dopant levels were limited to a maximum of 1 mol% regarding the acceptors and 0.5 mol% for the donor elements. In Figure 4.1.6 the individual results of all compositions are not shown, but there were no ceramics described having an average grain size below 2 μm. These relative large grains limit the development of dielectric layer thicknesses below 3 μm in MLCCs exhibiting Y5V properties. Thus material development had to change towards materials that exhibit X7R and X5R characteristics, which have finer grains, see Figure 4.1.5b. With X5R and X7R ceramics multilayer capacitors having dielectric layers below 2 μm can be produced.

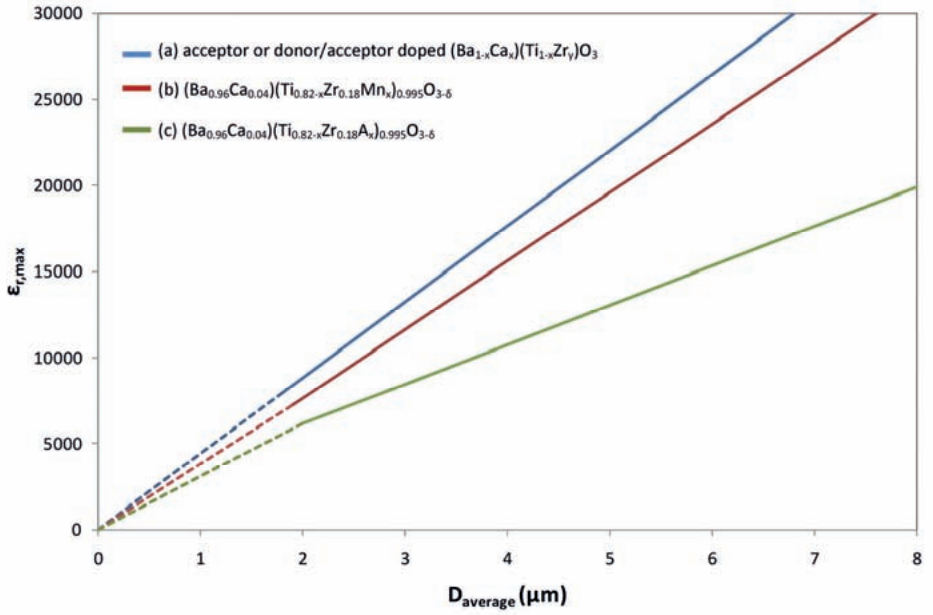

Figure 4.1.6: The trend lines of the maximum dielectric constant, measured at the Curie point, as function of the average grain size for (a) acceptor-doped or acceptor/donor-doped $(Ba_{1-x}Ca_x)(Ti_{1-y}Zr_y)O_3$ ceramics, (b) Mn-doped $(Ba_{0.96}Ca_{0.04})(Ti_{0.82-x}Zr_{0.18}Mn_x)_{0.995}O_{3-\delta}$ and (c) $(Ba_{0.96}Ca_{0.04})(Ti_{0.82-x}Zr_{0.18}Mn_x)_{0.995}O_{3-\delta}$ doped with various other acceptors.[20–21]

4.1.2 High-ε_r X5R multilayer capacitors with Ni electrodes

For thin film dielectrics fine $BaTiO_3$ powders are needed and high demands are set on powder properties, like high purity, homogeneous composition and cation distribution, uniform morphology, particle shape controllability and weak agglomeration.[5] The $BaTiO_3$ powders can be made by various production methods like mixed oxide, oxalate, alkoxide, sol-gel or hydrothermal route or other methods of synthesis.[5, 16, 22] Each method will produce $BaTiO_3$ powders with unique powder properties. The synthesis of $BaTiO_3$ is not within the scope in this work and will not be discussed further in detail.

The Y5V, X7R and X5R dielectrics are based on $BaTiO_3$ ceramics to which dopants are added in order to meet the electrical requirements. Two decades ago Y5V and X7R capacitors were made with noble metal electrodes like palladium or platinum, but due to high electrode layer count in the high-ε_r MLCCs and the high cost price of these metals currently the majority of the high-ε_r MLCCs are made with cheaper nickel as metal for the inner electrodes as discussed in Chapter 1.

Electron conduction suppressed by acceptor doping. When multilayer capacitors are manufactured with nickel electrodes the sintering process has to be performed in a reducing atmosphere like forming gas H_2/N_2 or CO/CO_2. Therefore the dielectric ceramics have to be reduction stable when fired at temperatures between 1200 and 1350°C at low oxygen pressures. When $BaTiO_3$ is sintered in a reducing atmosphere the conductivity of the ceramics changes, which can be represented by:[23–24]

$$BaTiO_3 + y/2\ H_2 \rightarrow BaTiO_{3-y}[V_O^x]_y + y/2\ H_2O \qquad (4.1.3)$$

when the oxygen vacancies, V_O^x, are ionized (activation energy E_a < 0.1 eV) electrons and double ionized oxygen vacancies are formed:

$$[V_O^x] \rightarrow [V_O^{\cdot\cdot}] + 2\ e' \qquad (4.1.4)$$

The formation of electronic and ionic charge carriers have a large influence on the insulation resistivity of the ceramics. Especially the conduction electrons, which are formed during sintering in a reducing atmosphere, contribute to a higher conductivity of the ceramics, which increases with 10–12 orders of magnitude. The ceramics are completely reduced and become semi-conductive.

The electron conduction can be suppressed by adding certain ions to $BaTiO_3$. When transition ions like Fe^{3+}, Mn^{2+} and Cr^{3+} are incorporated at the Ti^{4+} site, the conduction electrons are trapped by these acceptor ions according to;[23]

$$A_{Ti}^x + n\ e' \rightarrow [A_{Ti}^{n'}] \qquad (4.1.5)$$

where A = Ca^{2+}, Mg^{2+}, Cr^{3+}, Cr^{2+}, Mn^{3+}, Mn^{2+}, Fe^{3+} etc. The stronger acceptor ions are incorporated in the $BaTiO_3$ lattice, the more electrons can be trapped and the more insulating the dielectrics becomes. The insulation resistance improved from 10^2 to 10^{13} Ω·cm (E_a > 2 eV).[24]
Conduction electrons can be effectively trapped by incorporation of acceptor ions, like Ca^{2+} at the Ti^{4+} site, in the $BaTiO_3$ lattice;

$$CaO \rightarrow Ca_{Ti}" + O_O^x + V_O^{\cdot\cdot} \qquad (4.1.6)$$

Whereby ionized oxygen vacancies are formed in similar concentrations;

$$[Ca_{Ti}"] = [V_O^{\cdot\cdot}] \qquad (4.1.7)$$

Thus the incorporation of only acceptors in the $BaTiO_3$ lattice causes a higher conductivity due to electromigration of charged oxygen vacancies, even at room temperature, under the influence of an electrical field.[22, 24] In thin dielectric layers this results in degradation of the ceramic and considerable shortening of the life time of Ni-MLCCs.
Lifetime stability improvement. The concentration of oxygen vacancies can be reduced or even eliminated by gentle re-oxidation to improve the lifetime of the MLCCs. Therefore the MLCCs are heat treated after sintering at a moderate temperature in an atmosphere in which the oxygen partial pressure is low enough to avoid oxidation of the nickel electrodes. The concentration of oxygen vacancies is decreased during re-oxidation due to change of the vacancy state of unstable acceptor ions like Cr^{3+}, Fe^{2+}, Mn^{2+} etc.[23–24] As an example the valence state of Mn^{2+} is changed during re-oxidation to Mn^{3+} or Mn^{4+};

$$2\,[Mn_{Ti}"] + 2\,[V_O^{\cdot\cdot}] + ½O_2 \leftrightarrow 2\,[Mn_{Ti}'] + [V_O^{\cdot\cdot}] \qquad (4.1.8)$$

while the concentration of oxygen vacancies is diminished and less oxygen vacancies are needed to compensate the Mn-acceptors:

$$[Mn_{Mn}"] \approx [V_O^{\cdot\cdot}] \qquad (4.1.9)$$

$$[Mn_{Mn}'] \approx ½\,[V_O^{\cdot\cdot}]$$

$$[Mn_{Mn}] \approx \text{nil}$$

Thus, if the ceramics could be completely re-oxidized to Mn^{4+}, all oxygen vacancies would be diminished. However, re-oxidation of the MLCCs has to be carried out

under mild conditions. Therefore oxygen vacancies were still present in the ceramics. Nevertheless the lifetime of these type of MLCCs, acceptor doped $BaTiO_3$ dielectrics, were improved after the re-oxidation process.

The lifetime of BME MLCCs, which consist of acceptor-doped $BaTiO_3$ dielectrics, were still not optimal. Further improvement of lifetime stability was established by incorporation of a mixture of donor and acceptor ions into the $BaTiO_3$ lattice. Examples of a donor/acceptor combinations are Mn^{3+}/Nb^{5+} or Mn^{2+}/W^{6+}:[23–25]

$$[Mn_{Ti}'] + [Nb_{Ti}^{\cdot}] \leftrightarrow \{[Mn_{Ti}'][Nb_{Ti}^{\cdot}]\}^0 \qquad (4.1.10)$$

$$[Mn_{Ti}''] + [W_{Ti}^{\cdot\cdot}] \leftrightarrow \{[Mn_{Ti}'']][W_{Ti}^{\cdot\cdot}]\}^0 \qquad (4.1.11)$$

The incorporation of the donor ions reduces the concentration of oxygen vacancies. Furthermore, the incorporation of donor and acceptor ions forms very stable charge complexes. The charge complexes of Mn^{3+} and Nb^{5+} are so strong that Mn^{3+} cannot be oxidized further into Mn^{4+}, even when the re-oxidation is carried out in a pure oxygen atmosphere. The donor and acceptor charge complexes are determined primarily by the ionic charge of the ions and this charge complex is a strong barrier against oxygen vacancy migration.

The 'magic' ions. Further enhancement of lifetime can be achieved by the incorporation of the so-called 'magic ions' Y^{3+}, Dy^{3+} and Ho^{3+}. These rare earth (RE^{3+}) ions have a relatively small ionic radius and they can enter at the A and the B sites in the $BaTiO_3$ lattice, see Figure 4.1.7. Due to their amphoteric character these ions can either act as donor, when incorporated at the A-site, or as acceptor when introduced on the B-site.[23, 26]

$$\text{A-site: } RE_2O_3 \xrightarrow{2\ TiO_2} 2[RE_{Ba}^{\cdot}] + [V_{Ba}''] + 3\ [O_o^x] \qquad (4.1.12)$$

$$\text{B-site: } RE_2O_3 \xrightarrow{2\ BaO} 2[RE_{Ti}'] + [V_o^{\cdot\cdot}] + 3\ [O_o^x] \qquad (4.1.13)$$

The A/B ratio determines the distribution of amphoteric ions over the A and B-sites. However, when the 'magic ions' distribute evenly over the A and B-sites in the $BaTiO_3$ lattice they compensate each other and form acceptor-donor complexes. Therefore the concentration of oxygen vacancies is quite low. The Y5V and X7R dielectrics which are based on rare earth-doped $BaTiO_3$ ceramics exhibit excellent lifetime properties.[1, 23] When Ni-MLCCs based on these kind of dielectrics are sintered and re-oxidized in a controlled way their lifetime is comparable or even better than Pd-MLCCs.

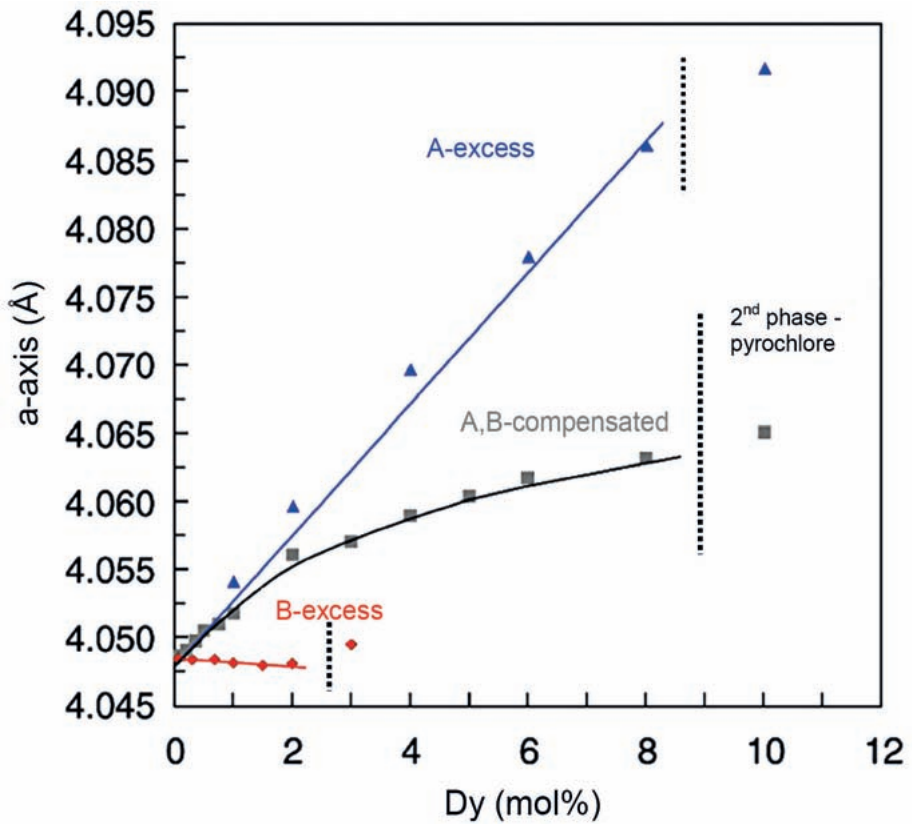

Figure 4.1.7: Lattice parameters of Dy^{3+} incorporated in $BaTiO_3$ depending on A/B ratio.[23–24]

Besides the three 'magic ions', also other rare earth ions can enter the $BaTiO_3$ lattice. Depending on the ionic radii of the rare earth ions and the material properties of $BaTiO_3$, like microstructure and A/B ratio, the rare earth ion can be incorporated at the A or B site or at both.[9] The elements with large ionic radii, like La^{3+} or Nd^{3+}, will be preferably incorporated on the A site and replace Ba^{2+}. The elements with small ionic radii, like Tm^{3+}, Yb^{3+} and Lu^{3+}, will be incorporated on the B-site and replace Ti^{4+}. The rare earth elements which have an intermediate ionic radius may incorporate on both A and B sites in $BaTiO_3$. The elements of group IIIB, Sc^{3+}, Y^{3+} and La^{3+}, show a similar relationship regarding site occupancy as the rare earth elements. La^{3+}, which is a rare earth element with a large ionic radius, prefers to incorporate at the B site, while Sc^{3+} will be located primarily at the A site. The ion Y^{3+} is amphoteric and has similar chemical properties as Er^{3+} and will be dissolved on both locations until the solubility of the elements in $BaTiO_3$ is reached. When larger concentrations of amphoteric elements are added to $BaTiO_3$ the remaining amount will reside in the grain boundary region.[26–29]

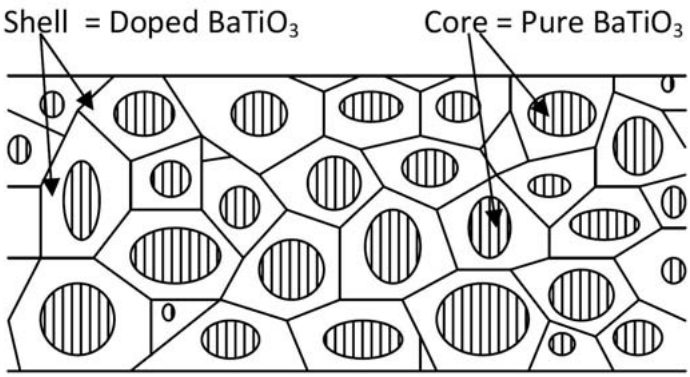

Figure 4.1.8: Schematic microstructure of core-shell dielectrics.

Core-shell microstructure. Besides the composition of the ceramics also the microstructure of the ceramics plays an important role in making reliable X5R and X7R ceramics. The first types of X7R dielectrics have a core-shell structure. These ceramics consist of grains having a core of pure ferroelectric tetragonal $BaTiO_3$, which is surrounded by a doped shell phase. The shell is a formed by adding small amount of donor, acceptor and/or amphoteric dopants to $BaTiO_3$ to form a solid solutions of various concentrations of the added elements in the shell. With controlled diffusion of the dopants during sintering a temperature stable dependence of the dielectric constant can be achieved. The first type of core-shell X7R dielectrics were based on additions of donor/acceptor combinations, like Nb_2O_5/Co_3O_4 and Nb_2O_5/Bi_2O_3, which were incorporated in $BaTiO_3$.[30–34] Later dielectrics based on MgO and RE_2O_3 additions to $BaTiO_3$ were investigated for production of X7R Ni-MLCCs. The grains of MgO-RE_2O_3 doped $BaTiO_3$ ceramics had a core-shell structure, see Figure 4.1.8. The core consists of almost pure ferroelectric $BaTiO_3$, and the shell is a paraelectric solid solution of $BaTiO_3$ and added elements. The core-shell structure is formed during sintering. A study of MgO-Ho_2O_3 doped $BaTiO_3$ materials revealed that MgO reacts with $BaTiO_3$ at low temperatures and forms an initial core-shell structure.[1, 35–36] Ho_2O_3 reacts at higher temperatures, but MgO suppresses the diffusion of Ho_2O_3 into the core. Further grain growth is inhibited by MgO at high sintering temperatures.[1, 37] A study of other MgO/RE_2O_3 dopant combinations revealed that MgO suppresses grain growth of the ceramics. Furthermore, diffusion of RE_2O_3 ions into the core-shell grains is dependent on the amount of MgO and the ionic radius of the rare earth ions. The concentration of MgO, the choice and concentration of Re_2O_3-type ions and the ratio between MgO/RE_2O_3 influences the microstructure and the electrical properties of the ceramics.

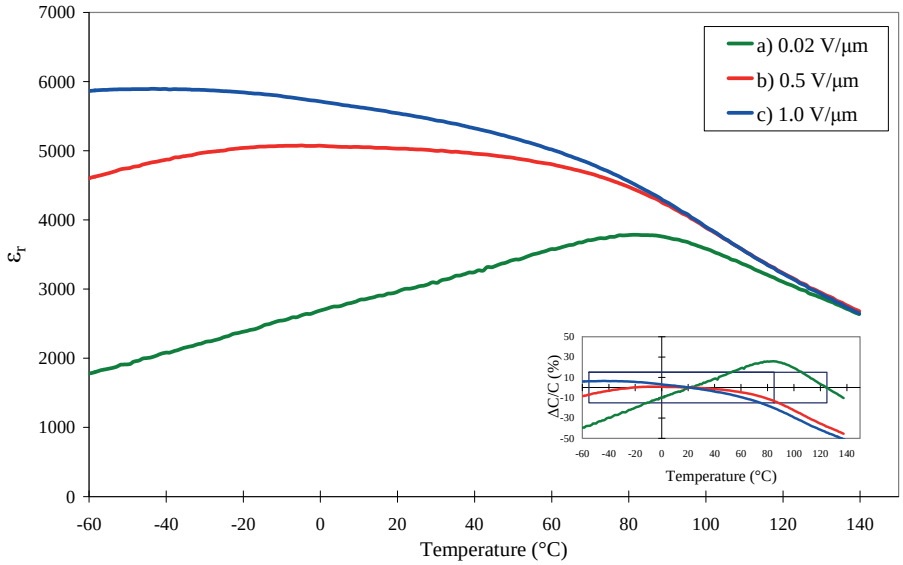

Figure 4.1.9: The relationship between relative permittivity and temperature of a 0603–10 µF MLCC with a dielectric thickness of 1 µm, measured with an AC current at 1 kHz and field strength (a) 0.02 V/µm, (b) 0.5 V/µm and (c) 1.0 V/µm. The inset shows the capacitance drift (ΔC/C in %) in relation to temperature with respect to X5R and X7R specification.

Temperature characteristics. The incorporation of MgO, MnO, rare earth oxides and, if necessary, other metal ions in the $BaTiO_3$ lattice influences the temperature characteristics of the dielectric phase. As mentioned above the ferro-electric core consists of nearly pure $BaTiO_3$ domains. The incorporation of various elements in the shell of the core-shell grains will locally shift the Curie point (T_c), depending on the concentration of the added elements. For pure $BaTiO_3$ the Curie temperature is around 125 °C, but addition of other elements decreases T_c depending on type and concentration of the cations. The shell exhibits paraelectric properties due to the incorporation of various elements.

Thus the core-shell grains consist of a ferroelectric core and a paraelectric shell, each having locally varying relative permittivity values. The superposition of inhomogeneously distributed domains with varying relative permittivity values can result in a flat capacitance-temperature dependency as is needed for X5R and X7R dielectrics as shown in Figure 4.1.9.[38–39]

4.1.3 Electrical characteristics of high-ε_r multilayer capacitors

When the dielectric layers are reduced in thickness, serious attention has to be paid not only to the permittivity but also to the insulation resistance of the materials. For good performance in terms of reliability and lifetime, the dielectric materials have to withstand leakage currents. In X5R and X7R core-shell materials the insulation resistance is dependent on the grain boundary characteristics, which play an important role in avoiding degradation of the dielectrics.[40–42] The dielectric layers should therefore have at least some 4 core-shell grains on top of each other to achieve high insulation resistance. Hence, when the dielectric thickness is reduced, the grain size has to be decreased as well. Thus finer powders are needed. Unfortunately, when the grain size of $BaTiO_3$, which is the main material responsible for high permittivity values, is decreased the relative permittivity of the dielectrics is reduced as well.[43–44] The development is therefore focused on implementing smaller grains with higher relative permittivity values in thinner dielectric layers to produce high capacitive multilayer capacitors.[4]

AC/DC field dependency. The electrical properties of the multilayer capacitors are important. Capacitors up to 10 μF are measured with an AC current of 1 kHz and 1 V_{rms} with no DC bias at room temperature (25 °C), according to the EIA guidelines. MLCC which have capacitances larger than 10 μF are measured with an AC current of 120 Hz and 0.5 V_{rms} with a 0 V DC bias.[45] These are the standard measurement conditions to classify the multilayer capacitors. However, in real applications the capacitors are used under other conditions and the capacitance is very dependent on the applied current and voltage. For example, thin layer X5R multilayer capacitors show a large AC and DC voltage dependence to capacitance. The relationships between permittivity and applied AC and DC voltage of a 0805 10 μF multilayer capacitor are shown in Figure 4.1.10 and Figure 4.1.11, respectively. The 0805–10 μF MLCCs have a dielectric thickness of 2 μm and the MLCCs exhibit X7R characteristics. Both figures clearly show that the applied electrical field has a large effect on the polarization in the capacitors. When an AC electrical field ranging from 0.1 to 1 V/μm (i.e., 1 to 100 kV/cm) is applied to a high permittivity capacitor the capacitance varied from -30 to +10 % compared to its nominal value at 25 °C. When a DC bias with an electrical field from 0 to 12.5 V/μm (equivalent to 125 kV/cm) was applied to the X7R capacitor the capacitance decreased by 8 % of its nominal capacitance at 25 °C. These values show that the applied electrical field has a strong effect on the electric properties of the dielectric materials used for X5R and X7R multilayer capacitors.

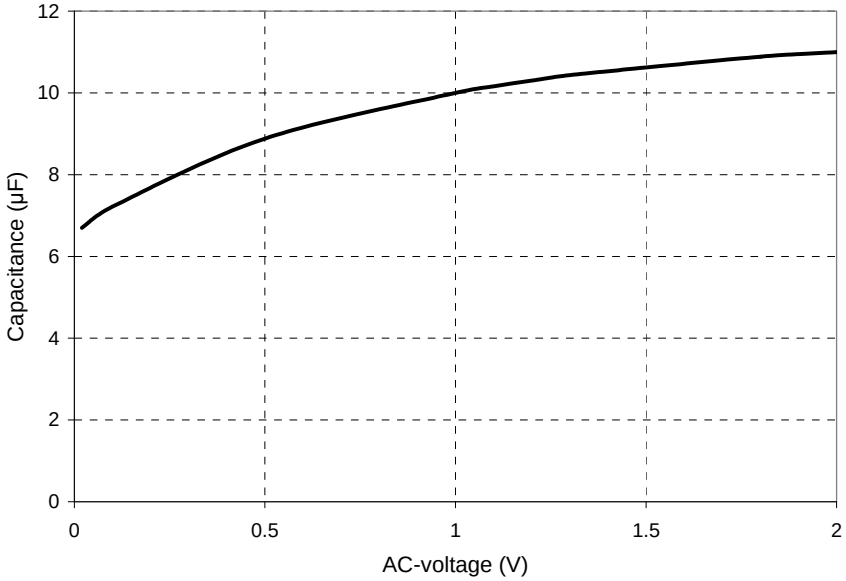

Figure 4.1.10: AC voltage dependence for 0805–10 µF X7R MLCCs with dielectric layers of 2 µm thickness. Measured at 1 kHz without DC bias.

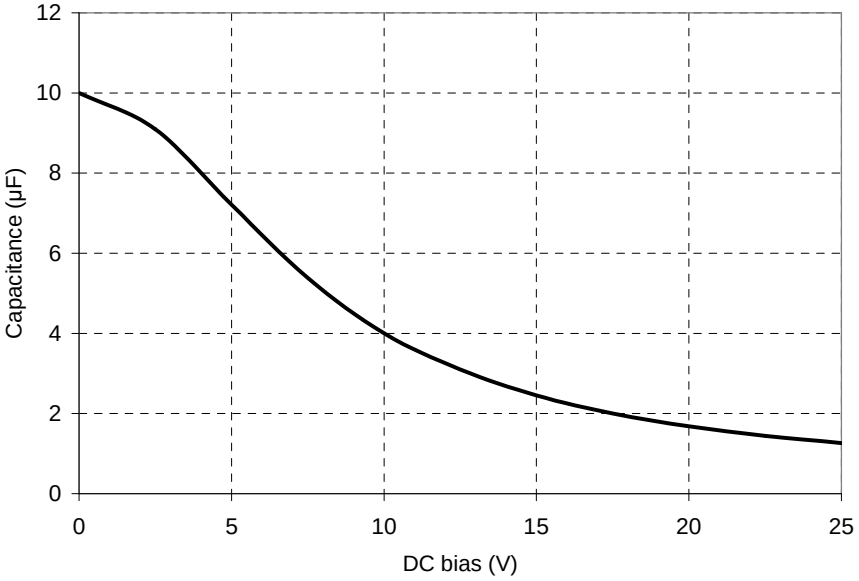

Figure 4.1.11: DC voltage dependence of 0805–10 µF X7R MLCCs with dielectric layers of 2 µm thickness. Measured with an electrical load at 1 kHz and 1 V_{rms} AC voltage.

Effect on thin dielectric layer. Besides the strong influence of applied electrical field on capacitance, the capacitance is also strongly dependent on the working temperature when capacitors are applied under an electrical field. In Figure 4.1.9 the temperature coefficient of capacitance (TCC) of a 0603 10 μF MLCC, with a dielectric layer thickness is 1 μm, is shown for various electrical fields at a frequency of 1 kHz. A distinct variation of capacitance with varying electrical field and temperature can be seen in the figure. For development of high capacitance dielectrics not only a large relative permittivity is needed. A reasonably flat relationship between capacitance and temperature, measured at specified frequency and electrical field, is also of great importance.

With decreasing dielectric layer thickness the electrical field is increased accordingly, when the capacitors have to be measured with one similar measurement condition. The polarization within the dielectrics will be influenced when a higher electrical field is applied and that will also influence the TCC characteristics. Therefore, when thinner dielectric layers are used in high-ε_r MLCCs, the composition of the dielectrics has to be modified. Thinner dielectric layers also affect other properties like insulation resistance (IR), aging rate and breakdown voltage (V_B) of MLCCs, especially when the dielectric layers are less than 1 μm thick and the applied electrical field is relatively large. Thus, when dielectric layers of less than 1 μm thickness are applied in multilayer capacitors, the dielectrics have to perform at relatively high electrical fields and still the multilayer capacitors should have reliable electrical properties.

Scope of this chapter. In the next chapters X5R dielectric materials, which are used in multilayer capacitors having nickel electrodes, will be described. The scope of this chapter is to evaluate various materials in order to make high capacitive efficient capacitors. In Chapter 4.2 the influence of AC electrical fields over the dielectric layers is discussed with respect to material composition. In particular, the dielectric characteristics of ceramic disc capacitors and multilayer capacitors, made of dielectrics having various yttrium concentrations, are compared. As the dielectric properties are also dependent on the raw materials, their ratio and the initial particle size distribution prior to the firing process, is described in Chapter 4.3. The results show that high permittivity dielectrics, based on $BaTiO_3$ to which Y_2O_3, MgO, $MnCO_3$, SiO_2 and some other elements are added, yield high capacitance multilayer capacitors. An alternative strategy to make high permittivity dielectrics is proposed in Chapter 4.4. The main raw materials are not only based on pure $BaTiO_3$, but also contain $BaTiO_3$ powders with high concentrations of yttrium and copper. To this mixture extra dopant was added to produce a new type of high permittivity dielectrics. Furthermore, the microstructure of a typical high-ε_r dielectric was examined in detail and the results are discussed in Chapter 4.5.

References

1) Kishi, H.; Mizuno, Y. and Chazono, H. *Base-metal electrode-multilayer ceramic capacitors: Past, present and future perspectives*; Japanese Journal of Applied Physics Part 1-Regular Papers Short Notes & Review Papers, 2003 **42**(1): p. 1–15.
2) Anklekar, R. M.; Fish, J.; Christofferson, J. and Cooke, V. *Insulation resistance production testing of high-capacitance base metal electrode multilayer ceramic capacitors*; conference paper CARTS USA 2003, p. 88.
3) Pan, M. J. and Randall, C. A. *A Brief Introduction to Ceramic Capacitors*; IEEE Electrical Insulation Magazine, 2010 **26**(3): p. 44–50.
4) Randall, M.; Skamser, D.; Kinard, T.; Qazi, J. and Tajuddin, A. *Thin film MLCC*; Conference paper CARTS USA, 2007: p. 1–12.
5) Pithan, C.; Hennings, D. and Waser, R. *Progress in the synthesis of nanocrystalline $BaTiO_3$ powders for MLCC*; International Journal of Applied Ceramic Technology, 2005 **2**(1): p. 1–14.
6) *Electroceramics*; 2nd ed.; Moulson, A. J. and Herbert, J. M.; John Wiley & Sons Ltd.: Chichester, 2003; p 71.
7) Xu, N.; Zhao, H.; Zhou, X.; Wei, W.; Lu, X.; Ding, W. and Li, F. *Dependence of critical radius of the cubic perovskite ABO_3 oxides on the radius of A- and B-site cations*; International Journal of Hydrogen Energy, 2010 **35**(14): p. 7295–7301.
8) Johnsson, M. and Lemmens, P. *Perovskites and thin films - Crystallography and chemistry*; Journal of Physics Condensed Matter, 2008 **20**(26): p 36.
9) Shannon, R. D. *Revised effective ionic-radii and systematic studies of interatomic distances in halides and chalcogenides*; Acta Crystallographica Section A, 1976 **32**(SEP1): p. 751–767.
10) Bhalla, A. S.; Guo, R. and Roy, R. *The perovskite structure - A review of its role in ceramic science and technology*; Materials Research Innovations, 2000 **4**(1): p. 3–26.
11) Goudochnikov, P. and Bell, A. J. *Correlations between transition temperature, tolerance factor and cohesive energy in 2^+:4^+ perovskites*; Journal of Physics Condensed Matter, 2007 **19**(17): p. 6201
12) Reaney, I. M. and Ubic, R. *Dielectric and structural characteristics of perovskites and related materials as a function of tolerance factor*; Ferroelectrics, 1999 **228**(1–4): p. 23–28.
13) Tsur, Y.; Dunbar, T. D. and Randall, C. A. *Crystal and defect chemistry of rare earth cations in $BaTiO_3$*; Journal of Electroceramics, 2001 **7**(1): p. 25–34.
14) Mitchell, R. H. and Liferovich, R. P. *A structural study of the perovskite series $Ca_{1-x}Na_xTi_{1-x}Ta_xO_3$*; Journal of Solid State Chemistry, 2004 **177**(12): p. 4420–4427.
15) Itoh, M. and Taniguchi, H. *Ferroelectricity in perovskite-type oxides*; Ferroelectrics, 2008 **369**(1 PART 3): p. 127–132.
16) Yoon, D. H. *Tetragonality of barium titanate powder for a ceramic capacitor application*; Journal of Ceramic Processing Research, 2006 **7**(4): p. 343–354.
17) *Piezoelectric ceramics*; Jaffe, B.; Cooke, W. R. and Jaffe, H.; Academic Press: London, 1971; p 53.
18) *Electroceramics*; 2nd ed.; Moulson, A. J. and Herbert, J. M.; John Wiley & Sons Ltd.: Chichister, 2003; p 313.
19) *Electroceramics*; 2nd ed.; Moulson, A. J. and Herbert, J. M.; John Wiley & Sons Ltd.: Chichister, 2003; p 73.

20) Hansen, P.; Hennings, D. and Schreinemacher, H. *High-K dielectric ceramics from donor/acceptor-codoped ($Ba_{1-x}Ca_x$)($Ti_{1-y}Zr_y$)O_3 (BCTZ)*; Journal of the American Ceramic Society, 1998 **81**(5): p. 1369–1373.
21) Hansen, P.; Hennings, D. and Schreinemacher, H. *Dielectric properties of acceptor-doped (Ba,Ca)(Ti,Zr)O_3 ceramics*; Journal of Electroceramics, 1998 **2**(2): p. 85–94.
22) *Electroceramics*; 2nd ed.; Moulson, A. J. and Herbert, J. M.; John Wiley & Sons Ltd: Chichester, 2003; p 100–101.
23) Hennings, D. F. K. *Dielectric materials for sintering in reducing atmospheres*; Journal of the European Ceramic Society, 2001 **21**(10–11): p. 1637–1642.
24) Lee, W. H.; Groen, W. A.; Schreinemacher, H. and Hennings, D. *Dysprosium doped dielectric materials for sintering in reducing atmospheres*; Journal of Electroceramics, 2000 **5**(1): p. 31–36.
25) Albertsen, K.; Hennings, D. and Steigelmann, O. *Donor-acceptor charge complex formation in barium titanate ceramics: Role of firing atmosphere*; Journal of Electroceramics, 1998 **2**(3): p. 193–198.
26) Sakabe, Y.; Hamaji, Y.; Sano, H. and Wada, N. *Effects of rare-earth oxides on the reliability of X7R dielectrics*; Japanese Journal of Applied Physics Part 1-Regular Papers Short Notes & Review Papers, 2002 **41**(9): p. 5668–5673.
27) Xue, L. A.; Chen, Y. and Brook, R. J. *The influence of ionic-radii on the incorporation of trivalent dopants into $BaTiO_3$*; Materials Science and Engineering B-Solid State Materials for Advanced Technology, 1988 **1**(2): p. 193–201.
28) Mizuno, Y.; Kishi, H.; Ohnuma, K.; Ishikawa, T. and Ohsato, H. *Effect of site occupancies of rare earth ions on electrical properties in Ni-MLCC based on $BaTiO_3$*; Journal of the European Ceramic Society, 2007 **27**(13–15): p. 4017–4020.
29) Yang, W. C.; Hu, C. T. and Lin, I. N. *Effect of Y_2O_3/MgO co-doping on the electrical properties of base-metal-electroded $BaTiO_3$ materials*; Journal of the European Ceramic Society, 2004 **24**(6): p. 1479–1483.
30) Chazono, H. and Kishi, H. *Sintering characteristics in $BaTiO_3$-Nb_2O_5-Co_3O_4 ternary system: I, electrical properties and microstructure*; Journal of the American Ceramic Society, 1999 **82**(10): p. 2689–2697.
31) Chazono, H. and Kishi, H. *Sintering characteristics in the $BaTiO_3$-Nb_2O_5-Co_3O_4 ternary system: II, stability of so-called "core-shell" structure*; Journal of the American Ceramic Society, 2000 **83**(1): p. 101–106.
32) Hennings, D. F. K. and Schreinemacher, B. S. *Temperature-stable dielectric materials in the system $BaTiO_3$-Nb_2O_5-Co_3O_4*; Journal of the European Ceramic Society, 1994 **14**(5): p. 463–471.
33) Pathumarak, S.; Alkhafaji, M. and Lee, W. E. *Microstructural development on firing Nb_2O_5 and Bi_2O_3 doped $BaTiO_3$*; British Ceramic Transactions, 1994 **93**(3): p. 114–118.
34) Park, Y. and Kim, Y. H. *The dielectric temperature characteristics of additives modified Barium-Titanate having core-shell structured ceramics*; Journal of Materials Research, 1995 **10**(11): p. 2770–2776.
35) Kishi, H.; Kohzu, N.; Sugino, J.; Ohsato, H.; Iguchi, Y. and Okuda, T. *The effect of rare-earth (La, Sm, Dy, Ho and Er) and Mg on the microstructure in $BaTiO_3$*; Journal of the European Ceramic Society, 1999 **19**(6–7): p. 1043–1046.

36) Mizuno, Y.; Okino, Y.; Kohzu, N.; Chazono, H. and Kishi, H. *Influence of the microstructure evolution on electrical properties of multilayer capacitor with Ni electrode*; Japanese Journal of Applied Physics Part 1-Regular Papers Short Notes & Review Papers, 1998 **37**(9B): p. 5227–5231.
37) Kishi, H.; Okino, Y.; Honda, M.; Iguchi, Y.; Imaeda, M.; Takahashi, Y.; Ohsato, H. and Okuda, T. *The effect of MgO and rare-earth oxide on formation behavior of core-shell structure in $BaTiO_3$*; Japanese Journal of Applied Physics Part 1-Regular Papers Short Notes & Review Papers, 1997 **36**(9B): p. 5954–5957.
38) Liu, X. A.; Cheng, S. G. and Randall, C. A. *The core-shell structure in ultrafine X7R dielectric ceramics*; Journal of the Korean Physical Society, 1998 **32**: p. S312-S315.
39) Park, Y. and Song, S. A. *Influence of core-shell structured grain on dielectric properties of cerium-modified barium titanate*; Journal of Materials Science-Materials in Electronics, 1995 **6**(6): p. 380–388.
40) Mizuno, Y.; Hagiwara, T. and Kishi, H. *Microstructural design of dielectrics for Ni-MLCC with ultra-thin active layers*; Journal of the Ceramic Society of Japan, 2007 **115**(1342): p. 360–364.
41) Chazono, H. and Kishi, H. *Dc-electrical degradation of the BT-based material for multilayer ceramic capacitor with Ni internal electrode: Impedance analysis and microstructure*; Japanese Journal of Applied Physics Part 1-Regular Papers Short Notes & Review Papers, 2001 **40**(9B): p. 5624–5629.
42) Morita, K.; Mizuno, Y.; Chazono, H. and Kishi, H. *Effect of Mn addition on electrical properties of Ni-MLCC*; Asian Ceramic Science for Electronics Ii and Electroceramics in Japan V, Proceedings, 2002 **228–2**: p. 195–198.
43) Arlt, G.; Hennings, D. and Dewith, G. *Dielectric-properties of fine-grained barium-titanate ceramics*; Journal of Applied Physics, 1985 **58**(4): p. 1619–1625.
44) Frey, M. H.; Xu, Z.; Han, P. and Payne, D. A. *The role of interfaces on an apparent grain size effect on the dielectric properties for ferroelectric barium titanate ceramics*; Ferroelectrics, 1998 **206**(1–4): p. 337–353.
45) Mosley, L. E. *Capacitor impedance needs for future microprocessors*; Conference paper CARTS USA 2006, p. 193–203.

Chapter 4.2

A quick method to determine the capacitance characteristics of thin layer X5R multilayer capacitors[1]

4.2.1. Introduction

Developments in the electronics industry are driven by miniaturization, the addition of more functionality in electronic devices, and cost reduction. As a consequence passive components like multilayer ceramic capacitors (MLCC) should achieve an increasingly high volumetric efficiency. There is an ongoing demand to increase the volumetric density by using thinner dielectric layers and higher layer numbers in successively smaller case size capacitors. Currently the thickness of dielectric layers of high capacitive MLCCs has already been reduced to below 1 µm and the number of active layers can range from 500 to 1000. Furthermore, the demand of temperature stable capacitors and high relative permittivity increased over the last decade. The dielectrics should also perform better and their electrical properties should be more reliable. Thus, capacitors having X5R characteristics are being used in electronic applications.[1–4] The X5R capacitors, as specified by the Electronics Industries Alliance (EIA), show a capacitance drift that may not exceed 15% of the nominal capacitance value at 25 °C in a temperature range from -55 to 85 °C. These types of dielectrics are based on modified $BaTiO_3$ with a microstructure of core-shell grains. The core-shell grains consist of a ferroelectric core of almost pure $BaTiO_3$ and a para-electric shell of doped $BaTiO_3$, which is formed by controlled addition of various elements.

Nowadays X5R multilayer capacitors are produced with nickel electrodes because of their low cost. Sintering of MLCCs therefore has to be carried out in an

[1] Published in Journal of the European Ceramic Society

atmosphere having a low oxygen partial pressure (pO_2) in order to prevent nickel from oxidizing. Numerous studies on the development of high permittivity dielectrics with high insulation resistivity values and good stability regarding temperature and applied electrical fields have been carried out since the 1980s. For X5R capacitors with base metal electrodes typically dielectrics based on $BaTiO_3$, doped with MgO, MnO, SiO_2 and one of the ´magic´ dopants, Ho_2O_3, Dy_2O_3 and Y_2O_3, are used.[5–10]

When the thickness of the dielectric layers in MLCCs is decreased, the electrical field is increased accordingly when a specific alternating current (AC) or direct current (DC) is applied. Therefore changes in dielectric properties occur, e.g. permittivity, loss factors, temperature stability, and reliability. Furthermore, the temperature independency of the dielectric constant is affected by changes of applied electrical field. It has nonetheless been possible to make temperature stable dielectrics for ultra thin layers with X5R characteristics by modifying the chemical composition and microstructure of the ceramics.

It is common in materials development to examine the properties of dielectrics in terms of electrical characteristics like relative permittivity and temperature coefficient of capacitance (TCC) directly on multilayer capacitors having ultrathin dielectric layers. However, the making of multilayer capacitors is laborious and costly. If ceramics disc capacitors (CDC) could be made and their electrical properties could be correlated directly with the behaviour in MLCCs, development time could be reduced significantly.

In the present study a method is proposed to evaluate the relative permittivity (ε_r) of CDCs in response to an applied AC electrical field by measuring the polarization versus applied electrical field. The slope of the hysteresis loops corresponds to $\varepsilon_r \cdot \varepsilon_0$, where ε_0 is the permittivity of vacuum.[3] These results are compared to the results from relative permittivity measurements on MLCCs versus applied AC electrical field.

4.2.2. Sample preparation and characterization

The ceramic disc capacitors (CDC) were made starting from powders of $BaTiO_3$ (NCI) and Y_2O_3 (Rhodia), SiO_2 (Degussa, Aerosil R975), $MnCO_3$ (J.T. Baker, 99.0%) and MgO (Konoshima, 99%). The powders were weighed according the formula

$BaTiO_3 + x$ mol% $YO_{1.5} + 0.4$ mol% MgO + 0.2 mol% $MnCO_3 + 1.0$ mol% SiO_2

where x = 3.0, 2.6, 2.1 or 1.5. The powders were ball-milled with 2 mm YTZ beads in an ethanol-toluene solvent mixture until a D_{50} of 0.2 μm was reached. The powders were dried, grounded and then the powders were pressed uniaxially (Fontijne SRA100) into pellets of 10 mm diameter x 2 mm height. Nickel electrodes were applied and the CDCs were sintered in a tube kiln (Carbolite) at 1280 °C for 2 h in a wetted 0.3% H_2/N_2 atmosphere. They were then re-oxidized at 1000 °C for 2 h in wetted N_2. The P-$U_{applied}$ hysteresis loops were measured at AC fields of 50, 150, 300, 450, 800, 900 and 1000 V/mm with an RT6000 HVS-2 analyzer (Radiant Technologies Inc.).

Green MLCC chips of above-mentioned compositions were produced on regular production equipment at Yageo in Roermond, The Netherlands. The MLCCs of 3.2 mm x 1.6 mm x 0.4 mm in size consisted of 50 electrode layers. The dielectric thickness of the MLCCs after sintering were between 2.2 and 2.6 μm; the electrode thickness was around 1 μm. Copper terminations were applied onto the chips, which were cured at 900 °C in a N_2 atmosphere.

The capacitances were measured at 1 kHz and under an applied electrical field ranging from 0.02 to 5 V_{rms} using a HP4284A LCR meter. The temperature coefficients of capacitance (TCC) of the samples were measured by measuring the capacitances respectively at 1 kHz/1V_{rms} and 1 kHz/0.02V_{rms} from -55 to +125 °C using a HP4284A LCR meter. The temperature was controlled using a Keithley 740 system scanning thermometer. This measurement setup was controlled by a computerized control system with data acquisition. The microstructures of the ceramics were examined using a scanning electron microscope (Philips XL20) after the MLCC samples were chemically etched for several seconds using a 1% HCl / 1% HF solution. The I-V curves were measured by determining the leakage current at 150 °C using a setup consisting of a Keithley K617 electrometer and an oven.

4.2.3. Discussion of CDC and MLCC results

The relationship between relative permittivity and applied AC field was investigated for X5R dielectrics with varying Y_2O_3 concentrations. The relative permittivity values of the ceramic disc capacitors were determined by polarization hysteresis loops of samples at electrical fields strengths of 50 to 1000 V/mm. Figure 4.2.1 shows an example of polarization (P) versus applied electrical field ($U_{applied}$) curves for a CDC sample measured at various electrical fields. The P-$U_{applied}$ loops were measured at 1 kHz. From the slope of the P-$U_{applied}$ curves the relative permittivity was calculated by dividing the maximum polarization by the maximum applied electrical field. Figure 4.2.2 shows the results of the relationship between ε_r and $U_{applied}$ of the four CDC samples. The ε_r-$U_{applied}$ dependency seems to have a

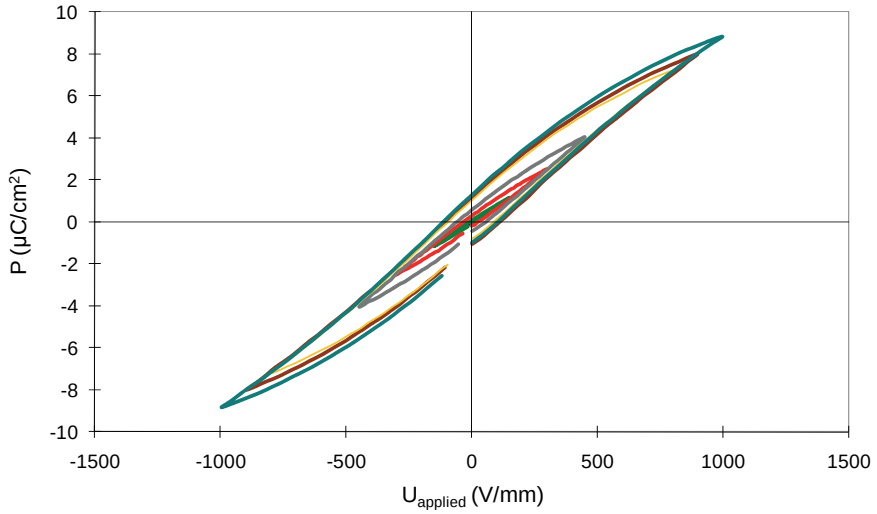

Figure 4.2.1: Hysteresis loop of CDC sample containing 1.5 mol% Y_2O_3.

maximum at 500–700 V/mm. At low $U_{applied}$ the value of ε_r is low because of random polarization in the domains. When $U_{applied}$ is increased the domain walls shift and an enhanced polarization is accomplished due to an increase of dipole motion, until a maximum polarization is reached at a certain $U_{applied}$. At even higher electrical fields the relative permittivity is decreased due to the non-linearity of the P-$U_{applied}$ curve. The results in Figure 4.2.2 also show that the ε_r-$U_{applied}$ curves vary depending on the Y_2O_3 concentration in the compositions. The value of ε_r of dielectrics with a low Y_2O_3 concentration show low dielectric constants compared to the dielectrics with higher Y_2O_3 concentration.

The dependency between ε_r and applied AC electrical field was also examined for the same dielectrics via measurements on MLCCs. The results in Figure 4.2.3 indicate a similar relationship between applied electrical field and relative permittivity. Initially an increase of the relative permittivity versus $U_{applied}$ is seen, until a maximum ε_r is reached at a certain applied electrical field. When higher AC fields were applied the ε_r decreased to lower values. This trend is similar as in CDCs.

The ε_r-$U_{applied}$ curves of the dielectrics with 1.5 and 2.0 mol% yttrium were similar. At higher Y concentrations the values of ε_r at given $U_{applied}$ were higher. At electrical field strengths below ~0.8 V/µm, the permittivity seems to be slightly lower for dielectrics having 2.6 mol% Y than for dielectrics with 3.0 mol% Y. Above 1 V/µm, the dielectrics with 3.0 mol% Y had slightly lower ε_r values than the dielectrics with 2.6 mol% Y. In any case the difference between the two curves was small and we assume that these curves are identical within experimental error.

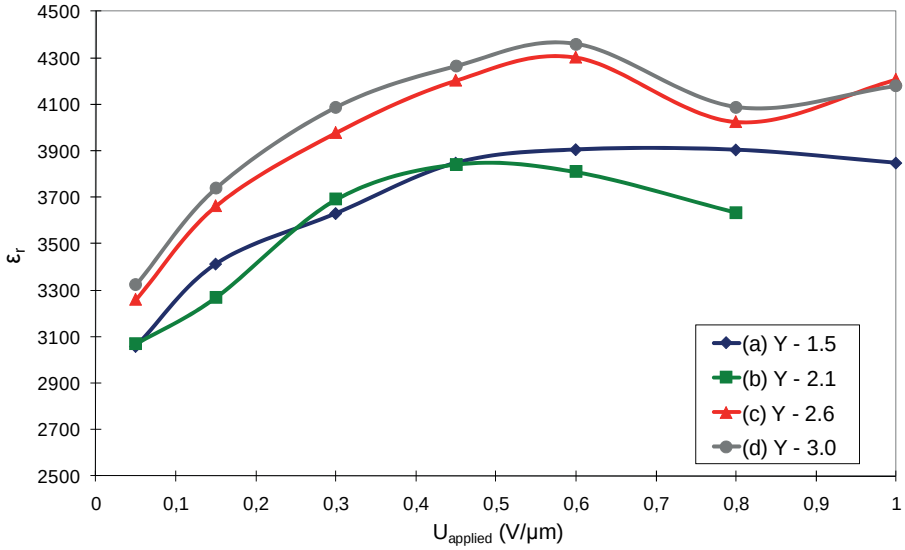

Figure 4.2.2: Relative permittivity as function of applied E in CDC samples.

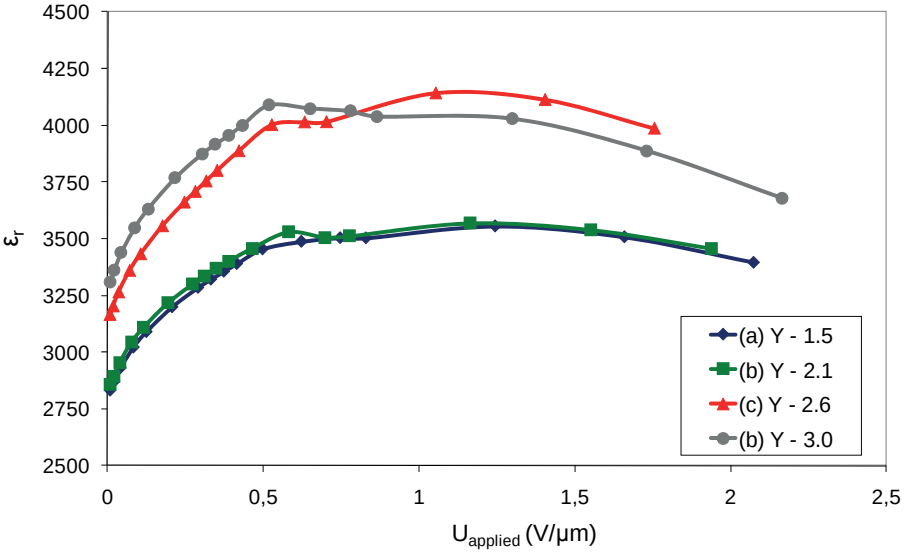

Figure 4.2.3: Relative permittivity as function of applied E in MLCC samples.

The results shown in Figure 4.2.3 suggest that two distinct types of microstructures formed, depending on yttrium concentration. The microstructure with low concentrations of yttrium had low permittivities, while the microstructure with high concentrations of Y_2O_3 showed higher permittivities. The difference between the ε_r-$U_{applied}$ characteristics of samples with lower (1.5–2.0 mol%) and higher (2.4–3.0 mol%) Y concentrations was also observed in Figure 4.2.2. Because both trend and absolute ε_r values were approximately similar for the series of measurements on CDCs and MLCCs, it can be concluded that direct measurements on CDCs are a good indicator for the ε_r values of MLCCs.

The temperature dependency of ε_r of MLCCs is very dependent on field strength. Because the core consists of ferroelectric $BaTiO_3$ the applied field strength dictates the ε_r.[3] To study the effect of field strength on the ε_r-*T* relationship, measurements were performed on MLCCs at both high and low applied field, employing field strengths of 0.4 V/μm and 0.008 V/μm, respectively. The frequency in both measurements was 1 kHz. Figure 4.2.4-I and 4.2.4-II show the temperature dependency of ε_r and TCC of the MLCC samples measured at high field. The results in Figure 4.2.4-II shows that the TCC curves of the four samples are relatively flat and that the capacitors can meet the X5R specification. Figure 4.2.4-I shows that the ε_r-*T* curves are dependent on the Y_2O_3 concentration and the ε_r-*T* curves of the four samples follow a similar trend in relation to temperature change above room temperature.

Figure 4.2.5-I and 4.2.5-II shows the results of temperature dependency of ε_r and TCC of MLCCs at low applied field. The permittivity ε_r of these samples is less dependent on *T* than at higher AC field. However, due to the smaller field the ε_r-values dropped, especially when measured well below the Curie temperature of 125 °C.

Around and above 125 °C ε_r was not influenced by an AC field. The Curie temperature of the core phase did not change due to the presence of Y. At lower temperatures ε_r is much more dependent on the applied AC electrical fields due to the occurrence of ferro-electricity, which is related to the tetragonal and orthorhombic crystal structure of $BaTiO_3$.

When foreign elements are reacted with $BaTiO_3$, then a shell of inhomogenously distributed chemical composition with different properties than the core phase forms. The incorporation of foreign elements usually shifts the Curie temperature. When the TCC of the samples were measured at low AC field the shift of the Curie temperature of the shell phase could be determined. The results are shown in Figure 4.2.5-II. The TCC of the various MLCC samples show a maximum that represents the Curie temperature of the shell phase. The results show that with increasing amount of Y the Curie point shifts to lower temperatures, see Table 4.2.1.

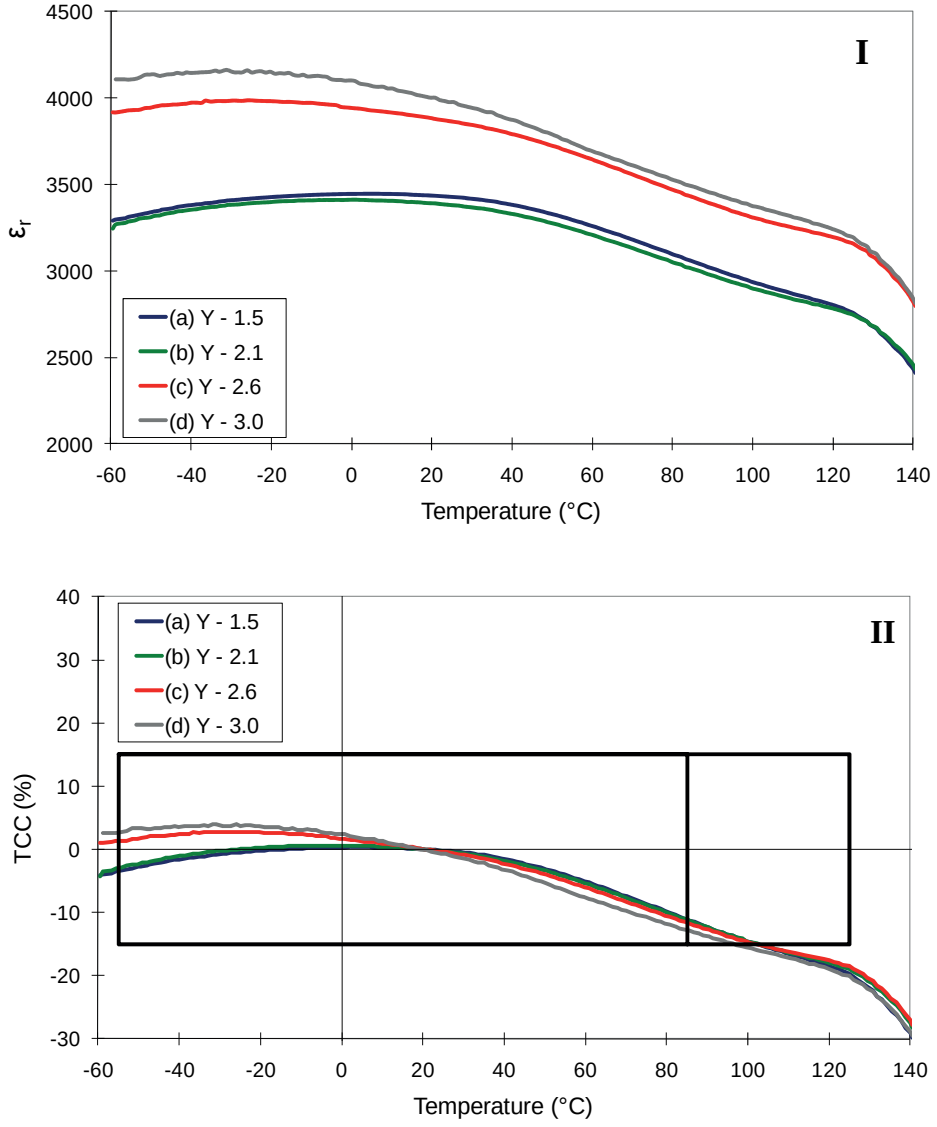

Figure 4.2.4: (I) Relative permittivity and (II) ΔC/C of MLCCs as function of temperature measured at 0.4 V/µm and 1 kHz. The X5R and X7R specification boxes are highlighted.

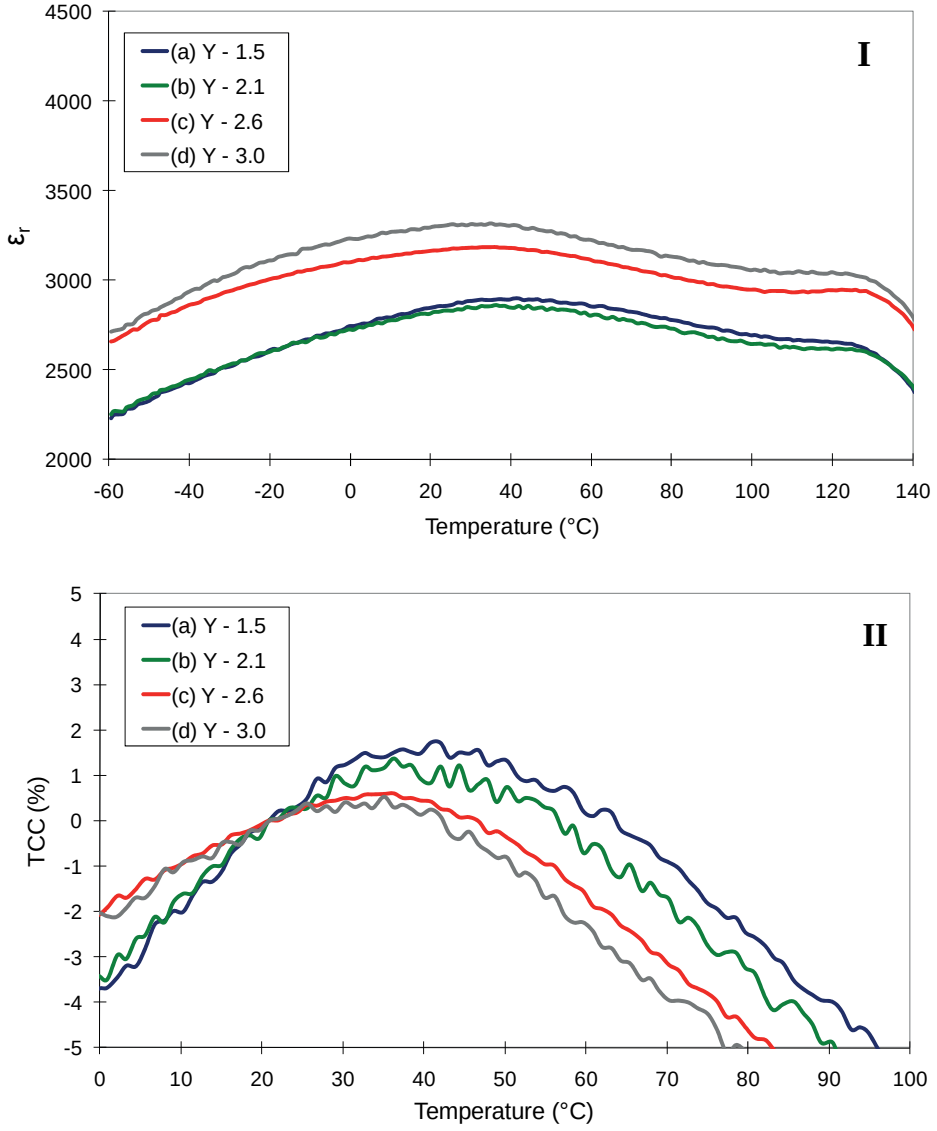

Figure 4.2.5: (I) Relative permittivity and (II) ΔC/C of MLCCs as function of temperature measured at 8 mV/μm and 1 kHz.

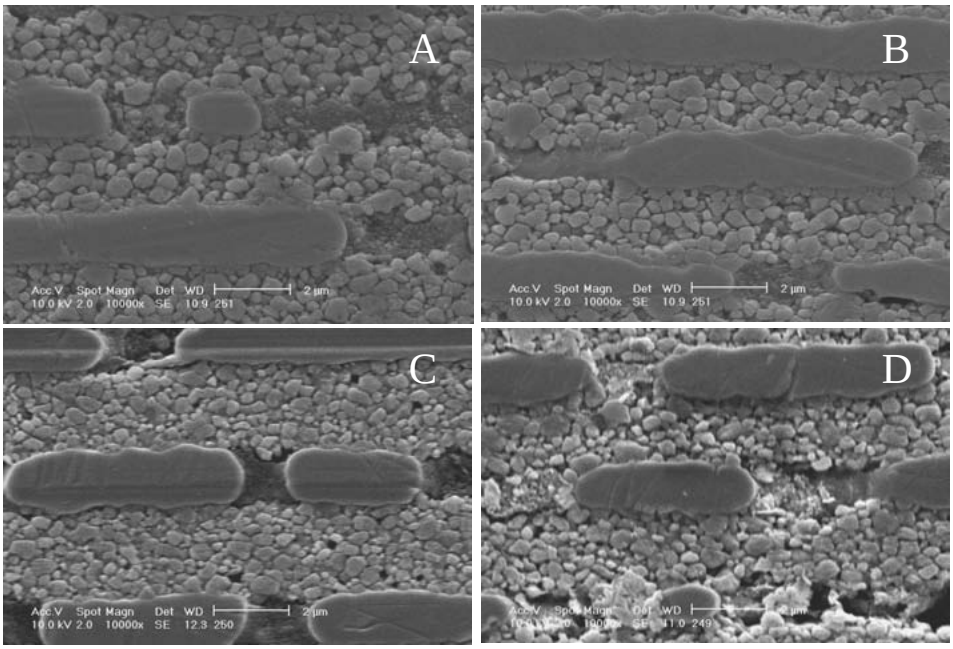

Figure 4.2.6: SEM micrographs of X5R dielectrics with a concentration of (a) 1.5 mol% Y, (b) 2.1 mol% Y, (c) 2.6 mol% Y and (d) 3.0 mol% Y. The MLCCs were sintered at 1280 °C in a wetted 0.3% H_2/N_2 atmosphere.

As the dielectric properties can be controlled by adjusting the formulation, the influence of Y concentration on microstructure was examined. Figure 4.2.6 shows the SEM micrographs of various dielectric ceramics sintered at 1280 °C. The Y_2O_3 concentration is important as grain growth of the core-shell grains can be largely influenced by the ratio and amount of added elements like MgO, Y_2O_3 or Mn_3O_4.

Table 4.2.1: T_c of shell phase.

$YO_{1.5}$ (mol %)	Curie Temperature (°C)
1.5	42.0
2.1	38.0
2.6	36.2
3.0	35.0

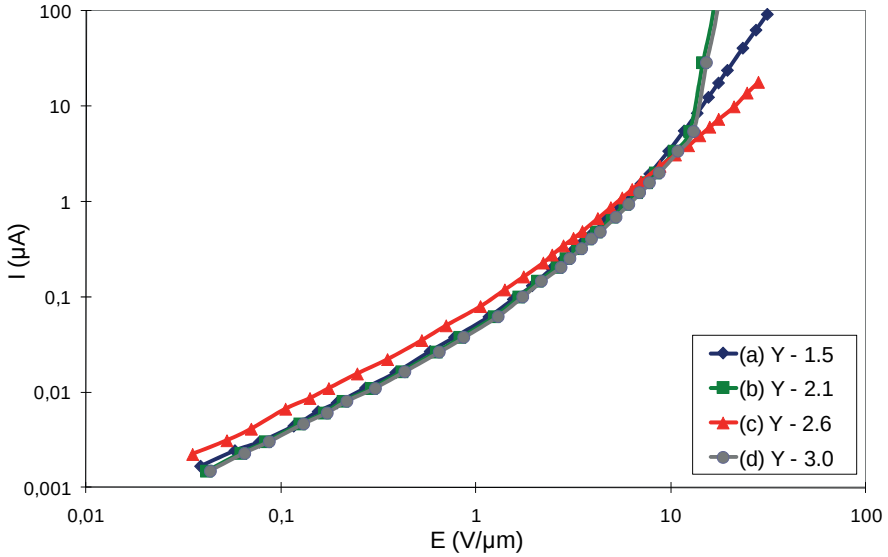

Figure 4.2.7: I-V curves of MLCCs with a concentration of (a) 1.5 mol% Y, (b) 2.1 mol% Y, (c) 2.6 mol% Y and (d) 3.0 mol% Y in the dielectric composition. The MLCCs were sintered at 1280 °C in a wetted 0.3% H_2/N_2 atmosphere.

From our results, it was observed that dielectrics having an Y concentration of 3 mol% had a relatively fine grain structure of small grains combined with few larger grains. When the Y_2O_3 concentration was smaller, the average grain size was slightly larger. However, this slight variation of grain size will have an effect on the electrical characteristics of the dielectrics.

To realize highly reliable dielectrics, MgO, Mn_3O_4 and one of the magic dopants, Y_2O_3, Ho_2O_3 or Dy_2O_3, are usually added to produce core-shell X5R dielectrics. The electrical resistivity of these types of dielectrics is determined by the chemistry of the grain boundaries and generally show varistor-like I-V characterics.[11] Therefore, the I-V characteristics were measured at 150 °C. The results are shown in Figure 4.2.7. The data show that there is no large difference between the four dielectric compositions when the DC electrical field was increased up to 10 V/µm. A gradual increase of the current was observed. The leakage current increases sharpely at DC fields >10 V/µm, indicating that the current passes via the grain boundaries and the resistivity of the dielectrics was decreased considerably. Thus, the concentration of Y_2O_3 has no significant influence on the I-V characteristics.

4.2.4. Conclusions

The relative permittivity as function of the AC electrical field dependency was determined by measuring the P-$U_{applied}$ hysteresis loops on CDCs. The results were compared with ε_r versus $U_{applied}$ measured on MLCCs. Comparison of data from these two methods showed that the trends in ε_r versus AC field strength were similar. This suggests that the ε_r of dielectric compositions can be determined directly on CDCs, thereby avoiding the laborious fabrication of MLCC samples to examine the electric properties of their ultra thin dielectrics.

The electrical measurements also showed that the relative permittivity at room temperature increased with increasing Y_2O_3 concentration. A distinct difference was observed between ε_r values of different compositions. Two types of microstructures could be distinguished. Microstructure analysis showed that the dielectrics consist of small grains and that the Y_2O_3 concentration has a very small effect on the average grain size. With increasing concentration of Y_2O_3 the average size decreased only slightly.

The Curie point of the dielectrics at 125 °C did not shift upon variation of the Y concentration, except at low AC fields, where a shift of the Curie point to lower temperatures was observed when more yttrium was incorporated in the ceramics.
The MLCC made from these dielectrics had good insulation resistance properties. The I-V measurements at 150 °C showed that the yttrium concentration had almost no effect on the leakage current of the ceramics.

References

1) Kishi, H.; Mizuno, Y. and Chazono, H. *Base-metal electrode-multilayer ceramic capacitors: Past, present and future perspectives*; Japanese Journal of Applied Physics Part 1-Regular Papers Short Notes & Review Papers, 2003 **42**(1): p. 1–15.
2) Randall, M.; Skamser, D.; Kinard, T.; Qazi, J. and Tajuddin, A. *Thin film MLCC*; Conference paper CARTS USA, 2007: p. 57.
3) Tsurumi, T.; Adachi, H.; Kakemoto, H.; Wada, S.; Mizuno, Y.; Chazono, H. and Kishi, H. *Dielectric properties of $BaTiO_3$-based ceramics under high electric field*; Japanese Journal of Applied Physics Part 1-Regular Papers Short Notes & Review Papers, 2002 **41**(11B): p. 6929–6933.
4) Morita, K.; Mizuno, Y.; Chazono, H.; Kishi, H.; Yang, G. Y.; Liu, W. E.; Dickey, E. C. and Randall, C. A. *Electric conduction of thin-layer Ni-multilayer ceramic capacitors with core-shell structure $BaTiO_3$*; Japanese Journal of Applied Physics Part 1-Regular Papers Brief Communications & Review Papers, 2007 **46**(5A): p. 2984–2990.
5) Hennings, D. F. K. *Dielectric materials for sintering in reducing atmospheres*; Journal of the European Ceramic Society, 2001 **21**(10–11): p. 1637–1642.

6) Yang, W. C.; Hu, C. T. and Lin, I. N. *Effect of Y_2O_3/MgO co-doping on the electrical properties of base-metal-electroded $BaTiO_3$ materials*; Journal of the European Ceramic Society, 2004 **24**(6): p. 1479–1483.
7) Mizuno, Y.; Okino, Y.; Kohzu, N.; Chazono, H. and Kishi, H. *Influence of the microstructure evolution on electrical properties of multilayer capacitor with Ni electrode*; Japanese Journal of Applied Physics Part 1-Regular Papers Short Notes & Review Papers, 1998 **37**(9B): p. 5227–5231.
8) Mizuno, Y.; Hagiwara, T. and Kishi, H. *Microstructural design of dielectrics for Ni-MLCC with ultra-thin active layers*; Journal of the Ceramic Society of Japan, 2007 **115**(1342): p. 360–364.
9) Wen, H.; Wang, X. H.; Gui, Z. L. and Li, L. T. *Modeling of the core-shell microstructure of temperature-stable $BaTiO_3$ based dielectrics for multilayer ceramic capacitors*; Journal of Electroceramics, 2008 **21**(1–4): p. 545–548.
10) Morita, K.; Mizuno, Y.; Chazono, H. and Kishi, H. *Effect of Mn addition on dc-electrical degradation of multilayer ceramic capacitor with Ni internal electrode*; Japanese Journal of Applied Physics Part 1-Regular Papers Short Notes & Review Papers, 2002 **41**(11B): p. 6957–6961.
11) Villamil, S. S.; Lee, H. Y. and Burton, L. C. *The resistance of grain-boundaries in $BaTiO_3$-based ceramic*; IEEE Transactions on Components Hybrids and Manufacturing Technology, 1987 **10**(4): p. 482–486.

Chapter 4.3.

The effect of milling process and dopant composition on electrical properties of X5R dielectrics in thin dielectric layers

4.3.1. Overview of raw materials for X5R dielectrics

In the early 1990s the minimum dielectric layer thicknesses of X7R MLCCs were in the range of 10 to 14 μm. Typically the number of grains per dielectric layer was about 8 to 10, which had an average grain size of about 1 μm. Since then the dielectric thicknesses of the Class 2 MLCCs were progressively reduced. In 2008 thickness of dielectric layers of high capacitive X5R MLCCs were already reduced to below 1 μm. These types of dielectrics have at least 4 to 5 grains per dielectric layer to meet the materials requirements with regard to quality and reliability.[1–5] As a consequence decreasing dielectric thickness requires smaller grains. Therefore finer $BaTiO_3$ powders and dopant metal oxides have to be used or existing powders have to be milled to finer particle sizes to achieve small grains, typically less than 200 nm, when used for dielectric layers of around 1 μm in thickness. Moreover, X5R ceramics have core-shell grains, which consist of a relatively pure $BaTiO_3$ core surrounded by a shell containing all dopant elements, which are inhomogeneously distributed to form a gradient concentration of the dopant elements, as described in detail in Chaper 4.1.[6–7] The average dielectric constant of the core-shell ceramics is then a function of the dielectric constant of the grain core and the dielectric constant of the grain shell.[8–9] The core-shell microstructure in X5R dielectrics is important with respect to the electrical properties and reliability, because the grain boundary resistance play an important role in keeping a high resistivity and low degradation of the dielectrics.[10] Therefore in ultra thin dielectric layers the grain size must be reduced, while a high dielectric constant must be maintained.

The microstructure of X5R dielectrics is defined by the material properties of $BaTiO_3$ and the dopant elements. The initial grain size and A/B ratio, the ratio between the ions located on the A^{2+}-site and the ions located on the B^{4+}- site within the perovskite lattice, of pure $BaTiO_3$ will have impact on the microstructure and dielectric constant (ε_r) of the dielectrics. It has been reported that the grain size of $BaTiO_3$ has an influence on the relative permittivity and ε_r-*T* characteristics. The dielectric constant will be lower when the dielectric grains become smaller.[11–13] A study on the effect of A/B ratio on pure $BaTiO_3$ revealed that abnormal grain growth was observed when excess Ti was present.[14] In stoichiometric ceramics and systems with Ba^{2+}-excess, fine grains were found. However, for X5R/X7R dielectrics various metal oxides have to be added to $BaTiO_3$ in order to alter the microstructure and electrical properties in order to obtain a flat ε_r-T dependency and high reliability. In literature the effect of metal oxide addition, like the rare earth oxides Y_2O_3, MgO, Mn_3O_4, SiO_2 and mixtures thereof, on microstructures and electrical properties have been described. Especially X5R-X7R dielectrics in base metal electrode technology are typically of interest.[3–4, 6, 10, 15–18]

Besides the effect of dopant formulation, process parameters like grain size effect, sintering temperature and method of addition of the dopant elements were also studied on material systems described as $BaTiO_3$ + *a* mol% RE_2O_3 (one of the 'magic dopants' Y^{3+}, Ho^{3+} or Er^{3+}) + *b* mol% MgO + *c* mol% Mn_3O_4 + *d* mol% SiO_2.[19–25] Moreover, the effect of milling raw materials on microstructure and electrical properties of the X5R dielectrics has been studied for several material compositions $BaTiO_3$ + *a* mol% Ho_2O_3 + *b* mol% MgO + *c* mol% MnO + *d* mol% $BaSiO_2$.[26] The latter study showed that high-energy milling has an influence on microstructure and electrical properties. The milling process will cause an increased damage of the surface of the $BaTiO_3$ grains leading to increased incorporation of the elements into the shell grains during the sintering process. High-energy milling has also an influence on the ε_r-*T* characteristics of the sintered ceramics. The dielectric constant was decreased when longer or higher-energy milling activity was applied on the precursor oxides, whereas the loss factor (tan δ) was increased. These results suggest that fierce milling of $BaTiO_3$ should be avoided and that initial material properties of $BaTiO_3$ must be chosen in such way that the initial grain size before sintering process is optimal, so that the desired properties can be achieved in the sintered dielectrics.

In this chapter the effect of dopant formulation and milling process on dielectric properties is examined. These dopant compositions are tested on four different commercially available BaTiO3 powders, which differ in grain size distribution and A/B ratio. Table 4.3.1 shows the materials properties of the four BaTiO3 powders. The first two BaTiO3 samples were manufactured by Nippon Chemical Industry (NCI) using the oxalate synthesis method. The difference between these 2 powders

Table 4.3.1: Ba/Ti ratio, particle size and surface area of commercial $BaTiO_3$ powders. Values provided by the vendors of the powders.

$BaTiO_3$	1	2	3	4
Type	Oxalate	Oxalate	Solid State	Hydrothermal
Ba/Ti	1.003	1.004	0.999	1.000
D_{50} (μm)	0.47	0.42	0.49	0.63
D_{90} (μm)	0.60	0.53	0.65	0.87
B.E.T. (m^2/g)	3.6	5.3	4.5	3.9

was primarily the grain size, see Table 4.3.1. A solid state powder (NCI) and a relatively coarse $BaTiO_3$ powder, manufactured via hydrothermal synthesis method by Sakai, were used for comparison. Besides the difference in synthesis method and grain size of the powders, the A/B ratio in powder number 3 and 4 were also different from the two oxalate powders.

As mentioned above the first 2 powders, see Table 4.3.1, were made via the oxalate process. The oxalate process is a precipitation method starting with Ti-precursors like titaniumchloride ($TiCl_4$) or titaniumoxychloride ($TiOCl_2$). The titanium precursor is hydrolysed within the acidic environment of an oxalic acid solution. To the saturated oxalic solution a Ba salt, like $BaCl_2$, is added whereby the barium titanate oxalate complex is precipitated;[27–28]

$$Ba^{2+} + TiO(OH)_2^{2-} + 2C_2O_4^{2-} + 2H_3O^+ \rightarrow BaTiO(C_2O_4)_2 \cdot 4H_2O \qquad (4.3.1)$$

The precipitated powder is then decomposed at temperatures of about 1000 °C to produce fine cubic or tetragonal $BaTiO_3$ powders of well-controlled stoichiometry.
The solid state method, often also called mixed oxide method, is based on a well controlled diffusion reaction between equimolar amounts of barium carbonate ($BaCO_3$) and titanium dioxide (TiO_2) powders. After the fine precursor powders are activated by an high-energy milling process the precursor powders typically react at temperatures above 820 °C, to produce aggregated coarse $BaTiO_3$ powders according to the overall reaction:[28–29]

$$BaCO_3(s) + TiO_2(s) \quad \rightarrow \quad BaTiO_3(s) + CO_2(g) \qquad (4.3.2)$$

The $BaTiO_3$ phase is formed during sintering at the surface of the TiO_2 grains and the diffusion rate is controlled by the diffusion of Ba^{2+} into the TiO_2 lattice.[29–30]. Typically the initial morphology of TiO_2 powder determines the particle size and

Table 4.3.2: Dopant mixtures added to $BaTiO_3$.

Material	Dopant mix A mol / mol $BaTiO_3$ (%)	Dopant mix B mol / mol $BaTiO_3$ (%)	Dopant mix C mol / mol $BaTiO_3$ (%)	Dopant mix D mol / mol $BaTiO_3$ (%)
SiO_2		0.50		
$BaCO_3$		0.25		
$BaSiO_3$	0.25		0.25	0.25
Y_2O_3	0.25	0.50	0.25	0.25
MgO	1.00	0.25	1.00	1.00
$MnCO_3$	0.20	0.20	0.25	0.30
CuO	0.10	0.10	0.10	0.30
MoO_3	0.10			
V_2O_5		0.05	0.05	0.05

morphology of the final synthesized $BaTiO_3$. Intermediate phases like Ba_2TiO_4 and other polytitanates can be present before completion of the reaction.

Typically, hydrothermal $BaTiO_3$ powders are synthesized in water at moderately high temperatures and at atmospheric or high pressures, often in an autoclave for several hours. The synthesis starts by making a hydrated TiO_2 gel from precursors like titanium tetrachloride ($TiCl_4$), titanium oxychloride ($TiOCl_2$) or other titanium salts.[27, 29] The reactive TiO_2 gel is then added to a barium hydroxide solution and the reaction:

$$Ba(OH)_2 \cdot 8H_2O + TiO_2 \xrightarrow{p,\,T} BaTiO_3 + 9H_2O \qquad (4.3.3)$$

will occur at high temperatures, typically between 350 and 500 °C, and pressures in the range of 160 to 1300 bar.[28, 31] However, lower temperatures and pressures can be applied when more reactive TiO_2 precursors are used beforehand. Particle size and morphology of the hydrothermal $BaTiO_3$ powders can be controlled by the choice of reactive precursor and the process conditions. The particle size of hydrothermally processed $BaTiO_3$ powders can range between 20 nm and 1 um.[29]

The $BaTiO_3$ powders used in this study were synthesized via 4 different methods. The effect of dopant formulation and high-energy milling are compared for these 4 different $BaTiO_3$ powders. The dopant formulations used in this work consisted of various elements and the exact composition is described in Table 4.3.2. The basic formulation is based on $BaTiO_3$ + *x* mol% Y_2O_3 + *y* mol% MgO + *z* mol% $MnCO_3$ + *v* mol% SiO_2. However, in this study extra elements like CuO, V_2O_5 and

MoO_3 were incorporated in the material composition. The CuO was added to improve sintering behaviour of the ceramics. It is known to decrease the sintering temperature of $BaTiO_3$ ceramics.[32] The other 2 elements, V_2O_5 and MoO_3, are typically used to modify the ε_r-T characteristics and reliability of the dielectrics.

4.3.2. Experimental procedure of sample preparation

Ceramic disc capacitors. The ceramic disc capacitors (CDC) were fabricated using 4 different $BaTiO_3$ powders. See Table 4.3.1 for the material properties. The dopant powders were $BaCO_3$ (Solvay, BM20), SiO_2 (Degussa, Aerosil R975), $BaSiO_3$ (Yageo), Y_2O_3 (Rhodia, UF39), $MnCO_3$ (J.T. Baker, 99.0%), MgO (Konoshima, HP-30), CuO (PCC, 99%), MoO_3 (HC Starck, 99%) and V_2O_5 (Sigma-Aldrich, 99%). These dopant powders were pre-milled to a D_{50} of approximately 100 nm by ball milling and kept as a slurry mixture. The $BaTiO_3$ powders were milled to the required particle size. The $BaTiO_3$ and dopant slurries were mixed according to the composition formulations shown in Table 4.3.2. Then pellets of 10 mm in diameter x 2 mm thickness were prepared. Nickel electrodes were applied onto the pellets. The CDC´s were co-sintered in a tube kiln at various temperatures according a temperature profile used for Ni electrodes as described in Chapter 2. The sintering behaviour of the ceramic powders was examined using a NETZSCH Dil 402 C dilatometer. The ceramic pellets were sintered at a heating rate of 5 °C/min up to 1350 °C before cooling down.

Multilayer capacitors. Green MLCC chips of above-mentioned compositions were produced on regular production equipment at Yageo in Roermond, the Netherlands. The MLCCs of 3.2 mm x 1.6 mm x 0.4 mm in size consisted of 50 electrode layers. The dielectric thickness after sintering was around 2.2 μm; the electrode thickness was around 1 μm. Copper terminations were applied onto the chips, which were cured at 900 °C in a N_2 atmosphere. The microstructures of the ceramics was examined using a scanning electron microscope (HR-SEM LEO 1550) after the cross-sections of MLCC samples were chemically etched.

4.3.3. Results and Discussion

The dopant formulation has a strong effect on microstructure and electrical properties and small variations of the dopant composition can have large effect on the dielectric properties. In the first part of this chapter this is demonstrated by comparing two typical X5R formulations, called dopant mix A and B, see Table 4.3.2. Dopant mixtures A and B were added to the 4 different $BaTiO_3$ powders of

Table 4.3.1. The second part of this chapter discusses the effect of milling on microstructure and electrical properties of $BaTiO_3$ powders. While the particle size has an effect on the dielectric properties the dopant formulation will have a simultaneous effect. Two other X5R formulations, called dopant mix C and D, were examined to investigate the effect of milling on microstructures and dielectric properties of the sintered ceramics.

4.3.3.1 The effect of dopant composition on X5R based dielectrics

The four $BaTiO_3$ powders, see Table 4.3.1, were all milled for several hours to de-agglomerate and mill the powders. The particle size and surface areas of these powder mixes are shown in Table 4.3.3. The various samples were prepared by mixing the $BaTiO_3$ slurries and the 2 dopant slurries to produce 8 different samples, which are coded BTO-*x*-A and BTO-*x*-B, were *x* refers to the $BaTiO_3$ powder number. The digits A and B refer to the 2 dopant mixtures.

Sintering behaviour examination did show a distinct difference between compositions with dopant mix A and B, see Figure 4.3.1 and Figure 4.3.2, respectively. The ceramics containing dopant mix A shows gradual sintering behaviour, whereas ceramics with dopant mix B seems to sinter with several steps. Furthermore, the ceramics containing dopant mix A seem to sinter at lower temperatures than B-type ceramics.

Tabel 4.3.3: Particle size and surface area after milling of $BaTiO_3$.

$BaTiO_3$	1	2	3	4
Type	Oxalate	Oxalate	Solid State	Hydrothermal
D_{50} (μm)	0.30	0.24	0.28	0.38
D_{90} (μm)	0.59	0.54	0.53	0.65
B.E.T. (m^2/g)	6.07	6.51	5.77	4.86

The sintering profiles of dopant A ceramics suggest that sintering behaviour is defined by the particle size of the powders, rather than the method of synthesis of $BaTiO_3$ or the A/B ratio. In this case, the powders with the largest grain size, BTO-4-A, have to be sintered at higher temperature than the ceramics with the finest grains, BTO-2-A, see Figure 4.3.1. The peculiar sintering profile of sample BTO-2-A shows a typical decrease of the relative change in length at temperatures above 1250 °C. The sample was bloated due to formation of a larger amount of liquid phase during sintering at these temperatures.

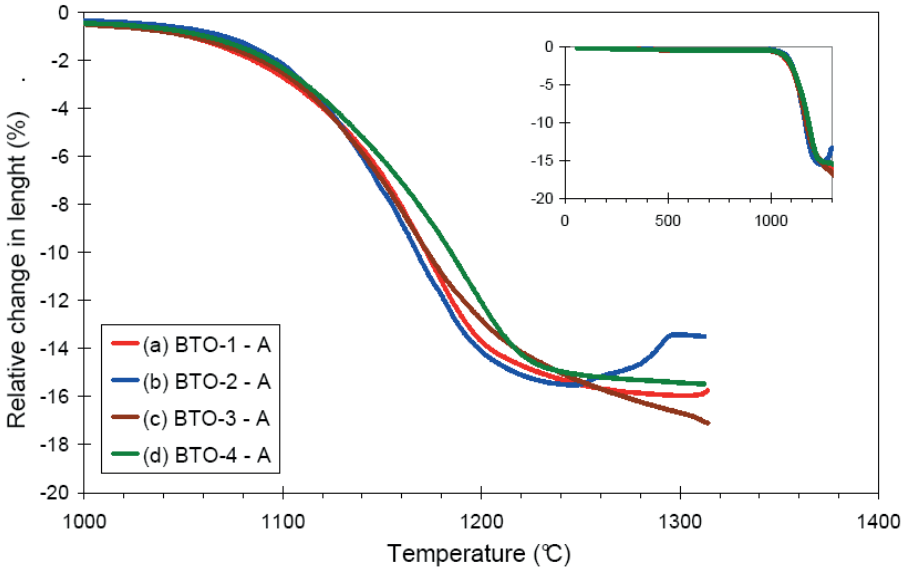

Figure 4.3.1: TMA curves of (a) BTO-1-A, (b) BTO-2-A, (c) BTO-3-A and (d) BTO-4-A.

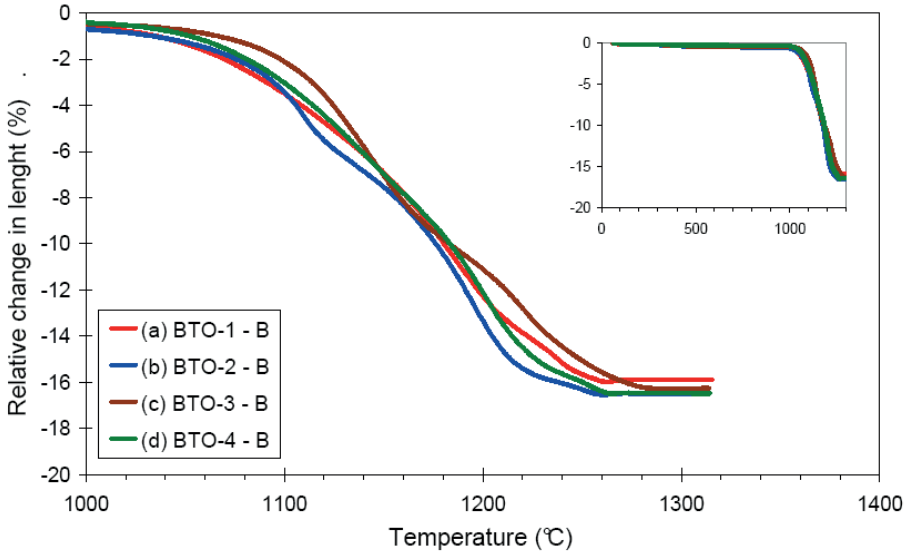

Figure 4.3.2: TMA curves of (a) BTO-1-B, (b) BTO-2-B, (c) BTO-3-B and (d) BTO-4-B.

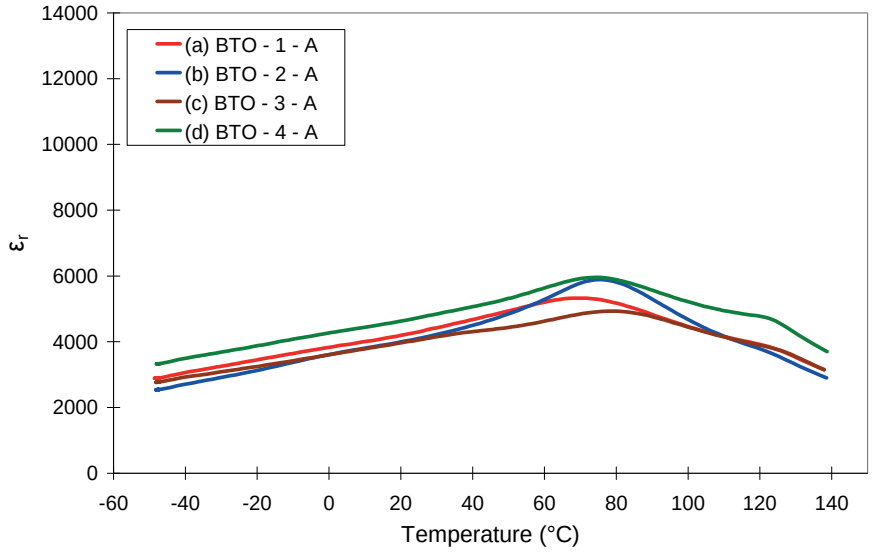

Figure 4.3.3: The ε_r versus T curves of (a) oxalate $BaTiO_3$ (BTO-1-A), (b) oxalate $BaTiO_3$ (BTO-2-A), (c) solid state $BaTiO_3$ (BTO-3-A) and (d) hydrothermal $BaTiO_3$ (BTO-4-A), to which dopant composition A was added. The CDC's were measured at 1kHz/1V_{rms}.

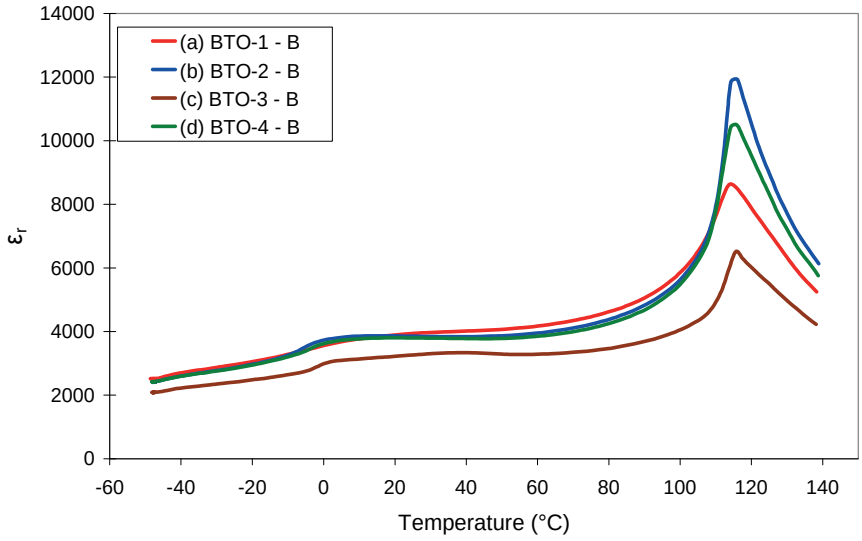

Figure 4.3.4: The ε_r versus T curves of (a) oxalate $BaTiO_3$ (BTO-1-B), (b) oxalate $BaTiO_3$ (BTO-2-B), (c) solid state $BaTiO_3$ (BTO-3-B) and (d) hydrothermal $BaTiO_3$ (BTO-4-B) to which dopant composition B was added. The CDC's were measured at 1kHz/1V_{rms}.

The sintering profiles of dopant B ceramics indicate that not only grain size is the dominant factor with respect to sintering. Comparing BTO-1-B and BTO-2-B, sintering is dictated by grain size, as BTO-2-B can be sintered dense at a lower temperature than the coarser BTO-1-B. The BTO-3-B powder sinters fully dense at higher temperatures than the coarsest powder BTO-4-B. Thus another effect also seems to play a role.

Since the A/B ratios were equal, the grain size or the synthesis method to make $BaTiO_3$ powder could be of influence. However, the samples BTO-1-B and BTO-3-B, having similar initial grain size, have different sintering characteristics. That indicates that the grain size is not the main cause of the difference. Thus different synthesis methods to make the initial $BaTiO_3$ powders or powder morphology could contribute as well to the different sintering characteristics.

The ceramic disc capacitors were sintered at 1250 °C in a moist 0.3% H_2/N_2 atmosphere. The ε_r-*T* curves of the CDC´s of the A and B formulations are shown in Figure 4.3.3 and Figure 4.3.4, respectively. The ε_r-*T* curves of dopant A dielectrics are relatively flat compared to dopant B ceramics. The samples BTO-1-A and BTO-2-A show one transition peak, indicating that the Curie points (T_c) are shifted due to strong diffusion of dopant elements into the $BaTiO_3$ lattice. The Curie point (T_c) of the cubic-tetragonal transition shifted to lower temperatures, whereas the T_c of the orthorhombic-tetragonal and rhombohedral-orthorhombic transitions shifted to higher temperatures. For samples BTO-3-A and BTO-4-A the T_c at 125 °C is observed, which indicates that a larger volume fraction of the pure $BaTiO_3$ core is still present in these ceramics.

The BTO-4-A sample had the highest ε_r at room temperature, having a value of 4650. The samples BTO-2-A and BTO-3-A had both a dielectric constant of around 4000, whereas BTO-1-A had an ε_r of 4200. These results suggest that the relative permittivities are related to the initial grain size of the milled $BaTiO_3$.

The ε_r-T curves of the dopant B compositions show a different profile and the shapes of the 4 samples are more or less identical. The tetragonal-cubic transition of the 4 samples shifted to 115 °C, while the T_c of the orthorhombic-tetragonal transition shifted by +5 °C. The ε_r at room temperature of BTO-1-B, BTO-2-B and BTO-4-B was 3850, while the ε_r of BTO-3-B was 3200. The maximum ε_r values of the dielectric constants, measured at T_c of 115 °C, show large differences between the 4 dielectrics. Based on these results no clear relationship between initial particle size of the milled $BaTiO_3$ and the dielectric properties can be established.

The micrographs of the strongly etched surfaces of the mix A doped ceramics reveal that the grain size distribution is not very homogeneous, see Figure 4.3.5a. The average grain sizes of the four dopant mix A ceramics were almost equal, with values of about 0.23 μm, see Table 4.3.4. The BTO-3-A ceramics had the smallest

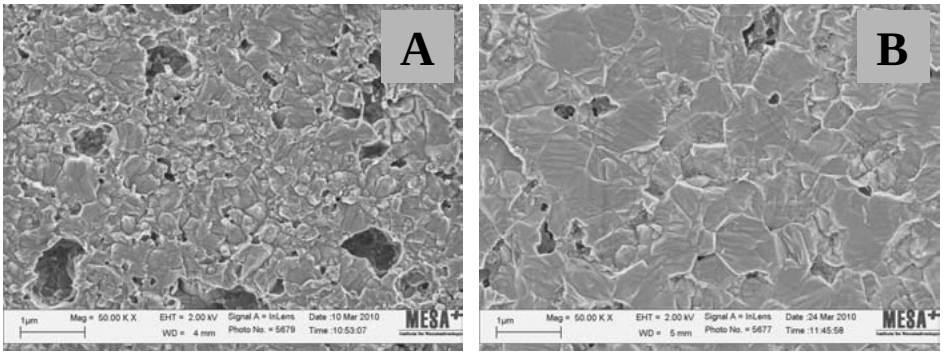

Figure 4.3.5: SEM micrographs of the ceramic surface after chemical etching of (a) BTO-2-A and (b) BTO-2-B.

grains within the A-ceramics series, but this was not reflected directly in the dielectric constants values, as shown in Figure 4.3.3.

The microstructure of the ceramics made with dopant B was completely different compared to dopant A, see Figure 4.3.5b. Dopant mix B dielectrics showed excessive grain growth, especially for samples BTO-2-B and BTO-3-B. Grain growth was less pronounced in sample BTO-1-B. However, the average grain sizes of BTO-4-B were almost comparable to the ceramics with dopant mix A, but the average grain size was still somewhat larger.

The elements Y^{3+} and Mg^{2+} are known to act as grain growth inhibitors.[1, 33] Moreover, Y^{3+} will dissolve first in the $BaTiO_3$ lattice and above a certain concentration it suppresses grain growth. In dopant formulation A the combined amount of Mg^{2+} and Y^{3+} is higher than in dopant B. Therefore the ceramics made with dopant B showed more grain growth, assuming that the elements Cu^{2+}, V^{5+} and Mo^{6+} did not make a large contribution to grain growth during sintering.

Since the A/B ratios were equal, the grain size or the synthesis method to make $BaTiO_3$ powder could be of influence. However, the samples BTO-1-B and BTO-3-B, having similar initial grain size, have different sintering characteristics. That indicates that the grain size is not the main cause of the difference. Thus different synthesis methods to make the initial $BaTiO_3$ powders or powder morphology could contribute as well to the different sintering characteristics.

Table 4.3.4: Average grain size of samples in μm.

$BaTiO_3$	Dopant A	Dopant B
BTO-1	0.23	0.34
BTO-2	0.18	0.50
BTO-3	0.23	0.55
BTO-4	0.22	0.25

4.3.3.2. The effect of milling process using dopant C

$BaTiO_3$ powder number 1, BTO-1, was de-agglomerated and milled to various particles sizes. The four different BTO-1 slurries were mixed with dopant C to prepare 4 individual samples. The grain size distributions and surface areas are shown in Figure 4.3.6. It is assumed that besides the de-agglomeration of the $BaTiO_3$ powders also the surface of the $BaTiO_3$ grains are damaged by the milling process.[26] Due to milling small chipped particles will be formed and the amount will increase with increasing duration of the milling process. The effect of milling was studied on a composition of $BaTiO_3$ to which dopant C had been added. Dopant C is an X5R formulation and is almost similar to dopant A. However, the Mn^{2+} concentration is a bit higher and V_2O_5 was used instead of MoO_3. Thus, 4 different powders were prepared and analyzed.

Sintering of the coarse powders occurs at higher temperatures. Figure 4.3.7 shows this trend for the first 3 samples. The finest powder, with D_{50} of 0.21 μm, seems to sinter at slightly higher temperatures compared to the powder that is milled to a D_{50} of 0.25 μm.

The CDCs made of these powders were sintered at 1250 °C in a moist 0.3% H_2/N_2 atmosphere. The ε_r-T curved of these CDCs were measured and the results are shown in Figure 4.3.8. The T_c of the tetragonal-cubic transition of the coarse powders, D_{50} = 0.42 μm and D_{50} = 0.32 μm, lies at 120 °C and is shifted 5 °C below the T_c of pure $BaTiO_3$. The T_c of the orthorhombic-tetragonal transition moved to higher temperatures when particle size D_{50} was decreased. The two powders with the smallest particle sizes did not exhibit the Curie point of either transition, and a new T_c peak was found at around 71 °C in the ε_r-T curve. The ε_r of these four samples at room temperature and at 125 °C decreased when the particle size is reduced. However, a large shift of the ε_r-T curve occurred when the particle size of the powders was reduced from 0.25 μm to 0.21 μm.

The same powders were also used to fabricate MLCCs that were sintered at 1200 and 1250 °C under the exact same sintering conditions as the CDC samples. The results show that temperature and particle size have an effect on ε_r, loss factor (tan δ) and insulation resistance (IR), see Table 4.3.5. The dielectrics sintered at 1200 °C had larger dielectric constants than the ceramics sintered at 1250 °C, irrespective of the initial particle size. The maximum ε_r is reached when the particle size, D_{50}, is around 0.25 μm. The dielectric constant decreased considerably for the dielectrics made from powders that had been milled to a D_{50} of 21 μm. The loss factor and insulation resistance the values also increased when the $BaTiO_3$ powders were milled towards smaller particles sizes, until the optimum powder with D_{50} of 0.25 μm was reached. Further milling of the powders to D_{50} of 0.21 μm led to a decrease of tan δ and IR values. Especially the IR values dropped considerably.

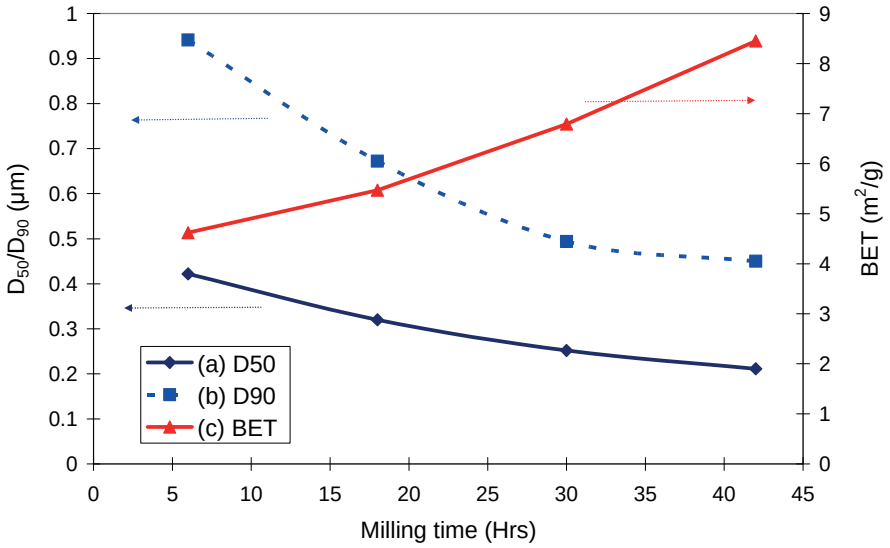

Figure 4.3.6: Effect of milling BTO-1 on (a) D_{50}, (b) D_{90} and (c) specific surface area.

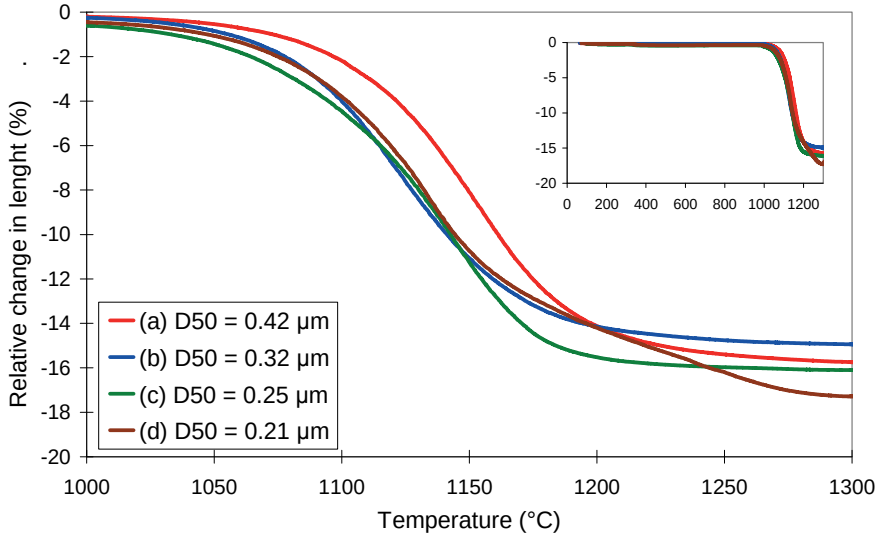

Figure 4.3.7: TMA curves of BTO-1-C milled to (a) D_{50} of 0.42 µm,(b) D_{50} of 0.32 µm, (c) D_{50} of 0.25 µm and (d) D_{50} of 0.21 µm.

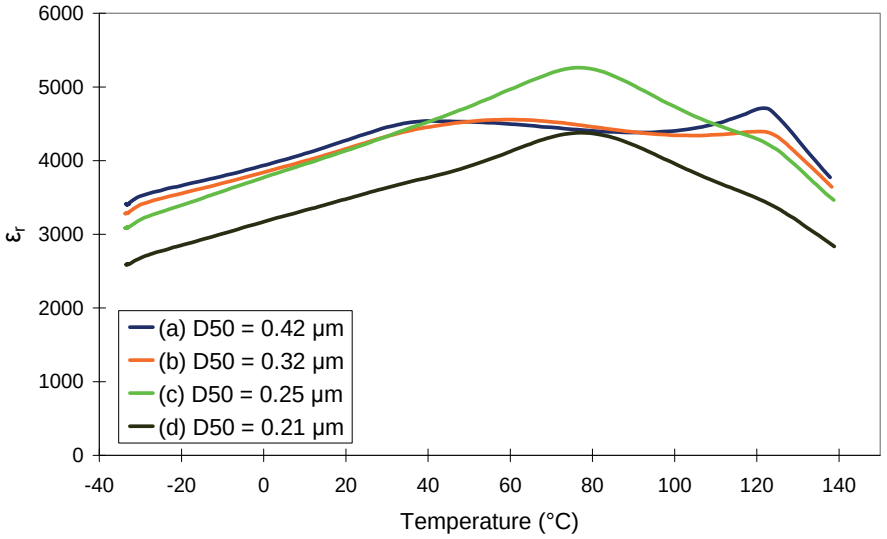

Figure 4.3.8: The ε_r versus T curves of BTO-1-C milled to (a) D_{50} of 0.42 µm, (b) D_{50} of 0.32 µm, (c) D_{50} of 0.25 µm and (d) D_{50} of 0.21 µm. The CDC's were sintered at 1250 °C in wetted 0.3% H_2/N_2 atmosphere. Capacitance was measured at 1kHz/1V_{rms}.

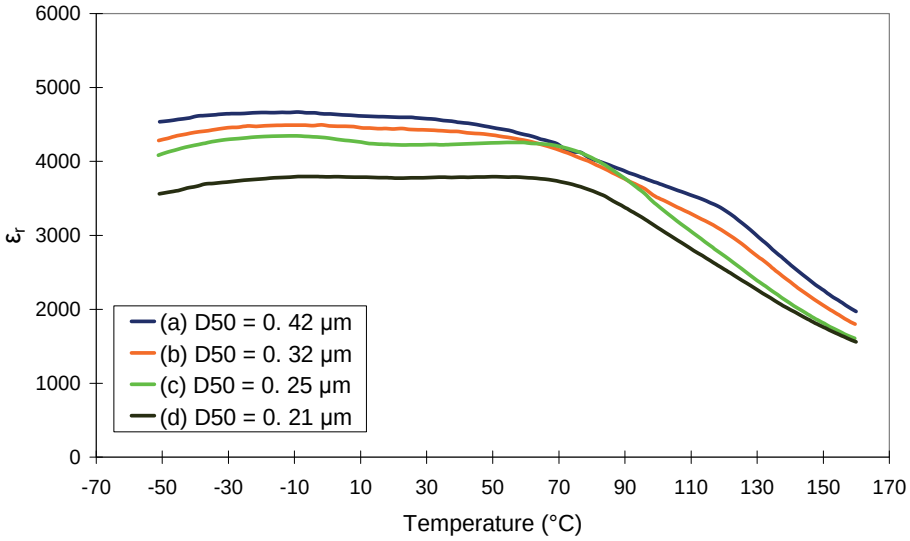

Figure 4.3.9: The ε_r versus T curves of BTO-1-C milled to (a) D_{50} of 0.42 µm, (b) D_{50} of 0.32 µm, (c) D_{50} of 0.25 µm and (d) D_{50} of 0.21 µm. The MLCC's were sintered at 1250 °C in wetted 0.3% H_2/N_2 atmosphere. Capacitance was measured at 1kHz/1V_{rms}.

Table 4.3.5: Electrical properties of MLCCs made of BTO-1-C sintered at 1200 and 1250 °C in moist 0.3 % H_2/N_2. The ε_r and tan δ were measured at 1 kHz/1Vrms.

Particle size (μm)	Temperature (°C)	ε_r	Tan δ (10^{-4})	IR at 10V (Ω)	IR at 50V (Ω)
D_{50} = 0.42	1200	4540	663	$1.01 \cdot 10^9$	$1.83 \cdot 10^9$
	1250	4598	668	$1.07 \cdot 10^9$	$1.77 \cdot 10^9$
D_{50} = 0.32	1200	4567	801	$1.34 \cdot 10^9$	$1.98 \cdot 10^9$
	1250	4432	759	$1.37 \cdot 10^9$	$2.89 \cdot 10^9$
D_{50} = 0.25	1200	4730	978	$1.78 \cdot 10^9$	$3.41 \cdot 10^9$
	1250	4223	1033	$1.76 \cdot 10^9$	$1.98 \cdot 10^9$
D_{50} = 0.21	1200	3882	903	$3.05 \cdot 10^8$	$6.01 \cdot 10^6$
	1250	3777	902	$1.29 \cdot 10^7$	$5.92 \cdot 10^4$

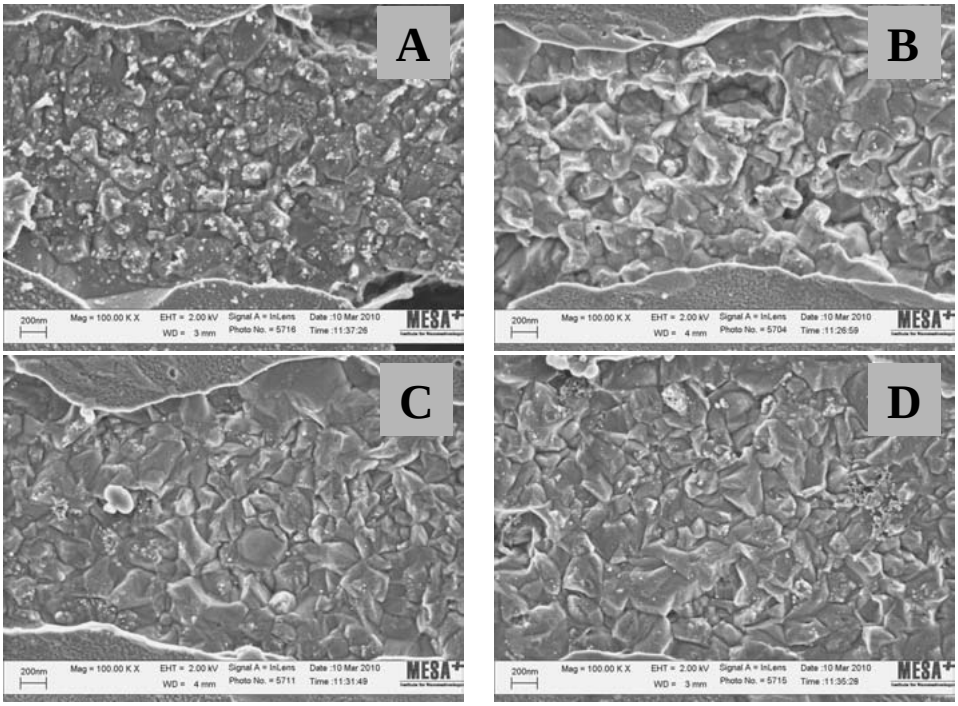

Figure 4.3.10: SEM micrographs of BTO-1-C milled to (a) D_{50} of 0.42 μm, (b) D_{50} of 0.32 μm , (c) D_{50} of 0.25 μm and (d) D_{50} of 0.21 μm.

The drop in insulation resistance indicated that the chemistry and microstructure of the grain boundary had changed. Thus, the main trend is that with increasing damage of the $BaTiO_3$ grains and increasing amount of chipped particles, the loss factor and insulation resistance increase simultaneously until a turning point is reached.

The ε_r-*T* curves of the MLCCs show that particle size has an effect on the dielectric constant of the dielectrics, see Figure 4.3.9. Over the temperature range between -55 and +150 °C the ε_r-*T* curves decreased as the particle size was reduced. The ε_r-*T* curves of the MLCCs are different compared to the ε_r-*T* curves of the CDC samples, because the actual applied AC field over the dielectric layer is different, as discussed in Chapter 4.2. However, the T_c of the orthorhombic-tetragonal transition at 71 °C is also observed in the 2 finest powder samples. Furthermore, the ε_r-*T* curve of the coarsest powder shows a T_c at 120 °C. Despite the decrease of ε_r, which is an effect caused by particle size, the curves are flat within the -55 to +85 °C range, making the ceramics fulfil the X5R requirements.

Table 4.3.6: Average grain size after sintering of BTO-1-C as function of particle size after milling.

$BaTiO_3$ sample	D_{50} (μm)	AGS (nm)
BTO-1-C	0.42	180
BTO-1-C	0.32	230
BTO-1-C	0.25	240
BTO-1-C	0.21	240

The microstructures of the ceramics made with the coarse powder show a grain distribution of fine grains with a few larger grains, see Figure 4.3.10. The grains are bigger in the ceramics when $BaTiO_3$ of lower particle sizes are sintered. Furthermore, even grains with excessive grain growth are observed near the nickel electrodes. The effect of milled $BaTiO_3$ with dopant C showed that the average grain size of the ceramics sintered at 1250 °C increased, see Table 4.3.6. The relatively large values of D_{50} indicate that the powders had some degree of agglomeration. This means that the milled $BaTiO_3$ powder existed of several primary grains, which formed agglomerated particles.

4.3.3.3. The effect of milling process using dopant D

The effect of small adjustment of the dopant composition can have large effect on microstructure and electrical properties. Therefore a dopant mixture D, which is a modified composition of dopant C, was prepared. Dopant D consisted of the same elements as dopant C. However, the amount of Mn^{2+} was slightly larger and the amount of Cu^{2+} was increased from 0.1 mol% per mol $BaTiO_3$ to 0.3 mol%, see Table 4.3.2. The effect of milling was tested on $BaTiO_3$ powder number 1 (BTO-1) and compared to $BaTiO_3$ powder number 2 (BTO-2), see Table 4.3.1. Both $BaTiO_3$ powders were fabricated with the same synthesis method, an oxalate process. The only difference is that initial particle size of BTO-2, which is smaller than BTO-1. Other parameters regarding composition were kept equal, like A/B ratio.

The effect of milling on particle size distribution and surface area for BTO-1 powder is shown in Figure 4.3.11. The four different BTO-1 slurries were mixed with dopant D to prepare 4 individual samples. Figure 4.3.12 shows the effect of milling of BTO-2 on particle size distribution and surface area of the 2 mixed and milled samples.

Ceramic disc capacitors were fabricated and sintered at 1250 °C in a moist 0.3% H_2/N_2 atmosphere and annealed at 1000 °C in moist N_2. Figure 4.3.13 shows the ε_r-T curves of these 6 CDC samples. The ε_r-T curve of the coarse BTO1-D (D_{50} = 0.38 μm) has almost similar shape and dielectric constant values over the measured temperature range as BTO-1-C (D_{50} = 0.42 μm). However, ε_r values are increased at temperature below T_c at 120–125 °C. Furthermore, ε_r at this transition temperature did not change considerably when the ceramics were milled to a D_{50} of 0.31 μm. The tetragonal-cubic T_c shifted to 121 °C for the coarse BTO-1, whereas the T_c of the finer powders shifted to 124 °C. The top of the ε_r-T curve of the ceramics milled to 0.29 μm is located at 78 °C and the temperature shifts to 70 °C for the sample milled to a D_{50} of 0.22 μm.

The dielectric constant decreased considerably when $BaTiO_3$ was milled to below 0.30 μm. However, the results of the BTO-2-D samples, which were milled below a D_{50} of 0.30 μm, showed similar ε_r-T curves as the 2 coarse powders of the BTO-1-D samples. In fact the ε_r-T curve of BTO-2-D milled to 0.27 μm has the same ε_r values as the BTO-1-D sample, which was milled to 0.38 μm. When the samples were milled to a smaller average particle size the relative constant increased over the whole temperature range, except at temperature above the T_c of the tetragonal-cubic transition. This is identical to the samples of BTO-1-D milled from 0.38 μm to 0.31 μm.

Multilayer capacitors were fabricated from exactly the same powders. The MLCCs were sintered at 1200 and 1250 °C and the results of the electrical measurements are shown in Table 4.3.7. The values of the BTO-1-D samples

sintered at 1200 °C show that the dielectric constant increased when the particle size is reduced. Also the values of the loss factor, tan δ, and the insulation resistance increased after reduction of the particle size. The same trend is observed for the samples sintered at 1250 °C. The sample milled to a D_{50} of 0.22 μm had lower ε_r and IR values compared to the sample which was milled to 0.29 μm. This trend is also observed in the ε_r-T curves of the MLCC samples, see Figure 4.3.14. The ε_r-T curves moved to higher ε_r values when the particle size was reduced by the milling process. However, the shape of the ε_r-T curve remained the same, except for the sample with a D_{50} of 0.22 μm, which became more flattened in the temperature range between -55 to +85 °C.

In contrast to the CDC samples the MLCC samples fabricated with the BTO-2-D powders had lower ε_r values than all the BTO-1-D samples. A notable fact is that ε_r at room temperature and the whole ε_r-T curve, below the T_c at 120 °C, shifted to higher values when the particle size of BTO-2-D was reduced by the milling process.

Figure 4.3.15 shows the microstructures of BTO-1-D ceramics sintered at 1250 °C. The ceramics show a homogeneous distribution of grains with an average grain size of 200 nm, see Table 4.3.8. However, the grain size distribution of the ceramics, which were milled to 0.22 um, show large numbers of large grains near the nickel electrodes. This is due to diffusion of $BaTiO_3$ out of the nickel electrode. To avoid sintering mismatch during co-sintering of the ceramics and the metal electrodes an amount of pure $BaTiO_3$ was added to the nickel paste. During sintering this $BaTiO_3$ will diffuses partly into the dielectric layer. Therefore the chemical composition will be changed locally, which is the reason for the excessive grain growth near the electrode.

In the other ceramics an equal distribution of fine and coarse grains was observed. However, the BTO-2-D sample, which was milled to 0.27 μm, had the smallest average grain size. The microstructure show a higher concentration of smaller grains compared to the other ceramics, see Figure 4.3.16.

These results show that milling of $BaTiO_3$ to smaller particles does not automatically result in dielectrics with lower dielectric constants. High energy milling does have an effect on morphology. The $BaTiO_3$ powders are completely or partly de-aglomerated. Besides, the powder surface is damaged and small chipped particles are formed. The resulting effect of the milling process is that the core of pure $BaTiO_3$ is decreased, which should results in a reduction of the dielectric constant as described by Y. Mizuno *et al.*[26] However, the results discussed in this chapter show that the dopant composition also plays an important role. Small adjustments of the dopant composition can have a large influence on microstructure and electrical properties. Furthermore, the sintering process, actually the diffusion of

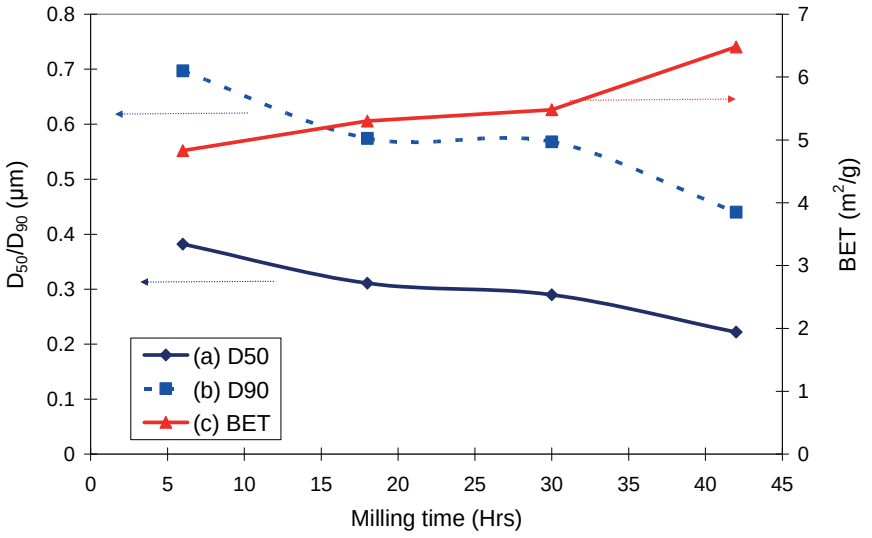

Figure 4.3.11: Effect of milling BTO-1 on (a) D_{50}, (b) D_{90} and (c) specific surface area.

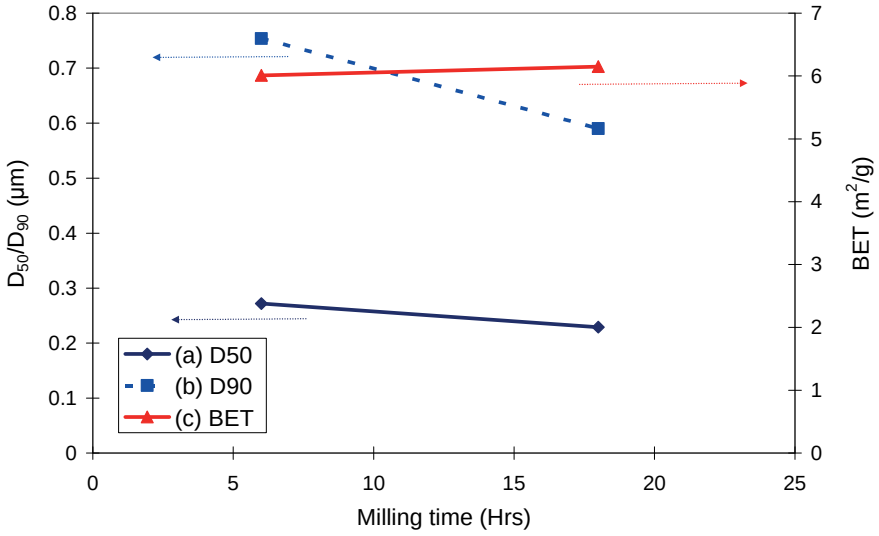

Figure 4.3.12: Effect of milling BTO-2 on (a) D_{50}, (b) D_{90} and (c) specific surface area.

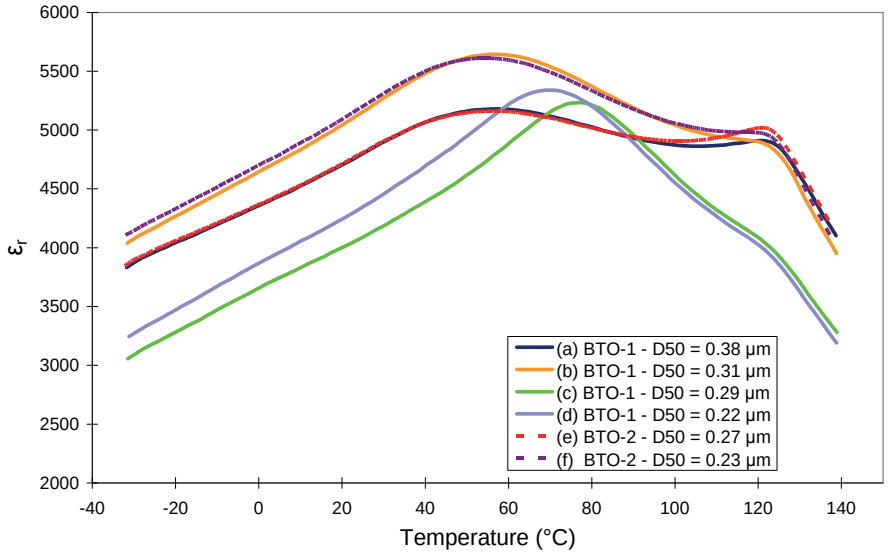

Figure 4.3.13: The ε_r-T curves of BTO-1-D milled to (a) D_{50} of 0.38 µm, (b) D_{50} of 0.31 µm, (c) D_{50} of 0.29 µm and (d) D_{50} of 0.22 µm. The ε_r-T curves of BTO-2-D milled to (e) D_{50} of 0.27 µm, and (f) D_{50} of 0.23 µm. The CDC's were sintered at 1250 °C in wetted 0.3% H_2/N_2 atmosphere. Capacitance was measured at 1 kHz/1V_{rms}.

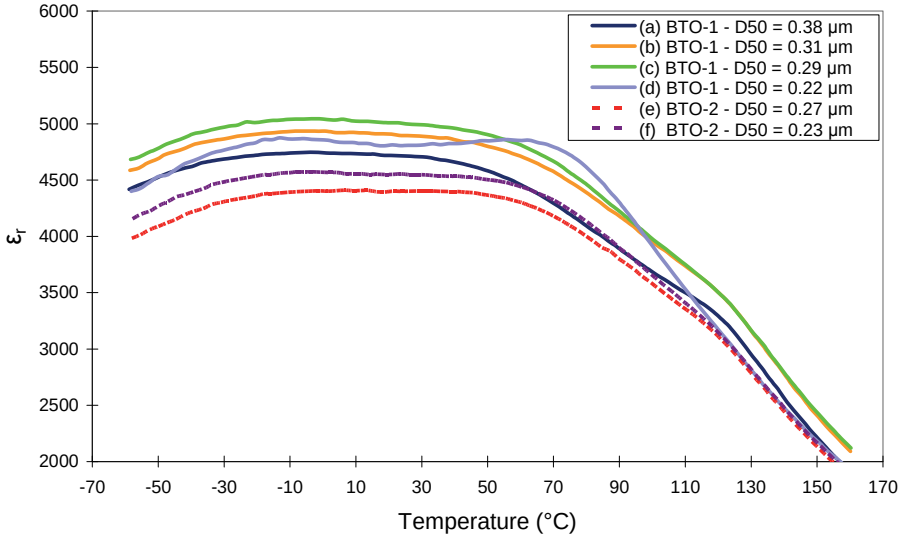

Figure 4.3.14: The ε_r-T curves of BTO-1-D milled to (a) D_{50} of 0.38 µm, (b) D_{50} of 0.31 µm, (c) D_{50} of 0.29 µm and (d) D_{50} of 0.22 µm. The ε_r-T curves of BTO-2-D milled to (e) D_{50} of 0.27 µm, and (f) D_{50} of 0.23 µm. The MLCC's were sintered at 1250 °C in wetted 0.3% H_2/N_2 atmosphere. Capacitance was measured at 1 kHz/1V_{rms}.

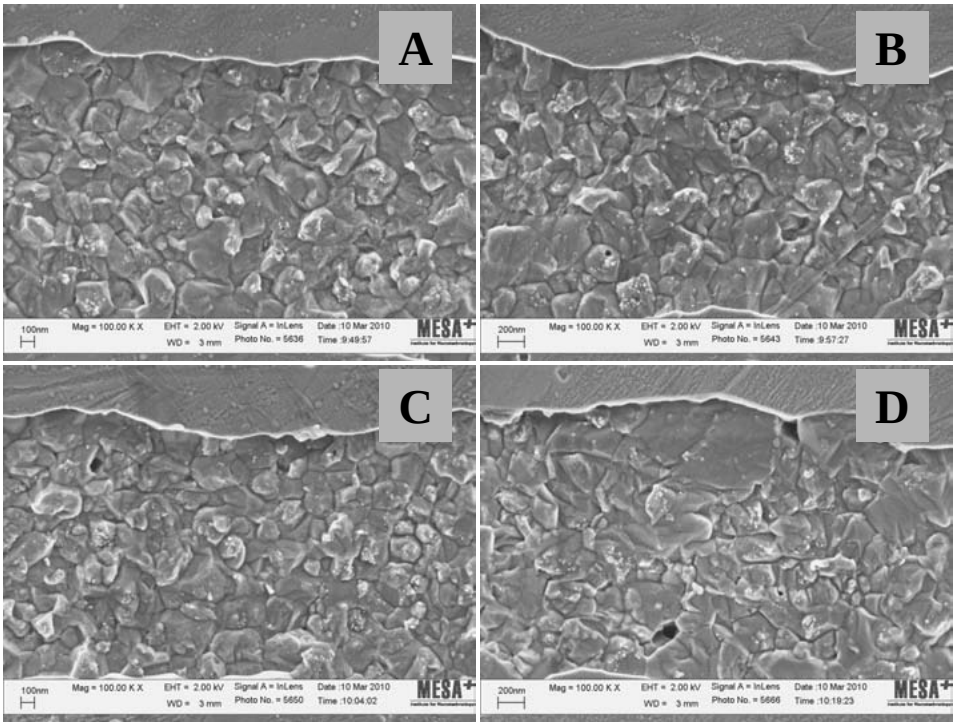

Figure 4.3.15: SEM micrographs of BTO-1-D milled to (a) D_{50} of 0.35 μm, (b) D_{50} of 0.31 μm, (c) D_{50} of 0.29 μm and (d) D_{50} of 0.22 μm after sintering at 1250 °C in 0.3% H_2/N_2.

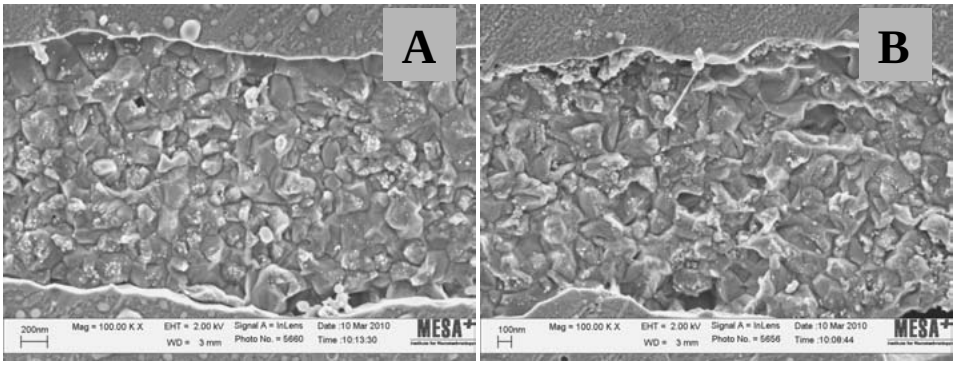

Figure 4.3.16: SEM micrographs of BTO-2-D milled to (a) D_{50} of 0.27 μm and (b) D_{50} of 0.23 μm after sintering at 1250 °C in 0.3% H_2/N_2.

Table 4.3.7: Electrical properties of MLCCs made with BTO-1-D and BTO-2-D.

$BaTiO_3$	Particle size (μm)	Temperature (°C)	ε_r	Tan δ (10^{-4})	IR at 50V (Ω)
BTO-1	D_{50} = 0.38	1200	4893	763	$1.64 \cdot 10^9$
		1250	4713	748	$1.75 \cdot 10^9$
BTO-1	D_{50} = 0.31	1200	4986	765	$1.77 \cdot 10^9$
		1250	4896	799	$2.19 \cdot 10^9$
BTO-1	D_{50} = 0.29	1200	5033	784	$2.08 \cdot 10^9$
		1250	4997	807	$2.35 \cdot 10^9$
BTO-1	D_{50} = 0.22	1200	5105	990	$3.00 \cdot 10^9$
		1250	4808	1033	$1.68 \cdot 10^9$
BTO-2	D_{50} = 0.27	1200	4223	702	$1.55 \cdot 10^9$
		1250	4400	754	$1.56 \cdot 10^9$
BTO-2	D_{50} = 0.23	1200	4625	746	$1.74 \cdot 10^9$
		1250	4554	788	$2.01 \cdot 10^9$

dopant elements, is also largely affected by amount and type of elements, but also by the volume concentration and size of the chipped particles. As a consequence the effect of milling also affects the tan δ and IR values. Both values were increased, due to the size reduction of $BaTiO_3$, the core-shell microstructures was altered.

Table 4.3.8: Average grain size after sintering of BTO-1-D as function of particle size after milling.

$BaTiO_3$ sample	D_{50} (μm)	AGS (nm)
BTO-1-D	0.38	210
BTO-1-D	0.31	200
BTO-1-D	0.29	180
BTO-1-D	0.22	220
BTO-2-D	0.27	170
BTO-2-D	0.23	210

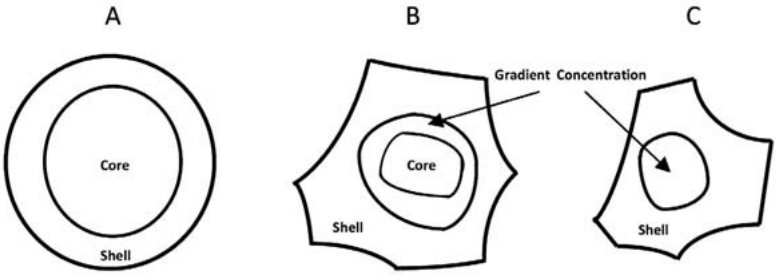

Figure 4.3.17: Schematic model of (a) simple core-shell structure, (b) core-shell structure with intermediate layer of gradient concentration of elements and (c) core-shell structure where the core contains a gradient concentration of elements.

Usually the simple core-shell model, Figure 4.3.17a, is used to explain the dielectric properties of X5R and X7R ceramics and is used for calculation models.[20, 34] This simple model is valid when the core consists of ferroelectric domains of pure or nearly pure $BaTiO_3$. The shell is formed by the dopant elements, which are inhomogeneously distributed in the shell structure. However, TEM studies revealed that with multiple elements an intermediate region exists, in which the elements are incorporated in the $BaTiO_3$ core, but have a decreasing elemental concentration from the shell towards the core of the particle, see Figure 4.3.17b.[35] Moreover, the whole core could also be include foreign metal elements. Then a gradient concentration within the core could be formed, see Figure 4.3.17c.[9]

In reality the microstructure of X5R dielectrics have a more complex structure. The ceramics consist of a mixture of the already mentioned core-shell grains. The core-shell structure is not only affected by the properties of $BaTiO_3$, like grain size, A/B ratio and degree of agglomeration, but also by the type and amount of added metal oxides. The reaction between $BaTiO_3$ powder and dopant powders depend on various parameters: (i) The particle size of the various dopant powders; (ii) The degree of agglomeration of the nanopowders, which is caused by the surface energy on the grain surface of each individual metal oxide; (iii) The overall distribution of all dopant elements in the powders. These factors influence the homogeneity of the powders before sintering. During sintering, the reaction between the chipped particles and the damaged surface of $BaTiO_3$ grains will lead to an inhomogeneously distributed pattern of grains. Such ceramics will contain various types of core-shell grains as described above. Because of the large amount of variables it is difficult to predict the microstructure and electrical properties when a dopant mixture contains various elements at the same time. Even the effect of milling contributes to a certain degree of uncertainty about the outcome of the experiments, as the amount of chipped particles influences the properties of the grain boundary and the shell structure of the sintered grains.

4.3.4. Conclusions

The effect of dopant formulation and milling of various $BaTiO_3$ starting powders on microstructure and dielectric properties were studied. The results showed that small variations of the dopant composition can contribute to large differences in microstructure, grain growth and electrical properties of the dielectrics. The effect of milling has as a consequence that more chipped particles are formed with increasing milling time, which influences the microstructure and dielectric properties of the X5R ceramics. However, the effect of milling can be affected by small adjustments of the dopant composition.

References

1) Kishi, H.; Mizuno, Y. and Chazono, H. *Base-metal electrode-multilayer ceramic capacitors: Past, present and future perspectives*; Japanese Journal of Applied Physics Part 1-Regular Papers Short Notes & Review Papers, 2003 **42**(1): p. 1–15.
2) Randall, M.; Skamser, D.; Kinard, T.; Qazi, J. and Tajuddin, A. *Thin film MLCC*; Conference paper CARTS USA, 2007: p. 1–12.
3) Tsurumi, T.; Adachi, H.; Kakemoto, H.; Wada, S.; Mizuno, Y.; Chazono, H. and Kishi, H. *Dielectric properties of $BaTiO_3$-based ceramics under high electric field*; Japanese Journal of Applied Physics Part 1-Regular Papers Short Notes & Review Papers, 2002 **41**(11B): p. 6929–6933.
4) Morita, K.; Mizuno, Y.; Chazono, H. and Kishi, H. *Effect of Mn addition on dc-electrical degradation of multilayer ceramic capacitor with Ni internal electrode*; Japanese Journal of Applied Physics Part 1-Regular Papers Short Notes & Review Papers, 2002 **41**(11B): p. 6957–6961.
5) Yoon, D. H. *Tetragonality of barium titanate powder for a ceramic capacitor application*; Journal of Ceramic Processing Research, 2006 **7**(4): p. 343–354.
6) Mizuno, Y.; Okino, Y.; Kohzu, N.; Chazono, H. and Kishi, H. *Influence of the microstructure evolution on electrical properties of multilayer capacitor with Ni electrode*; Japanese Journal of Applied Physics Part 1-Regular Papers Short Notes & Review Papers, 1998 **37**(9B): p. 5227–5231.
7) Liu, X. A.; Cheng, S. G. and Randall, C. A. *The core-shell structure in ultrafine X7R dielectric ceramics*; Journal of the Korean Physical Society, 1998 **32**: p. S312-S315.
8) Hennings, D. and Rosenstein, G. *Temperature-stable dielectrics based on chemically inhomogeneous $BaTiO_3$*; Journal of the American Ceramic Society, 1984 **67**(4): p. 249–254.
9) Park, Y. and Song, S. A. *Influence of core-shell structured grain on dielectric properties of cerium-modified barium titanate*; Journal of Materials Science-Materials in Electronics, 1995 **6**(6): p. 380–388.
10) Mizuno, Y.; Hagiwara, T. and Kishi, H. *Microstructural design of dielectrics for Ni-MLCC with ultra-thin active layers*; Journal of the Ceramic Society of Japan, 2007 **115**(1342): p. 360–364.

11) Arlt, G.; Hennings, D. and Dewith, G. *Dielectric-properties of fine-grained barium-titanate ceramics*; Journal of Applied Physics, 1985 **58**(4): p. 1619–1625.
12) Frey, M. H.; Xu, Z.; Han, P. and Payne, D. A. *The role of interfaces on an apparent grain size effect on the dielectric properties for ferroelectric barium titanate ceramics*; Ferroelectrics, 1998 **206**(1–4): p. 337–353.
13) Sakabe, Y.; Wada, N. and Hamaji, Y. *Grain size effects on dielectric properties and crystal structure of fine-grained $BaTiO_3$ ceramics*; Journal of the Korean Physical Society, 1998 **32**: p. S260-S264.
14) Lee, J. K.; Hong, K. S. and Jang, J. W. *Roles of Ba/Ti ratios in the dielectric properties of $BaTiO_3$ ceramics*; Journal of the American Ceramic Society, 2001 **84**(9): p. 2001–2006.
15) Kishi, H.; Kohzu, N.; Sugino, J.; Ohsato, H.; Iguchi, Y. and Okuda, T. *The effect of rare-earth (La, Sm, Dy, Ho and Er) and Mg on the microstructure in $BaTiO_3$*; Journal of the European Ceramic Society, 1999 **19**(6–7): p. 1043–1046.
16) Kishi, H.; Okino, Y.; Honda, M.; Iguchi, Y.; Imaeda, M.; Takahashi, Y.; Ohsato, H. and Okuda, T. *The effect of MgO and rare-earth oxide on formation behavior of core-shell structure in $BaTiO_3$*; Japanese Journal of Applied Physics Part 1-Regular Papers Short Notes & Review Papers, 1997 **36**(9B): p. 5954–5957.
17) Sakabe, Y.; Hamaji, Y.; Sano, H. and Wada, N. *Effects of rare-earth oxides on the reliability of X7R dielectrics*; Japanese Journal of Applied Physics Part 1-Regular Papers Short Notes & Review Papers, 2002 **41**(9): p. 5668–5673.
18) Morita, K.; Mizuno, Y.; Chazono, H.; Kishi, H.; Yang, G. Y.; Liu, W. E.; Dickey, E. C. and Randall, C. A. *Electric conduction of thin-layer Ni-multilayer ceramic capacitors with core-shell structure $BaTiO_3$*; Japanese Journal of Applied Physics Part 1-Regular Papers Brief Communications & Review Papers, 2007 **46**(5A): p. 2984–2990.
19) Park, Y.; Kim, Y. H. and Kim, H. G. *The effect of grain size on dielectric behavior of $BaTiO_3$ based X7R materials*; Materials Letters, 1996 **28**(1–3): p. 101–106.
20) Yasukawa, K.; Nishimura, M.; Nishihata, Y. and Mizuki, J. *Core-shell structure analysis of $BaTiO_3$ ceramics by synchrotron X-ray diffraction*; Journal of the American Ceramic Society, 2007 **90**(4): p. 1107–1111.
21) Chen, C. S.; Chou, C. C. and Lin, I. N. *Microstructure of X7R type base-metal-electroded $BaTiO_3$ capacitor materials co-doped with MgO/Y_2O_3 additives*; Journal of Electroceramics, 2004 **13**(1–3): p. 567–571.
22) Wada, N.; Tanaka, H.; Hamaji, Y. and Sakabe, Y. *Microstructures and dielectric properties of fine-grained $BaTiO_3$ ceramics*; Japanese Journal of Applied Physics Part 1-Regular Papers Short Notes & Review Papers, 1996 **35**(9B): p. 5141–5144.
23) Yuan, Y.; Zhang, S. R. and Li, C. M. *The effect of doping process on microstructure and dielectric properties of $BaTiO_3$-based X7R materials*; Journal of Materials Science-Materials in Electronics, 2004 **15**(9): p. 601–606.
24) Tian, Z. B.; Wang, X. H.; Zhang, Y. C.; Fang, J.; Song, T. H.; Hur, K. H.; Lee, S. and Li, L. T. *Formation of Core-Shell Structure in Ultrafine-Grained $BaTiO_3$-Based Ceramics Through Nanodopant Method*; Journal of the American Ceramic Society, 2010 **93**(1): p. 171–175.
25) Zhou, X. H.; Zhang, S.; Yuan, Y.; Li, B. and Liu, J. S. *Preparation of $BaTiO_3$-based nonreducible X7R dielectric materials via nanometer powders doping*; Journal of Materials Science-Materials in Electronics, 2006 **17**(2): p. 133–136.

26) Mizuno, Y.; Hagiwara, T.; Chazono, H. and Kishi, H. *Effect of milling process on core-shell microstructure and electrical properties for $BaTiO_3$-based Ni-MLCC*; Journal of the European Ceramic Society, 2001 **21**(10–11): p. 1649–1652.
27) Gijp van der, S. *Preparation of homogeneously-doped barium titanate*; dissertation 1998
28) Phule, P. P. and Risbud, S. H. *Low-temperature synthesis and processing of electronic materials in the BaO-TiO_2 system*; Journal of Materials Science, 1990 **25**(2B): p. 1169–1183.
29) Pithan, C.; Hennings, D. and Waser, R. *Progress in the synthesis of nanocrystalline $BaTiO_3$ powders for MLCC*; International Journal of Applied Ceramic Technology, 2005 **2**(1): p. 1–14.
30) Buscaglia, M. T.; Bassoli, M. and Buscaglia, V. *Solid-state synthesis of nanocrystalline $BaTiO_3$: Reaction kinetics and powder properties*; Journal of the American Ceramic Society, 2008 **91**(9): p. 2862–2869.
31) Maurice, A. K. and Buchanan, R. C. *Preparation and stoichiometry effects on microsctructure and properties of high-purity $BaTiO_3$*; Ferroelectrics, 1987 **74**(1–2): p. 61–75.
32) Derling, S.; Muller, T.; Abicht, H. P.; Felgner, K. H. and Langhammer, H. T. *Copper oxide as a sintering agent for barium titanate based ceramics*; Journal of Materials Science, 2001 **36**(6): p. 1425–1431.
33) Yang, W. C.; Hu, C. T. and Lin, I. N. *Effect of Y_2O_3/MgO co-doping on the electrical properties of base-metal-electroded $BaTiO_3$ materials*; Journal of the European Ceramic Society, 2004 **24**(6): p. 1479–1483.
34) Wen, H.; Wang, X. H.; Gui, Z. L. and Li, L. T. *Modeling of the core-shell microstructure of temperature-stable $BaTiO_3$ based dielectrics for multilayer ceramic capacitors*; Journal of Electroceramics, 2008 **21**(1–4): p. 545–548.
35) Park, Y. and Kim, Y. H. *The dielectric temperature characteristics of additives modified Barium-Titanate having core-shell structured ceramics*; Journal of Materials Research, 1995 **10**(11): p. 2770–2776.

Chapter 4.4

An alternative strategy towards high ε_r dielectrics

4.4.1. Introduction to new high ε_r X5R dielectrics

Temperature stable X5R multilayer capacitors consist of chemically doped $BaTiO_3$ dielectrics in order to get a flat capacitance temperature curve and high reliability. This type of dielectrics have in general a microstructure of core-shell grains. The core consists of pure or nearly pure $BaTiO_3$ and the shell is formed by incorporating various elements into the $BaTiO_3$ lattice. Typically the dielectrics are schematically drawn in literature as shown in Figure 4.1.8. However, this schematic representation of the microstructure suggests that all grains have more or less the same basic core-shell structure. To achieve high relative permittivity values in ultrathin dielectric layers, other possible strategies to obtain high ε_r dielectrics are also investigated. Dielectric materials having an ε_r of 5000 or more based on a different type of materials synthesis method are described in an application note.[1] The application note describes a dielectric material based on grains, which are partly rich in one of the rare earth elements and copper, and grains with a low concentration of these elements, see Figure 4.4.1. Besides the differences in concentration of rare earth element and copper, the volume ratio between the two type of grains also has to be within a certain range. The claim also describes the possibility that the dielectrics do not have the typical core-shell structure, an idea that was proposed by N. Wada *et al.*[2]

Furthermore, it has also been reported that ceramics in ultrathin dielectrics, which have a very fine grain size distribution, do not have the typical core-shell structure because the grains are believed to be too small and all added elements diffuse into the core during the sintering process.[3–4] However, these fine grained ceramics possess a high dielectric constant and they seem to be used already in MLCCs with 1 μm dielectric layers in thickness.[2]

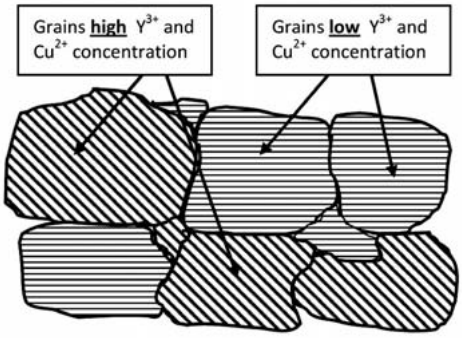

Figure 4.4.1: Schematic microstructure of X5R in ultrathin dielectric layer.

The application note describes a process method of manufacturing according to the following procedure. First the Ba_mTiO_3 or $(Ba_{1-x}Ca_x)_mTiO_3$ powders, where $0<x<0.3$ and $1.001<m<1.012$, are reacted with RE_2O_3 and CuO to form grains having a core-shell structure, see Figure 4.4.2b. Then the core-shell grains have to be grinded by a milling process to form chipped particles rich in RE^{3+} and Cu^{2+}, besides grains with low concentration of these elements, see Figure 4.4.2c. Then the RE^{3+}/Cu^{2+}-rich grains and almost pure $BaTiO_3$ grains are sintered together with other elements like MgO, MnO and SiO_2 to form a X5R type of dielectrics. It is noted that this method does not allow good control of the ratio and composition of the various grains.

X5R ceramics are normally fabricated by mixing the dopant elements by adding these in nano-powder form to coarse grains of pure $BaTiO_3$, see Figure 4.4.3a. However, to control the ratio between the grains with high and low concentration of rare earth elements and copper, an alternative method is proposed in this chapter to study and optimize the materials properties. A homogeneous powder of modified $BaTiO_3$ with Y_2O_3 and CuO was fabricated by the solid state reaction. Then the modified $BaTiO_3$ and pure $BaTiO_3$ powders were mixed in specific ratios together with the nano-dopant powders, which are for instance MgO, MnO, SiO_2 and Y_2O_3, to make dielectric ceramics, see Figure 4.4.3b.

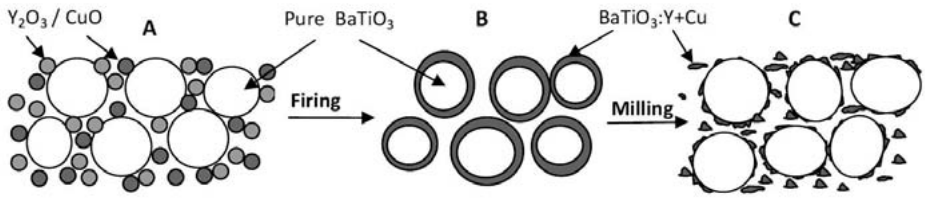

Figure 4.4.2: Schematic process flow of making of high dielectric powders by (a) adding Y_2O_3 and CuO to $BaTiO_3$. Then (b) core-shell grains formed by firing process and (c) chipped particles rich in Y^{3+} and Cu^{2+} in the $BaTiO_3$ lattice are formed by a milling process.

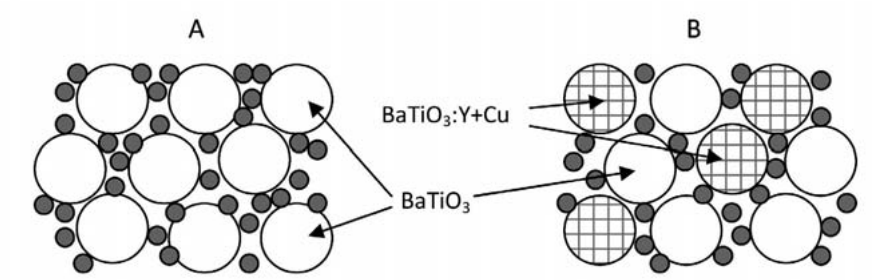

Figure 4.4.3: Schematic view of particle grains consisting of the nano-dopant particles besides (a) pure $BaTiO_3$ grains and (b) a mixture of pure $BaTiO_3$ and modified $BaTiO_3$ grains.

The material and electrical properties of these types of dielectrics were evaluated. In particular the effect of $BaTiO_3$ and $BaTiO_3$:Cu:Y ratio was examined. All powders were made with the solid state method. However, the effect of addition of a $BaTiO_3$:Cu:Y compound to various commercial $BaTiO_3$ powders having different material properties was evaluated as well.

4.4.2. Preparation method to make new type X5R dielectrics

The $BaTiO_3$ and $BaTiO_3$:Cu:Y (=BTCY) powders were made according to the composition $BaTi_{1.003}O_3$ + *x* mol% Y_2O_3 + *y* mol% CuO. Table 4.4.1 shows the exact compositions. The $BaCO_3$ (Solvay, BM20), TiO_2 (TOHO, HT3201), Y_2O_3 (Rhodia, UF39) and CuO (PCC, 99%) powders were weighed and overnight milled in isopropanol. After drying the powders, they were calcined at 1000 and 1150 °C ,respectively, for 4 h in air.

Tabel 4.4.1: Overview of $BaTiO_3$ and modified $BaTiO_3$ with Y^{3+} and Cu^{2+}.

Sample	BT	BTCY-1	BTCY-2	BTCY-3	BTCY-4
$BaTiO_3$	$Ba_{1.003}TiO_3$	$Ba_{1.003}TiO_3$	$Ba_{1.003}TiO_3$	$Ba_{1.003}TiO_3$	$Ba_{1.003}TiO_3$
x = Y_2O_3 (mol%/mol BT)	-	0.5	1.0	1.5	3.0
x = CuO (mol%/mol BT)	-	0.3	0.6	0.9	1.8

The powders for the ceramic disc capacitors were weighed in the ratio *u* mol% BT + *v* mol% BTCY-*x*, so that *u* + *v* = 100 mol%. This is the main compound and will be referred as BT/BTCY. The ratio *u*/*v* represents the molar ratio between the pure $BaTiO_3$ phase and the Y^{3+}/Cu^{2+}-rich powders. To these BT/BTCY powders the dopant elements are added according to the following composition

Table 4.4.2: Overview of dielectric compositions.

Experiment	E-1	E-2	E-3	E-4	E-5
Precursor $BaTiO_3$	BT	BTCY-1	BTCY-2 BT	BTCY-3 BT	BTCY-4 BT
BTCY/$BaTiO_3$ (*u*/*v*)	0/100	100/0	50/50	25/75	17/83
a = Y_2O_3 (mol%/mol BT)	0.5	-	-	-	-
b = CuO (mol%/mol BT)	0.3	-	-	-	-
c = MgO (mol%/mol BT)	1.0	1.0	1.0	1.0	1.0
d = $MnCO_3$ (mol%/mol BT)	0.35	0.35	0.35	0.35	0.35
e = SiO_2 (mol%/mol BT)	0.5	0.5	0.5	0.5	0.5

100 mol% BT/BTCY + *a* mol% Y_2O_3 + *b* mol% CuO + *1.0* mol% MgO + *0.35* mol% $MnCO_3$ + *0.5* mol% SiO_2.

Table 4.4.2 shows the overall compositions of the 5 experimental samples. All these mixtures yielded exactly the same overall composition. The raw materials used for the dopant mixtures were Y_2O_3 (Rhodia, UF39), CuO (PCC, 99%), MgO (Konoshima, HP-30), $MnCO_3$ (J.T. Baker, 99.0%) and SiO_2 (Degussa, Aerosil R975). Pellets of 8 mm diameter x 2 mm height were prepared. The pellets were sintered in a wetted 0.3% H_2/N_2 atmosphere at temperatures between 1250 and 1350°C for 2 hours in a Nabertherm tube kiln according the temperature profile as described in Chapter 2. Gold terminations, with a thickness of 200 nm, were applied on the pellets by sputtering using a Perkin-Elmer sputtering system Model 2400.

4.4.3. Discussion of electrical properties and XRD results

The $BaTiO_3$ and BTCY-*x*, where *x* is 1 to 4, were calcined at 1000 and 1150 °C, respectively. Figure 4.4.4 shows the ε_r-*T* curves of the samples sintered at 1350 °C from precursor powders BT and BTCY-*x* that had been calcined at 1000 °C. Figure 4.4.5 shows the results of dielectrics that were sintered at 1350 °C from precursors that had been calcined at 1150 °C. The difference in ε_r-*T* characteristics is obvious and shows the effect of calcination temperature on electrical properties. The ε_r-*T* curve of the ceramics calcined at 1000 °C show a large peak between 70 and 84°C, reaching maximum ε_r values in the range of 8200 to 8900. This is a typical type of the ε_r-*T* curve, and is often observed for core-shell grains.[5] Furthermore, in these ε_r-*T* curves the T_c of the cubic-tetragonal transition of $BaTiO_3$ were not

observed, whereas the ε_r-*T* curves of the ceramic powders calcined at 1150 °C showed a T_c at 125 °C. The ε_r-*T* curves measured on the ceramic disc capacitors show a very flat ε_r-*T* dependency, in which various curves overlap each other. On the other hand, the ε_r of the dielectrics with a calcination temperature of 1000 °C varied more.

In Figure 4.4.4e the ε_r-*T* curve of sample E-5 show very low ε_r values. This is probably due to the fact that these ceramics were not fully dense. This hypothesis is supported by the results on the E-5 ceramics calcined at 1150 °C. These ceramics were not fully dense after sintering at 1350 °C, and that is why the ε_r-*T* dependency was not measured for this sample. The data from Table 4.4.3 indicate that the particle size of the powders calcined at 1150 °C were coarser than the powders calcined at 1000 °C. Moreover, the sintering temperatures increased from sample E-1 towards sample E-5, independent of particle size of the milled powders.

Table 4.4.3: The surface area of the mixed powders after being milled overnight with dopant addition.

Experiment	B.E.T. (g/cm^3) Calc. 1000°C	B.E.T. (g/cm^3) Calc. 1150°C
E-1	8.6	5.1
E-2	8.6	5.4
E-3	7.7	5.1
E-4	7.9	5.1
E-5	8.3	5.8

To sinter all samples fully dense, sintering temperatures of 1350 °C were required. For samples E-1 and E-2 a sintering temperature of 1250 °C was high enough to produce fully dense ceramics.

Figure 4.4.6 show the x-ray diffraction patterns of the dielectrics that had been successively calcined at 1000 °C and sintered at 1350 °C. All patterns show two different crystal structures. The first phase consisted of pure $BaTiO_3$ and had the tetragonal crystal phase for samples E-1 to E-4, see Figure 4.4.7.[6] The split of the peaks of the {200}and {002} planes of the tetragonal phase for 2θ between 44° and 46° is clearly observed. However, sample E-5 seemed to have the cubic crystal structure as only 1 peak, the {200} plane, was observed.

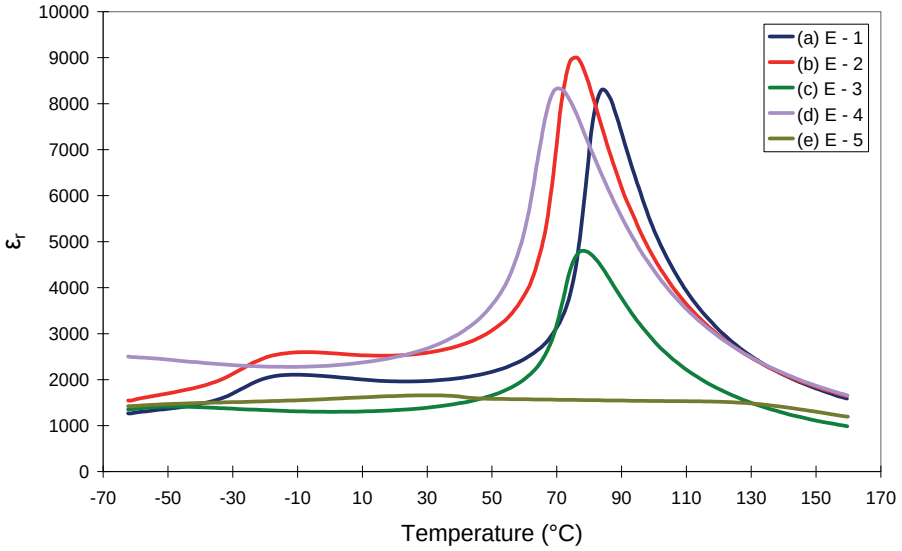

Figure 4.4.4: The ε_r versus *T* curves of (a) E-1, (b) E-2, (c) E-3, (d) E-4 and (e) E-5 samples calcined at 1000 °C and sintered at 1350 °C. The CDC's were measured at 1kHz/1V_{rms}.

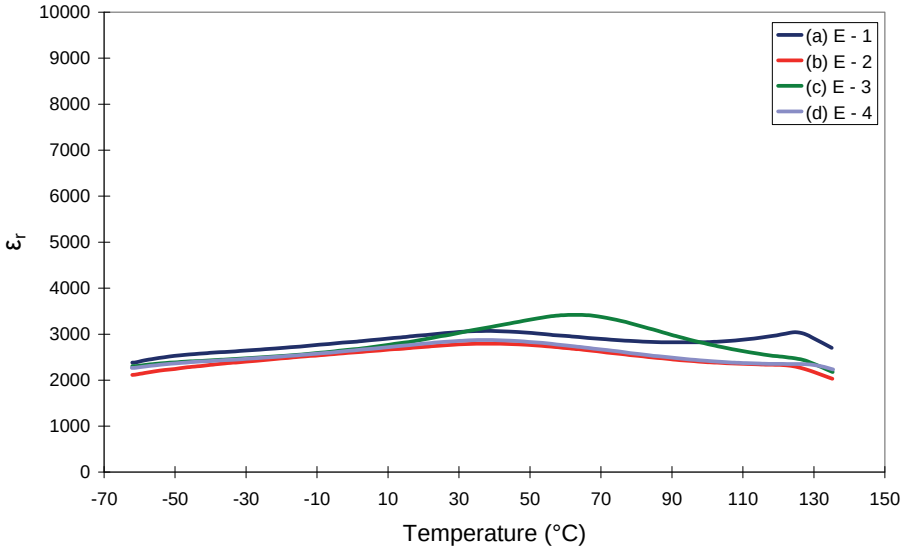

Figure 4.4.5: The ε_r versus *T* curves of (a) E-1, (b) E-2, (c) E-3 and (d) E-4 samples calcined at 1150 °C and sintered at 1350 °C. The CDC's were measured at 1kHz/1V_{rms}.

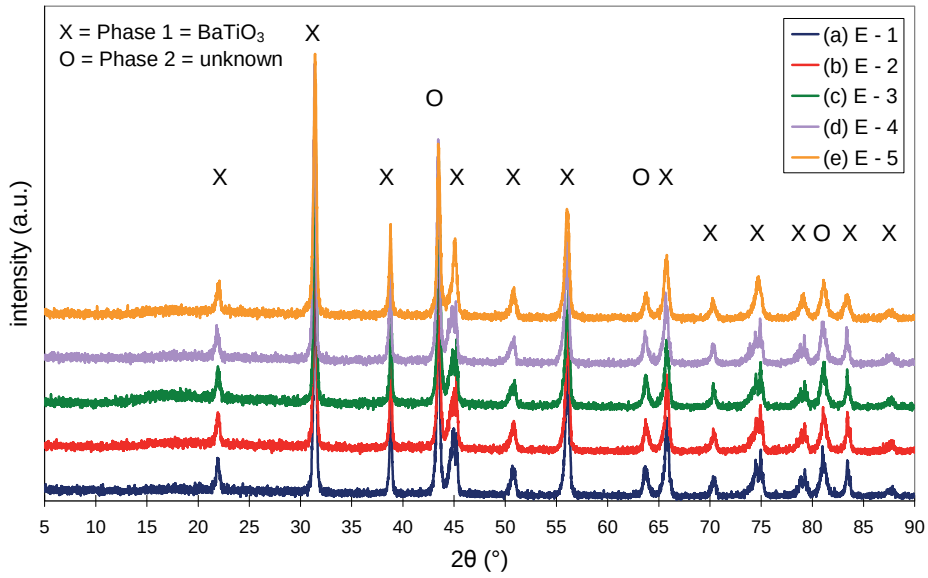

Figure 4.4.6: X-ray diffraction patterns of dielectrics E-1 to E-5, which were successively calcined at 1000 °C and sintered at 1350 °C.

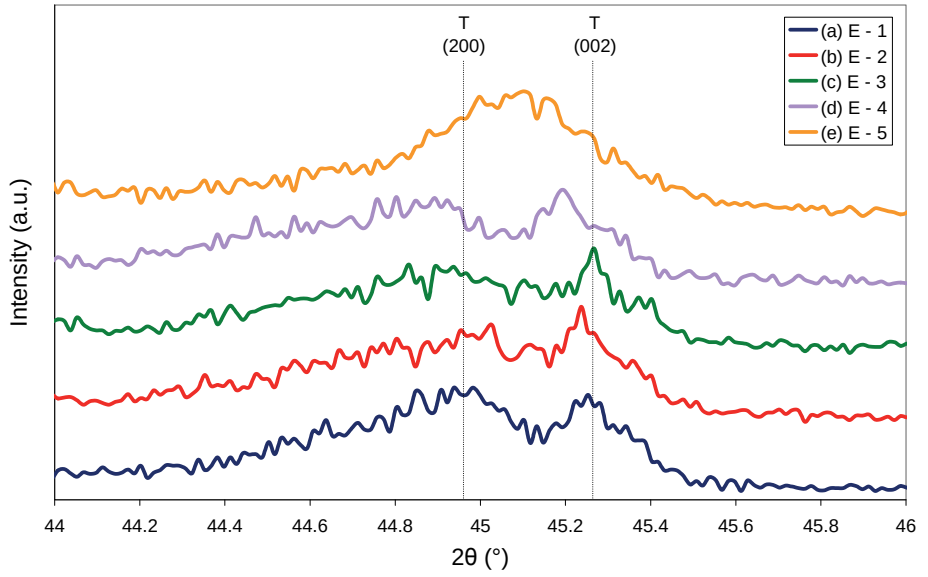

Figure 4.4.7: Deformation of the {200} and {002} peaks of samples E-1 to E-5, successively calcined at 1000 °C and sintered at 1350 °C.

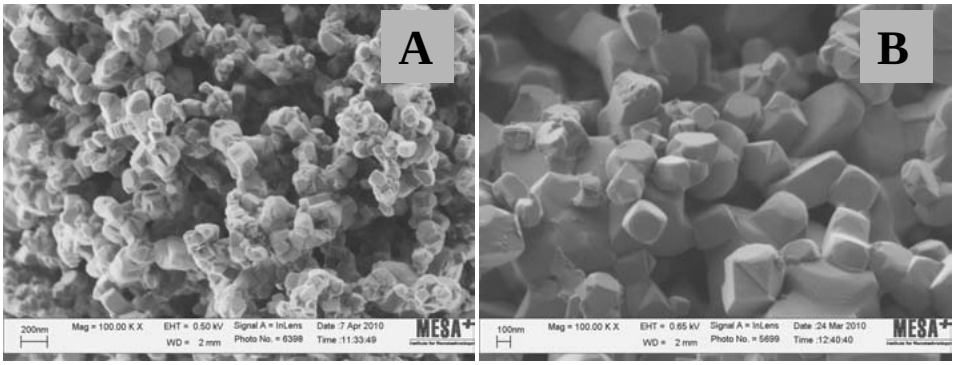

Figure 4.4.8: Powder morphology of $BaTiO_3$ after calcination at (a) 1000 °C and (b) 1150 °C for 4 h in air.

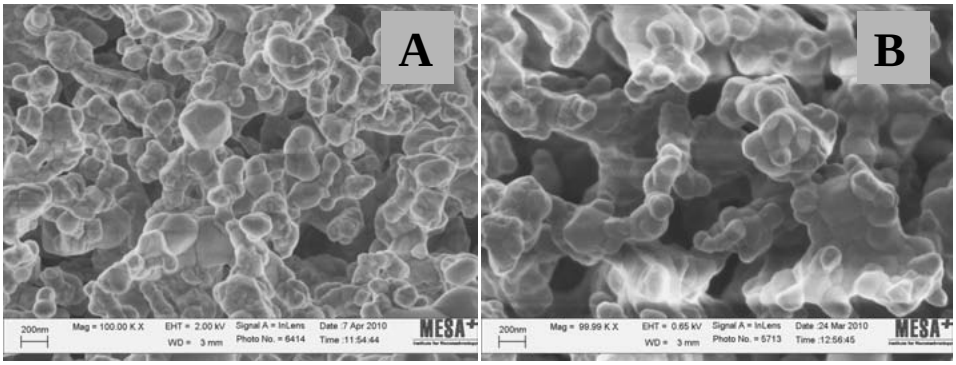

Figure 4.4.9: Powder morphology of BTCY-4 after calcination at (a) 1000 °C and (b) 1150 °C for 4 h in air.

The second phase is an unidentified crystal structure. The phase should contain Ba^{2+}, Ti^{4+}, Cu^{2+} and/or Y^{3+} elements, which are incorporated in the BTCY powders. The other elements, Mg^{2+}, Mn^{2+} and Si^{4+}, will also be present in the $BaTiO_3$ lattice. The second phase will most likely consist of grains with high concentration of the added foreign elements or it could be the shell phase, when core-shell grains were formed instead. The phase fraction of this unknown phase is quite large having a volume fraction value of 42.5 %. This means that the amount of the pure $BaTiO_3$ and the second phase were almost equal. In the temperature dependent ε_r measurement the tetragonal-cubic transition of $BaTiO_3$ was not observed. The relative permittivity is therefore not only dominated by the ferroelectric domains in $BaTiO_3$, but also by the dielectric properties of the second phase.

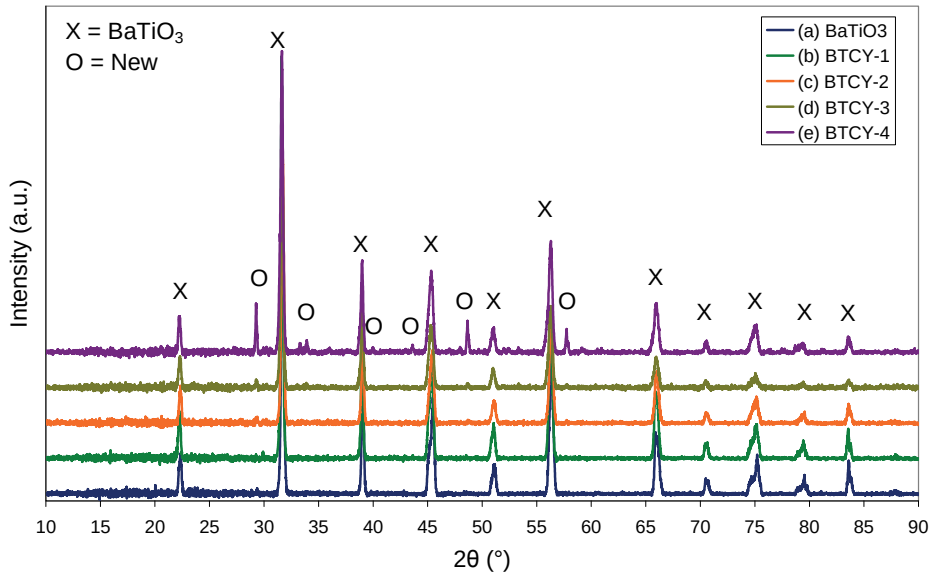

Figure 4.4.10: The X-ray diffraction patterns of powders (a) $BaTi_{1.003}O_3$, (b) BTCY-1, (c) BTCY-2, (d) BTCY-3 and (e) BTCY-4, which were fired at 1000 °C.

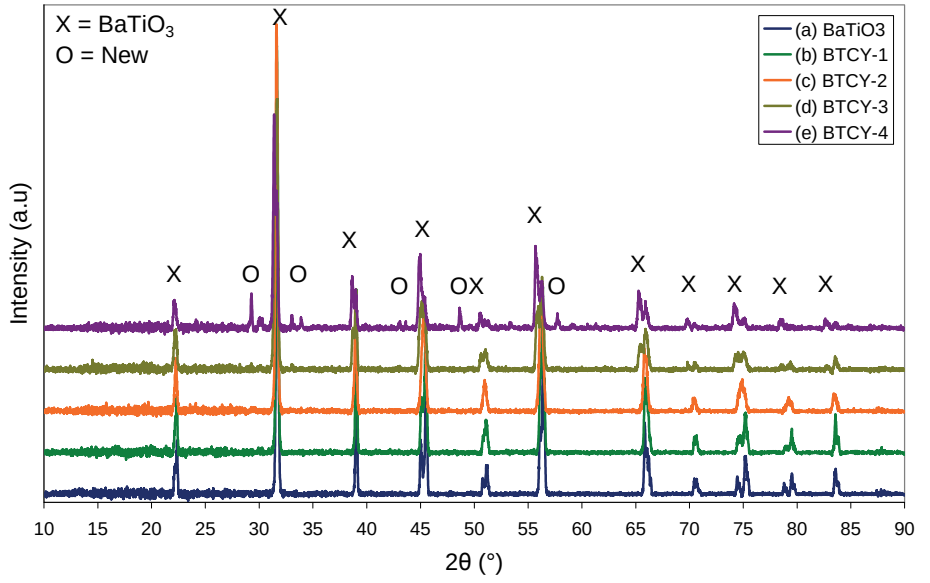

Figure 4.4.11: The X-ray diffraction patterns of powders (a) $BaTi_{1.003}O_3$, (b) BTCY-1, (c) BTCY-2, (d) BTCY-3 and (e) BTCY-4, which were fired at 1150 °C.

The calcination temperature had a large impact on the sintering behaviour and electrical properties of the dielectrics. Figure 4.4.8 shows the powder morphology of $Ba_{1.003}TiO_3$. This powder forms larger cubic particles having a relatively wide grain size distribution. The powders fired at a calcination temperature of 1150 °C had larger particles than the powders calcined at 1000 °C. However, the series of the BTCY-*x* powders showed a different morphology, see Figure 4.4.9.

The powders calcined with CuO and Y_2O_3 showed an agglomerated structure after the firing process. These structures could be de-agglomerated by a milling process. However, the milled powders of E-4 were not very reactive. This is probably due to the formation of a crystal phase as observed in the x-ray diffraction pattern of BTCY-4, see Figure 4.4.10 and Figure 4.4.11. Except for powder BTCY-4 the XRD patterns are representative of $BaTiO_3$. However, the samples fired at 1000°C had a cubic crystal structure, whereas the powders fired at 1150°C had a tetragonal structure.

In the BTCY-4 powders a second crystallographic phase was found, next to tetragonal or cubic $BaTiO_3$. The analysis of the new phase did not reveal a known crystal structure that is commonly found in the Ba-Ti-O phase diagram. It is known that the element Y^{3+} is incorporated both on the Ba and Ti lattice sites. Furthermore, Cu^{2+} is a small ion, which will be incorporated on the Ti^{4+} site.[7] The Ba^{2+}/Ti^{4+} ratio will therefore be largely influenced when a large amount of Cu^{2+} is incorporated into $BaTiO_3$. From literature it is known that Cu^{2+} addition to the $BaTiO_3$ lattice changes the crystal structure at room temperature from tetragonal to hexagonal, when a certain minimum amount of Cu^{2+} is added and the ceramics are sintered at 1400 °C.[8] However, the amount to incorporate Cu^{2+} is limited and depends largely on the Ba/Ti ratio of $BaTiO_3$. Most likely the simultaneously added Y^{3+} element will influence the solubility and crystal structure as well. Probably due to the large concentration of elements incorporated at the Ti-site, a crystal structure is formed that is different from the phases commonly found in $BaTiO_3$. More knowledge about the formation of this unknown crystal structure should be gained with a new set of experiments.

4.4.4. Conclusions

A new method of solid state synthesis to make high ε_r dielectrics is proposed That differs from the conventional method of preparing a core-shell structure by adding various elements to $BaTiO_3$. With the new approach grains rich in rare earth elements and copper are combined with pure $BaTiO_3$ and other dopants in a solid state reaction to fabricate high ε_r and reliable dielectrics suitable for ultrathin layers in multilayer capacitors. The microstructure of the dielectrics is different than the

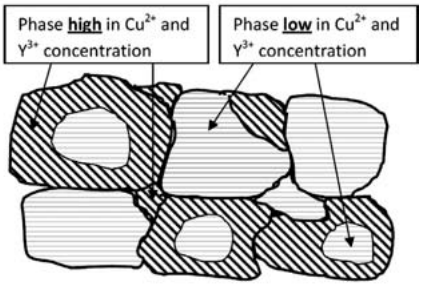

Figure 4.4.12: Proposed microstructure of X5R in ultrathin dielectric layer.

typical core-shell structure. Proposed is a microstructure, see Figure 4.4.12, in which core-shell grains are present besides grains with most probably a gradient of elements, or grains with high and low contents of rare earth elements and copper. Due to the small sizes of the grains a mixture of these types of grains will be found in dielectrics when processed as mentioned above.

The combination of $BaTiO_3$ and $BaTiO_3$:Y:Cu grains produced high ε_r dielectrics in ceramic disc capacitors. The influence of the calcination temperature was found to have a large effect on the dielectric properties. However, the effect of the material properties under a higher applied AC field such as found in multilayer capacitors were not evaluated. It would be interesting to evaluate this type of dielectrics in more detail.

References

1) Sasabayashi, T.; Ishihara, M.; Nakamura, T. and Sano, H. *Dielectric ceramic, method for manufacturing dielectric ceramic and monolithic ceramic capacitor*; US application note 7501371, 2007.
2) Wada, N.; Hiramatsu, T.; Tamura, T. and Sakabe, Y. *Investigation of grain boundaries influence on dielectric properties in fine-grained $BaTiO_3$ ceramics without the core-shell structure*; Ceramics International, 2008 **34**(4): p. 933–937.
3) Sakabe, Y.; Wada, N.; Hiramatsu, T. and Tonogaki, T. *Dielectric properties of fine-grained $BaTiO_3$ ceramics doped with CaO*; Japanese Journal of Applied Physics Part 1-Regular Papers Short Notes & Review Papers, 2002 **41**(11B): p. 6922–6925.
4) Wada, N.; Tanaka, H.; Hamaji, Y. and Sakabe, Y. *Microstructures and dielectric properties of fine-grained $BaTiO_3$ ceramics*; Japanese Journal of Applied Physics Part 1-Regular Papers Short Notes & Review Papers, 1996 **35**(9B): p. 5141–5144.
5) Tsurumi, T.; Adachi, H.; Kakemoto, H.; Wada, S.; Mizuno, Y.; Chazono, H. and Kishi, H. *Dielectric properties of $BaTiO_3$-based ceramics under high electric field*; Japanese Journal of Applied Physics Part 1-Regular Papers Short Notes & Review Papers, 2002 **41**(11B): p. 6929–6933.

6) Yoon, D. H. *Tetragonality of barium titanate powder for a ceramic capacitor application*; Journal of Ceramic Processing Research, 2006 **7**(4): p. 343–354.
7) Shannon, R. D. *Revised effective ionic-radii and systematic studies of interatomic distances in halides and chalcogenides*; Acta Crystallographica Section A, 1976 **32**(SEP1): p. 751–767.
8) Langhammer, H. T.; Muller, T.; Bottcher, R. and Abicht, H. P. *Crystal structure and related properties of copper-doped barium titanate ceramics*; Solid State Sciences, 2003 **5**(7): p. 965–971.

Chapter 4.5

Microstructure of X5R dielectrics

4.5.1. Short introduction to microstructures of X5R dielectrics

To achieve high volumetric efficiencies in X5R multilayer ceramic capacitors high-ε_r dielectrics are used. Nowadays relative permittivity values of about 5000 can be reached and such dielectrics are described in Chapter 4.3. Typically, these high-ε_r X5R ceramics consist of grains having a core-shell structure. For X7R dielectrics the microstructure is quite often schematically represented in literature as shown in Figure 4.1.9. This schematically drawn microstructure suggests that all grains of X5R and/or X7R dielectrics have the typical core-shell structure. Initially, this type of microstructure was used to describe the donor/acceptor doped X7R dielectrics.[1–4]

Because the average grains size of the dielectrics had to be decreased to fulfil the requirements to make thin layer dielectrics, the microstructures of these high-ε_r X5R could be different. Nowadays the dielectrics, used for X5R BME capacitors, are based on formulations, which contain MgO, one of the three 'magic ions' (Y^{3+}, Ho^{3+} and Er^{3+}), Mn_3O_4 and a sintering flux based on SiO_2. The effect of incorporating these metal oxides in particular ratios into the $BaTiO_3$ lattice has been intensively studied, not only for the electrical properties, but also regarding their microstructures.[5–11]

Some of these studies suggest that the dielectrics, which are composed of the above-mentioned elements, have a core-shell structure for every grain. Other studies focused their examination of the microstructure mainly on the grains with a core-shell structure. For instance, the effect of milling of raw materials on the volume fractions of the core and shell phase after sintering was investigated and the examination was primarily focused on the core-shell grains.[12]

A more careful study of the microstructure of the grains by transmission electron microscopy (TEM) revealed that only a limited number of the grains had the core-shell structure. The typical 90° domain patterns were present in a fraction of the ceramics grains, but a considerable number of grains did not show these typical

ferro-electric domains.[13–14] Moreover, some studies revealed that the microstructures show an inhomogeneous distribution of the para-electric phase. Furthermore, the ferroelectric domains are only present in the larger grains as their presence is dependent on the individual grain size.[15–16]

In this chapter the microstructure of a typical high-ε_r dielectric, manufactured according to the process described in Chapter 4.3, is examined in more detail by TEM. There is a relationship between the microstructure of the ceramics and their electrical properties. The microstructure analysis by TEM can help to reveal this relationship.

4.5.2. CDC and MLCC preparation and characterization

The ceramic disc capacitors (CDC) were fabricated starting from powders of $BaTiO_3$ (NCI; in Table 4.3.1 described as $BaTiO_3$ no 1), $BaCO_3$ (Solvay, BM20), SiO_2 (Degussa, Aerosil R975), $BaSiO_3$ (Yageo), Y_2O_3 (Rhodia, UF39), $MnCO_3$ (J.T. Baker, 99.0%), MgO (Konoshima, HP-30), CuO (PCC, 99%), MoO_3 (HC Starck, 99.5%) and V_2O_5 (Sigma-Aldrich, 99.8 %). The dopant powders were ball-milled in ethanol to a D_{50} of approximately 100 nm and kept as a slurry. The $BaTiO_3$ powders were milled to a D_{50} of 0.34 μm. The $BaTiO_3$ and dopant slurries were mixed according the formula

100 mol% $BaTiO_3$ + *0.25* mol% Y_2O_3 + *2.0* mol% MgO + *0.2* mol% $MnCO_3$ + *0.25* mol% SiO_2 + *0.25* mol% $BaCO_3$ + *0.025* mol% Nb_2O_5 + *0.06* mol% V_2O_5

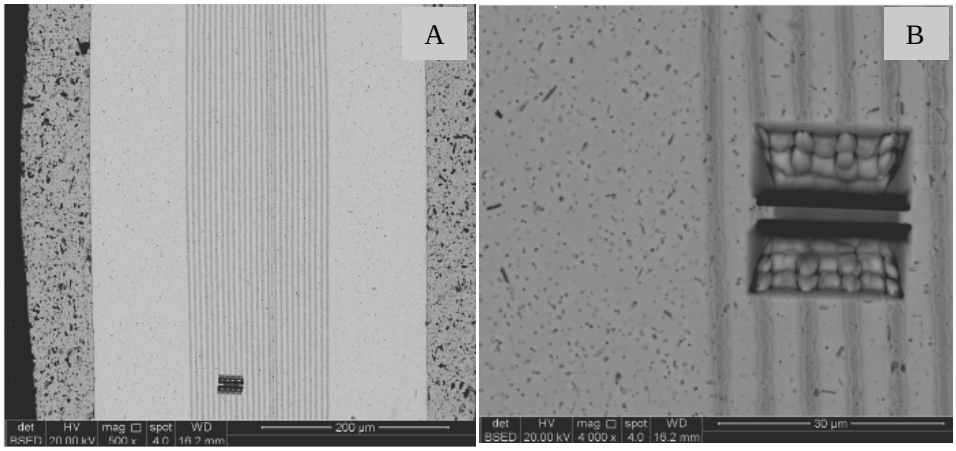

Figure 4.5.1: SEM micrographs showing (a) the location of the FIB trench and (b) FIB trench details.

CDC samples of 10 mm in diameter x 2 mm in thickness having nickel electrodes were made. Green multilayer ceramic capacitor (MLCC) chips of above-mentioned composition of 3.2 mm x 1.6 mm x 0.4 mm in size were produced, which consisted of 50 electrode layers. The CDCs and MLCCs were sintered at 1250 °C for 2 hours in a wetted 0.3% H_2/N_2 sintering atmosphere according to a sintering profile as described in Chapter 2.

Samples were prepared from a MLCC using the lift-off technique via a focused ion beam (FIB) scanning electron microscope, see Figure 4.5.1. The microstructures of the dielectrics were determined by transmission electron microscopy, Technai 20 and JEOL 2010F, which operated at 200 kV.

4.5.3. Electrical properties and microstructure characteristics

CDC and MLCC samples were fabricated and fired at 1250 °C according to the typical sintering profile used for BME multilayer capacitors. The ceramics were sintered close to full density. Some porosity was observed in the ceramics of the MLCC´s cover layers. This porosity is often observed in the cover layer, but it does not affect the capacitor's reliability. As long as the ceramics of the capacitors active dielectric layers are fully dense then reliability and long lifetime are guaranteed.

For reference the sintering behaviour of this ceramics was determined by dilatometer analysis and the results are shown in Figure 4.5.2. The CDC and MLCC capacitances and loss factors were measured using an AC field of 1 kHz and 1 V_{rms}. The calculated relative permittivity values showed a difference between the CDC and the MLCC samples, see Table 4.5.1. The CDC samples had permittivities of about 4430, while the calculated permittivity values of the MLCCs dielectrics were somewhat higher and up to a value of 4830, due to a higher applied electrical field over the dielectric layer. In fact the electrical fields applied over the CDC and MLCC dielectric layers were quite different. The electrical fields over the dielectrics in the CDC and MLCC were ~0.0005 V/μm and ~0.4 V/μm, respectively, which influenced the degree of electric polarization.

Table 4.5.1: Electrical properties of CDC and MLCC.

	Temp (°C)	Cap (nF)	ε_r	Tan δ (10^{-4})
CDC	1250	1125	4434	345
MLCC	1250	3079	4834	932

The losses, tan δ, were lower in the CDC samples than in the MLCC samples. The tan δ values of CDC samples were primarily determined by the dielectric losses. However, in MLCCs the ESR is not only determined by the dielectric loss, but also by the electrode resistivity, multilayer construction and termination resistivity, as already discussed in Chapter 3.1 and Chapter 3.5. The nickel electrodes of the MLCC samples were discontinuous; the average thickness was about 1 μm. The sum of the dielectric losses and the total of the electrode resistivities, due to for instance inner electrode quality and construction, led to higher tan δ values in the MLCCs than in the CDC samples.

The ε_r-T curves of the multilayer capacitors were within X5R specification, see Figure 4.5.3. The CDC samples had different ε_r-T curves because they were measured at lower applied electrical fields compared to the dielectrics of the MLCCs. Thus, the polarization of the dielectrics in the CDC samples was much lower than in the MLCC. The effect of the electrical field on the ε_r-T curves is explained in detail in Chapter 4.1. Anyway, the dielectric composition used in this study was used as an example that can be used to make multilayer capacitors for mass production. The electrical characteristics were known, yet the appearance of the ceramic microstructure had to be analyzed.

Transmission electrode microscopy was performed to observe the general microstructure of the ceramics, see Figure 4.5.4. The micrographs showed a significant number of grains having a core-shell structure. However, only a fraction of the grains showed the typical 90° ferro-electric domains. Moreover, the core-shell structures were not very pronounced, see Figure 4.5.5. Most of the grains were relatively small. It seemed that especially the smaller grains, < 200 nm, did not show the typical 90° domains structure. The stripe patterns were typically found in the larger grains, between 200 and 500 nm. Furthermore, the shell phase did not cover the core phase in a uniform manner, because the surrounding shell phase varied in thickness. Therefore the grains did not show a nice spherical core–shell structure. The overall picture showed a microstructure wherein a considerable amount of small para-electric grains were mixed with larger ferro-electric grains, which were surrounded by a para-electric shell of varied thickness.

The chemical composition of several core-shell grains were analyzed using a scanning transmission electron microscope equipped with energy dispersive spectroscopy (EDS). Elemental analysis did not reveal large differences in the dopant concentration within the grains. In fact there were no large concentration gradients detected between core and shell grains with respect to the added elements.

An attempt was also made to analyze the Ba/Ti ratios of the core and the shell phases. Again, no significant differences in the Ba/Ti ratios between core and shell phases were detected.

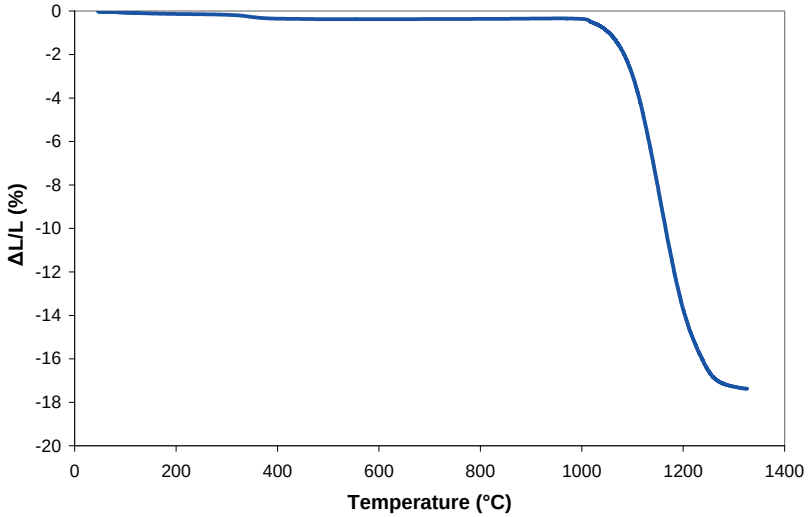

Figure 4.5.2: TMA curve of high-ε_r X5R composition.

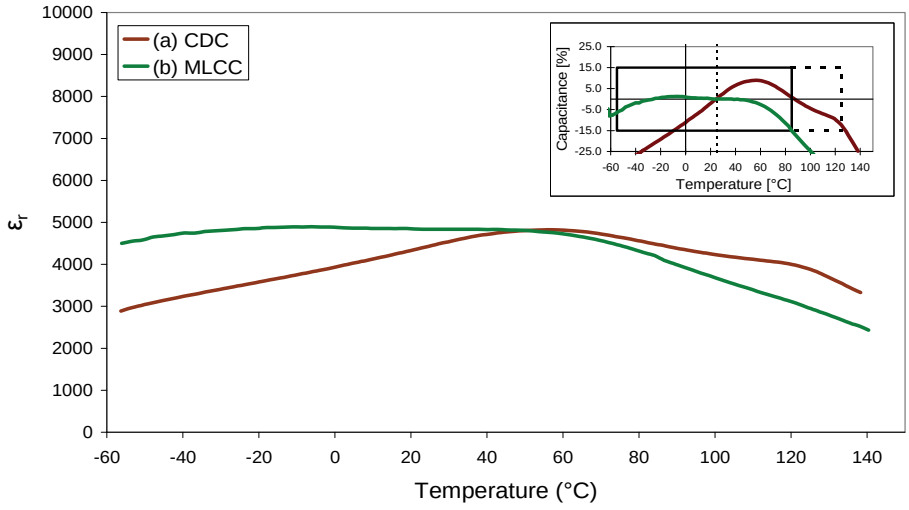

Figure 4.5.3: The ε_r versus temperature curves for (a) CDC and (b) MLCC. The inset shows the capacitance versus temperature for both samples. The X5R and X7R specification boxes are highlighted.

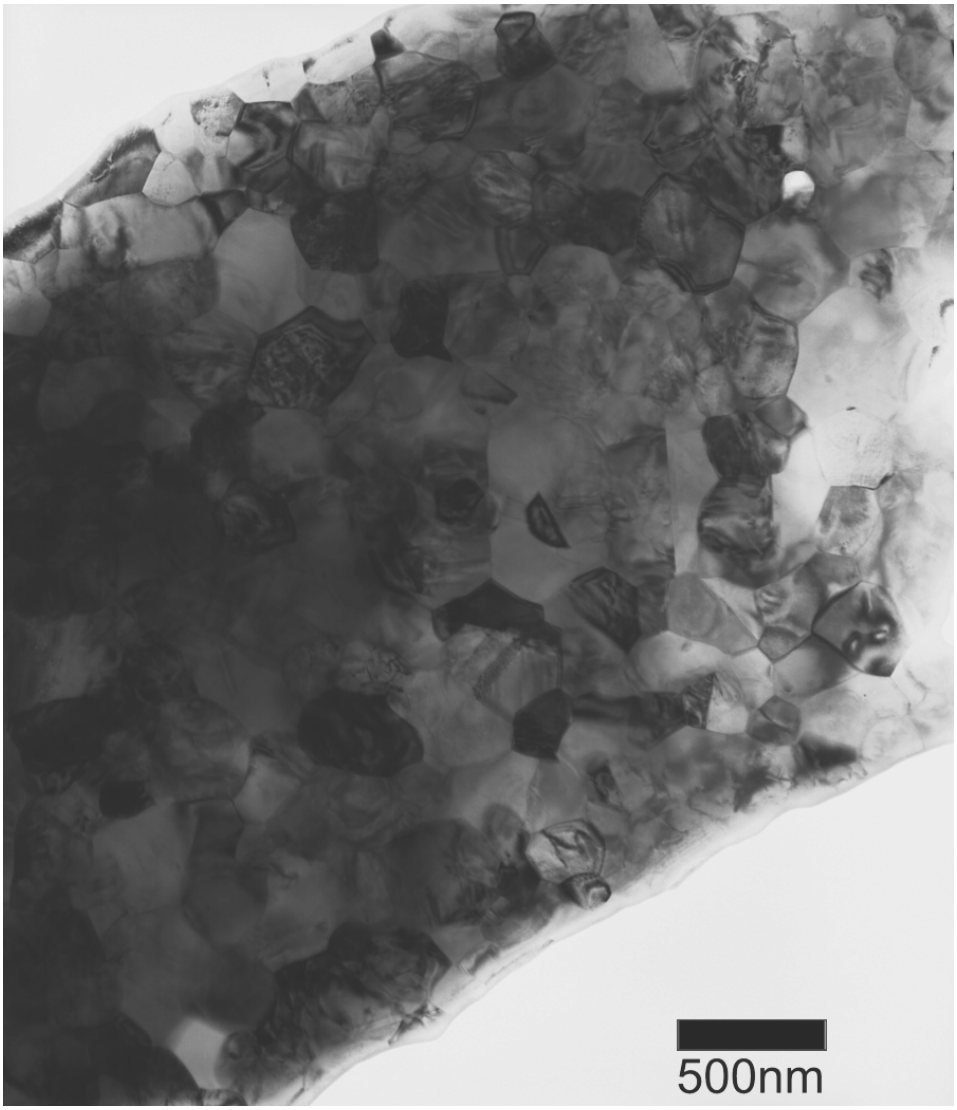

Figure 4.5.4: TEM micrograph of a ceramic region showing a significant number of grains with a core-shell structure and grains without a core-shell structure.

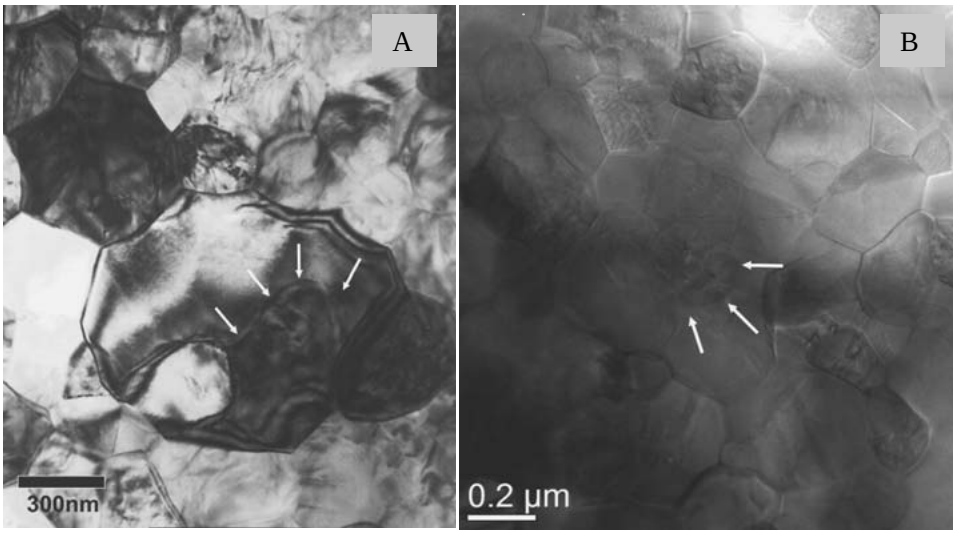

Figure 4.5.5: Micrographs showing the core-shell structure by (a) TEM and (b) STEM.

Two other phases were observed quite frequently. The EDS analysis revealed that the first phase was composed of primarily Mg and Ti oxide with some traces of Mn, see Figure 4.5.6. The EDS spectrum showed also Ni and Cu, but they originated from the TEM sample holder and re-deposited material from the ion beam sputtering, respectively. When the enlarged region was examined in more detail a layered pattern was observed. This was confirmed by the diffraction pattern which showed closely spaced spots pointing into one direction. The d-spacing is quite large and we were not able to determine the crystallographic phase precisely of the this needle like inclusion. Anyway, the inclusion consisted primarily of Mg-Ti-oxides. Possible crystallographic phases could be rhombohedral $MgTiO_3$, cubic Mg_2TiO_4 or orthorhombic $MgTi_2O_5$. The EDS results suggested that the crystallographic structure of the Mg-Ti rich inclusions could be orthorhombic $MgTi_2O_5$.

The other phase is a square inclusion which consisted primarily of Mg and Si oxide with some traces of Ti and Mn, see Figure 4.5.7. These square grains were observed quite often within the dielectrics. As the inclusion had a square shape it was concluded that this Mg-Si rich phase could be either perovskite $MgSiO_3$ or spinel Mg_2SiO_4. Both phases crystallize in the orthorhombic crystal structure. However, to get more certainty about the exact compositions and the crystal structures of both inclusions more experimental data have to be collected.

Silica, SiO_2, was used as sintering aid and therefore added to the raw materials. After sintering it could be expected that silica-rich phases had formed in the ceramics, because silica forms a liquid phase during sintering. Then amorphous Si-rich phases would be located at the grain boundaries or at other interfaces. However, the high resolution images in Figure 4.5.8 did not reveal any Si-rich amorphous

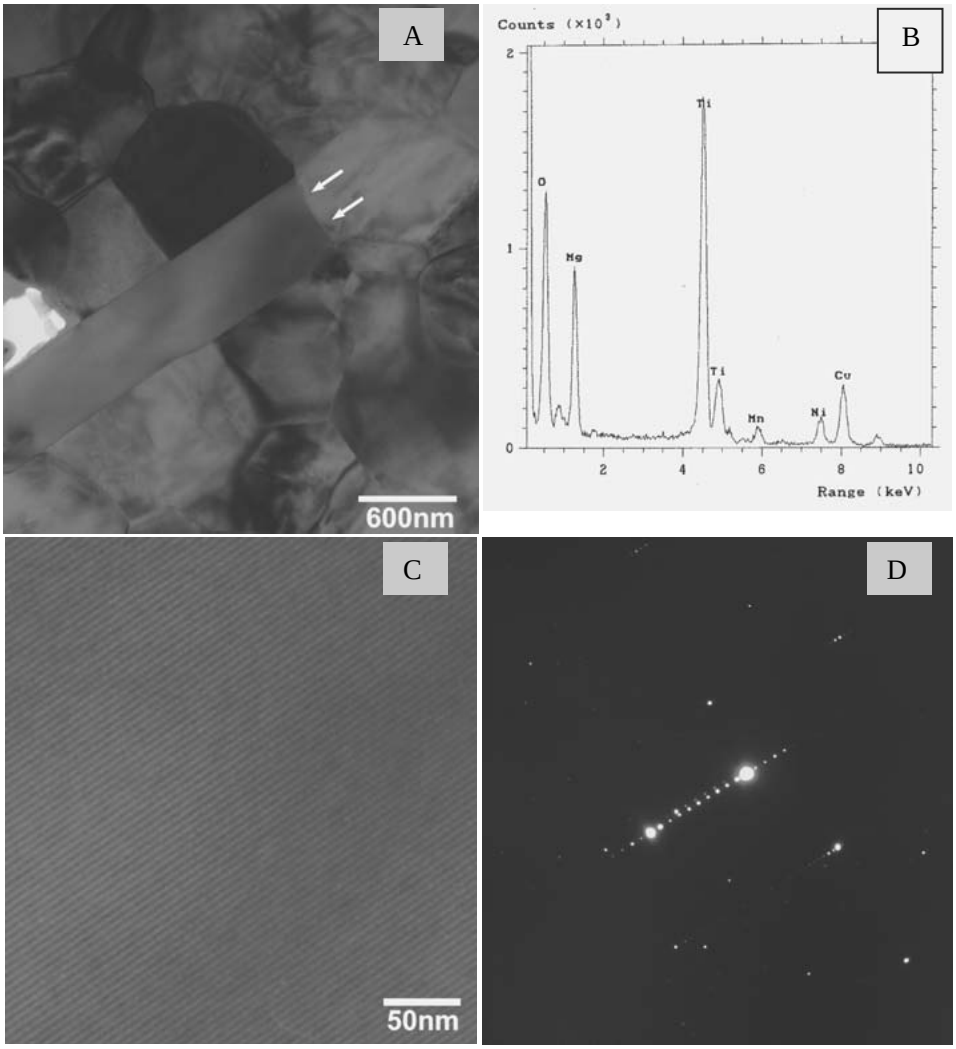

Figure 4.5.6: (a) Micrograph showing a needle-like inclusion, (b) the EDS spectrum, (c) an enlarged region of the inclusion and (d) a diffraction pattern of the enlarged region.

phase at the nickel/ceramic interfaces nor at the grain boundaries of the $BaTiO_3$ grains. Within these ceramics a grain boundary thickness of about 1 nm was observed between the $BaTiO_3$ grains. The interface between the nickel electrode and the ceramics was visible and the grain boundary thickness was less than 1 nm thick. No extra secondary phases were observed. That would suggest that SiO_2 reacted partly into the Mg-Si oxide rich phase or was dissolved into the $BaTiO_3$ lattice during sintering.

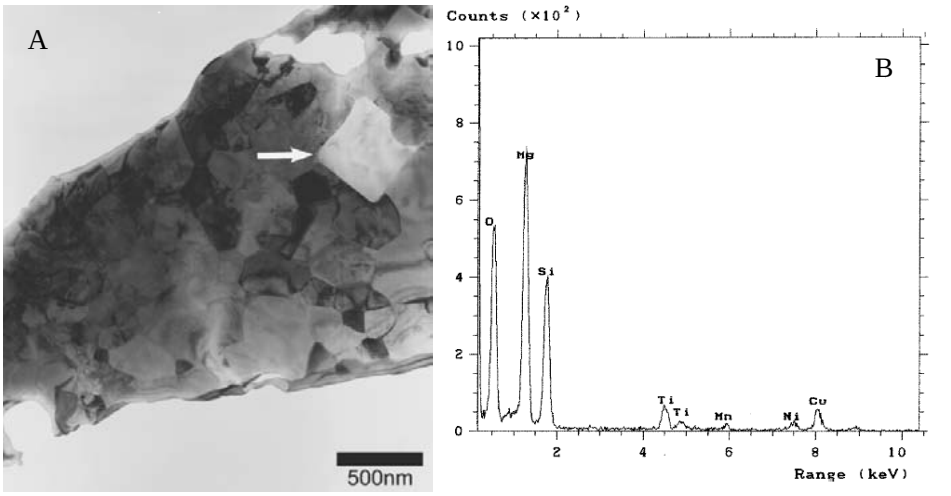

Figure 4.5.7: (a) TEM micrograph showing a square inclusion in the ceramics sample and (b) the EDS spectrum of the inclusion.

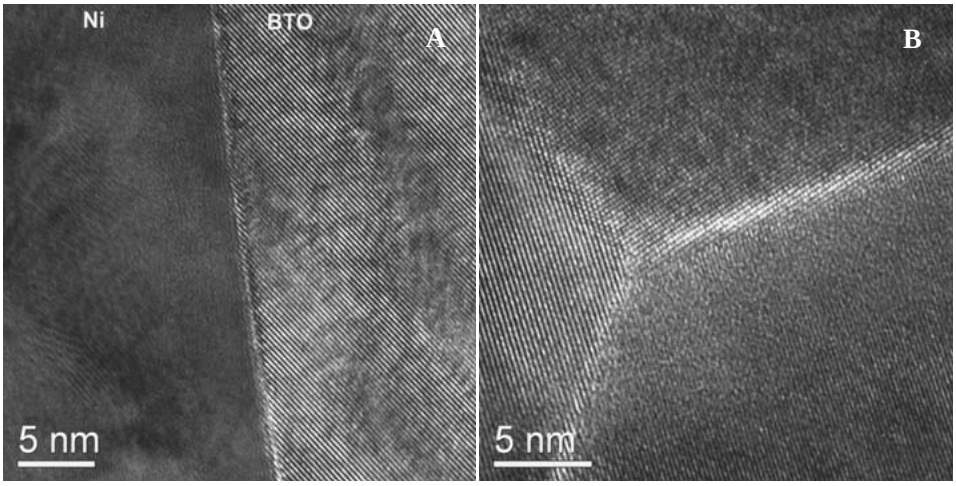

Figure 4.5.8: High resolution micrograph of (a) nickel electrode and ceramic interface and (b) a triple point within the ceramics.

4.5.4. Conclusions

A typical ceramic formulation, used to make high-ε_r X5R multilayer ceramic capacitors, was evaluated for its electrical properties by examining CDC and MLCC samples. The results showed that these ceramics had high dielectric permittivities and that the electrical properties met the X5R specification limits. This typical X5R dielectric was used as an example to study the microstructure of the ceramics.

TEM and EDS analysis revealed that a significant number of the grains showed typical ferro-electric stripe patterns. Grains that were larger than ~200 nm showed the typical 90° domains. When the grains were smaller than ~200 nm the grains did not have these typical striped patterns. Actually the microstructure consisted of a mixture of small grains that were para-electric. Grains having the typical core-shell structure had a shell phase which varied in thickness. The core was not surrounded uniformly by the shell.

EDS analysis did not reveal large concentration differences between the grains. No large differences in Ba/Ti ratios were found between core and shell phase.
Two extra secondary phases were observed. The first consisted of Mg-Ti oxide rich grains, presumably $MgTi_2O_5$. The other phase is a Mg-Si oxide rich phase. This phase could be perovskite $MgSiO_3$ or spinel Mg_2SiO_4. In any case no other secondary phases were found in these ceramics.

References

1) Hennings, D. and Rosenstein, G. *Temperature-stable dielectrics based on chemically inhomogeneous $BaTiO_3$*; Journal of the American Ceramic Society, 1984 **67**(4): p. 249–254.
2) Park, Y. and Kim, Y. H. *The dielectric temperature characteristics of additives modified Barium-Titanate having core-shell structured ceramics*; Journal of Materials Research, 1995 **10**(11): p. 2770–2776.
3) Chazono, H. and Kishi, H. *Sintering characteristics in the $BaTiO_3$-Nb_2O_5-Co_3O_4 ternary system: II, stability of so-called "core-shell" structure*; Journal of the American Ceramic Society, 2000 **83**(1): p. 101–106.
4) Yoon, D. H.; Lee, J. H. and Kim, D. Y. *Core-shell structure of acceptor-rich, coarse barium titanate grains*; Journal of the American Ceramic Society, 2002 **85**(12): p. 3111–3113.
5) Kishi, H.; Kohzu, N.; Sugino, J.; Ohsato, H.; Iguchi, Y. and Okuda, T. *The effect of rare-earth (La, Sm, Dy, Ho and Er) and Mg on the microstructure in $BaTiO_3$*; Journal of the European Ceramic Society, 1999 **19**(6–7): p. 1043–1046.
6) Kishi, H.; Okino, Y.; Honda, M.; Iguchi, Y.; Imaeda, M.; Takahashi, Y.; Ohsato, H. and Okuda, T. *The effect of MgO and rare-earth oxide on formation behavior of core-shell structure in $BaTiO_3$*; Japanese Journal of Applied Physics Part 1-Regular Papers Short Notes & Review Papers, 1997 **36**(9B): p. 5954–5957.

7) Mizuno, Y.; Okino, Y.; Kohzu, N.; Chazono, H. and Kishi, H. *Influence of the microstructure evolution on electrical properties of multilayer capacitor with Ni electrode*; Japanese Journal of Applied Physics Part 1-Regular Papers Short Notes & Review Papers, 1998 **37**(9B): p. 5227–5231.
8) Morita, K.; Mizuno, Y.; Chazono, H.; Kishi, H.; Yang, G. Y.; Liu, W. E.; Dickey, E. C. and Randall, C. A. *Electric conduction of thin-layer Ni-multilayer ceramic capacitors with core-shell structure $BaTiO_3$*; Japanese Journal of Applied Physics Part 1-Regular Papers Brief Communications & Review Papers, 2007 **46**(5A): p. 2984–2990.
9) Tian, Z. B.; Wang, X. H.; Zhang, Y. C.; Fang, J.; Song, T. H.; Hur, K. H.; Lee, S. and Li, L. T. *Formation of Core-Shell Structure in Ultrafine-Grained $BaTiO_3$-Based Ceramics Through Nanodopant Method*; Journal of the American Ceramic Society, 2010 **93**(1): p. 171–175.
10) Park, K. J.; Kim, C. H.; Yoon, Y. J.; Song, S. M.; Kim, Y. T. and Hur, K. H. *Doping behaviors of dysprosium, yttrium and holmium in $BaTiO_3$ ceramics*; Journal of the European Ceramic Society, 2009 **29**(9): p. 1735–1741.
11) Yasukawa, K.; Nishimura, M.; Nishihata, Y. and Mizuki, J. *Core-shell structure analysis of $BaTiO_3$ ceramics by synchrotron X-ray diffraction*; Journal of the American Ceramic Society, 2007 **90**(4): p. 1107–1111.
12) Wang, T.; Wang, X. H.; Wen, H. and Li, L. T. *Effect of milling process on the core-shell structures and dielectric properties of fine-grained $BaTiO_3$-based X7R ceramic materials*; International Journal of Minerals Metallurgy and Materials, 2009 **16**(3): p. 345–348.
13) Mizuno, Y.; Hagiwara, T.; Chazono, H. and Kishi, H. *Effect of milling process on core-shell microstructure and electrical properties for $BaTiO_3$-based Ni-MLCC*; Journal of the European Ceramic Society, 2001 **21**(10–11): p. 1649–1652.
14) Mizuno, Y.; Hagiwara, T. and Kishi, H. *Microstructural design of dielectrics for Ni-MLCC with ultra-thin active layers*; Nippon Seramikkusu Kyokai Gakujutsu Ronbunshi/Journal of the Ceramic Society of Japan, 2007 **115**(1342): p. 360–364.
15) Chen, C. S.; Chou, C. C. and Lin, I. N. *Microstructure of X7R type base-metal-electroded $BaTiO_3$ capacitor materials co-doped with MgO/Y_2O_3 additives*; Journal of Electroceramics, 2004 **13**(1–3): p. 567–571.
16) Chou, C. C.; Chen, C. S.; Lin, I. N.; Yang, W. C. and Cheng, H. F. *Development of X7R type base-metal-electroded $BaTiO_3$ capacitor materials by co-doping of MgO/Y_2O_3 additives*; Ferroelectrics, 2006 **332**: p. 35–39.

Chapter 5

General conclusions and future trends

In electronics the trend to produce smaller handheld equipment like notebook PCs, smart phones, GPS units and so on, which are equipped with higher functionalities, is still continuing. In the last two decades, development was focussed on producing smaller multilayer capacitors, which have higher capacitive densities. Besides, in the last 2 decades the raw material costs is continuously increasing, which led to cost-effective design of new electronic devices and components. This work describes several highlights with respect to the development of the several important multilayer ceramic capacitors types. Various dielectric material systems were studied, which can be applied in ceramic multilayer capacitors to use in various electronic devices.

5.1. Temperature stable dielectrics

The first part of this thesis described various C0G-type Class 1 dielectrics, i.e. new dielectrics based on relative high permittivity non ferro-electric materials. Goal was to develop and produce dielectrics which are suitable to co-fire with low cost electrode materials like pure silver or copper. It is proposed that the sintering temperature of multilayer capacitors must be at least 100 °C below the melting point of the used electrode material in order to produce reliable capacitors. This general rule can be applied successfully to all dielectric systems described in this work. For instance, modifications to reduce the sintering temperature of a commercial dielectric Ferro powder, AD850DZ, were successfully applied. The sintering temperature can be reduced to 950 °C by adding a sinter aid based on a B_2O_3-ZnO-CuO-Bi_2O_3-SiO_2 material system. The co-firing temperature is only 10 °C below the melting point of pure silver. However, study on electrode quality of 95Ag/5Pd and 90Ag/10Pd electrodes revealed that reliable dielectrics can only be obtained when silver diffusion into the dielectric ceramics can be avoided. Best results were achieved when the new C0G dielectric material was used in combination with 90Ag/10Pd electrodes.

Furthermore, a dielectric material, which can be used to co-fire with pure silver electrodes, based on (Zn,Mg)TiO_3 was developed. This new material system can be sintered fully dense at temperatures of about 900 °C. Multilayer capacitors with pure silver electrodes were made using $Zn_{0.95}Mg_{0.05}TiO_3$ + 0.25 mol% TiO_2 + *2* wt% $Zn_4B_6O_{13}$ + *2* wt% Bi_2O_3 ceramics. The electrical properties and reliability were evaluated and it showed promising electrical properties at room temperature. The material has an ε_r of 30, meets the C0G properties and has a high insulation resistance. However, insulation resistance and time constant decreased substantially, due to the presence of a semi-conductive spinel Zn_2TiO_4, when measured at 140 °C. Specifically the time constant dropped from a few hundred seconds, measured at room temperature, to well below 10^{-6} seconds at 140 °C. Unfortunately, that means that this material is not suitable to use in high reliable multilayer ceramic capacitors.

In order to make multilayer capacitors suitable for co-firing with pure copper electrodes a commercial dielectric, AD850DZ, was modified by adding a reduction stable sintering aid, composed of Li_2O-MgO-SiO_2 and CuO. Multilayer capacitors were made using this new dielectric ceramics and co-fired with copper electrodes in a reducing sintering atmosphere at 1040 °C. The dielectric constant of this ceramic is around 70 and the electrical properties meet C0G specifications. However, the time constants at room temperature and 140 °C were about 150 and 45 s, respectively, which is relatively low. In any case depending on the requirements of the capacitors function the material can possibly be used for HF applications.

To reduce costs a lot of effort was put in the development of new dielectrics suitable to co-sinter with low cost electrode materials like pure silver or copper. Another important condition was to reduce the equivalent series resistance of the multilayer ceramic capacitors in order to avoid self-heating of the component, which is caused by high energy dissipation during application at high frequencies. It was therefore thought in the 1990s and early 2000s that multilayer capacitors have to be made with pure silver or copper electrodes, because these metals have the lowest resistivities. This study shows that the equivalent series resistance is mainly dependent on the resistivity of the inner electrodes. Lowest equivalent series resistances are obtained with MLCCs having pure copper electrodes. However, nowadays most C0G multilayer ceramic capacitors are made with nickel electrodes to reduce costs. The drawback of using MLCCs having nickel electrodes is the fact that due to the skin effect, whereby the equivalent series resistance increases, these capacitors can only be used at moderately high frequencies. MLCCs having nickel electrodes are most commonly used for bypassing, impedance matching and temperature compensation applications.

There are a lot of multilayer ceramic capacitors manufacturers, i.e. Yageo, Murata, Kemet, Samsung, Taiyo Uden and others, which produce a wide variety of capacitors. Most of them use in-house powder manufacturing, so that the exact

formulation of the ceramics is not known outside the companies. In fact it is also not very simple to know the inner-electrode composition just by reading the companies datasheets. However, there are companies, which sell ready-to-use dielectric powders, e.g. Ferro, Prosperity Dielectrics, MRA laboratories and others.[1–5] It is interesting to note that none of these companies have dielectric formulations that can be co-fired with pure silver electrodes. Ferro claims to have 2 compositions, ULF140 (ε_r of 13–15) and ULF800 (ε_r of 75; BaO-$(Gd,Nd)_2O_3$-TiO_2 based composition), which can be co-fired with 99Ag/1Pd electrodes. The recommended firing temperature of the ULF800 is 860 °C for 3 h. That is 100 °C below the melting point of pure silver. Despite the fact that this material can be sintered well below the melting point of silver, it is noticeable that pure silver is not recommended. MRA laboratories also claim to have a dielectric material, VLF-220Aq4, that can be co-sintered with an Ag/Pd alloy of high silver content and even with pure silver.[3] The material is a $(Zn,Mg)TiO_3$-type ceramic having an ε_r of around 23. This dielectric powder can be sintered fully dense when fired at 940 °C for 5 h. The sintering temperature is just below the melting point of pure silver and most probably a considerable amount of silver will diffuse into the ceramics during sintering. Most probably an Ag/Pd alloy with higher palladium content will have to be used to produce reliable capacitors. In general most high ε_r C0G dielectric formulations have to be sintered with Ag/Pd alloys of high Pd content. The various dielectric powder manufacturers offer C0G raw materials, which have to co-fire with Ag/Pd alloys which contain at least 10 % Pd.

It is reported that C0G MLCC with Cu electrodes were mass produced, which were based on modified $CaZrO_3$ dielectrics. These type of dielectrics have dielectric constants of about 35.[6] However, high ε_r C0G dielectrics having values of 70 were not reported in literature as an option for high frequency applications. No multilayer ceramic capacitors having pure copper electrodes are currently mass produced. The majority of BME C0G capacitors are being produced with nickel electrodes, which are primarily based on modified $CaZrO_3$ or $SrZrO_3$ ceramics.[7] Depending on actual use, i.e. in low or high frequency applications, the proper multilayer capacitor can be chosen from a wide variety of dielectric materials.

5.2 High-ε_r X5R dielectrics

The second part of this work describes development issues of X5R Class II dielectrics. These types of dielectrics are based on modified ferroelectric $BaTiO_3$ ceramics. They have dielectric constants exceeding 3000 and the main industrial strategy is to produce multilayer capacitors having higher capacitive volume efficiency. Nowadays these type of multilayer capacitors are being made with nickel

inner electrodes and development is not primarily focused on reducing material costs by implementation of new raw materials. The main goal is to maximize the capacitive efficiency by optimizing the construction of the multilayer capacitors by stacking the electrode and dielectric layers more efficiently. The layers are stacked in such way that the capacitors body volume is optimally used, meaning that the margins between the active area and the capacitors body is kept as small as possible. An optimal configuration of the MLCC is obtained as the dielectric layer and electrode thickness are reduced as much as possible. However, currently the technology is reaching its limits and both the dielectric and electrode layer thicknesses are already reduced to about 1 μm. Therefore the aim is focused on developing X5R dielectrics having higher dielectric constants. In general dielectric properties are studied after making multilayer capacitors, which have dielectric layers thinner than 2 to 3 μm. This is a very laborious and time consuming manner to evaluate material properties. A proposal is made to evaluate the dielectric properties by measuring the electrical properties via P-U hysteresis loop measurements directly on ceramic disc capacitors. In this manner the dielectric capacitive trend in AC fields can be studied quickly. This technique builds a good correlation between the dielectric properties of ceramic disc capacitors and capacitors having very thin dielectric layers.

The multilayer capacitor's fabrication process had also to be improved in order to make high-ε_r multilayer capacitors. Especially the slurry/slip preparation is an important production step. In the 1980s and 1990s milling of the raw material powders was done by a ball milling step whereby large milling media, typically beads of 2 mm in diameter, were used. With this technique it was not possible to decrease the particle size sufficiently. Therefore new techniques were introduced, like bead mills and milling beads with an average sizes of 100 to 200 nm. Hereby the raw materials can be de-agglomerated, mixed and milled to particles size distributions well below 1 micron. This manufacturing process is suitable for thin dielectric multilayer technology.

Usually for high-ε_r dielectrics the main component is $BaTiO_3$ powder to which small amounts of metal oxides, called dopants, are added. The milling process of the raw materials has an influence on the final dielectric properties of the X5R ceramics. This is related to the properties of the $BaTiO_3$ powders as well as to the final particle size of the milled powder mixture. However, not only the raw materials grade or the particle sizes of the powders are important. Also small adjustments of the dopant concentrations have a large impact on the microstructure, dielectric constant, temperature dependency and insulation resistance of the dielectrics. High permittivities can be achieved when to $BaTiO_3$ powders a well specified concentration of metal elements is added. Typical elements which can be used to

make high-ε_r dielectric are combinations of Yttrium (Y), Magnesium (Mg), Manganese (Mn), Silicium (Si), Copper (Cu), Molybdenum (Mo) and Vanadium (V). The combination of $BaTiO_3$ grade, elemental concentrations, and milling process have impact on the electrical properties of multilayer capacitors. In general capacitors having dielectric constants of about 5000 can be made successfully.

Typically a trend in industry is to decrease the dielectric thickness of the multilayer capacitors.[8] It is already possible to make X5R multilayer capacitors having dielectric thicknesses of 0.5 μm, produced by Murata.[9] However, the trend to reduce dielectric thicknesses using thick film/wet processes will reach the limits of its technology. To make even thinner dielectrics other processes have to be used instead; i.e physical vapor deposition, chemical vapor deposition, spin coating or other techniques.[10] All these techniques have drawbacks in manufacturing devices in large quantities.

To avoid the trend in making thinner dielectrics, an attempt was made to develop a very high-ε_r dielectric material via an alternative method. Normally dopant elements in the form of metal oxides are added in specific concentrations to $BaTiO_3$. The alternative route will use a mixture of pure $BaTiO_3$ powders and powders of $BaTiO_3$ that are rich in yttrium (Y) and copper (Cu). To this mixture elements are added to form X5R dielectrics. This method yields high-ε_r dielectrics, values are between 2500 and 3000, when measured on ceramic disc capacitors. This alternative method is a complete new synthesis route which can be used to make reliable high-ε_r X5R Class II multilayer ceramic capacitors.

Usually the large ceramic multilayer capacitors manufacturers develop the ceramic formulations themselves. That also means that these large companies will have their own strategies to make and mass produce the components. It is common to buy the $BaTiO_3$ powders from specialized powder manufacturers, like Sakai, Nippon Chemical Industries or KCM Corporation.[5, 11–12] Besides, it is also possible to buy full composition Class II powders from some of these manufacturers and companies like Ferro and Prosperity dielectrics.[1–2] However, none of these companies have commercial very high-ε_r dielectrics. The ε_r of their powders is limited to values below 4000.

5.3. General remarks and future trends

In the last 2 decades, the development of Class I and Class 2 capacitors was mainly focused on decreasing raw materials costs, miniaturization of passive components and increasing capacitive volume efficiency. The majority of ceramic multilayer capacitors, especially the Class II and Class III (X5R, X7R and Y5V) capacitors were already being produced with nickel electrodes. In the last decade most Class 1

(C0G) MLCCs are also produced using nickel metal as inner electrodes.[7] Further options to decrease raw materials costs are limited. Moreover, miniaturization of components is limited by the mounting techniques, which have to handle small case size components. The smallest case size is the 01005 sized multilayer capacitors for both C0G and X5R dielectrics. However, the maximum possible capacitance is limited to the dielectric properties of various materials.

The dielectric layer thickness of X5R multilayer capacitors were decreased considerably in the past decade. That led to higher electrical fields over the dielectric layers, which had impact on the use of these components. As the dielectric layers became thinner the rated voltage of the capacitors had to be decreased as well, because the long term reliability of the components has to be quaranteed.[13] The rated voltages of current capacitors have already reached very low values, X5R at 4 V and X6R at 2.5 V. The trend of using lower DC voltages could only happen due to the lower power supply of the semiconductor chips on various circuit boards, whereby the chips work at about 1.0 V.[9] However, the current technology is reaching the limits with respect to the ceramic materials and technology. New materials and manufacturing technologies have to be developed to meet the requirements for the future central processing units (CPU) decoupling applications and other purposes.
The latest trends in multilayer ceramic capacitors development are focussed mainly on two routes: (1) higher reliability at temperatures above 125 °C and (2) continuing miniaturization of electronic devices.

For automotive, military and aviation applications the operating temperatures are typically in the range of 150 to 300 °C, depending on the specific application.[14] Investigations towards materials to obtain C0G up to 200 °C and X8R, X9S or even X9G capacitors are already reported.[15–16] At these operating temperatures it is even possible that PME materials, Ag/Pd, have to be used instead of nickel (BME) in multilayer components, because nickel has the tendency to oxidize at these higher temperatures.[16]

For miniaturization there are several strategies to make smaller electronic devices. As the minimum case size is limited to a 01005 dimension and further size reduction is limited to pick-and-place costs, other strategies are investigated to reduce manufacturing costs. It is possible to integrate various electronic components using embedding techniques. That means that the passive and active components are directly formed during Printed Circuit Board (PCB) manufacturing, whereby currently existing or specially designed components are inserted into the inner layers of the PCB.[17] In the latter case the thickness of the multilayer capacitors is important. The thicknesses of the components are adjusted to meet new requirements and thicknesses of these types of capacitors are already reduced to a maximum of 150 µm. This dimension is adopted for all case sizes and is already accepted as a standard in industry.

Another way to save space is to make components according to an array structure. That means that multiple capacitors, normally 2 or 4 individual multilayer capacitors, are processed in such way that one single component is produced. The application of these type of array components reduces space and mounting costs.[9] Furthermore, PCB manufacturers are mainly focussed on improvement of electrical performance, reliability, resistance to mechanical stress and improved thermal properties.[17] To meet these requirements dielectric materials with even higher dielectric constants and higher reliability have to be developed.

References

1) www.ferro.com
2) www.pdc.com.tw/product/mlcc.asp
3) www.mralabs.com/
4) http://hcc.hanwha.co.kr/english/pro/cbt_detail.jsp?idx=198
5) www.kyoritsu-kcm.co.jp/english/electronic/electronic_top.html
6) Kishi, H.; Mizuno, Y. and Chazono, H. *Base-metal electrode-multilayer ceramic capacitors: Past, present and future perspectives*; Japanese Journal of Applied Physics Part 1-Regular Papers Short Notes & Review Papers, 2003 42(1): p. 1–15.
7) Xu, X.; Niskala, M.; Gurav, A. S.; Laps, M.; Saarinen, K.; Tajuddin, A.; Montanari, D.; Bergamaschi, F. and Boni, E. *Advances in Class-I C0G MLCC and SMD Film capacitors*; conference paper CARTS USA 2008.
8) Randall, M.; Skamser, D.; Kinard, T.; Qazi, J. and Tajuddin, A. *Thin film MLCC*; Conference paper CARTS USA, 2007: p. 1–12.
9) www.murata.com
10) Pan, M. J. and Randall, C. A. *A Brief Introduction to Ceramic Capacitors*; IEEE Electrical Insulation Magazine, 2010 26(3): p. 44–50.
11) www.sakai-chem.co.jp/english/index.html
12) www.nippon-chem.co.jp
13) Hendricks. C.R.; Min Y.K. and Lane. T. *Reliability challanges for CPU decoupling MLCC*; conference paper CARTS USA; 2010.
14) Devoe A.; Hofmaier R.L. and Ngo L. *New high temperature ceramic capacitor*; conference paper CARTS USA; 2009.
15) Xu X.; Magee J.; Hoskins A.; Laps M. and Gurav A. *Robust Class-I dielectric for high temperature applications*; conference paper CARTS USA; 2009.
16) Polotai, A. V.; Maher, G. H.; Wilson, J. M. and Maher, G. H. *Selection od dielectric materials for high temperature applications*; conference paper CARTS USA; 2010.
17) Uher, U. and Zednicek, T. *Ultrathin discrete capacitors for emerging embedded technology*; conference paper CARTS USA; 2010.

Appendix 1

Commercial dielectrics for multilayer capacitors with nickel electrodes

A.1. Introduction to C0G capacitors with nickel electrodes

In Chapter 3.5 multilayer capacitors with nickel electrodes are discussed. In this appendix chapter two types of commercially available dielectrics are evaluated to give an impression of the chemical composition and electrical properties of these types of dielectrics. The dielectrics for the Ni-MLCCs are based on $SrZrO_3$ and $CaZrO_3$ ceramics, which are known to be stable against reduction during sintering.[1–2] The $SrZrO_3$ and $CaZrO_3$ dielectrics exhibit good electronic properties in high frequency applications. The dielectrics have relative permittivity (ε_r) values of 38 and 30, respectively. The temperature coefficient of capacitance (TCC) are +120 and +40 ppm/°C, respectively, and the losses (tan δ) is approximately $3 \cdot 10^{-4}$ for both dielectrics. They can be used for C0G capacitors when the TCC properties of the zirconates, which have positive TCC values, are mixed with titanates, which have negative TCC values. For instance $SrZO_3$ can form a solid solution with $SrTiO_3$, which exhibits a near-zero TCC. However, $CaZrO_3$ and $SrZrO_3$ powders are sintered dense at temperatures above 1450 °C, therefore the dielectrics have to be adjusted to sinter well below the melting temperature of nickel, 1435 °C. Furthermore, the nickel electrodes must be protected from oxidation. Therefore the multilayer capacitors have to be sintered in a reducing atmosphere. To meet these requirements the addition of sintering aids, addition of acceptor ions and process conditions have been investigated and they are reported in literature.[2–8] Various C0G dielectrics with good lifetime and breakdown strengths are available on the market. In this appendix two dielectric powders are discussed. The first is a dielectric powder called YK30, which was developed by Yageo and is currently used to produce Ni-MLCCs in mass production. The second dielectric ceramics is the commercially available powder from Ferro called AD350N, see Table A.1.

Table A.1: Composition of dielectric powders for Ni-MLCC.

Component	YK30 mol%	AD350N mol%
CaO	35.8	0.1
SrO	14.1	48.8
ZrO_2	46.1	47.5
TiO_2	1.7	2.8
HfO_2	0.5	0.5
SiO_2	1.0	0.3
MnO	0.5	0.0
Nb_2O_5	0.1	0.0

A.2. Experimental - Ceramic Disc Capacitors

The powders YK30 (Yageo) and AD350DZ (Ferro) were ball milled overnight in 2-propanol using a PE flask with 2 mm YTZ beads. The powders were dried, crunched and sieved over 300 µm mesh. For the examination of sintering behaviour 1200 mg powder was weighed and uniaxially pressed (Fontijne SRA100) with a pressure of 8 bar into bars of 8 mm diameter x 7.50 mm height. Thereafter the pellets were cold-pressed isostatically (EPSI *Engineered Pressure Systems International* B.V.) at 4000 bar for 3 minutes. The pellets were measured using a NETZCH Dil 402 C dilatometer. The samples were sintered at a 5 °C/ min heating rate in static air. Then the samples were kept at 1400 °C for 30 minutes before the samples were cooled down by 10 °C/min.

For examination of the other properties 300 mg powders were weighed and uniaxially pressed with a pressure of 8 bar (Fontijne SRA100) into pellets of 8 mm diameter x 2 mm height. The pellets were sintered in air, moist N_2 and moist 0.3% H_2/N_2 atmosphere in a tube kiln (Nabertherm), respectively. The densities of the sintered samples were measured using an Archimedes method. The crystal structures of the sintered powders were determined by X-Ray diffraction (XRD) using Cu Kα radiation (PanAnalytical PW1830). The compositions of the powders were determined by X-Ray fluorescence spectrometry using a Philips XRF spectrometer type PW1480.

Ceramic Disc Capacitors were prepared by sputtering gold terminations of 200 nm thickness on the pellets using a Perkin-Elmer sputtering system Model 2400.

A.3. Results and Discussion

The two dielectric powders were analyzed by X-ray fluorescence (XRF) to determine the composition. The compositions of the two dielectrics are shown in Table A.1. The dielectric YK30 is based on a mixture of $CaZrO_3$ and $SrZrO_3$ at which TiO_2, SiO_2, MnO and Nb_2O_5 is added. The use of various dopants in this dielectric were described by W.S. Lee and his colleagues.[8] SiO_2 is added to enhance densification of the ceramics during sintering and is therefore the sintering aid. Mn^{2+} and Nb^{5+} are both incorporated at the Zr-site. The Mn^{2+} ion is therefore considered as acceptor and Nb^{5+} as donor dopant. Due to higher concentration of Mn^{2+} in the dielectrics compared to Nb^{5+}, the effect of Nb^{5+} is overruled and the incorporation of excess Mn^{2+} will yield good insulation resistances and lifetime properties of the ceramics.

The commercial powder AD350N is mainly $SrZrO_3$ to which TiO_2 and SiO_2 is added. In literature it is described that the dielectric is composed of $SrTiO_3$, which has a large negative TCC, and $SrZrO_3$, which has a positive TCC, and the mixture therefore has a near-zero TCC.[9] The sintering aid SiO_2 is added to improve sintering behaviour. The AD350N dielectrics can be sintered at top temperatures ranging from 1200 to 1300 °C. The sintered AD350N dielectrics have a relative permittivity near 35 and can meet the C0G specification easily. In the XRF results also HfO_2 is mentioned, but it is known that HfO_2 is an impurity in TiO_2 and ZrO_2 and therefore it was not added on purpose.

The sintering behaviour of the two dielectrics were examined, see Figure A.1. The analysis revealed that AD350N ceramics can be sintered at lower temperatures in comparison to YK30. In literature it is written that AD350N can be sintered fully dense at 1200 °C, while YK30 has to be sintered at 1300 °C. However, AD350N can also be sintered at 1300 °C and yields dielectrics with good electrical properties. For the sake of comparison pellets of these two powders were sintered at 1300 °C in air, moist N_2 and moist 0.3% H_2/N_2, respectively. In practice MLCCs are produced in large production kilns together with other types of MLCCs with nickel electrodes. In Figure 2.3 an example of a sintering curve of Ni-MLCCs is shown. In the evaluation a similar sintering profile was carried out to sinter the ceramic pellets. Sintering in air and in moist N_2 was done with an easy sintering profile by just heating up by 5°C per minute to a maximum temperature. The pellets were kept at maximum temperature for 2 hours before cooling down to room temperature.

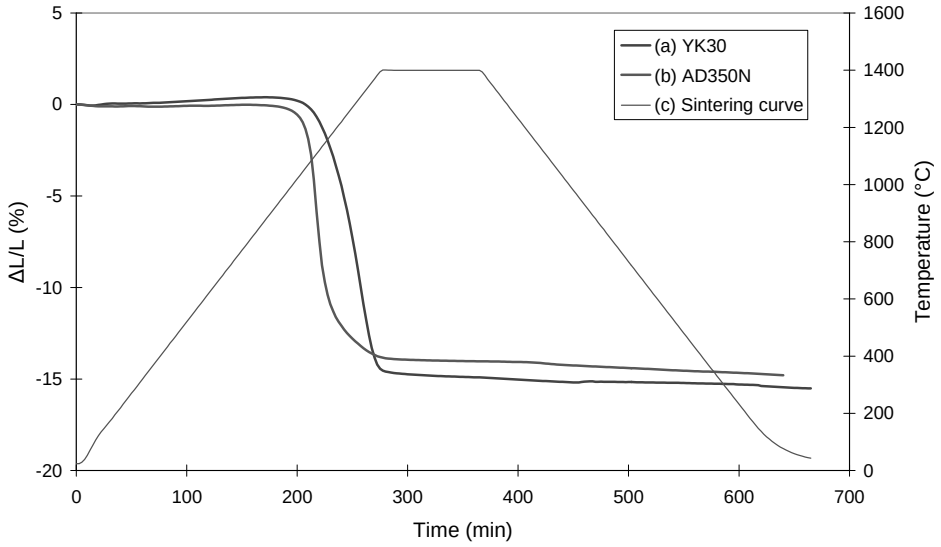

Figure A.1: TMA curves of dielectric powders (a) YK30 and (b) AD350N.

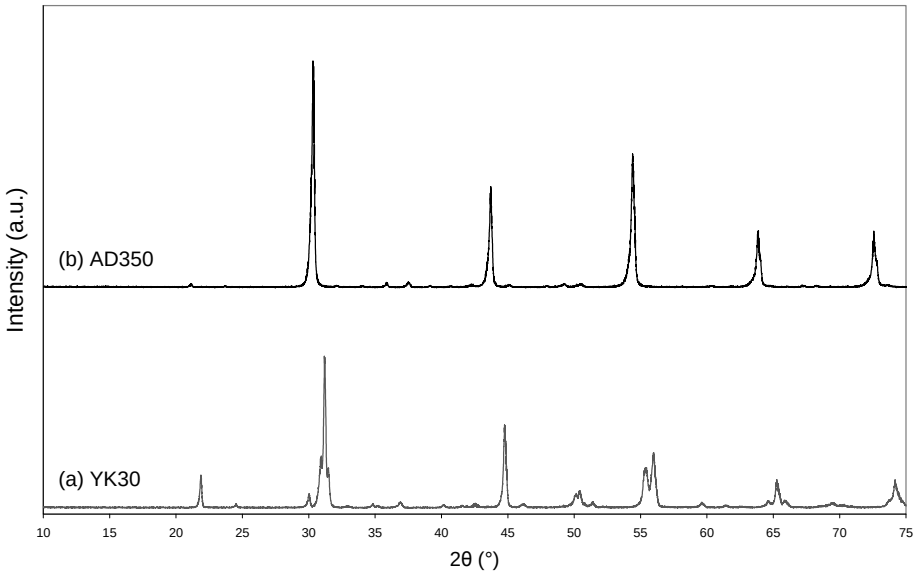

Figure A.2: X-ray diffraction pattern of (a) YK30 and (b) AD350N ceramics sintered at 1300°C in air.

Table A.2: Density (g/cm^3) of pellets sintered at 1300 °C in various atmospheres.

Dielectrics	Air	N_2	0.3% H_2/N_2
YK30	4.87	4.79	4.73
AD350N	5.37	5.44	5.35

After the pellets were sintered at 1300 °C in moist 0.3% H_2/N_2 the crystal structures of the ceramics were identified by X-ray diffraction, see Figure A.2. The sintered YK30 ceramics mainly consisted of $Ca_xSr_{1-x}ZrO_3$ with an orthorhombic crystal structure. Furthermore some traces of cubic $CaZrO_3$ were also found.[10–11] The phase composition of AD350N consisted mainly of tetragonal $SrZrO_3$ with traces of cubic $SrTiO_3$.[12–13] The density of the dielectrics was measured after sintering, see Table A.2. The YK30 ceramics showed density values which seem to depend on sintering temperature. The density of the pellets sintered in moist 0.3% H_2/N_2 had a density of 4.73 g/cm^3. The pellets of AD350N had a density of 5.35 g/cm^3, which is in agreement with data from literature.[9]

Table A.3: Electrical properties of CDC sintered at 1300 °C at various atmospheres.

	Air			N_2			0.3% H_2/N_2		
	ε_r	Tan δ	IR	ε_r	Tan δ	IR	ε_r	Tan δ	IR
Dieletrics		(10^{-4})	(Ω)		(10^{-4})	(Ω)		(10^{-4})	(Ω)
YK30	32	24	$1.6 \cdot 10^{14}$	27	18	$9.5 \cdot 10^{13}$	32	22	$6.3 \cdot 10^{13}$
AD350N	41	18	$7.1 \cdot 10^{14}$	40	22	$1.5 \cdot 10^{14}$	38	25	$1.3 \cdot 10^{14}$

The basic electrical properties were measured, see Table A.3, and it becomes clear that YK30 has a lower permittivity than AD350N. The tan δ values are relatively large, because the electrodes were made of gold that were sputtered on the pellets. The adhesion between the gold contacts and the dielectrics are not optimal, and therefore, higher losses were measured. The insulation resistance of YK30 dielectrics is lower than AD350N, but is still at a very high level. The values of IR also show that the dielectrics sintered in a higher reductive sintering atmosphere were reduced to a larger extent than the ones sintered in air. This indicates that some reduction of the ceramics took place during sintering.

References

1) Kell, R. C.; Greenham, A. C. and Olds, G. C. E. *High permititivity temperature-stable ceramic dielectrics with low microwave loss*; Journal of the American Ceramic Society, 1973 **56**(7): p. 352–354.
2) Lee, W. J.; Wakahara, A. and Kim, B. H. *Decreasing of $CaZrO_3$ sintering temperature with glass fritaddition*; Ceramics International, 2005 **31**(4): p. 521–524.
3) Tsurumi, T.; Teranishi, T.; Wada, S.; Kakemoto, H.; Fukunaga, O.; Nakada, M. and Akedo, J. *Ultra wide range dielectric spectroscopy of strontium titanate-strontium zirconate solid solution*; Journal of the Ceramic Society of Japan, 2006 **114**(1333): p. 774–781.
4) Hu, X.; Ling, Z. Y.; Guo, D. and He, X. H. *Effective Sintering Aids of Boric Frit and Lithium Salts for Low-Temperature Sintering of Dielectric Ceramics*; Ferroelectrics, 2009 **388**: p. 120–127.
5) Kim, B. H.; Lee, G. Y.; Lee, W. J. and Kim, J. H. *Dielectric properties in $(1-x)CaZrO_3$–$0.1CaTiO_3$-$xTiO_2$ system*; Materials Science and Engineering B-Solid State Materials for Advanced Technology, 2004 **113**(3): p. 198–202.
6) Pollet, M. and Marinel, S. *Lowering of $CaZrO_3$ sintering temperature using lithium-calcium fluoride flux addition*; Materials Science and Engineering a-Structural Materials Properties Microstructure and Processing, 2003 **362**(1–2): p. 167–173.
7) Pollet, M.; Marinel, S. and Desgardin, G. *$CaZrO_3$, a Ni-co-sinterable dielectric material for base metal-multilayer ceramic capacitor applications*; Journal of the European Ceramic Society, 2004 **24**(1): p. 119–127.
8) Lee, W. S.; Su, C. Y.; Lee, Y. C.; Lin, S. P. and Yang, T. *Effects of dopant on the dielectric properties of $CaZrO_3$ ceramic sintered in a reducing atmosphere*; Japanese Journal of Applied Physics Part 1-Regular Papers Brief Communications & Review Papers, 2006 **45**(7): p. 5853–5858.
9) Megherhi, M.; Symes, W.; Chu, M.; Romer, E. and Coppens, W. *COG Base metal electrode dielectric composition for thin layer MLCC*; conference paper CARTS USA 2004, p. 21–24.
10) *ICSD powder diffraction card 01–089–8016: $Ca_{0.612}Sr_{0.388}ZrO_3$.*
11) *ICSD powder diffraction card 00–024–1074: $CaZrO_3$.*
12) *ICSD powder diffraction card 01–089–9001: $SrZrO_3$.*
13) *ICSD powder diffraction card 01–084–0443: $SrTiO_3$.*

Dankwoord

Tot een paar jaar geleden had ik niet gedacht dat ik ooit een proefschrift zou schrijven. Ik had namelijk al met ´plezier´ ruim 12 jaar gewerkt aan het ontwikkelen van keramische condensatoren en andere componenten. Het kwam dan ook als een verassing, dat ik de mogelijkheid kreeg om onderzoek te mogen doen en dit proefschrift te mogen schrijven. Hiervoor moet ik Pim Groen en Andre ten Elshof bedanken. Zij hebben mij kunnen overtuigen, gelukkig, dat ik op basis van het materiaal onderzoek, die ik in de voorgaande jaren had verricht, zou kunnen gebruiken voor het schrijven van dit proefschrift. Echter, als ik dat een aantal jaar eerder had geweten, dan zou ik mijn gegevens trouwens wel anders, minder chaotisch dus, hebben opgeschreven. Met de hoeveelheid informatie die ik tot de beschikking had, was het een grote puzzel die ik moest oplossen. Gelukkig eens eentje die ik überhaupt heb kunnen oplossen. Maar wel met behulp van de goede raad van en de discussies met Andre.

Ik ben ook Dave Blank, Guus Rijnders en de andere leden van de wetenschappelijke staf van de vakgroep ‘Inorganic Material Science’ dankbaar, die me de mogelijkheid hebben gegund om nog een groot aantal maanden experimenten te kunnen uitvoeren in hun laboratoria. Deze periode was, behalve nuttig, ook zeer de moeite waard. Ik heb kunnen ervaren wat het verschil is tussen het doen van onderzoek bij een universiteit en het werken in een ontwikkelingsafdeling binnen het bedrijfsleven. Het was een mooie periode in mijn carrière.

Zoals iedereen nu wel kan begrijpen, moet ik een groot aantal personen bedanken, omdat dit proefschrift zonder hun inbreng niet tot stand zou zijn gekomen. Met name de collega’s met wie ik heb kunnen discussiëren, die voor mij de verschillende monsters en condensatoren hebben gemaakt, die voor mij analyses hebben uitgevoerd, die samen met mij koffie tijdens de pauzes hebben gedronken, waarmee ik samen, na het werk, ben wezen stappen om het werk tijdelijk te vergeten, of die mij op ander wijze geestelijk hebben ondersteund in al die jaren.

Enkele van deze (oud)-collega’s zijn intussen ook goede vrienden geworden. Hier moet ik zeker Pim Groen en Oliver Steigelmann noemen. Zij hebben mij al vanaf mijn afstudeerstage (in 1996!) in Aken met kennis gevoed en met wie ik veel over het werk heb kunnen discussiëren. En ik zal de meeste van de vele avonden die we gezellig met een pot bier hebben doorgebracht niet vergeten. Ik hoop dat we dit nog vaak samen kunnen blijven doen.

De (oud)-collega's, die ik heb leren in Roermond, Laura Beekman, Harold Brentjens, Rob Coninx, Gerard Dortant, Rob van der Drift, Jos van der Heijden, Hans Heynen, Paul Hilgers, Ruud Lammers, Harrie Nabben, Xenofon Nikolaou, Sietse Oostra, Frank Peeters, Truus Stienen, Peter van der Straten, Mat Vossen, Dick Vroling, Jacques Warnier en Johan Wolters wil ik met name noemen, omdat zij direct of indirect hebben bijgedragen aan het tot stand komen van dit proefschrift. Daarnaast wil ik degenen bedanken die voor mij veel praktisch werk hebben uitgevoerd; Christien Berger, Sandra Briels, Winnie van Garling, Hendrik de Haan, Wenny Maessen, Jos van der Sanden, Bianca Weekers.

This work was not possible if I didn't had the possibility to co-operate with my colleagues at Philips Forzungszentrum in Aachen. Especially I would like to thank Knuth Albertsen, D. Bausen, Petra Huppertz, Christof Metzmacher, H.G. Kohler, Dr. A. Comberg, Dr. D. Hennings and Tilman Schlenker. For the detailed information with respect to high permittivity C0G materials and its properties, I also thank Yukiko Furukawa for her detailed explanations.

Ook moet ik de Wilma Derks bedanken. Zij heeft gezorgd voor de verschillende diëlektrische poeders en de bijbehorende informatie. Bovendien wil ik Gerald Koebrugge bedanken voor het meten van de temperatuurafhankelijkheid van de capaciteit van de verschillende condensatoren, die ik heb gemaakt op de universiteit.

Furthermore, I want to thank Ian Reaney and Denis Cumming (University of Sheffield) for the hospitality, when I visited you in Sheffield, and for doing the TEM analysis of the capacitor samples.

Ondanks dat ik niet al zo vaak op de universiteit te vinden was, het is een behoorlijk stuk rijden van Maastricht naar Enschede, wil ik iedereen bedanken van de vakgroep IMS voor de gezellige tijd. Met name wil ik mijn 'oude' bekenden Tomek Stawski en Sjoerd Veldhuis bedanken, die me in ieder geval, voor hun onbewust denk ik, geestelijk gesteund hebben. Maar ook dank ik de kamergenoten Josée Kleibeuker, Michiel Maas, Frank Vroegindeweij en Ole Göbel voor de nodige gezelligheid. Suresh Kumar voor zijn hulp bij de praktische werkzaamheden. Mark Smithers voor het maken van de mooie SEM afbeeldingen en Gerrit van Hummel voor de hulp bij de röntgendiffractie.

Tot slot wil ik Daan van de Ende en Theo Wehrung bedanken voor het doorlezen van het manuscript en het geven van hun commentaar.

Het is de bedoeling dat ik ieder bedank die me geholpen heeft met het tot stand komen van dit proefschrift. Ik hoop oprecht dat ik niemand vergeten ben.

Publications

Articles

R. Mikkenie, O. Steigelmann, W.A. Groen and J.E. ten Elshof, *A quick method to determine the capacitance characteristics of thin layer X5R multilayer capacitors*, Journal of the European Ceramic Society, 2012, Volume 32, Issue 1, pages 167-173.

R. Mikkenie, W.A. Groen and R. van der Drift, *Diffusion of silver during sintering in high permittivity C0G dielectrics*, Integrated Ferroelectrics, 2010, Volume 114, Issue 1, pages 72-80.

C. Metzmacher, R. Mikkenie and W.A. Groen, *Indium-containing ceramics with negative temperature coefficient characteristics*, Journal of the European Ceramic Society, 2000, Volume 20, Issue 7, pages 997-1002.

Application note

R. Mikkenie, G.C.M. Dortant, K. Albertsen, H.G. Kohler, T. Schlenker, *Dielectric composition, method of manufacturing a ceramic multilayer element, and electronic device*, 2006, US patent number 7041615.

Samenstelling van de promotiecommissie

Voorzitter en secretaris:

Prof. J.J.M.L. Cornelissen (University of Twente, The Netherlands)

Promotor:

Prof.dr.ing. A.J.H.M. Rijnders (University of Twente, The Netherlands)

Co-promotor:

Prof.dr.ir. J.E. ten Elshof (University of Twente, The Netherlands)

Referent:

Dr. W.A. Groen (TNO Eindhoven, The Netherlands)

Leden:

Prof.dr.ing. D.H.A. Blank (University of Twente, The Netherlands)
Prof.dr.ir. L. Lefferts (University of Twente, The Netherlands)
Prof. I.M. Reaney (University of Sheffield, United Kingdom)
Prof.dr.ir. S. van der Zwaag (Delft University of Technology, The Netherlands)